Characterising Mer and Axl receptor tyrosine kinase expression and transcriptomic profiling of myeloid cells in hepatocellular carcinoma

Sujit Mukherjee

July 2022

Thesis submitted for the degree of Doctor of Philosophy

Imperial College London

Department of Metabolism, Digestion and Reproduction
Imperial College London

Primary Supervisor:
Professor Mark Thursz

Declaration of Originality

I declare that all work in this thesis is my own and is appropriately referenced.

Copyright Declaration

Dedication

To the memory of my late supervisor, Harry Antoniades

To my wife Magda and our two daughters, Norah and Sofia

Acknowledgements

I would like to thank my supervisor Professor Thursz for his guidance and for helping me to move this project forward. I am indebted to my secondary supervisors, Dr Wafa Khamri and Dr Evangelos Triantafyllou for their wisdom, support with flow cytometry and *in vitro* work, and unwavering advice and help throughout my time in research.

I received enormous help and wisdom from Professor Alberto Quaglia in reviewing the immunohistochemistry. I would also like to thank Dr Rosa Miquel and the histopathology team at King's College Hospital for their support and help with specimens, the surgical and transplant teams including the transplant co-ordinators and Professor Heaton. I would like to thank key members of my lab group for their advice and support over the years – in particular, Dr Naveenta Kumar and Dr Arjuna Singanayagam.

For bioinformatic support, I would like to thank Dr Laura Martinez-Gili. In addition, Dr David Britton and Professor Pedro Cutillas for their support with managing the data from the mass spectrophotometry. I would also like to express my sincere gratitude to the Wellcome Trust for awarding me the Research Training Fellowship to allow me to conduct this work.

I would like to thank my family – my parents Kalpana and Mihir, and my sisters Leena and Lisa, who have encouraged me and given me strength over the years.

Lastly, I would like to thank my wife for everything she has done to help me complete this thesis – without her support this would not have been possible, and I will be forever grateful for everything that she has done for me and for our two girls.

Abstract

Background: TAM receptor tyrosine kinases attenuate pro-inflammatory signalling in myeloid cells and maintain tissue homeostasis through apoptotic cell clearance (efferocytosis). Two members of the TAM-RTK family, MerTK and Axl, are overexpressed in human cancers; MerTK+ macrophages display a regulatory phenotype (M2c) similar to tumour associated macrophages (TAMϕs). MerTK+ and Axl+ macrophages contribute to immune paresis in liver disease. Little is known about MerTK and Axl expressing myeloid cells in HCC. In this thesis I characterise their expression and phenotype in circulating and tissue-resident myeloid cells, explore drivers for their expansion and function *in vitro* and utilise transcriptomics to interrogate wider TAMϕ phenotype in human HCC.

Methods: Tissue and blood were collected from patients undergoing surgery or awaiting treatment for HCC. TAM-RTK expressing myeloid cells were identified using immunohistochemistry. Flow cytometry of isolated immune cell populations was utilised to understand their abundance and phenotype; *in vitro* conditioning and co-culture experiments were devised to recapitulate the tumour microenvironment, identify potential drivers for MerTK and Axl expression and assay their function. Serum and tissue homogenates were analysed for levels of TAM-RTK ligands. Transcriptomic analysis of tumour and liver derived myeloid cells was undertaken.

Results: MerTK+ macrophages are evident within inflammatory infiltrates in HCC. There is modest expansion of myeloid cells expressing MerTK and Axl in the tumour microenvironment, however gene expression is not upregulated and neither are downstream signalling cascades. *In vitro* conditioning does stimulate Axl but not MerTK expression and promotes immune-regulatory cytokine production. TAMϕs exhibit a 'post-phagocytic' phenotype with upregulation of C1Q, scavenger receptor Stabilin-1 and APOE.

Conclusions: TAM-RTK signalling is not activated within the tumour microenvironment. Transcriptomic analysis has identified an immune regulatory post-phagocytic and efferocytotic phenotype; further work is needed to evaluate the significance of this in the tumour biology of HCC, if it is not mediated through MerTK and Axl signalling.

Abbreviations

Axl – Axl tyrosine kinase

AFP – alpha-fetoprotein

AKT – protein kinase B

ARLD – alcohol related liver disease

BCLC – Barcelona Clinic Liver Cancer

DAMP – damage-associated molecular pattern

DMSO – dimethyl sulfoxide

ELISA – enzyme-linked immunosorbent assay

FACS – fluorescence-activated cell sorting

Gas6 – growth-arrest-specific 6

HC – healthy control

HBV – hepatitis B virus

HCV – hepatitis C virus

HFE – haemochromatosis

HLA-DR – human leukocyte antigen-DR

IFN – interferon

INR – international normalized ratio

JAK – Janus kinase

LC/MS – liquid chromatography/ mass spectrometry

LPS – lipopolysaccharide

MACS – magnetic associated cell sorting

MAPK – mitogen-activated protein kinase

M-CSF – macrophage colony stimulating factor

MDSC – myeloid-derived suppressor cell

MELD – model for end stage liver disease

MerTK – Mer tyrosine kinase

MerTK-/- – Mer tyrosine kinase knockout

MFI – median fluorescence intensity

MoMF – monocyte-derived macrophage

NAFLD – non-alcoholic fatty liver disease

NASH – non-alcoholic steatohepatitis

NF-κB – nuclear factor NF-kappa B

PAMP – pathogen-associated molecular pattern

PBMC – peripheral blood mononuclear cell(s)

PCA – principal component analysis

PCR – polymerase chain reaction

PI3K – phosphoinositide 3 kinase

Pros1 – Protein S

PS – performance status

PtdSer – phosphatidylserine

SLE – systemic lupus erythematosus

SLUG – zinc-finger protein SNAI2

SNAIL – zinc-finger protein SNAI1

SOCS – suppressor of cytokine signalling protein

TLR – toll-like receptor

TNF-α – tumour necrosis factor-alpha

TAMϕ – tumour associated macrophage

TAM-RTK – TAM (Tyro3-Axl-MerTK) receptor tyrosine kinase

TME – tumour microenvironment

TWIST – twist related protein 1

VEGF – vascular endothelial growth factor

Abstracts and publications related to this work

International

- Mukherjee S. K., Kumar N., Graham J., Miquel R., Quaglia A., Thursz M., Khamri W., Antoniades C.G., *Axl positive myeloid cells are expanded within tumours and in the peripheral circulation in patients with hepatocellular carcinoma,* Poster Presentation, EASL HCC Summit, Lisbon, Portugal, March 2019

- Mukherjee S. K., Pop O.T., Triantafyllou E., Khamri W., Bernsmeier C., Li K., Suddle A., Weston C., Curbishley S., Thursz M., Adams D. H., Heaton N., Quaglia A., Antoniades C. G., *Mer tyrosine kinase positive tumour associated macrophages are a novel therapeutic target in hepatocellular carcinoma*, Poster Presentation, International Liver Congress, Barcelona, April 2016

- Mukherjee S. K., Pop, O. T., Triantafyllou, E., Khamri, W., Suddle, A., Curbishley, S., Thursz, M.R.T., Adams, D.H., Heaton, N., Quaglia, A., Antoniades, C.G. *TAM receptor tyrosine kinase expression modulates macrophage function in hepatocellular carcinoma,* Poster Presentation, Academy of Medical Sciences Spring Meeting for Clinician Scientists in Training, London, February 2017

Table of Contents

List of Figures

List of Tables

CHAPTER 1

Introduction

1. Background

1.1 Epidemiology of hepatocellular carcinoma

As the third leading cause of premature death in the United Kingdom and the second leading cause of lost working years in Europe, liver disease is unique amongst other major causes of chronic disease (including heart disease, stroke and respiratory disease) in having an increasing mortality: rates have increased by 400% since the 1970s (Williams *et al.*, 2014). Excess alcohol consumption and increasing rates of obesity are key risk factors in the development of liver disease in the UK - alcohol accounts for 75% of liver related deaths and the incidence of non-alcoholic fatty liver disease (NAFLD) continues to rise. Since 1990 there has been an increase in the number of deaths in Europe attributable to liver disease from 2.3% to 3% of all deaths (Karlsen *et al.*, 2022).

Alongside this burgeoning rate of death related to liver disease is a worrying rise in the number of deaths related to hepatocellular carcinoma, a key pathological endpoint in the natural history of chronic liver disease and cirrhosis. Since 1990, there has been a 70% increase in the number of deaths related to HCC, with a total of 63500 in Europe in 2019 alone (GBD 2019 Diseases and Injuries Collaborators, 2020). Rates are projected to increase to 22 deaths per 100,000 people in the UK by 2035. At the current rate of increasing deaths from HCC, it is projected to move from its current place as the fourth to the third most common cause of cancer worldwide by 2030 (Rahib *et al.*, 2014). In the UK currently, five-year survival is just 13.7% for men and 10.7% for women (Llovet, 2005; Cancer Research UK, 2019).

The majority of cases (90%) arise on a background of chronic liver disease; 80% of all cases have cirrhosis (European Association for the Study of the Liver, 2018). The annual incidence of cirrhosis varies, according to estimates, between 1% to 6% annually (Trinchet *et al.*, 2015);

approximately one-third of patients with cirrhosis will develop HCC at some point during their lifetime (Llovet, 2005). The incidence of HCC in chronic liver disease can vary across the world, due in part to varying aetiological burdens for chronic liver disease: age standardised rates of HCC can vary from between 3 to 9 cases per 100000 people (Llovet *et al.*, 2021). In east Asia the burden is skewed towards hepatitis B virus (HBV) - 53.4% of cases relate to hepatitis B infection and there is a higher incidence of HBV related HCC in endemic areas, up to 15% at 5 years in patients with cirrhosis (Fattovich *et al.*, 2004; Liu *et al.*, 2019). HBV can also develop aggressively and on a non-cirrhotic background, on account of HBV being capable of incorporating into hepatocyte DNA and promoting transformation of hepatocytes. If combined with exposure to aflatoxin B1 in sub-Saharan Africa, presentation can be earlier and more aggressive (Kew, 2003); taken together these facts explain the higher burden of HCC in areas with higher endemic HBV.

Hepatitis C (HCV) remains the commonest aetiology of chronic liver disease underlying HCC in Europe and North America, with 40.1% and 37.5% of cases attributable to it according to recent estimates (Liu *et al.*, 2019). With the advent of direct acting anti-virals and the prospect of eradication of HCV in the coming decade, this incidence is hoped to reduce, however the risk of HCC remains significant after eradication in cirrhotic patients (around 2% per annum).

Alcohol and non-alcoholic fatty liver disease (NAFLD) are an increasing proportion of cases, with alcohol accounting for 34.5% of cases in Western Europe at present. This proportion is likely to increase as eradication of HCV results in a reduction in the incidence of HCV related HCC. The incidence of HCC is lower than in patients with viral hepatitis (particularly HBV) at around 8% at 5 years in patients with alcohol related liver disease (ARLD) as the primary aetiology of cirrhosis. Survival from HCC in this group is lower as well, even after adjusting

for age, demographics, co-morbidity and severity of liver disease. (Fattovich *et al.*, 2004; Brar *et al.*, 2020). With regard to NAFLD related cirrhosis and HCC, there is a lower incidence (1 – 2% per annum) but it can develop in approximately 25% of cases on a non-cirrhotic background, making surveillance of NAFLD patients with fibrosis and steatohepatitis (non-alcoholic steatohepatitis, NASH) a valid question; currently evidence does not support the need for it (Mittal *et al.*, 2016).

1.2 Survival and mortality in hepatocellular carcinoma

Although there is some contribution from aetiology of liver disease, survival rates are primarily dependent upon the stage of disease at presentation. The Barcelona Clinic Liver Classification (BCLC) report median survival of greater than 5 years for patients with very early stage or Stage A HCC at diagnosis (well compensated liver disease with a solitary HCC or less than 3 nodules, each <3cm), 2.5 years for those patients with intermediate disease (patients with multinodular disease) and between 3 months to 2 years for those with advanced disease, dependent on the presence of concurrent decompensated cirrhosis (Reig *et al.*, 2022). In other (older) cohorts, these categories have been described to have 36 months, 16 months and 6 months respectively (Llovet *et al.*, 1999) – survival has improved in the last 10 years on account of wider use of curative and locoregional therapies. Unfortunately, the majority of cases (60-75%) present at too advanced a stage for curative treatment (Llovet, Fuster and Bruix, 2004; Llovet, 2005).

1.3 Pathophysiology of hepatocellular carcinoma

The development of HCC requires either activating mutations or insertion of viral DNA, resulting in accelerated transformation of hepatocytes or cholangiocytes in the hepatic parenchyma. The most common activating driver mutations in hepatocellular cancer cells

include those that result in activation of the Wnt-β-catenin pathway, through activating mutations in CTNNB1 (β-catenin) or inhibitory mutations that impair the regulatory effect of AXIN1 or APC on β–catenin signalling. These mutations can account for between 30% to 50% of all driver mutations in HCC. Activation of this pathway promotes cell stemness, proliferation and differentiation (Zhang and Wang, 2020).

Histological subtypes can determine the genetics of certain tumours and help predict their biology. Two key subtypes of HCC include the proliferative and non-proliferative tumour types – the proliferative subtype has a poorer prognosis and is classically associated with HBV related liver disease, with activation mutations in oncogenes such as TP53, and cell proliferation signalling pathways Wnt-β-catenin, PI-3 kinase and AKT. (Zucman-Rossi *et al.*, 2015). Activation of these pathways results in proliferation and histologically this group are often macrotrabecular, or a mixed cellular type of tumour. They are more commonly secretors of alpha-fetoprotein (AFP) and result in micro and macrovascular invasion (Llovet *et al.*, 2021). The non-proliferative sub-type has mutations in Wnt-β-catenin signalling, are commonly seen in patients with alcohol related liver disease and have a better prognosis; histologically these can be steatohepatitic or cholestatic.

These genetic drivers are commonly seen on a background of chronic inflammation and regeneration, with HCCs classically developing from regenerative nodules with progressive dysplasia. There is evidence that chronic inflammation in the hepatic parenchyma can stimulate transformation of the hepatocytes within regenerative nodules, resulting in the selection of a proliferative, malignant clone and the development of a malignant nodule. A common mutation in most HCCs is a reactivating mutation in the TERT (telomerase reverse transcriptase) gene, which results in proliferation of a malignant clone on a background of dysplastic nodules (Nault

et al., 2013). In addition, it is thought that the secretion of angiogenic and proliferative cytokines by activated macrophages including TNF-α, hepatocyte growth factor, IL-6 and VEGF can directly stimulate hepatocytes to proliferate through NF-κB. In addition, stellate cells in the inflammatory environment are often activated and produce pro-fibrogenic cytokines including TGF-β and extracellular matrix, which can promote the formation of a malignant clone (Llovet *et al.*, 2016).

1.4 Treatment options and the BCLC (Barcelona Clinic Liver Cancer) guidance for therapy in hepatocellular carcinoma

1.4.1 Curative and locoregional therapy

Curative therapies, when feasible, offer the best prognosis. Survival after transplant can be as high 70% at 5 years and 50% at 10 years, with a recurrence rate at 5 years of 10 -15% (Tabrizian *et al.*, 2022). Other curative strategies (resection or ablation) offer similar outcomes at 5 years but with higher recurrence rates – approaching 50 – 70% at five years for both therapies (Roayaie *et al.*, 2013). As transplant is a limited resource, patient selection is key and means to attempt to improve recurrence rates after resection or ablation are key gaps in our therapeutic armoury.

Therapeutic benefit of approved options for patients with intermediate disease are significantly less encouraging - transarterial chemoembolization (TACE) is the accepted standard of care for patients with intermediate (Stage B) HCC and studies have demonstrated an extension of survival of between 26 to 30 months (Llovet and Bruix, 2003) and recent trials of adjuvant systemic therapy with sorafenib had no beneficial effect on survival (Lencioni *et al.*, 2016). TACE is not a curative therapy but can be used for ‘downstaging’ a patient to within transplantation criteria, if appropriate.

1.4.2 Systemic therapies

For those with in whom TACE is not appropriate, either because of portal hypertension or because of multinodular disease, systemic therapies are the first option in advanced (Stage C) disease. The IMbrave150 trial demonstrated survival benefit for the combination of atezolizumab (an anti-PDL1 monoclonal antibody) and bevacizumab (an anti-VEGF monoclonal antibody) over sorafenib, with an increase in median overall survival from 13.4 months to 19.2 months (Finn *et al.*, 2020). Prior to this, the REFLECT trial had demonstrated the non-inferiority of lenvatinib, a multi-tyrosine kinase inhibitor when compared with sorafenib (Kudo *et al.*, 2018). Both act on a range of tyrosine kinase inhibitors including VEGF, FGFR and PDGFR; Lenvatinib had few side effects and similar survival benefit first line. These data went head to head with sorafenib, which had previously demonstrated an increase in survival in the SHARP trial of just 2.8 months (10.7 months vs 7.9 months) versus placebo in patients with well compensated (Childs-Pugh Class A) disease and advanced HCC (Llovet *et al.*, 2008).

Second line therapies after Atezolizumab-bevacizumab include Sorafenib and Lenvatinib, and second line after sorafenib includes cabozantinib, regorafenib and ramucirumab (Vogel *et al.*, 2018). There are a range of other therapies, including anti-CTLA-4 and anti-PDL1 combination therapy tremelimumab-durvalumab, which has shown a modest increase in median overall survival first line when compared with sorafenib (16.6 vs 13.8 months) (G.K. Abou-Alfa. *et al.*, 2022) but is not yet licensed in the UK. In addition, selective internal radiotherapy (SIRT) has been licensed for inoperable tumours in patients with compensated liver disease and for whom TACE is not appropriate, thereby increasing the range of option in this group of patients.

A key point in these trials is the selection of patients with compensated, Child Pugh A liver disease. There are limited options (apart from liver transplantation) for patients with decompensated disease. Cirrhotic liver disease is a characterised by limited physiological and hepatic reserve: if hepatocellular function is impaired (even temporarily) by drug toxicity, the patient is vulnerable to hepatic decompensation, which carries significant mortality.

Therefore, new therapies must be targeted and with a safe side-effect profile for liver disease. Nevertheless, in the era of immunotherapy, it is encouraging that there are a number of new therapies of this category within reach for patients with advanced HCC. Further work is needed to ascertain these therapies' benefit in other settings or parts of BCLC algorithm, perhaps as adjuvant or neo-adjuvant therapies for resection or ablation (T. Zhang *et al.*, 2020). Given our growing understanding of the role of other immune cell populations in the tumour microenvironment, there is a need to develop a wider and more varied range of therapeutic options, both to individualise therapy in HCC but also to develop further options for combination therapy – it is clear that the synergistic effects of combination therapy are of real benefit, given the results from the IMbrave150 trial (Finn *et al.*, 2020).

1.5 Cancer inflammation and the immuno-editing hypothesis

1.5.1 Chronic inflammation is a driving factor for carcinogenesis

There has long been observed an association between tumours and inflammation. There is clear evidence from clinical practice: there is an increased incidence of cancers in a number of chronic inflammatory conditions, not least hepatocellular carcinoma, which develops on a background of liver cirrhosis in 80% of cases (Llovet *et al.*, 2021). Other examples include colorectal malignancy associated with inflammatory bowel disease and the increased incidence of both solid tumours and haematological malignancy in patients with autoimmune conditions

such as systemic lupus erythematosus. It is estimated that chronic inflammation accounts for 20% of cases of human cancer (Aggarwal, Vijayalekshmi and Sung, 2009). In addition to this, there is an increased risk of malignancy in patients with either acquired or iatrogenic immunosuppression (HIV infection, transplant recipients on long-term anti-rejection therapies) (Hadden, 2003).

Chronic inflammation releases reactive oxygen species and when combined with recurrent direct cytotoxicity can lead to mutagenesis and a pre-malignant state. Pro-inflammatory cytokine release (IL-1β, TNF-α) by immune cells activates transcription factors NF-κB, AP-1 and STAT3. These are intended to promote cell survival, growth and proliferation in immune cells but can have the same effect on any pre-malignant cells within the inflamed tissue. In the diethylnitrosamine (DEN) mouse model of hepatocellular carcinoma, IL-1β released from necrotic hepatocytes results in Kupffer cell recruitment and release of IL-6. This activates STAT3 mediated hepatocyte survival and promotes tumorigenesis (Grivennikov, Greten and Karin, 2010).

1.5.2 Pro-inflammatory cytokines support early tumour development

Once an early tumour is established, a significant immune response is maintained by the tumour and elicited by two principal mechanisms. Firstly, activating mutations in oncogenes, for example within the Ras/Raf/MAP-kinase pathway can result in the production of pro-inflammatory cytokines and chemotactic agents including IL-1β, IL-8 and cyclooxygenase-2. Secondly, as a tumour develops in size and its blood supply outstrips its metabolic requirements, hypoxic and necrotic areas release chemotactic IL-1β and TNF-α which, in addition to stimulating angiogenesis, recruits further populations of immune cells in a feed-forward mechanism (Tu *et al.*, 2008; Grivennikov, Greten and Karin, 2010).

1.5.3 Immunodeficiency increases susceptibility to malignancy

Protective immune responses to cancer had been predicted in the early 20th century by Ehrlich, Burkett and Thomas. The 'immunosurveillance' theory centred around the concept that a functioning immune system can kill aberrant malignant cells by recognising mutated, 'neo-antigen' from mutated proteins presented on their cell surface. Early enthusiasm for this hypothesis was muted by observations in athymic mice, in whom higher incidences of cancer were not detected in mice after injection with a potent carcinogen. Modern, targeted knockout mouse models helped to give credence to the theory in the 1990s and early 21st century: firstly, mice lacking the IFN-γ receptor or perforin developed more carcinogen induced tumours than wild-type counterparts (Dighe *et al.*, 1994). These are cytokines produced by cytotoxic T cells and NK cells and help mediate their function. In addition, RAG-2 knockout mice also displayed the same increased propensity to carcinogenesis compared to wild-type mice; RAG-2 is a recombination activation gene which is responsible for maintaining DNA rearrangement required to produce variation in lymphocyte receptors. This underlines the importance of antigen presentation to lymphocytes in the process of immune mediated protection from carcinogenesis. This was compounded by the discovery of human tumour antigens and data from human transplant databases showing a higher incidence of solid tumours of non-viral aetiology in transplant recipients, thereby providing a clinical correlate for observations in mice (Dunn *et al.*, 2002).

These seemingly opposing views of the role of immunity in tumour biology have led to the hypothesis that the interaction between the two is dynamic and context specific – indeed numerous studies have demonstrated contradictory functional phenotypes of almost every immune cell type when found within tumour tissue, from macrophages and dendritic cells, natural killer (NK) cells, regulatory and even cytotoxic T cells. This dynamic relationship is

dependent on the milieu of the tumour microenvironment: the cytokine and chemokine composition both within and around a tumour can orchestrate the functionality of the immune cell infiltrate from tumour-inhibitory to permissive and even tumour-promoting.

1.5.4 The immune-editing hypothesis

The natural history of cancer would suggest that this relationship is ultimately 'won' by the tumour. The 'immunoediting' hypothesis (first described by Dunn *et al.* in 2002) suggests that immunity is not simply 'overcome' by a developing tumour but that the interaction ultimately benefits its biology. This was based on observations from, amongst others, a series of informative experiments by Shankaran *et al*. in 2001 in mice. Carcinogens were administered to both immune competent and immunodeficient mice strains; solid tumours developed and transplanted into both immunocompetent and deficient recipient mice. Tumours developed in mice with and without a functioning immune system grow equally well when transplanted into immunodeficient mice: all 37 cases of methlycholanthrene (MCA) induced tumours continued to progress when transplanted into RAG-2 knockout mice. However, when tumours raised on an immunodeficient background were transplanted into immunocompetent mice, 8 of the 20 mice showed regression of the tumour (Shankaran *et al.*, 2001). Lacking an immune system during tumour development results in the development of a tumour which is more vulnerable to immune mediated attack i.e., is more 'immunogenic'. The immunoediting hypothesis highlights three distinct phases:

1) Elimination: this is broadly similar to the concept of immune surveillance and is the dominant role of immunity in early tumorigenesis.
2) Equilibrium: this (likely protracted) phase encompasses a period in which ongoing selective pressure within a tumour, exerted by both anti-tumour immune responses and

genomic instability, helps to generate clones of highly resistant malignant cells within a tumour. These are sustained by pro-tumorigenic cytokine and chemokine release by tumour intrinsic and extrinsic (immune cell derived) pathways.

3) Escape: once sufficiently resistant to immunological attack, the tumour begins to grow rapidly and exponentially.

The implication of Dunn's theory is that in a growing tumour, any immune-mediated methods of controlling tumour growth are overcome, and there is clear evidence of an immune-suppressive environment within a developing tumour. Numbers of regulatory T cells, which play a key role in dampening cytotoxic T cell function, correlate with disease progression and survival. Similarly, cytotoxic cells (CD8+ T cells and NK cells) often display an 'exhausted' phenotype and are unable to kill malignant cells. In addition, myeloid cells within advanced tumours are not only hypo-functional in antigen uptake and presentation but secrete growth factors and cytokines which promote tumour cell survival, epidermal to mesenchymal transformation (which facilitates invasiveness) and metastasis (Dunn *et al.*, 2002).

Immunotherapies have therefore focussed on altering the balance in immunity towards a reinvigorated, cytotoxic immune profile. In recent years immune-checkpoint blockade therapy has yielded promising results by enabling this switch.

1.6 Intrahepatic immunity is tolerogenic in steady state

The tolerogenic immune environment of the liver is an adaptation to its function: as the recipient of a large antigenic load from the portal blood supply, it must maintain the ability to efficiently clear pathogens swiftly yet avoid over-activation of immunity in steady state. Hepatic tolerance relies on attenuated responses from both innate and adaptive immune cell

populations within the hepatic parenchyma and the production of immune regulatory cytokines (such as IL-10) in addition to mechanical and structural factors including the slow kinetics of flow through the hepatic sinusoids to mediate this effect (Jenne and Kubes, 2013).

1.6.1 Kupffer cells, dendritic cells and liver sinusoidal epithelial cells

Kupffer cells are specialised hepatic macrophages and make up a significant proportion of the total intrahepatic immune cell population. This liver resident population is the largest population of resident macrophages in the body. They are derived from a combination of sources – there is data to suggest that they are replenished locally from embryonic precursors, however they can be replaced by infiltrating monocytes after episodes of liver injury (Bilzer, Roggel and Gerbes, 2006). Their principal functions are in clearance of pathogens and antigen presentation. Situated within the liver sinusoidal lumen, they are adept at engulfing and removing pathogens from the circulation via ligation of pathogen associated molecular patterns to Toll-like receptors. Engulfment by phagocytosis does not result in the propagation of an inflammatory response in steady state; instead, it is thought that chronic exposure to low levels of antigen (e.g. lipopolysaccharide) results in refractory responses via ligation of toll-like receptor (TLR) 4; a phenomenon known as 'endotoxin tolerance'. Importantly, Kupffer cells maintain phagocytic capacity, effectively clearing antigen without inducing a local inflammatory response which could be deleterious over time. Instead, IL-10 is released – this contributes to an immune-regulatory cytokine milieu within the hepatic sinusoids and promotes tolerogenic responses across the lobule and in other cell populations (Jenne and Kubes, 2013). Kupffer cells interact with CD4+ T cells in the sinusoids, resulting in the formation of regulatory T cells, perhaps as a result of high expression of inhibitory co-stimulation molecules – Kupffer cells express abundant surface PD-L1 (Tacke, 2017).

One particular cell population affected by IL-10 are dendritic cells. Known as 'professional antigen presenting cells', IL-10 exposure results in an alteration in phenotype, with a reduction in surface expression of MHC class II molecules and a reduction in key co-stimulatory molecules when compared with its non-hepatic or circulating counterparts. This results in ineffective antigen presentation and anergic T cell responses. In addition to IL-10, dendritic cells maintain their hyporesponsive phenotype through ongoing cell to cell contact with liver sinusoidal epithelial cells (LSECs) and with hepatocytes (Jenne and Kubes, 2013; Sana *et al.*, 2014).

LSECs play a similar role within the sinusoids – these cells are effective scavengers of cellular debris and immune complexes and have similarly reduced surface expression of MHC class II molecules. At steady state, they can promote tolerogenic responses to antigen arriving from the GI tract and can also help to promote similar tolerogenic responses from dendritic cells and Kupffer cells in their vicinity (Jenne and Kubes, 2013).

1.6.2 CD8+ T cells

Cytotoxic (CD8+) T cell function is also attenuated by trafficking through the liver in physiological conditions. Slow flow within hepatic sinusoids allows for direct activation of patrolling CD8+ T cells with antigen presenting cells and with hepatocytes, but without co-stimulation from CD4+ T helper cells. Transient interactions such as these do not result in a proliferative response and eventually die by apoptosis. This mechanism prevents autoreactive T cells developing to antigenic load from the GI tract. The liver may act to sequester and remove activated CD8+ T cells from the circulation. Experiments in a mouse model with a transgenic T-cell receptor have shown that CD8+ T cells activated by systemic administration of the cognate peptide accumulate within the liver and undergo apoptosis. These observations

formed the basis of the 'graveyard' hypothesis, postulating that the liver is a key site of sequestration and removal of activated CD8+ T cells in steady state conditions (Crispe *et al.*, 2006).

1.7 Chronic inflammation in intrahepatic immune cell populations promote fibrosis and carcinogenesis

1.7.1 Chronic inflammation results in reversal of the tolerogenic phenotype

Central to the pathogenesis of cirrhosis in chronic liver disease is a cycle of tissue damage, regeneration and repair within the hepatic parenchyma, resulting in the formation of fibrous scar tissue and loss of hepatocellular function. This chronic inflammation is a result of continual direct insults (viral infection or ongoing alcohol intake, for example), but is also punctuated by discrete episodes of acute inflammation in relation to decompensating events, such as systemic infection or gastrointestinal bleeding.

This process ultimately results in progression to end-stage liver disease, with progressive loss of hepatic function, through loss of functioning hepatic parenchyma and replacement with expanses of bridging fibrosis between portal tracts. Inflammatory cytokines released during this process can directly stimulate hepatocytes to transform into malignant clones (Llovet *et al.*, 2016). This process is exacerbated by a range of resident immune cell populations, whose functions are altered in the setting of recurrent pro-inflammatory stimuli.

1.7.2 Macrophage and dendritic cell phenotype are altered in an inflammatory milieu

Despite a tolerogenic role for myeloid antigen presenting cells in steady state, in the setting of acute inflammation they are able to restore function: both Kupffer cells and dendritic cells can

become potent antigen presenting cells and stimulate the production of pro-inflammatory cytokines (Jenne and Kubes, 2013). In addition, there is evidence that in chronic inflammatory contexts, there is an increased infiltration of monocytes into the liver. These are recruited by liver derived TGF-β and IL-10 and differentiate locally into monocyte-derived macrophages (MoMFs). These macrophages possess a wide portfolio of pro-fibrotic chemokines and cytokines, including TNF-α, IL-6, IL-13 and CCL2. CCL2 can thereafter promote further accumulation of these activated macrophages. In a similar manner to the Kupffer and dendritic cells in this context, they are potent antigen presenters and highly phagocytic (Liaskou *et al.*, 2012).

1.7.3 Stellate cell activation promotes fibrosis and carcinogenesis

Activation of hepatic stellate cells (HSCs) is a key event in fibrogenesis and, ultimately, cirrhosis. Stimuli for this include the release of damage associated molecular patterns (DAMPs) from dying hepatocytes, disturbance of the existing extracellular matrix and release of growth factors from platelets at the site of injury including PDGF, transforming growth factor beta (TGF-β) and vascular endothelial growth factor VEGF. Activations alters their phenotype, promoting the release of TGF-β and VEGF (Higashi, Friedman and Hoshida, 2017). Stellate cells are not the only cell type to undergo this transformation during chronic hepatic inflammation and the result is an environment rich in growth factors which can promote tumour cell survival and angiogenesis.

1.7.4 Loss of parenchymal immune surveillance is potentially carcinogenic

Immune surveillance is primarily undertaken by cytotoxic CD8+ T cells and NK cells. In the liver, both cell types are enriched compared with the peripheral circulation. It is hypothesised

that their surveillance function is impaired by fibrosis within the subendothelial space of Disse. This fibrotic deposition can act as a physical barrier to these circulating lymphoid cells (Guidotti *et al.*, 2015). In addition to this the cytokine milieu of the cirrhotic liver as outlined above has been shown to inhibit the cytotoxic functions of both cell types and may be relevant to intrahepatic populations (Liu, Chen and Zhang, 2018).

1.8 The tumour microenvironment in hepatocellular carcinoma

Immune dysfunction is a pivotal feature in both tumour biology and in the pathophysiology of liver disease. More specifically, persistent inflammation provides a permissive substrate both for the formation of a pre-malignant state and for the propagation of a nascent tumour. In addition to this, tolerogenic and sub-optimal immune responses result in the early escape of such tumours from the 'equilibrium' phase of immunoediting. Taken together these neatly help to illustrate not only the predominant incidence of hepatocellular carcinoma on a background of cirrhosis but also that preponderance for the development of metastases from other solid tumours within the liver. The 'immunological weakness' of tumours formed in the setting of immune dysfunction highlights the potential for immunotherapy in HCC.

Ablative therapies including transarterial chemoembolization and radiofrequency ablation result in cell death by necrosis and apoptosis and release of cellular debris and DAMPs, which could stimulate a phagocytic immune response. Release of this 'neo-antigen' can help to prime adaptive immune responses by stimulating dendritic cell function (Greten, Wang and Korangy, 2015). This has been demonstrated in patients with HCC undergoing percutaneous ablation (Ali *et al.*, 2005). The rare but remarkable phenomenon of the abscopal effect underlines the powerful effect that cytolytic therapies can have in stimulating anti-tumour responses, however, and has been described in HCC (Nakanishi *et al.*, 2008; Saito *et al.*, 2014). In such

cases, direct cytolytic therapy to one cancerous lesion results in the resolution of a distant metastasis, presumably through reinvigoration of systemic anti-tumour immunity. It has been suggested that ablative therapies in conjunction with checkpoint inhibitor therapy may act synergistically to propagate anti-tumour responses which would otherwise be suppressed by tumour derived mechanisms.

1.9 Myeloid cells and cancer

Myeloid cells constitute the predominant immune cell population within the tumour microenvironment. They are recruited from the circulation by tumour derived chemokines, most notably CCL2 and CSF1 and the two key populations are myeloid derived suppressor cells (MDSCs) and tumour associated macrophages (TAMϕs). Broadly, they share similar mechanisms by which they alter the tumour microenvironment to promote tumour progression and metastasis (Ugel *et al.*, 2015).

1.9.1 Myeloid derived suppressor cells

MDSCs are a more immature myeloid population found in the peripheral circulation and within tumours. They are thought to derive from altered myelopoiesis in cancer, which is orchestrated by the release of CCL2 and CSF1. Their presence is often noted to be a poor prognostic indicator in the natural history of a malignancy.

1.9.2 Tumour associated macrophages

TAMϕs are the predominant leucocyte population in tumours. In parallel with established nomenclature and classification systems used for macrophages, both classically activated, ‘M1-like’ TAMϕs and alternatively activated (or post efferocytotic) ‘M2-like’ TAMϕs have been described. Although these extremes of phenotype have been described, a spectrum of

macrophage phenotype has been observed - it has been proposed that the ratio of M1/M2 macrophages can be informative when determining the prognostic significance of a significant TAMϕ infiltrate within the TME (Petrillo *et al.*, 2015; Tan *et al.*, 2020). There is some data to suggest that the M1 phenotype is tumoricidal (Xu *et al.*, 2015).

The key pro-tumorigenic roles that tumour associated macrophages are known to fulfil within the tumour microenvironment include:

1) Release of growth factors (including VEGF) to promote tumour growth and angiogenesis within the developing tumour
2) Promotion of cancer cell stemness through activation of NF-κB signalling
3) Promotion of metastasis through the production of matrix metalloproteinases (e.g. MMP9)
4) Inhibition of anti-tumour cytotoxic T cell proliferation and promotion of regulatory CD4+ T cell expansion.

This is achieved by a number of means. Surface expression of PD-L1 and CD80/CD86 activate inhibitory signalling pathways through PD-1 and CTLA-4 respectively. TGF-β directly promotes regulatory T cell expansion. They can also interfere with T cell metabolism and induce anergic responses through the production of nitric oxide and arginase (Ugel *et al.*, 2015).

In addition to these multiple roles in the TME, there is considerable evidence that the TAMϕs can inhabit a variety of different niches, with potentially diverse roles and functions depending on whether they are found at the tumour-stromal interface, within tumour nests or adjacent to areas of vascularity within the tumour microenvironment (Yang, McKay, Jeffrey W Pollard, *et al.*, 2018). Taken together, this implies that TAMϕs represent a diverse and abundant

population in the tumour microenvironment with an array of predominantly tumour promoting roles.

1.10 Transcriptomic profiling of myeloid cell populations in human liver and hepatocellular carcinoma

Recent advances in transcriptomics through the development of single-cell RNA sequencing technologies have allowed for a much higher resolution understanding of cell populations within human tissues. A number of recent studies have helped to further our understanding of the immune cell environment in chronic liver disease and hepatocellular carcinoma, and myeloid cell populations in particular. Spatial transcriptomic analyses have also helped us to gain further insight into the topography of myeloid cell niches within both the liver and the TME.

In the context of fibrosis and chronic liver disease, two studies in particular - by Ramachandran et al. and Guilliams et al. – have advanced our understanding of the myeloid cell niche. Ramachandran et al. undertook analysis from 5 cirrhotic human livers and identified 'scar associated' macrophages, which derive from tissue infiltrating monocytes, express CD9 and TREM2 and are expanded in fibrosis and cirrhosis. Their interaction with endothelial cells through Notch signalling promotes collagen deposition and scar formation in cirrhosis (Ramachandran *et al.*, 2019).

Guilliams et al. have confirmed distinct sub-populations of Kupffer cells, identifying TIMD4 expression as a marker differentiating resident Kupffer cells those derived from circulating monocytes. Spatial transcriptomic analyses identified embryonic Kupffer cells in the mid-zones between portal tracts and centrilobular veins. Furthermore, this study observed altering

distributions of a novel macrophage subset depending on the disease context – 'lipid associated macrophages' are found near portal tracts in healthy livers but are recruited to areas of steatosis in disease, and have an attenuated production of pro-inflammatory cytokines in response to direct antigenic stimulation (Guilliams *et al.*, 2022). These studies built on earlier work demonstrating distinct Kupffer cell populations with differing phenotypes – a CD1C+ subset expressing genes consistent with a pronounced ability for antigen presentation and another, MARCO+ population with an immune regulatory transcriptomic profile (Aizarani *et al.*, 2019).

This approach has extended into the analysis of human HCC. A number of subsets of tumour associated macrophages with distinct phenotypes have been described and light shed on their ontogeny. TAMϕs interact not only with endothelial cells and fibroblasts, but with most cell types within the TME, including tumour cells and most other immune cell populations (Liu *et al.*, 2022). Tumour-resident Kupffer cells have been shown to have higher expression of HLA-DR and genes related to hypoxic stress, such as heat-shock proteins when compared with hepatic counterparts (Aizarani *et al.*, 2019), perhaps reflecting the dynamic environment in which they are found.

TAMϕ subsets have been defined by the expression of particular genes, such as osteopontin (SPP1). SPP1 is thought to be a key mechanism by which TAMϕs interact with tumour cells via the SPP1-CD44 ligand receptor interaction. There is bi-directional crosstalk, resulting in a skewing of macrophage function towards a classical M2 phenotype. TAMϕs have been demonstrated to express higher SPP1 than liver Kupffer cells and other resident macrophage populations (Liu *et al.*, 2022); SPP1+ TAMϕs interact with cancer associated fibroblasts near tumour boundaries to stimulate production of collagen and extracellular matrix remodelling,

thus generating an 'immune barrier' which prevents the entry of tumour infiltrating immune cells (Liu *et al.*, 2023).

Further TAMϕ subsets have been described. Zhang et al. report 2 clusters of myeloid cells enriched in the TME – one expressing MDSC-like phenotype and another with a more classical TAMϕ-like profile which was associated with pro-inflammatory cytokine production, expression of TREM2 and poor prognosis. Further work is needed to understand the overlapping phenotypic and transcriptomic profiles of these macrophage subsets across a range of tumour stages and after treatment (Q. Zhang *et al.*, 2019).

Interestingly, recent work has demonstrated that both tumour infiltrating mononuclear cells and PBMCs from patients with HCC have shared transcriptomic profiles, including up-regulation of SMAD3, a key protein in the cell cycle and in TGF-β signalling. The mechanism for this is unclear and may reflect intra-tumoural myeloid cell trafficking; in any case this may present a precision medicine based diagnostic approach of the future to target appropriate myeloid cell based immunotherapy.

1.11 TAM receptor tyrosine kinase family

1.11.1 Structure and function

The TAM receptor tyrosine kinase family (so called in reference to their names, *T*yro-3 – *A*xl – *M*erTK) have key roles in immunity, cancer and in tissue homeostasis. Specifically, their signalling results in regulation of immune signalling cascades and in maintenance of tissue homeostasis through the clearance of apoptotic cellular debris. In addition, they are found to be overexpressed in range of human cancers and promote cell survival (Linger *et al.*, 2008). The family consists of three members – MerTK, Axl and Tyro-3; the receptors were originally

cloned from leukaemia cell lines. MerTK is found in most haematopoietic cells, as well as in some specific specialised epithelial cells such as retinal epithelial cells and microglia in the central nervous system; Axl is found in most cells in the body. Less is known about Tyro-3 but it has been widely described in neuronal tissue (Lemke and Rothlin, 2008).

1.11.2 Signal Transduction

Each member is a dimeric transmembrane receptor and requires the binding of phosphatidylserine in addition to one of its known ligands for maximal activation of downstream signalling. Figure 1.1 outlines this structure in detail. Each receptor shares a similar structure, with two external fibronectin III (FNIII) domains and two immunoglobulin like domains. Signalling downstream of these receptors is principally though survival pathways – principally MAP-kinase, PI3K and AKT, which promote cell survival and proliferation. Activation of these pathways occurs after autophosphorylation of the receptor, which allows binding of PI3K and MAP-kinase/MEK to the intracellular domains of the receptor (Graham *et al.*, 2014a).

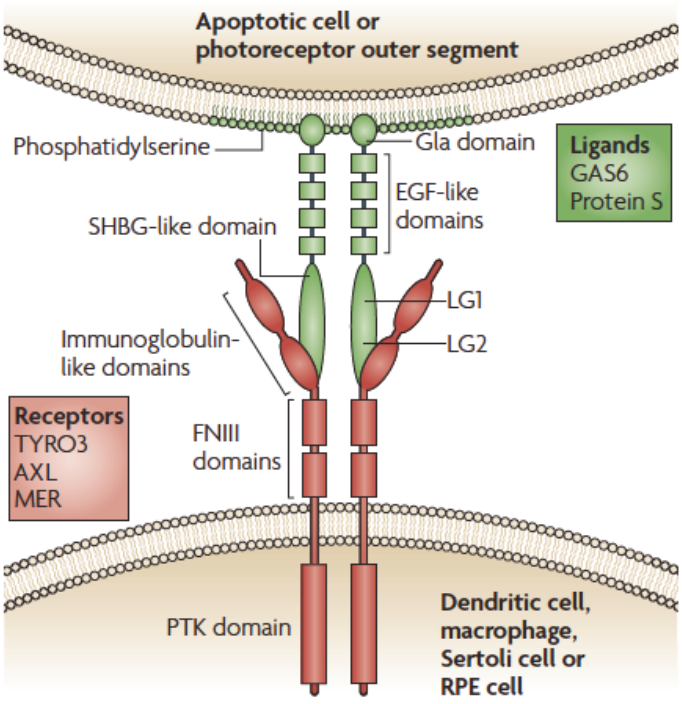

Figure 1.1: TAM family receptor tyrosine kinase structure and their ligands
TAM family receptor tyrosine kinase structure is highlighted in this figure (in red) consisting of two immunoglobulin-like and fibronectin III domains externally and the intra-cytosolic protein tyrosine kinase (PTK) domains. In addition, the broad structure of TAM-RTK ligands (in green) are outlined, and how they interact. Ligands consist of Laminin-G (LG) domains, sex-hormone binding globulin (SHBG) domains, four epidermal growth factor (EGF) domains and a Gla domain. It is the Gla domain that binds to phosphatidylserine; however TAM-RTKs can be activated without this interaction. *Abbreviations: RPE – retinal pigmented epithelium (Taken from Lemke et al., 2008 – permission granted from Springer Nature)*

1.11.3 TAM receptor tyrosine kinase ligands

TAM receptors have three principal ligands in addition to the contributory role of phosphatidylserine – Gas-6, Protein S (Pros-1) and Galectin-3. Gas-6 and Pros-1 share 40% homology of sequence. Gas-6 is known to activate Axl more readily than MerTK, and Pros-1 is known to be exclusively linked to MerTK. Gas6 is expressed most abundantly in vascular smooth muscle in addition to endothelial cells; it can bind and activate Axl without phosphatidylserine, indicating that it has roles outside of efferocytosis and indeed this has been described in models of cancer, where Gas-6 production stimulates Axl expression directly in tumour cells. Pros-1, being more MerTK specific, is produced in endothelial cells in tissues which MerTK expression is more abundant, as well as being produced by hepatocytes. Galectin-3 has been more recently identified as a TAM receptor ligand and acts primarily through MerTK, acting as an efferocytosis promoting signal on tissues.

1.11.4 Efferocytosis in tissue homeostasis

This interaction between receptor, ligand and exposed phosphatidylserine enables mobilization of the cellular cytoskeleton and results in an ability to facilitate uptake of apoptotic cells, in a process known as efferocytosis. Work in mice has shown how MerTK in particular is involved in this process, although Axl and Tyro-3 are able to facilitate efferocytosis in a similar manner (Seitz *et al.*, 2007). Within the specialised cells of the retinal pigment epithelium, MerTK$^{-/-}$ mice are unable to clear apoptotic debris and cellular remnants, resulting in persistent inflammation with the resultant development of fibrosis and ultimately retinal degeneration. In

a similar manner, MerTK signalling mediated efferocytosis is pivotal in involution of the epithelial glandular tissue after lactation and of apoptotic remnants of meiosis in Sertoli cells of testes. As with the resultant accumulation within the retinal pigmental epithelium, this accumulation in male TAM knockout mice causes significant inflammation and damage to seminiferous tubules, resulting in infertility in mouse models (Zhang *et al.*, 2013). Ineffective synaptic pruning and clearance of inappropriate synaptic connection in the central nervous system is the result of the same loss of function, and in mice results in impaired development of the hippocampus and persistent neuronal damage (Lemke and Rothlin, 2008; Lemke, 2013). In this way, in performing both homeostatic clearance of apoptotic cell debris and in enabling effective removal of apoptotic cells within developing tissue, TAM- mediated efferocytosis is crucial for tissue integrity and development.

1.11.5 TAM receptor tyrosine kinase signalling in cancer

TAM receptors have been reported to be overexpressed in a wide range of cancers, as is evident from their original cloning from leukaemic cells. Overexpression or ligation of these receptors activates a number of survival pathways through ERK, JAK-STAT, Rho kinase, AKT and p38 and has been demonstrated to confer an ability for cancer cells to survive in conditions of cellular metabolic stress. These are summarised in Figure 1.2. In cancer cells, MerTK results in activation of NF-κB, which results in inhibition of apoptosis; the opposite occurs in inflammatory cells but the effect is not to result in immune cell death, but in reduction in the production of pro-inflammatory cytokines (Graham *et al.*, 2014b).

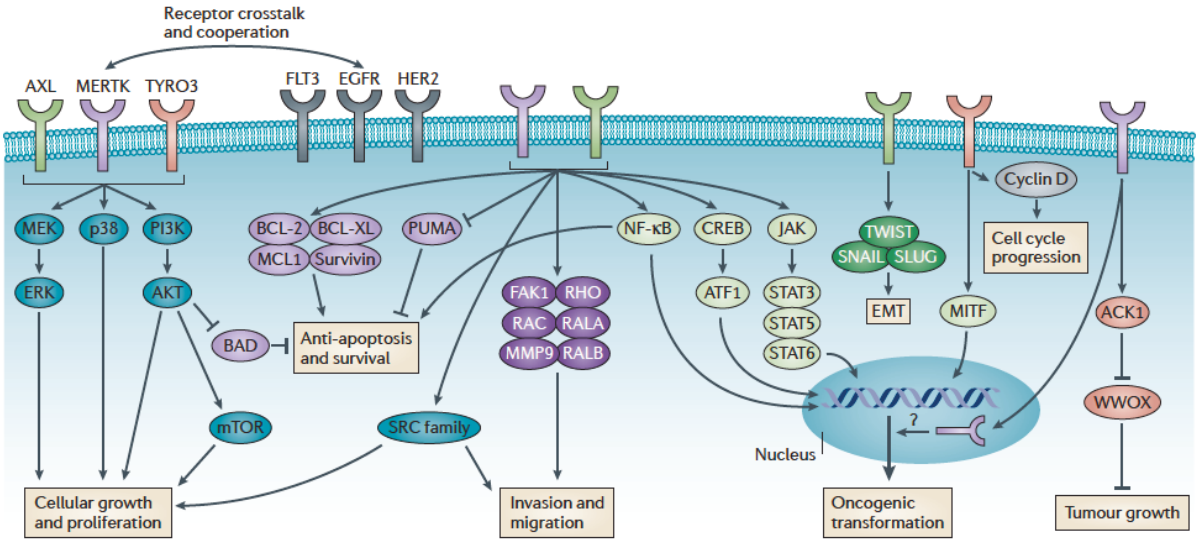

Figure 1.2 TAM receptor tyrosine kinase signalling in pathways in carcinogenesis
All three members of the TAM-RTK family (Axl in green, MerTK in purple and Tyro3 in red in this schematic) signal through PI3K and MAP kinase pathways in both immune and oncogenic contexts (on the left of this diagram). In addition, signalling through a number of additional pathways has direct proto-oncogenic effects including cell survival (activations of BCL-2/Survivin complex and NF-kB), cellular transformation (JAK-STAT pathway activation and TWIST/SNAIL/SLUG complex), cellular invasion and migration (Rho kinase, MMP9) and tumour growth through inactivation of ACK1. *Abbreviations: ACK1, activated CDC42 kinase 1; AKT, protein kinase B; ATF1, activating transcription factor 1; BAD, BCL-2-associated agonist of cell death; BCL – B-cell lymphoma; BCL-Xl, BCL-extra large, CREB, cAMP-responsive element-binding protein; EMT – epithelial – mesenchymal transformation; ERK, extracellular signalling-related kinase; FAK1, focal adhesion kinase 1; FLT-3, FMS-like tyrosine kinase 3; JAK, Janus kinase; MCL1, myeloid cell leukaemia 1; MEK – MAP kinase kinase; MITF, microphthalmia-associated transcription factor; MMP9 – matrix metalloproteinase 9; NF-kB, nuclear factor-kappaB; PI3K, phosphoinositide 3 kinase; PUMA, p53 upregulated modulator of apoptosis; RAC, Ras related C3 botox substrate; RAL – Ras related proteins A and B; RHO – Rho kinase; STAT, signal transducer and activator of transcription; WWOX, WW domain-containing oxidoreductase. (Taken from Graham et al., 20014 – Permission granted from Springer Nature)*

TAM-RTK signalling can also result in promotion of angiogenesis within the tumour microenvironment (TME). Axl mediated stimulation of Akt results in the production of vascular endothelial growth factor A (VEGFA). However, MerTK has been shown to down regulate this same pathway, making the overall contribution of TAM-RTK signalling context dependent (Graham *et al.*, 2014b).

TAM-RTK signalling has also been implicated in promoting tumour progression and metastasis. This is perhaps not surprising, given their ability to promote cell motility. Axl signalling through downstream transcription factor TWIST, SNAIL and SLUG are all stimulated by Axl overexpression in cancer cell lines. This results in epithelial to mesenchymal

transition, which is pivotal in promoting cell motility and metastasis. MerTK, though RHO and focal adhesion kinase (FAK1) can promote cell motility and promote cellular invasiveness (Graham *et al.*, 2014b).

1.11.6 TAM receptor tyrosine kinase signalling in immune regulation

TAM-RTK signalling has a key role in regulating and controlling the response to activation of the innate immune response. Loss of their function in animal models results in an inability to resolve the initial inflammatory insult and causes a more exaggerated response. This results in excessive tissue damage and destruction though inflammation. These observations have been made in both sterile and pathogen induced inflammation: MerTK knockout mice died rapidly from septic shock after exposure to lipopolysaccharide, with very high levels of TNF-α, IL-1 and resulting in excessive tissue damage (Camenisch *et al.*, 1999). In experimental models of lung injury with bleomycin, overexpression of MerTK in alveolar macrophages resulted in an increase in the production of TGF-β, reduced TNF-α and IL-1β and a resultant reduction in lung fibrosis in this sterile model of inflammation (Lee *et al.*, 2012).

The most extensive work on the immune regulatory roles of TAM-RTK signalling has been undertaken by Rothlin et al. Looking at pro-inflammatory signalling after activation of Toll-like receptor (TLR) in dendritic cells, they demonstrate inhibition of pro-inflammatory cytokine release that is mediated by TAM-RTK signalling. This effect is mediated by two inhibitory proteins - SOCS1 and 3 (suppressors of cytokine signaling) – whose expression is increased after TAM-RTK signalling is triggered. They have been shown to inhibit pro-inflammatory signalling at various points in the signalling pathway downstream of TLR-ligation.

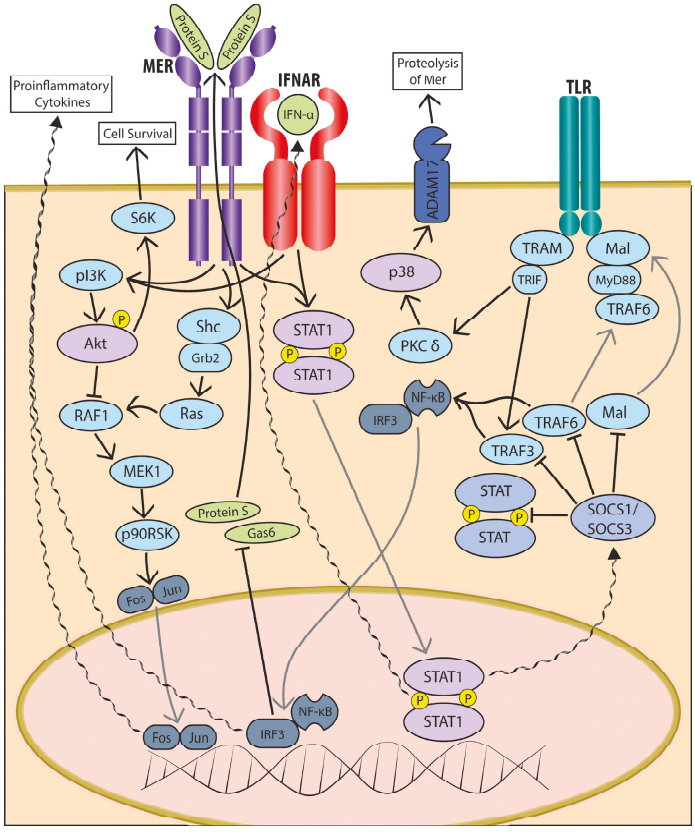

Figure 1.3 TAM receptor tyrosine kinase signalling in innate immune cells
This schematic outlines the immune specific regulatory downstream signalling cascades for both MerTK and Axl. Complex formation with the IFNAR orchestrates a negative feedback loop (outlined by the helical arrows on the schematic) in cytokine production and Toll-like receptor pro-inflammatory signalling and activation of NF-κB. *Abbreviations: IFNAR – interferon associated receptor; SOCS1/3 – suppressor of cytokine signalling; PKC – protein kinase C; TRAM – Toll-like receptor adaptor molecule; TRAF – TNF-receptor associated factor. (Taken from* (Wang *et al.*, 2018)*, permission granted).*

Upon direct stimulation of the TLR receptor with a pathogenic stimulus, an initial burst of pro-inflammatory cytokines bind to their respective receptors and activate STAT1. This transcription factor activates further pro-inflammatory cytokines to propagate the inflammatory response; however, STAT1 also induces the transcription of Axl. Axl can then directly bind to interferon associated receptor (IFNAR). The Axl:IFNAR complex is able to redirect STAT-1 signalling at this point, moving it away from a feed-forward amplification of pro-inflammatory cytokine production and towards SOCS1 and 3 induction. Through SOCS1 and 3 this mechanism acts to regulate and control cytokine release after pathogenic stimuli in dendritic cells (Rothlin *et al.*, 2007). These pathways are outlined in Figure 1.3.

The regulatory role of TAM-RTK signalling differs with respect to MerTK and, more specifically, in macrophages. The effect of efferocytosis mediated by MerTK in phagocytes is to skew the cytokine profile towards a regulatory, post-phagocytic, "M2c" phenotype, with increased production of IL-4, IL-10 and TGF-β (Zizzo *et al.*, 2012). This happens after ligation of the receptor with phosphatidylserine and either Pros-1 or Gas-6, and thereafter, ingested cholesterol breakdown products of efferocytosis act to further increase signalling by binding and activating the liver X receptor (LXR), which in turn activates transcription of the MerTK gene via its promoter (A-Gonzalez *et al.*, 2009). Furthermore, IL-10 produced also acts in an autocrine manner to further stimulate MerTK expression.

These examples highlight a diversification of immune regulatory roles for individual members of the TAM-RTK family within innate immune populations. Axl is more prominently expressed on dendritic cells and is more acutely induced in expression after TLR stimulation after encountering pathogens. In contrast, MerTK is more pronounced on macrophages, and is best induced by the mechanisms outlined above. Further evidence in support of this can be taken from experimental observations – MerTK is strongly induced in bone marrow derived macrophages by dexamethasone, whereas it has the very opposite effect on Axl expression. In this way, it has been postulated that Axl and MerTK share aspects of downstream signalling but have discrete roles in the regulation of inflammation, with Axl signalling mediating regulatory responses to acute stimuli and MerTK maintaining an immune regulatory environment that prevents overactivation of the immune system in tissue homeostasis (Zagórska *et al.*, 2014).

1.11.7 TAM receptor tyrosine kinase signalling and autoimmunity

In support of a key role for immune regulatory signalling mediated by TAM-RTKs in steady state, observations from knockout mouse models have demonstrated overt features of autoimmunity, in addition to the developmental defects described above. TAM triple (MerTK$^{-/-}$, Axl$^{-/-}$, Tyro3$^{-/-}$) knockout mice develop a poly-autoimmune syndrome akin to systemic lupus erythematosus (SLE) with elevated autoantibodies and dysregulated B and T cell proliferation and lymphadenopathy (Lu and Lemke, 2001). In humans, SLE is characterised by ineffective clearance of autoreactive lymphocytes in lymph nodes germinal centres by tingible body macrophages (Gaipl *et al.*, 2006) that are known to express MerTK in mice (Rahman *et al.*, 2010).

TAM RTKs are also key players in maintaining hepatic immunity – further information on this can be gained from the same TAM triple knockout mouse. These mice develop a spontaneous autoimmune hepatitis, with elevated transaminases and autoantibodies to smooth muscle antigen and antinuclear antigen, just like in humans, by the age of six months. Liver parenchyma is notable for an infiltrate of CD4+ T cells. Hepatocytes produce pro-inflammatory cytokines including IL-6, IL-1β, TNF-α and interferons as a result of activation of NF-κβ and interferon regulatory factor 3 (IRF3) – these promote further autoreactive inflammation (Qi *et al.*, 2013).

1.11.8 TAM receptor tyrosine kinase signalling and anti-tumour immunity

Immune regulatory mechanisms of action mediated by TAM-RTKs are also evident within the tumour microenvironment. In these settings, however, their regulatory and immune suppressive roles are deleterious for tumour biology. In keeping with this, Gas-6 is elevated in a number of solid tumours and haematological malignancies (Graham *et al.*, 2014b). Paolino *et al*. describe an inhibitory role in NK cell activation: Gas-6 administration was able to

attenuate the pro-inflammatory release of IFN-γ and proliferation of NK-cells. This effect was removed by the administration of a TAM-RTK inhibitor and, in mouse models, resulted in a reduction in tumour burden and restoration of the cytotoxic capacity of NK cells (Paolino *et al.*, 2014).

TAM-RTK signalling is thought to be contributory to tumour associated macrophage function; tumour derived IL-10 can induce the production of Gas-6 by tumour associated macrophages and result in increased MerTK signalling; $MerTK^{-/-}$ mice have been shown to have a much less permissive environment for adoptive transfer of syngeneic tumours including melanoma and breast cancer, with a reduction in tumour volume. In a similar way, irradiation and replacement of wild-type bone marrow with $MerTK^{-/-}$ haematopoeitic cells results in a switch in the macrophage phenotype towards an M1 phenotype and slowed growth of mammary tumours (Cook *et al.*, 2013).

A recent study by Zhou *et al.* has provided encouraging evidence of a pivotal role for MerTK modulation of signalling in altering macrophage phenotype towards anti-tumour immunity. In ectopic tumour mouse model of malignancy, administration of a MerTK blocking antibody resulted in a reduction in tumour growth and increased activation of CD8+ T cells, with a synergistic effect when given in combination with anti-PDL1 therapy. These data may indicate a role for MerTK blocking strategies as part of a combination therapy to enable effective results from existing immunotherapy – in blocking MerTK mediated efferocytosis (which may promote immune evasion through the removal of tumour antigen and apoptotic cell fragments) cytotoxic T cells were able to develop strong anti-tumour cytotoxic responses with the result of improving outcomes and survival. (Zhou *et al.*, 2020).

1.11.9 TAM receptor tyrosine kinase signalling in liver disease

TAM-RTK signalling has been demonstrated to play a key role in inflammation, injury and repair in the liver. MerTK has been shown to have a protective role in acute liver injury. In a mouse model of ischaemia (hepatic arterial ligation), phosphorylated MerTK rose shortly afterwards, as did Gas-6. When MerTK signalling was blocked by knocking down Gas-6, there was an exaggerated response to injury with higher levels of pro-inflammatory cytokines IL-1α, TNFα and worsening liver failure after partial ischemic injury (Llacuna *et al.*, 2010). There is evidence for activation of TAM-RTK signalling in chronic inflammatory contexts also. In a mouse model of chronic liver disease (carbon tetrachloride model), stellate cell activation was dependent upon Gas-6 and Axl (Bárcena *et al.*, 2015).

Work from our group has demonstrated a clear role for TAM-RTK signalling in monocytes and macrophages in both acute liver failure and acute on chronic liver failure in humans. Work by Triantafyllou et al. and Bernsmeier et al. have demonstrated that MerTK expressing monocytes are expanded in the circulation of patients with acute liver failure and acute on chronic liver failure respectively. These MerTK expressing monocytes have a reduced capacity to respond to antigenic stimulus, are skewed towards a regulatory phenotype with higher CD163 co-expression and Blockade of MerTK in these monocytes restored TNFα and IL-6 production in response to lipopolysaccharide. Intriguingly, MerTK also demonstrated an increased capacity to migrate across endothelial barriers, suggesting that they may have obtained this immune-paretic phenotype after trans-endothelial migration through the diseased liver in decompensated liver disease. (Bernsmeier *et al.*, 2015; Triantafyllou *et al.*, 2018)

1.12 Summary

The landscape of therapeutic options in hepatocellular carcinoma is gathering pace, however there is a burgeoning need for effective options with an increasing incidence across the globe. With the advent of small molecular inhibitors in the last decade, there has been incremental improvements in survival; this will hopefully be augmented by improvements in disease prevention, however there remain persistent problems with screening and early detection of HCC (Kanwal and Singal, 2019). Without a reliable serum biomarker, and with growing concerns over the development of HCC on a non-cirrhotic background (both in NAFLD/NASH and in patients with fibrosis after direct acting antiviral therapy (DAA) for HCV), the likelihood of patients presenting with intermediate or advanced disease remains high. Recent concerns about an increased risk of HCC after DAA therapy have not been borne out in subsequent data, however patients with hepatic fibrosis will require lifelong surveillance (Reig *et al.*, 2016; Pascut, Pratama and Tiribelli, 2020; Delgado Martínez, Gómez-Rubio and Gómez-Domínguez, 2021)

In addition to this increasing and persistent burden of disease, there remain the challenges of managing disease recurrence after ablation or resection and more pertinently, of managing unresectable disease with decompensated liver disease. The need for new therapies that can augment our current options is clear. Furthermore, in an era of personalised medicine there is a clear impetus to develop a range of therapeutic options and to adapt our strategies accordingly. Immunotherapy is currently the most likely source of further treatment options for patients with HCC, for a variety of reasons. Immunotherapeutic strategies that look outside of the CTLA-4 and PD-L1 paradigm of T cell mediated cytotoxicity are desperately required.

Firstly, as HCC is a tumour that develops on an inflammatory background; the end result of defective immune surveillance and a chronically inflamed environment that is permissive (and indeed promotes) the propagation of malignant clones. These facts make HCC an attractive candidate to respond to immunomodulatory therapy.

In addition, there is data to suggest that the effects of existing immunotherapy can be potentiated with the introduction of combination therapies. Myeloid cells and macrophages in particular play a pivotal role in the evolution of chronic liver disease and liver fibrosis, as well as having established roles within the tumour microenvironment as the predominant intra-tumoural immune cell population. Regulatory signalling via the TAM receptor tyrosine kinase family is potentially contributory to the tumour promotion and progression. This has been described in a recent study in a mouse model (Zhou *et al.*, 2020), using MerTK inhibition in combination with PD-L1 inhibition. In addition, resistance to existing immune checkpoint blockade has been posited to be related to the pro-tumour actions of tumour associated macrophages (Laviron and Boissonnas, 2019).

Lastly, the use of locoregional therapies as part of the treatment algorithm in HCC (radiofrequency ablation and TACE) has the potential to further augment responses to immunotherapy – by releasing tumour antigen into the tumour microenvironment, if combined with immune checkpoint inhibition therapy then the beneficial effects could potentially be maximised (Buonaguro *et al.*, 2019).

1.13 Aims of this study

In light of these findings, the aims of this study were as follows:

1) To characterise the MerTK and Axl expression phenotype in both tumour and liver macrophages in patients with HCC, using tissue extracted myeloid cells and tissue sections.

2) To ascertain if there is a circulating monocyte phenotype that reflects the intra-tumoural and/or intrahepatic monocyte and macrophage phenotype.

3) To determine if locoregional therapy with chemoembolisation has an effect on the MerTK and Axl expression on tumour associated macrophages.

4) To interrogate the functional profile of MerTK and Axl expressing monocytes and macrophages with a view to understanding their potential functional role within the tumour microenvironment and, therefore, their potential utility as a therapeutic target in HCC.

5) To utilise transcriptomic analysis to characterise and contextualise TAM-RTK signalling within the broader expression profiles of myeloid cell populations in HCC.

CHAPTER 2

Immunohistochemical evaluation of the MerTK and Axl expressing macrophage phenotype

2.1 Background and Aims

2.1.1 Background

Characterising MerTK and Axl expression within the tumour associated myeloid cell compartment is crucial to understanding if signalling through these immune regulatory and homeostatic signalling pathways is a feature of the immune microenvironment in hepatocellular carcinoma. Myeloid cells are the most abundant immune cell population in the tumour microenvironment, with an array of mechanisms by which they enable tumour evasion of immune surveillance and promoting cell survival, lesion growth and metastasis. In support of a pivotal role for TAM receptor tyrosine kinases in these processes, MerTK and Axl signalling in myeloid cells has been demonstrated to be immune regulatory in both steady state and in response to acute inflammatory stimuli. Furthermore, downstream signalling through PI3K, AKT and ERK promotes cell survival in both immune and non-immune cell populations, with MerTK and Axl overexpressed in a range of human cancers. MerTK and Axl signalling pathways are immune regulatory across a variety of immune cell populations, including NK cells and dendritic cells in addition to macrophages and monocytes. This is further suggestive of a wide role in mediating tumour immune evasion and make them an important potential therapeutic target.

The tumour microenvironment can present a complex and heterogenous immune landscape, however, with niches that can support and promote macrophage populations with apparently opposing phenotypes. There is a growing body of evidence suggesting that macrophage phenotypes are plastic and highly localised within tumours. In support of this, the presence of particular macrophage populations, or indeed skewing of the total macrophage population towards one particular phenotype can result in either beneficial or deleterious effects on prognosis and survival (C. Wu *et al.*, 2020). When characterising TAM receptor tyrosine kinase

expression in the tumour microenvironment it is therefore important to characterise expression based not only on co-expression of markers of immune phenotype, but to understand the distribution within different parts of the tumour microenvironment.

2.1.2 Hypothesis

Given our understanding of the role of TAM-RTK signalling both in cancer and in the response to tissue injury, it was hypothesised that expression of MerTK and Axl expressing immune cells would be identified in tumour microenvironment. TAM-RTK expression on macrophages and myeloid cells could play an important role in tumour biology by skewing macrophage function towards a regulatory phenotype, which is permissive for disease progression and by impairing cytotoxic and/or T-helper lymphocyte responses. In addition, it was hypothesised that hypoxia and tissue damage caused by locoregional therapy with chemoembolization could result in an expansion of TAM-RTK expression on tumour associated macrophages.

2.1.3 Aims

In order to confirm the presence of TAM-RTK expressing myeloid cells in human hepatocellular carcinoma (HCC), direct histological evaluation was required. Therefore, the aims of this chapter were as follows:

1. To identify the presence of TAM-RTK positive myeloid cells, both in HCC lesions and in the surrounding background liver using sections of formalin fixed and paraffin embedded (FFPE) tissue from patients with hepatocellular carcinoma and appropriate control cases. Double epitope enzymatic immunohistochemistry utilising macrophage marker (CD68) in conjunction with either MerTK or Axl was undertaken.
2. To characterise the distribution and topography of MerTK and Axl expressing macrophages within lesions.

3. To evaluate the effect, if any, of prior chemoembolization upon the characteristics outlined in Aim 2.
4. Previous work has suggested that MerTK expressing monocytes can impair T cell function in haematological malignancies (Cook *et al.*, 2013)*;* this is also an established function of tumour associated macrophages in solid malignancies. It was aimed to evaluate if MerTK and Axl expressing myeloid cells co-localise with T lymphocytes in the tumour environment in hepatocellular carcinoma, using double-epitope staining with MerTK or Axl in conjunction with T lymphocyte markers CD4 and CD8.

2.2 Materials and Methods

2.2.1 Patient selection, recruitment and sample collection

Patients were identified and recruited into the study as previously described. Cases for analysis by microscopy were identified and evaluated prospectively; from each case, the official consultant histopathologist report was reviewed to confirm the diagnosis, determine the presence of viable tumour tissue and to identify blocks containing lesional and surrounding non-lesional tissue. In all cases where possible, parenchymal (non-lesional) tissue blocks were sought distant to the tumour; for explant specimens a section from a contralateral lobe, is feasible, was identified. A group of HCC cases (n=10) in which there had been previous chemoembolization of a tumour and in which there was viable residual tumour was chosen in order to assess the effect of prior locoregional therapy.

Blocks were requested from the histopathology department at Kings College Hospital; ethical approval obtained for this study allowed for use of embedded tissue surplus to diagnostic requirement and was agreed with the laboratory in advance. Pathological control samples were taken from patients with liver cirrhosis but without hepatocellular carcinoma and from patients undergoing resection of either colorectal malignancy or of a benign lesion. For cirrhotic controls, cases were selected in whom no microscopic tumours had been identified at diagnostic sectioning after transplantation.

2.2.2 Clinical data acquisition

Supporting clinical data from the cases recruited and analysed were obtained from the electronic medical records at King's College Hospital. Such data included blood results (including alpha-fetoprotein levels), demographic data and information as to the aetiology of underlying liver disease, where appropriate. These data were collected with the patients'

consent and stored in a secure password protected database on an approved laptop computer. Official histopathological reports for each case were also stored digitally on this device. In accordance with requests from the local research ethics committee, backup data was stored on an external hard-drive and kept on hospital premises in a locked cabinet.

2.2.3 Double epitope enzymatic immunohistochemistry

Sections of tissue 4μm thick were cut using a Leica RM2235 rotary microtome (Leica Biosystems, UK) and placed onto slides coated with poly-L-lysine. Immunohistochemistry was then performed utilising Leica Bond III Polymer Refine Detection (BPRD) kits and automated protocols using Leica Bond III Autostainer. Double epitope staining was undertaken with brown chromogen 3,3'-Diaminobenzidine tetrahydrochloride hydrate (DAB) and Fast Red chromogens using the BPRD kits DS9800 and DS 9390 respectively (Leica Biosystems, UK) and in that order. Staining was undertaken in the liver histopathology lab at Kings College Hospital under the supervision of lead histopathology technicians. Pre-existing optimised protocols for staining of hepatocellular carcinoma and hepatic parenchymal tissue sections for common epitopes (CD68, CD4 and CD8) were adapted to enable double epitope staining using novel epitope targets MerTK and Axl.

Tissue section preparation and antigen retrieval

Paraffin embedded tissue sections were dewaxed and rehydrated, using sequential 5-minute washes in three solutions: Leica Bond dewaxing solution (Leica Biosystems, UK), industrial denatured alcohol and Leica Bond wash buffer. Retrieval of epitopes for immunohistochemistry was achieved using heat-induced epitope retrieval (HIER); for all antibodies used in this study, HIER was performed for 20 minutes at 100^{o}C, pH 9.0 using ethylenediaminetetraacetic acid (EDTA) based Epitope Retrieval 2 solution (Leica Biosystems, UK). Between each subsequent step, slides were washed by immersion in Leica

Bond wash buffer for 5 minutes unless otherwise stated. Endogenous peroxidase activity was quenched by incubation with 3% hydrogen peroxide diluted with methanol for 5 minutes at room temperature. This prevented endogenous tissue peroxidase reacting with DAB chromogen resulting in non-specific staining.

Sequential double epitope immunostaining

In all cases, primary antibody was applied for 15 minutes at room temperature; Table 2.1 below outlines the dilutions used, as well as the species in which they were raised. Optimal concentrations for both MerTK and Axl were determined by single staining of positive control slides for each epitope; MerTK staining was optimised using human lymph node tissue and Axl using hepatic parenchyma, as per manufacturers' instructions (Abcam, UK). For mouse primary antibodies, a 'post-primary' rabbit anti-mouse IgG antibody is then applied for 8 minutes at room temperature, as the horseradish peroxidase enzymatic complex (poly-HRP) utilised subsequently is conjugated to a mouse anti-rabbit IgG antibody. Poly-HRP was then added and incubated for 8 minutes before washing both with Leica Bond wash buffer and deionised water. DAB chromogen ('DAB refine' solution, Leica Biosystems, UK) was added for a 10-minute incubation and washed with deionised water. In this step HRP enzymatically activates the covalent linkage of brown pigment DAB to the tissue epitope.

Primary antibody to the second epitope was then added the Leica BPRD Red kit (DS9390, Leica Biosystems, UK) were used. Post primary rabbit anti-mouse IgG was incubated for 20 minutes, before adding mouse anti-rabbit IgG Polymer-AP (alkaline phosphatase) for 30 minutes. Fast red was added for 15 minutes and slides washed with wash buffer and de-ionised water, before counterstaining with Mayer's haematoxylin for 5 minutes to delineate nuclear structures. Mounting media and coverslips were then applied after dehydration with ethanol.

In each batch of cases stained in this manner, control slides were stained singly using anti-CD68 primary with both DAB and Fast-Red. These singly stained controls were utilised for spectral processing using Nuance imaging software as outlined below (paragraph 2.2.5).

Epitope	Species	Product Code	Manufacturer	Dilution
MerTK	Rabbit IgG	ab52968	Abcam, UK	1:4000
Axl	Rabbit IgG	ab219651	Abcam, UK	1: 250
CD68	Mouse IgG	NCL-L-CD68	Leica Biosystems, UK	Pre-mixed
CD4	Mouse IgG	NCL-L-CD4-368	Leica Biosystems, UK	Pre-mixed
CD8	Mouse IgG	NCL-L-CD8-4B11	Leica Biosystems, UK	Pre-mixed

Table 2.1: Antibodies used for double epitope enzymatic immunohistochemistry: *rabbit and mouse anti-human antibodies were used either at manufacturers' recommended instruction if pre-mixed, or at optimised concentrations determined manually.*

2.2.4 Image capture and multispectral imaging analysis

Fully stained slides were viewed on a Nikon Eclipse E600 light microscope and images were taken using multispectral imaging software Nuance™ v.3.0.2 (PerkinElmer, UK) at 100x, 200x and 400x magnifications. For each lesion, images were taken of the periphery and boundary with surrounding hepatic parenchyma and stroma, within central areas with nests of neoplastic cells and of areas of necrosis, especially in cases with prior chemo-embolisation. For surrounding liver tissue, pictures were taken both of hepatic plates and portal tracts. For each case, after routine images were taken, 10 fields at high-power magnification were taken to allow for cell quantification. For lesions, images away from the boundary with liver tissue and from areas of post-embolisation tumour necrosis were taken.

Multispectral image processing using Nuance software was undertaken to identify dual positive macrophages. Images of single stained slides were used to provide software with the spectral signature of pure DAB (brown) and Fast Red (red) signal. Colour images from double-stained cases were then 'unmixed' by the software, with brown and red signals from the chromogens

separated from the rest of the visible spectrum. Green, fluorescent labelling was digitally assigned to DAB, red to the Fast-Red signal and blue to the haematoxylin staining. All other colours were removed, generating a 'pseudo-immunofluorescent' image. Areas of overlapping red and green signal were then labelled with a yellow mask using the software, allowing for co-localisation of signal to be determined. Dual positive cells were determined as those associated with a nucleus, either with yellow signal or red and green signal closely co-located. For each batch of slides stained, separate single stained controls were used to generate the settings for spectral analysis to ensure consistency.

2.2.5 Case review and expert opinion

Each case was reviewed for the presence and distribution of dual positive cells in the lesions and in the surrounding liver. A selection of cases was submitted to expert review independently by a consultant liver histopathologist to assess both lesions and the background liver in the same manner.

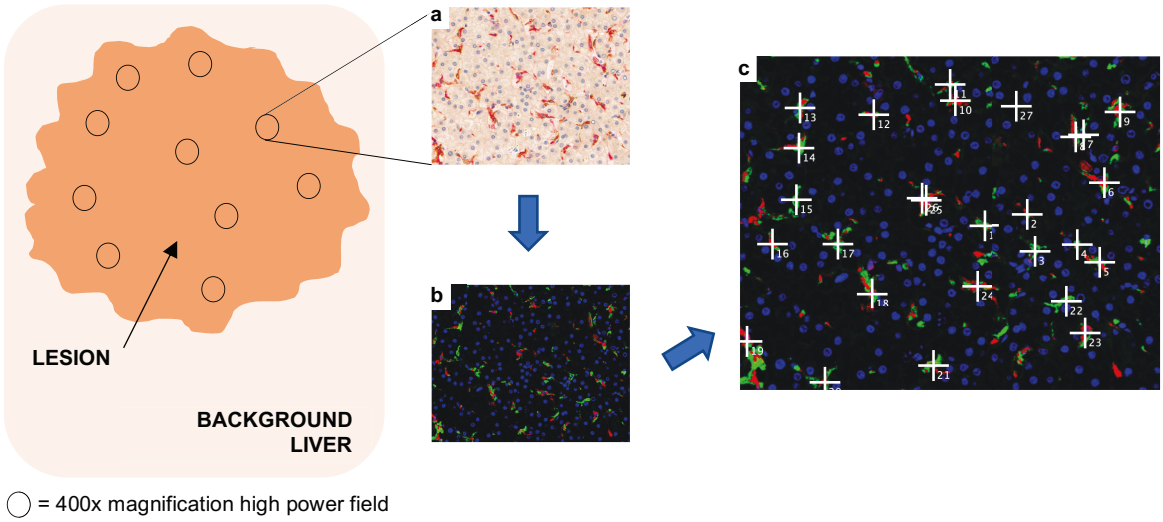

Figure 2.1: Schematic representation of the enumeration method for dual positive macrophages in both lesional and background liver tissue. (A) Random high-power field (400x) images were taken from within the tumour (away from the tumour/stroma interface) and from background liver **(B)** Multispectral analysis converted true colour images into a tri-colour, pseudo-immunofluorescent image. Counting of individual double positive cells used the Image J software cell counter.

2.2.6 Quantification and statistical analysis

Images at high power magnification taken for quantification were analysed using ImageJ (version 1.53a, National Institute of Health (Schneider, Rasband and Eliceiri, 2012)). Using the 'cell counter notice' plugin, each individual cell was marked and counted. Individual and summed cell counts from 10 images were obtained; a schematic of this process is outlined in Figure 2.1. Comparative (non-parametric) statistical analysis and graphical representation of the data was generated using GraphPad Prism version 9.3.1 for Macintosh (San Diego, California USA).

2.3 Results

2.3.1 Patient characteristics

Twenty-two cases were identified and utilised for this aspect of the study. Their baseline characteristics are outlined in Table 2.2; comparison of the cases that were the subject of chemoembolization with those that had resection or transplantation without this form of locoregional therapy is further outlined in Table 2.3. Pathological control samples (n = 9) were obtained from patients with liver cirrhosis without a confirmed histological or radiological diagnosis of hepatocellular carcinoma. For control cases without cirrhosis, patients were sought who were undergoing resection of either a colorectal liver metastasis (n = 3) or a benign liver lesion (n = 1, biliary cystadenoma).

There were no significant differences in the patient demographics between the diseased and healthy control groups. When the treated and untreated cases were compared (n=11 of each) there was a significant difference in the distribution of differentiation status on histological review of the tumours, with a wider range and more poorly differentiated tumours in the untreated group. This may reflect the effect of chemoembolisation, but this was not possible to determine in this small sample.

Table 2.2: Clinical and physiological characteristics of patients with hepatocellular carcinoma (and control cases) used for immunohistochemistry

	Cases (n = 22)	Controls (n = 9)	p-value
Age (years; range)	58.5 (48 – 82)	56 (43 – 67)	0.1495[a]
Sex (M:F)	16:6	6:3	>0.999[b]
Cirrhosis (%)	Cirrhosis: 18 (81.8%) Non-cirrhotic: 4 (18.2%)	Cirrhosis: 6 (67%) Non-cirrhotic: 3 (33%)	0.3841[b]
Aetiology of liver disease			
Alcohol	7	3	
NAFLD	4	3	
Viral	3	0	
Dual aetiology	6	1	
Sporadic	2	2	0.4819[c]
Tumour Differentiation			
Well	3	-	
Moderate	14	-	
Poor	2	-	
Necrotic	3	-	-
BCLC Stage (HCC)			
0	3	-	
A	18	-	
B	1	-	
C	0	-	-
Tumour Size* (mm)	27 (14 – 140)	-	-
Explant: Resection	13:9	6:3	>0.999
AFP [IU/ml]	5 (2 - 143)	-	-
Bilirubin (μmol/L)	16 (5 – 122)	47 (7 – 326)	0.397[a]
Platelets	163.5 (60 – 594)	127 (48 – 303)	0.541[a]
INR	1.32 (0.98 – 2.01)	1.57 (0.91 – 3.11)	0.259[a]
MELD score	15 (6 – 30)	10.5 (4 – 21)	0.246[a]

Abbreviations: BCLC = Barcelona Clinic Liver Cancer, HCC = hepatocellular carcinoma, NAFLD = non-alcoholic fatty liver disease, AFP = alpha-fetoprotein, IU = international units, MELD = Model for End-Stage Liver Disease, INR = international normalised ratio. Statistical tests used: [a]Mann-Whitney U test, [b]Fisher's Exact test, [c]Chi-square test. Values are written median [range]. **Multifocal cases not included in this range*

Table 2.3: Clinical and physiological characteristics of patients with hepatocellular carcinoma; comparing cases with and without prior chemoembolization

	Untreated Cases (no locoregional therapy) n = 11	Chemo-embolised cases n = 11	p-value
Age (range)	58 (50 – 82)	60 (48 – 77)	0.885[a]
Sex (M:F)	6:5	10:1	0.1486[b]
Cirrhosis (%)	Cirrhosis: 7 (63.6%) Non-cirrhotic: 4 (36.4%)	Cirrhosis: 11 (100%) Non-cirrhotic: 0	0.090[b]
Aetiology of liver disease			
Alcohol	4	3	
NAFLD	2	2	
Viral	1	2	
Dual aetiology	2	4	
Sporadic	2	0	0.534[c]
Tumour Differentiation			
Well	3	0	
Moderate	6	8	
Poor	2	0	
Necrotic	-	3	**0.041**[c]
BCLC Stage (HCC)			
0	3	0	
A	7	11	
B	1	0	
C	0	0	0.086[c]
Tumour Size* (mm)	27 (14 – 140)	25 (11 – 50)	0.664[a]
Explant: Resection	3:8	10:1	**0.008**[b]
AFP [IU/ml]	18.5 (2 – 10618)	6 (2 – 28)	0.239[a]
Bilirubin (μmol/L)	14 (5 – 122)	27 (6 – 62)	0.307[a]
Platelets	223 (60 – 594)	136 (64 – 269)	0.211[a]
INR	1.18 (0.98 – 2.01)	1.42 (1.06 – 1.60)	0.374[a]
MELD score	10.5 (6 – 21)	9 (4 – 17)	0.822[a]

Abbreviations: BCLC = Barcelona Clinic Liver Cancer, HCC = hepatocellular carcinoma, NAFLD = non-alcoholic fatty liver disease, AFP = alpha-fetoprotein, IU = international units, MELD = Model for End-Stage Liver Disease, INR = international normalised ratio. Statistical tests used: [a]Mann-Whitney U test, [b]Fisher's Exact test, [c]Chi-square test. Values are written median [range]. **Multifocal cases not included in this range.*

2.3.2 MerTK+ macrophages are present in the tumour microenvironment with a variable distribution and morphology

Double epitope enzymatic immunohistochemistry reveals the presence of MerTK expressing CD68+ cells, both within the tumour microenvironment and in the non-lesional hepatic parenchyma in patients with hepatocellular carcinoma. Representative pictures are demonstrated in Figure 2.2. At lower power magnification (200x), the presence within tumours of areas of dense and pronounced MerTK positivity can be seen, as marked by arrows on the right side of images on Panel A and C. These areas show some co-localisation and overlap with the CD68 signal, indicating the presence of dual positive cells within these areas. Furthermore, in other cases there is a more scattered and regular distribution of dual positive macrophages, as seen in Panel B in the same figure.

At higher magnifications, the prevalence and distribution of dual positive cells can be better appreciated. Not all intra-tumoural CD68+ cells are MerTK+ – MerTK-CD68+ cells were more prevalent in well or moderately differentiated lesions - Panel A and B in Figure 2.3 are representative images in lesions with a trabecular phenotype. In less well differentiated regions within tumours, more dual MerTK macrophages are seen, with clusters of cells nestling between disorganised, expanded trabecular sheets of hepatocytes (Panel C & D, Figure 2.3**)**. In other lesions these dual positive cells are seen near other mononuclear cells indicative of an inflammatory infiltrate (Panel E). Their morphology appears to mimic that of Kupffer cells, with a characteristic 'spider' shape, resting between the expanded chords of hepatocytes (Panel D, case AHCC31, Figure 2.3). Pseudo-immunofluorescence reveals that positive signal for MerTK can vary in individual cells, with surface staining (Panel D, arrow 1), intracellular staining (arrow 2) and eccentric MerTK positivity (arrow 3). These patterns were repeated across all dual positive cells within the samples analysed.

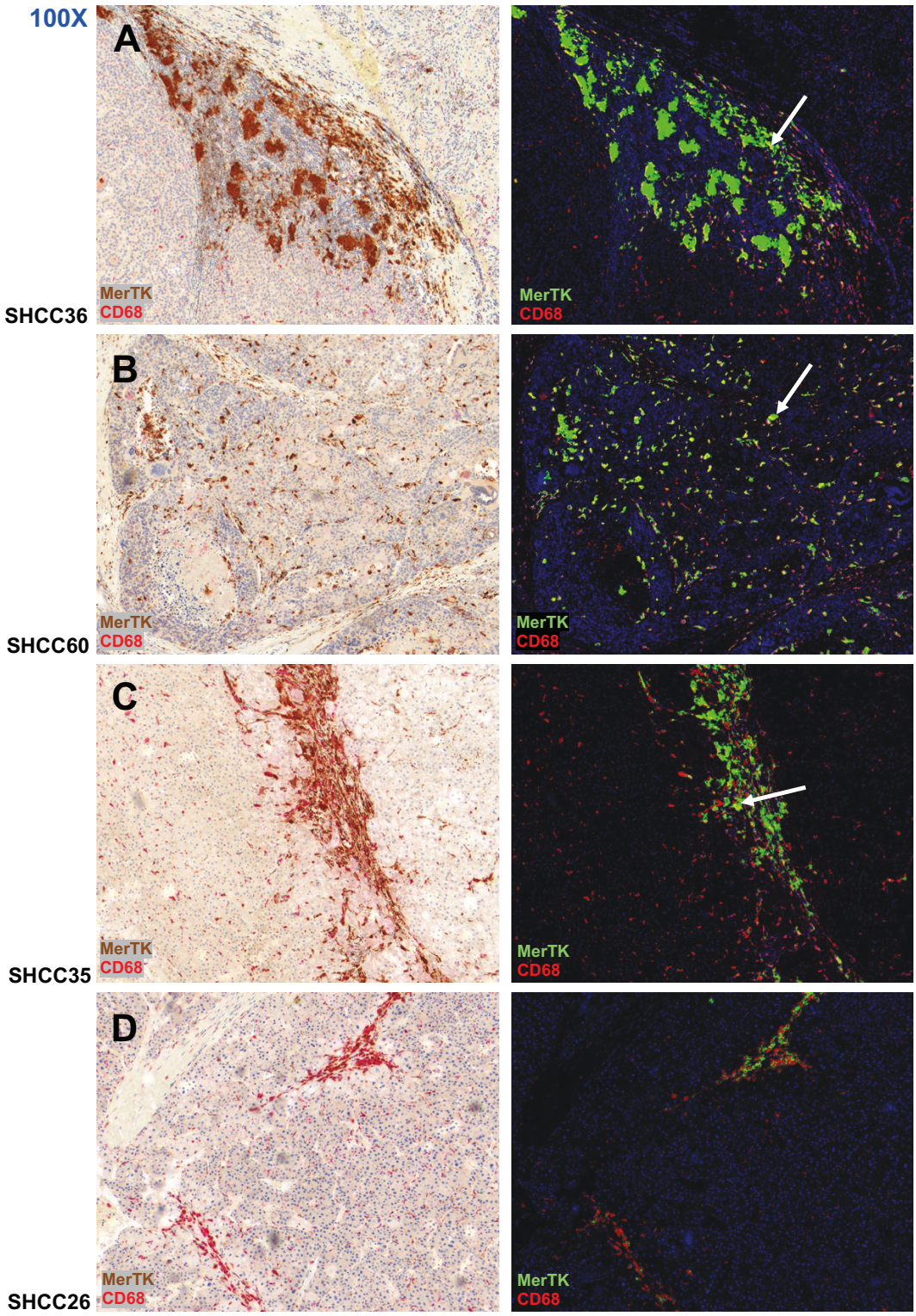

Figure 2.2: Double epitope enzymatic immunohistochemistry characterizes tumour MerTK+CD68+ macrophages in human hepatocellular carcinoma lesions

Representative true colour (left) and pseudo-immunofluorescent (right) images at low power magnification (100X) taken after double epitope immunohistochemistry and multispectral analysis of individual lesions from patients with HCC. MerTK positive signal is brown in true colour and green in pseudo-immunofluorescence respectively; CD68 signal is red in both image types. Areas of co-localization (or signal overlap) appear yellow on the right-hand side. Dense MerTK+ inflammatory infiltrates are seen at the boundaries between tumour and stroma (*Panel A, case SHCC36)* and within tumour nests *(Panel C and D, cases SHCC35 and SHCC26)*. Less well differentiated lesions *(Case SHCC60, panel B)* have more widespread MerTK+CD68+ macrophages. Arrows point to areas of both co-localization and overlap of signal. Study IDs of individual cases are labelled to the left.

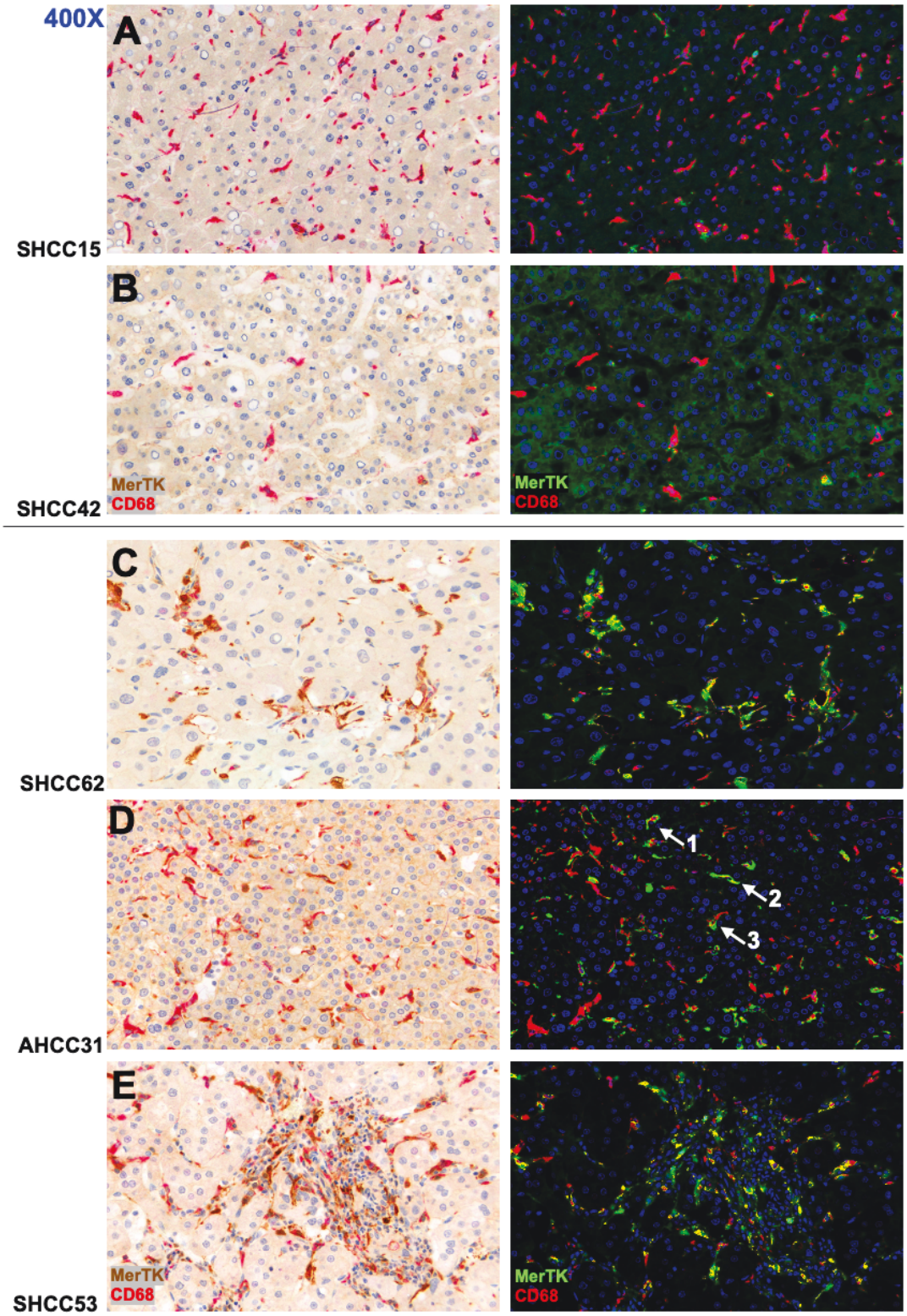

Figure 2.3: Tumour macrophage MerTK expression varies in distribution and density with degree of hepatocellular differentiation.

Images at high power magnification (400X). True colour and pseudo-immunofluorescent images are laid out right and left, as in Figure 2.2. Arrows highlight individual dual positive cells and the varied appearances and distribution of MerTK signal. Well differentiated lesions are represented in panel A and B; less well differentiated cancers are illustrated in Panels C – E. Study IDs of the individual cases are labelled to the left of each panel.

2.3.3 MerTK+ macrophages are numerically expanded in cirrhosis

Analysis of surrounding liver parenchyma revealed that MerTK+CD68+ cells are most commonly found in cases with cirrhosis, and that these are commonly Kupffer cells, as evidenced by their shape and location within hepatic sinusoids. Figure 2.4 provides representative pictures of non-cirrhotic liver (case SHCC31, upper panel) and a liver from a patient with cirrhosis (case AHCC31, lower panel). The MerTK dual positive cells are more abundant in the latter and this was reliably observed in other cases. Enumeration of dual positive cells confirmed this finding (Figure 2.5, D). Although the numbers of control cases were small, a significant increase in the number of positive cells was seen in cases with cirrhosis (median number of dual positive cells per high-powered field = 210 vs 94, p=0.023). In addition, a trend towards a statistically significant increase in MerTK positive CD68+ macrophages was seen between cases from controls and those non-cirrhotic cases with HCC (p=0.0571). MerTK positive cells were infrequently seen within the fibrous septa and within portal tracts in patients with cirrhosis; if these were sampled in the course of enumeration, these were counted in a similar fashion to the hepatic plates photographed.

2.3.4 Chemoembolised tumours have an intra-lesional expansion of MerTK+ macrophages when compared with their surrounding liver

Enumeration of dual positive macrophages included lesions that had received some locoregional therapy in which there was residual or recurrent tumour at the time of transplantation. Review of these cases at high power magnification did not reveal an expansion of macrophages when compared with untreated tumours (Fig 2.5 C). However, when compared with the paired background liver of the same individual, there was a significant increase within the tumour (Figure 2.5 B, 244 cells/HPF in the tumour vs. 101 cells/HPF in the background liver, p = 0.0382) which was more pronounced on paired analysis (p = 0.0098). These cases were all from patients who had undergone transplantation and non-lesional background

samples were taken from distant liver, usually the caudate lobe where feasible, if not the contralateral lobe to the lesions if one-sided. When comparing background liver from patients with HCC, there was a trend towards a reduced infiltrate of MerTK+ macrophages in cases with prior chemoembolization (Figure 2.5 B, 128 vs. 198 cells/HPF, p = 0.0903). When compared with cirrhotic livers from pathological control cases, this reduction was statistically significant (210 vs 101 cell/HPF; p=0.0158).

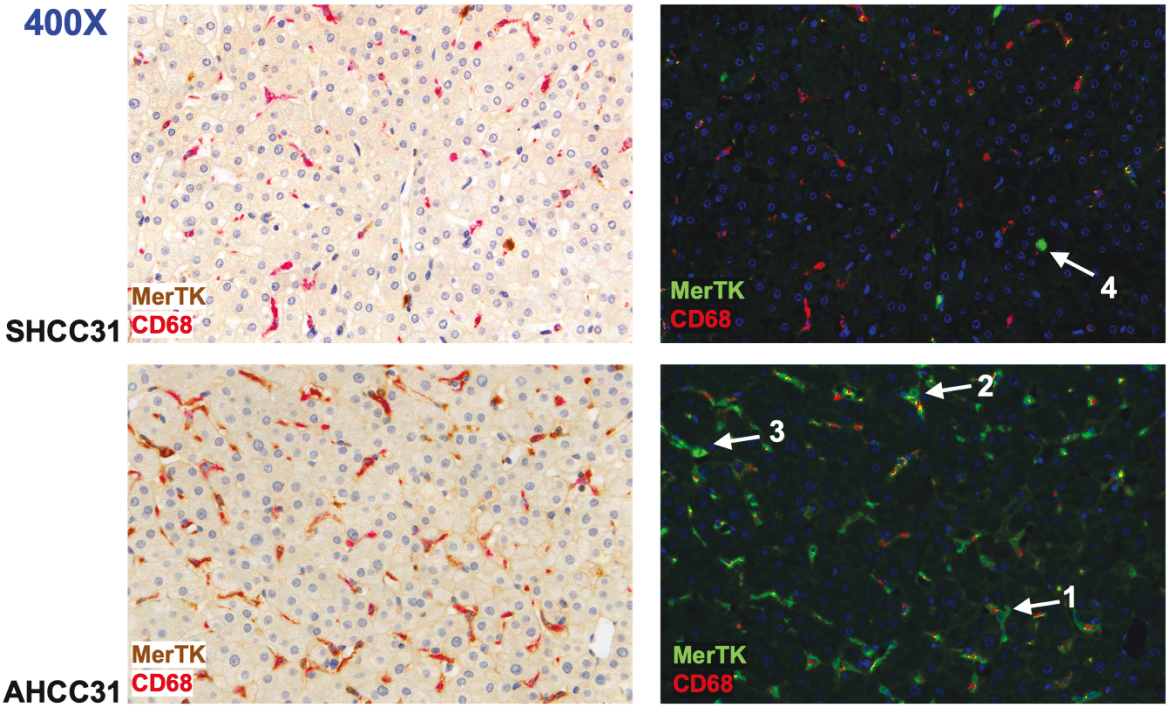

Figure 2.4: Background liver macrophages express MerTK more abundantly in cirrhosis
Representative pseudo-immunofluorescence and colour images demonstrate an increased MerTK+ signal in CD68+ cells in cases with cirrhosis – the lower images, from AHCC31, are from a patient with cirrhosis. MerTK+ signal is pronounced on Kupffer cells *(arrows 1, 2)*. Increased background MerTK signal in hepatocytes and endothelial spaces is evident in cirrhosis, particularly by pseudo-immunofluorescence. MerTK+CD68- cells *(arrows 3, 4)* are evident in the tumour microenvironment, without the characteristic classical features of a Kupffer cell.

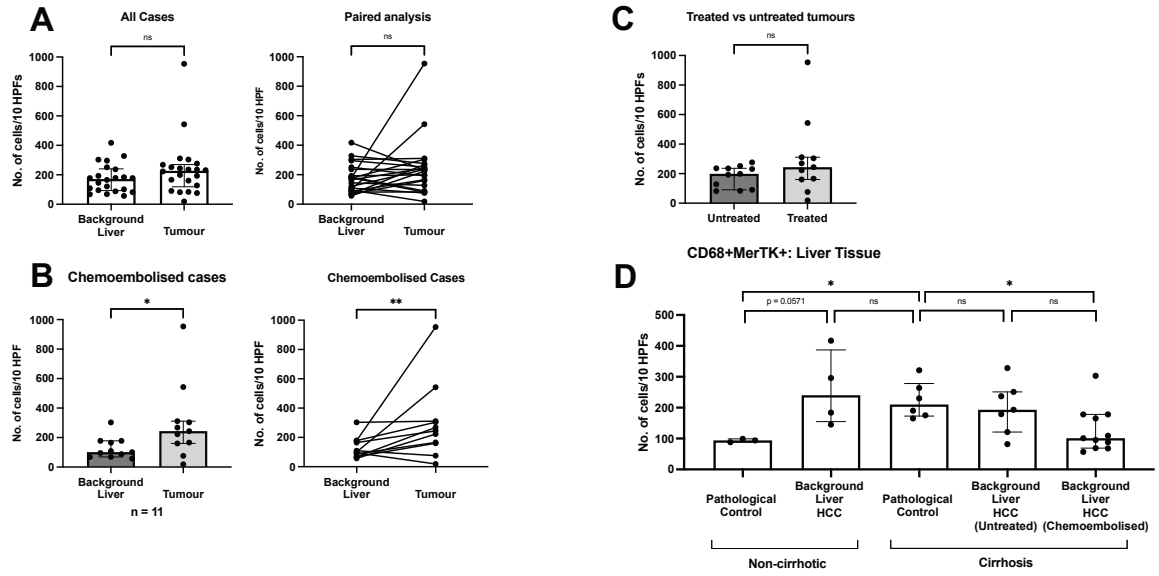

Figure 2.5: Enumeration of MerTK+CD68+ cells in tumour and background liver of patients with HCC

n = 22 cases were analysed. (**A**) Numbers of dual positive cells per high powered (400X) field were counted from within lesions and in parenchyma distant to the tumour. Unpaired and paired analyses are presented. (**B**) n = 11 cases in which prior chemoembolization of the lesion had been undertaken and residual tumour remained were analysed as a sub-group. (**C**) Treated and untreated lesions were similarly compared. (**D**) Background liver counts are presented and compared. Non-parametric analysis (Mann-Whitney for unpaired; Wilcoxon for paired data) was undertaken; data is presented as median values with interquartile ranges (IQR). *p<0.05, ** = p<0.01, ns – non-significant. *Abbreviations: HPFs = high-powered fields*

2.3.5 Axl+ macrophages are evident in the tumour microenvironment but less abundant than those expressing MerTK

Double epitope immunohistochemistry with Axl and CD68 characterised a different profile for Axl+ macrophages in the tumour microenvironment. Notably, considerable diffuse positive staining for Axl within both background parenchymal hepatocytes and within hepatocellular tumour cells was observed and has been previously described (Pinato *et al.*, 2019). Such diffuse Axl staining within the tumour varied in intensity between cases; those with areas of steatosis appeared to have a lower intensity of Axl positive staining (Figure 2.6 A). In these more steatotic areas, macrophages appeared less strongly positive for Axl than in other areas and other lesions analysed. Furthermore, some cases had strong 'background' Axl staining but a predominantly Axl- macrophage population (Figure 2.6 B, C); arrows 1 and 2 in Fig 2.6 B illustrate the presence of both Axl positive and negative macrophages. In Panel C, the lesion is

notable for a scant infiltrate of CD68+ cells without the characteristic 'Kupffer-like' appearance and without Axl expression (arrow 3). Despite these findings, some cases with well differentiated lesions had an abundance of dual positive, Kupffer like cells within well differentiated lesions (Fig 2.7 A, B). In all cases where Axl+ macrophages were found, staining was seen throughout the cytoplasm and on the cell surface. In less well differentiated cases, macro-trabecular areas were notable for the presence of Axl negative macrophages (Fig 2.7, C, D).

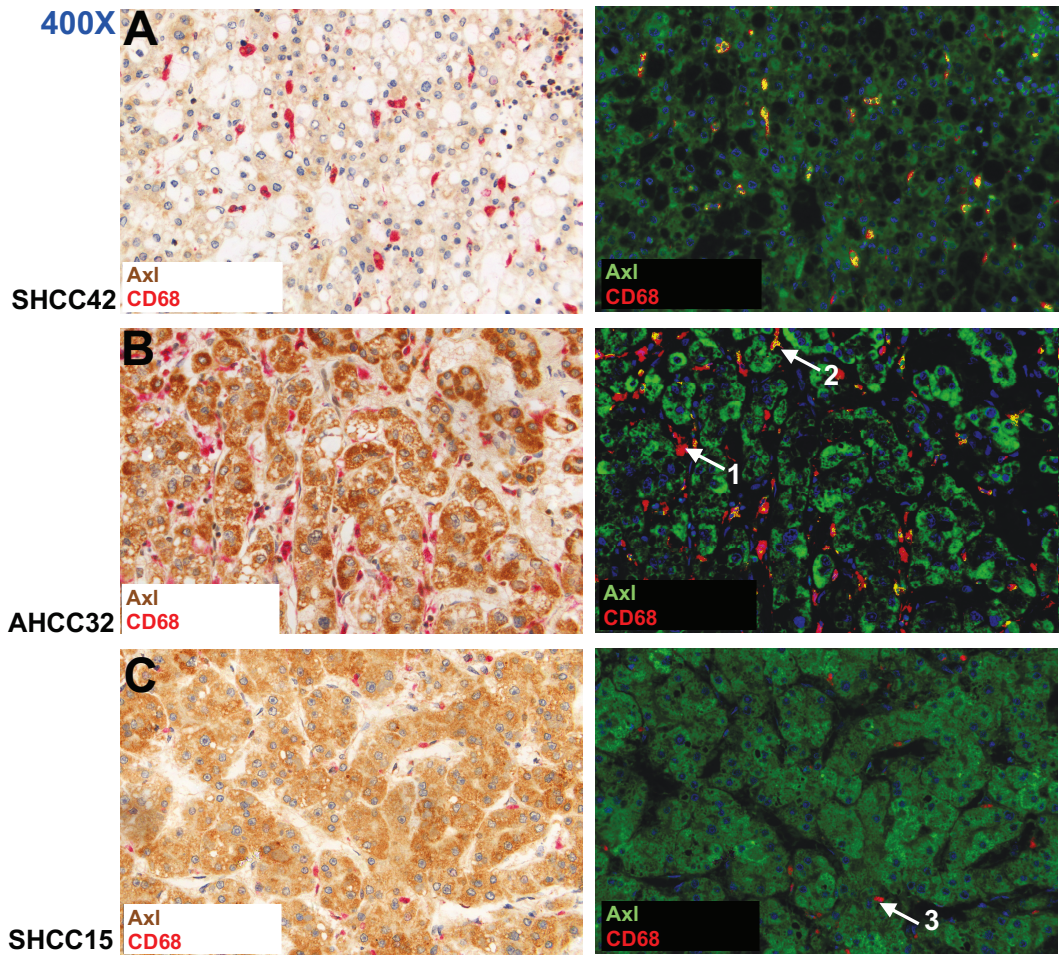

Figure 2.6: Tumour expression of Axl can be marked within tumour parenchyma
True colour (left) and pseudo-immunofluorescent (right) images at 400X taken after double epitope immunohistochemistry and multispectral analysis. Axl positive signal is brown in true colour and green after multispectral analysis; CD68 signal is red in both image types. Areas of co-localization appear yellow. There is marked variation in Axl positivity in the tumour hepatocytes, often less pronounced in the steatohepatitic variant of HCC (Panel A). Macrophages are predominantly Axl- and with variable density. Arrows 1 and 3 are Axl- macrophages; Arrow 2 is an Axl+ macrophage. These are representative cases, with Study ID to the left of the panel.

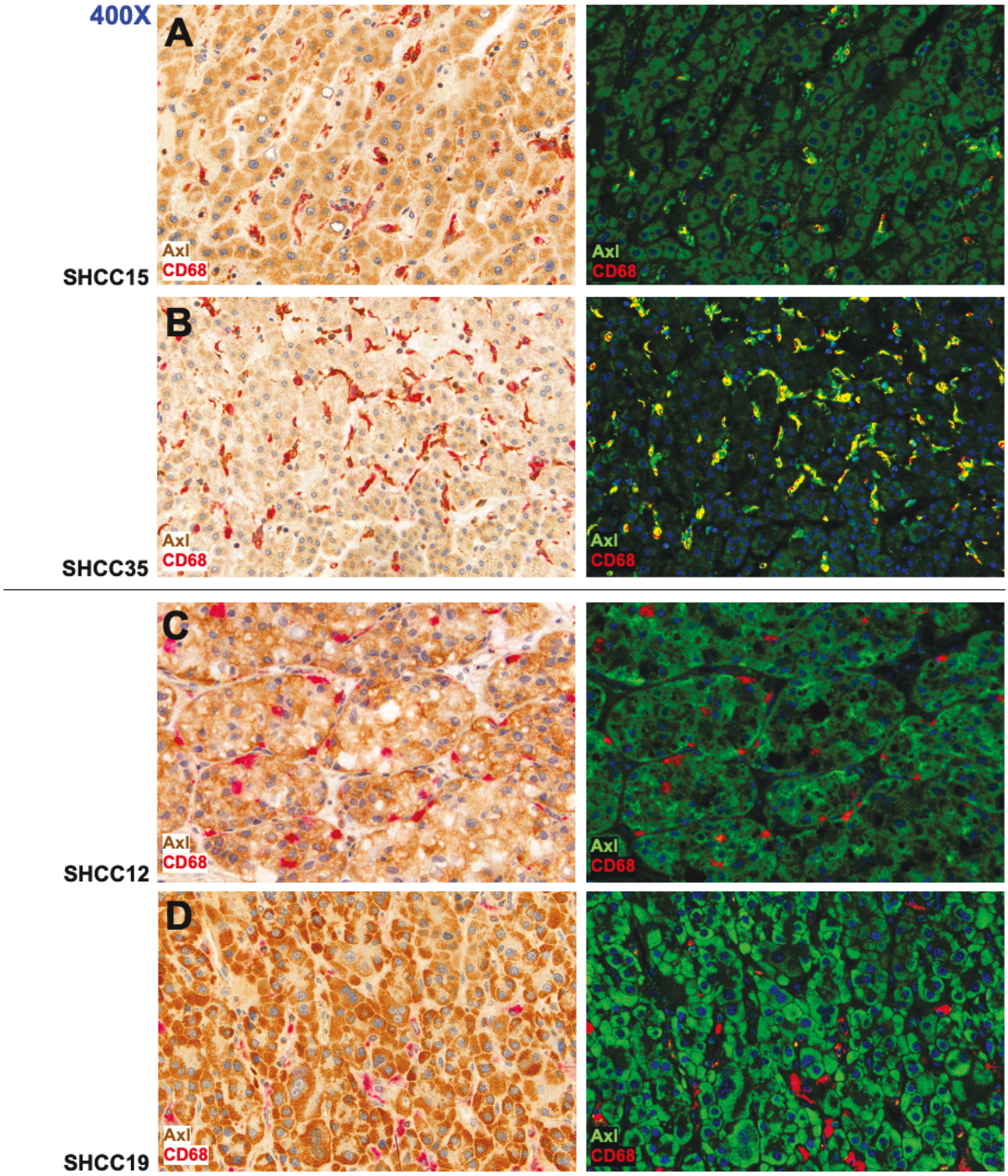

Figure 2.7: Tumour associated macrophage Axl expression varies with tumour differentiation
Well differentiated lesions are represented in panel (A) & (B); less well differentiated lesions are represented with macrotrabecular pattern, intracytoplasmic lipid (C) and marked nuclear atypia (D). Macrophage distribution, morphology and density varies between cases, with more Axl+CD68+ macrophages seen in less differentiated lesions. As before, Axl+ signal is brown in true colour; green after multispectral analysis; CD68 signal is red in both image types. Areas of co-localization appear yellow. These are representative cases; Study ID to the left of the panel.

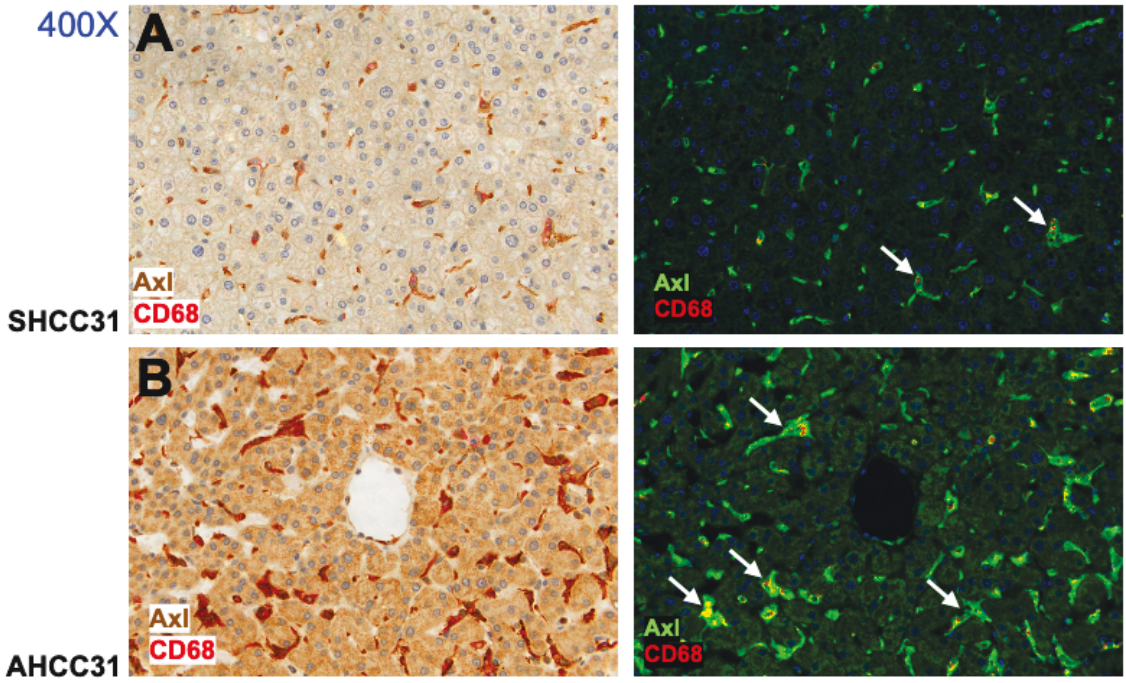

Figure 2.8: Kupffer cells are positive for Axl in both non-cirrhotic and cirrhotic liver
Non-cirrhotic (A) and cirrhotic (B) liver are notable for the presence of Axl positive Kupffer cells, seen here at high magnification (400x). These are distinct from the background parenchyma, which also stains for Axl and is more pronounced in cases with cirrhosis. Images are from two representative cases; Study IDs are to the left of the panel.

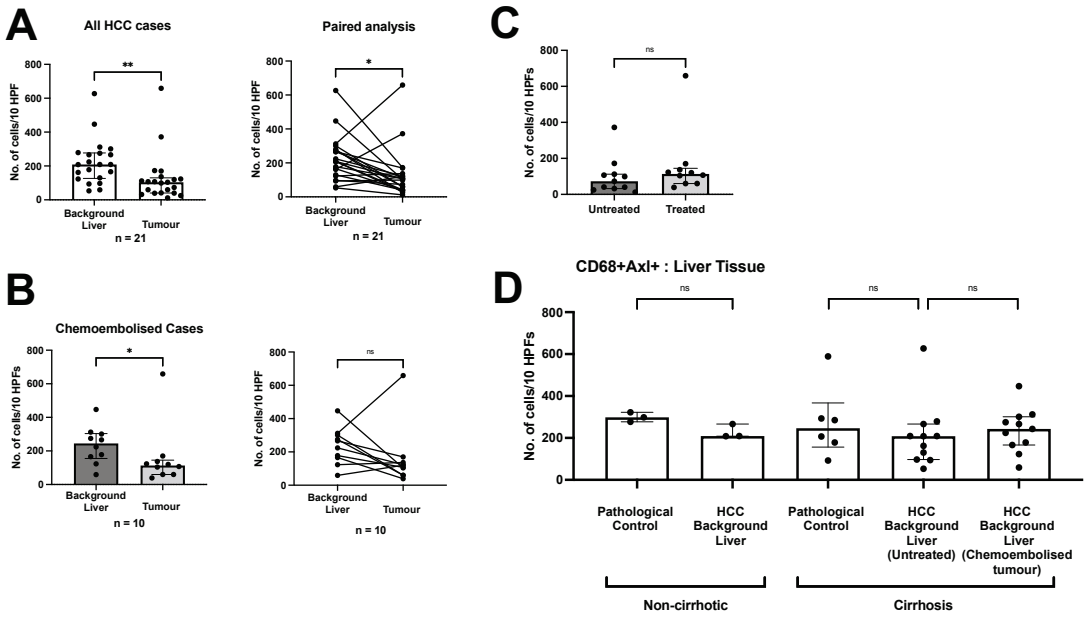

Figure 2.9: Axl+CD68+ cells are significantly less abundant within lesions than in surrounding liver in patients with HCC
(A) n = 22 cases were analysed and numbers of dual positive cells per high powered (400X) field were counted from within lesions and distant to tumour. Unpaired and paired analyses are presented. (B) n = 11 cases in which prior chemoembolization had been undertaken and residual tumour remained were analysed as a sub-group in the same fashion. (C) Treated and untreated lesions were compared. (D) Background liver counts are presented and

compared. Non-parametric analysis (Mann-Whitney for unpaired; Wilcoxon for paired data) was undertaken; data is presented as median values with interquartile ranges (IQR). *p<0.05, ** = p<0.01, ns – non-significant. *Abbreviations: HPFs = high-powered fields*

2.3.6 Kupffer cells express Axl irrespective of the presence of liver disease

Review of non-lesional background liver from cases with HCC and pathological control tissue revealed a consistent strong staining for Axl within Kupffer cells. This was also evident in cases without cirrhosis. Figure 2.8 illustrates these findings, Panel A in a liver without cirrhosis (case SHCC31) and Panel B a cirrhotic liver (case AHCC31). In both images, arrows indicate dual positive cells. True colour images also highlight the variation in hepatocyte Axl staining. Enumeration of sinusoidal macrophages confirmed this finding, demonstrating no significant difference between the different groups analysed (Figure 2.9, D).

Enumeration of Axl+ macrophages confirmed the findings on histological review when non-lesional background liver, which consistently stained well for Axl+ macrophages, was compared with the tumours. There was a statistically significant reduction in the numbers of dual positive macrophages counted within the tumour (Fig 2.9 A, 104 vs 209 cells/HPF; p = 0.0014); this effect was also observed with a paired non-parametric analysis (p = 0.0101). This observation was maintained when the sub-group of cases with prior locoregional therapy were reviewed (Fig 2.9 B, 113 vs 245 cells/HPF, p = 0.0303) and when tumours were compared with each other (Fig 2.9 C, p = 0.1780).

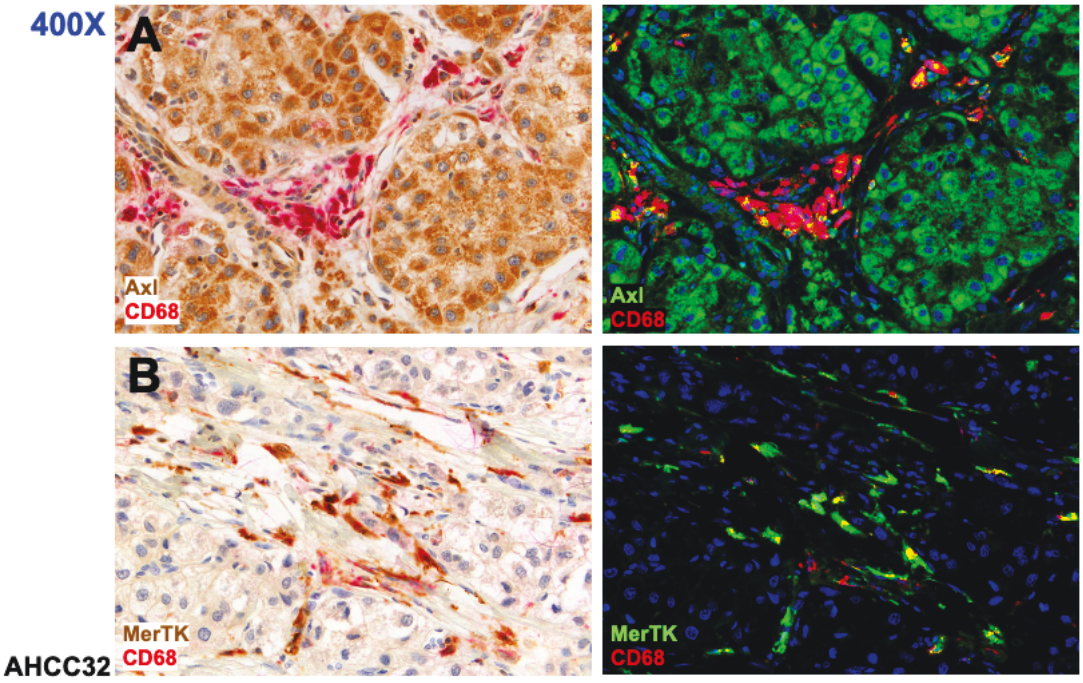

Figure 2.10: TAM-RTK positive macrophages are evident within stromal clusters in HCC
True colour (left) and pseudo-immunofluorescent (right) images at 400X taken after double epitope immunohistochemistry and multispectral analysis. Axl (panel A) and MerTK (panel B) positive signal is brown in true colour and green after multispectral analysis; CD68 signal is red in both image types. Areas of co-localization appear yellow. Images are representative from a single case (Study ID to the left of the panel)

2.3.7 Intralesional clusters of macrophages may have dual TAM-RTK positivity

As previously outlined in 2.3.2, lesions can harbour areas with clusters of macrophages, which may have infiltrated from the vasculature or be in direct contact with stromal cells seen within the lesions. These are more commonly positive only for MerTK (Figure 2.2 A), however certain lesions have Axl+ macrophages in clusters within stromal clusters (Fig 2.10 A) in addition to MerTK (Fig 2.10 B).

2.3.8 Macrophage infiltrates around necrotic tissue reveal differential TAM-RTK co-expression in the tumour microenvironment

Areas of pronounced macrophage infiltrate are seen around areas of necrosis; this is most clearly demonstrated in cases with successful embolization. Figure 2.11 outlines the comparative expression of both TAM-RTKs on macrophages in these areas. At the boundary

of lesions, dense infiltrates with strong positivity for CD68 represent multinucleate, large cell macrophages which appear to be recruited from surrounding areas in response to tissue damage. Such macrophages appear to be negative for Axl in this area, but strongly positive for MerTK (case SHCC19 and SHCC33; both cases received chemoembolisation), as evident from the strong brown (DAB) staining (highlighted with arrows). Of note, there is evidence of a gradient, with MerTK positive macrophages found at the boundary but MerTK negative macrophages within the necrotic tissue itself (noted with markers B and C; no such gradient is evident with Axl staining). Marker A denotes multinucleate macrophages engulfing embolization beads, which appear to be dual TAM-RTK positive.

2.3.9 MerTK+ and Axl+ macrophages co-localise with both CD4+ and CD8+ T lymphocytes in the tumour microenvironment

Separate double epitope immunohistochemistry and multispectral analysis was undertaken to evaluate T-cell – macrophage interactions within the tumour microenvironment. Two separate double epitope stains were optimised and performed – CD4:CD68 and CD8:CD68 to study both T cell subsets. Images taken at low and high-power magnification were then compared with matched images from the same location from sections that had undergone double epitope staining for both Mer:CD68 and Axl:CD68.

Direct contact between macrophages and T cells was evident with MerTK positive macrophages. In Figure 2.12, Arrows 1 and 2 highlight individual CD8 and CD4 T cells respectively in close proximity with macrophages. In this lesion, arrow 3 delineates an area that has MerTK+ macrophages (Panel A) seen in close proximity with CD8 T cells (Panel B) and nearby to CD4 lymphocytes (Panel C). Arrow 4 in panel A and B marks out a MerTK+CD68+ cell in direct association with 2 CD8+ T cells. At lower magnification in a separate lesion (SHCC27, Figure 2.13), areas of strong staining for MerTK co-localise with

both CD68+, CD8 and CD4 staining. This effectively illustrates a dense infiltrate of MerTK+ macrophages in close proximity with both CD4+ and CD8+ T cells in the tumour microenvironment.

A distinct pattern and differences between CD4 and CD8 staining was noted across all cases reviewed. CD8+ lymphocyte staining defined individual lymphocytes with a classical mononuclear cell appearance. CD4 staining, however, was more variable. In addition to similar classical mononuclear cells, areas with diffuse areas of positive staining not associated with individual nuclei were seen (Panel B, Fig. 2.13; arrow). CD4 expression has been described on monocytes and activated macrophages (Collman *et al.*, 1990; Zhen *et al.*, 2014). As a result, care was taken to identify distinct lymphocyte - macrophage interactions as opposed to double positive (CD4+CD68+) macrophages: arrow 5, Fig 2.12, Panel C and Arrow 4, Figure 2.14 are both examples of CD4+CD68+ macrophages.

In a parallel manner, Axl+CD68+ macrophages and lymphocytes were assessed. Lower magnification images in Figure 2.13 demonstrate that Axl expression in intra-tumoural aggregates of macrophages is less pronounced than MerTK on the same cells. Axl+ macrophages appear to be more prominent at the edges of these infiltrates, where they border onto nests of tumour cells. Higher magnification images in Figure 2.14 also confirm that although T-cell: macrophage interactions were similarly evident when compared with Mer+CD68+ double stains, they were less frequently observed. Arrows 1 and 2, Figure 2.14 highlight CD4+ T-lymphocytes in direct contact with CD68+ macrophages. In both instances CD4+ staining is morphologically consistent with true lymphocyte staining. Arrow 3 denotes a CD8 T cell and macrophage in proximity within a cluster of tumour cells.

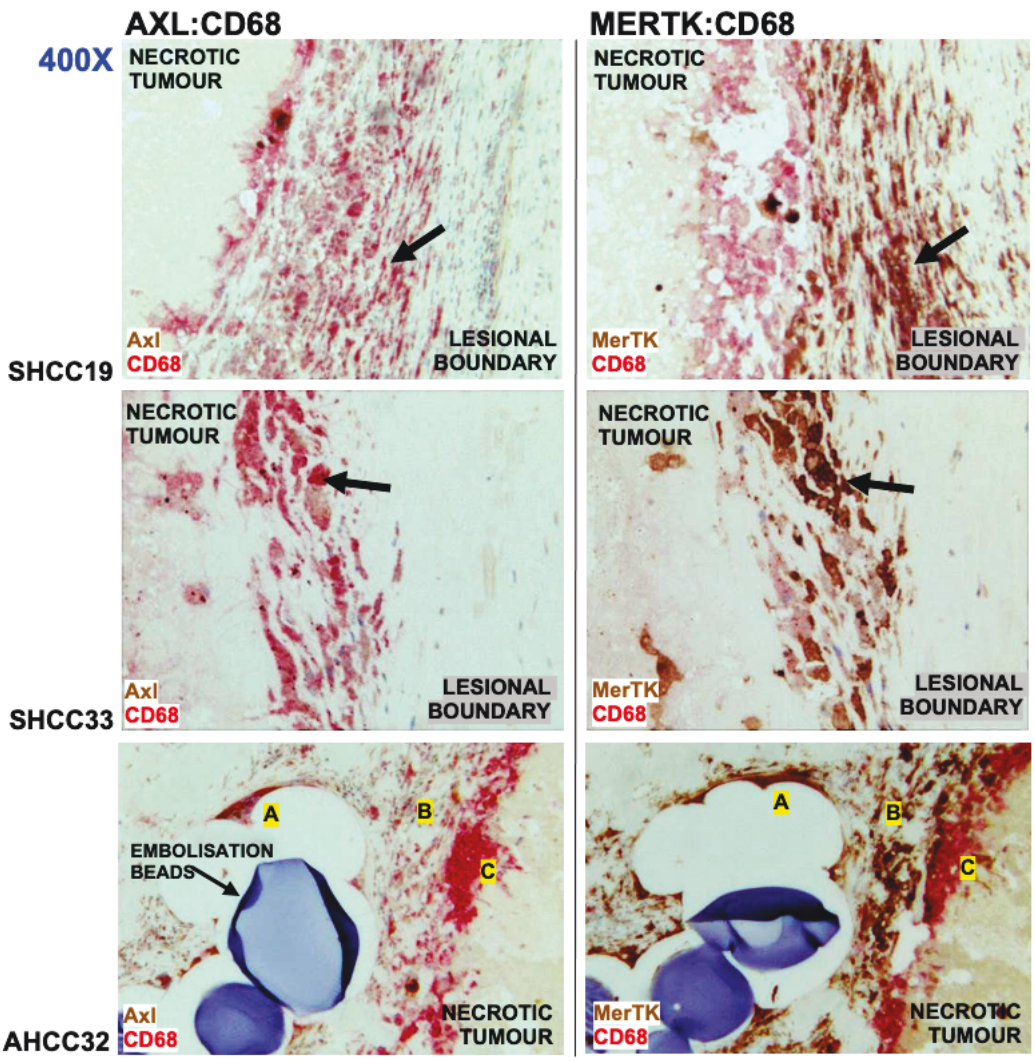

Figure 2.11: Macrophage infiltrates around areas of necrosis and prior chemoembolization differ in their TAM-RTK expression in HCC.

True colour images at 400X taken after double epitope immunohistochemistry. Images on the left are Axl:CD68 double stains; MerTK:CD68 double stains on the right. Axl and MerTK positive signal are brown, CD68 signal is red in all images. Images are representative of three separate cases (case IDs noted on the left of each panel).

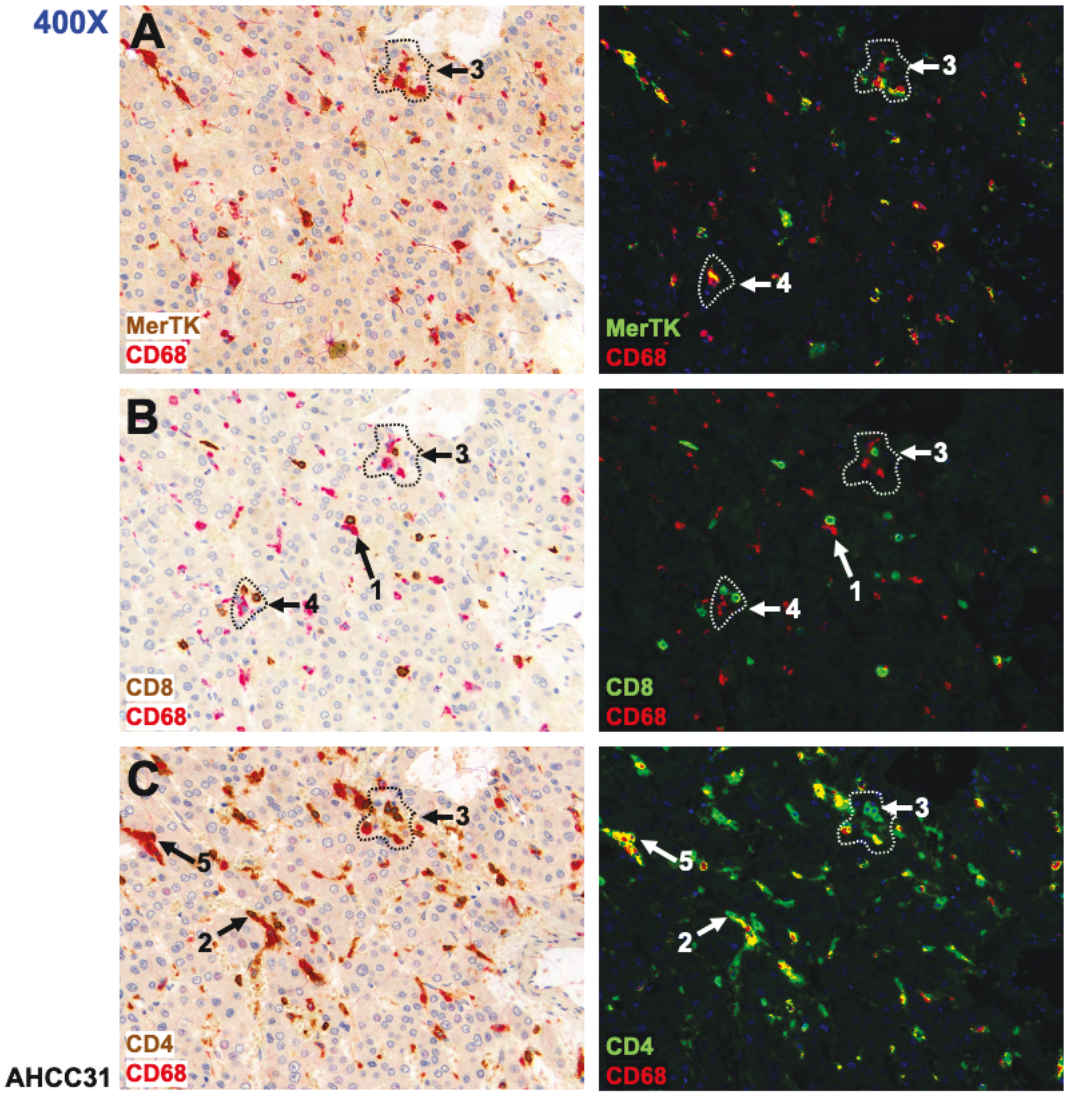

Figure 2.12: MerTK+ macrophages and T lymphocytes co-localize in the tumour microenvironment
Three separate double-epitope stains were undertaken (MerTK:CD68, panel **A**; CD8:CD68, panel **B** and CD4:CD68, panel **C**) in parallel and the high-powered field images in the same area were captured and analysed. Arrows 1&2 highlight macrophage-T lymphocyte pairs in proximity, Arrows 3 & 4 demonstrate multi-cellular aggregates within tumour nests. Arrow 5 demonstrates CD4+ macrophages in the background liver.

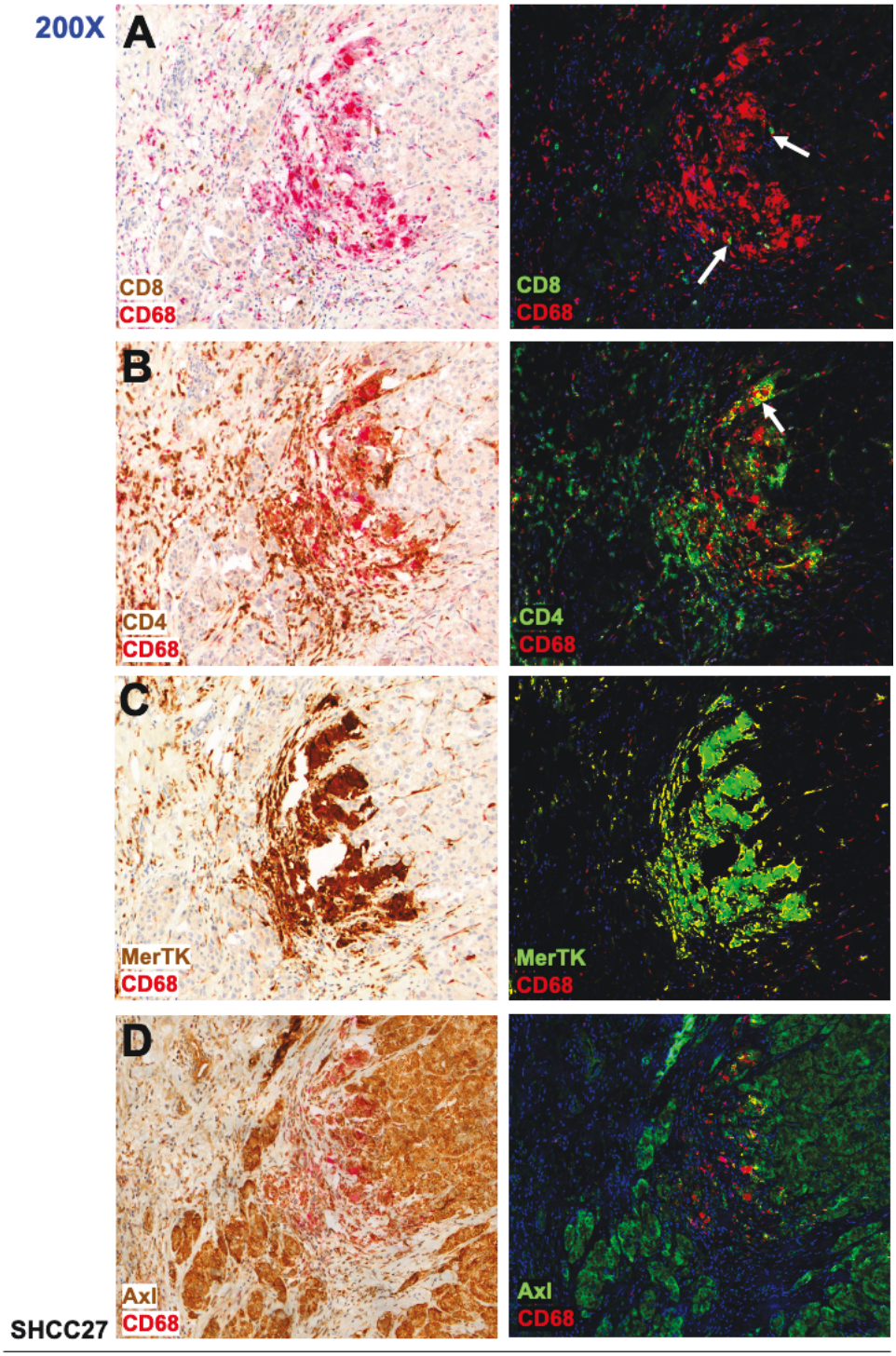

Figure 2.13: Inflammatory infiltrates in the tumour microenvironment are macrophage rich and differentially express MerTK

Low magnification images demonstrate aggregates of MerTK positive macrophages in proximity with both CD4+ and CD8+ T cells. Axl expression on macrophage aggregates is less pronounced. Arrows in panel A highlight CD8+ T cells, in panel B, an arrow highlights areas of diffuse CD4+ staining.

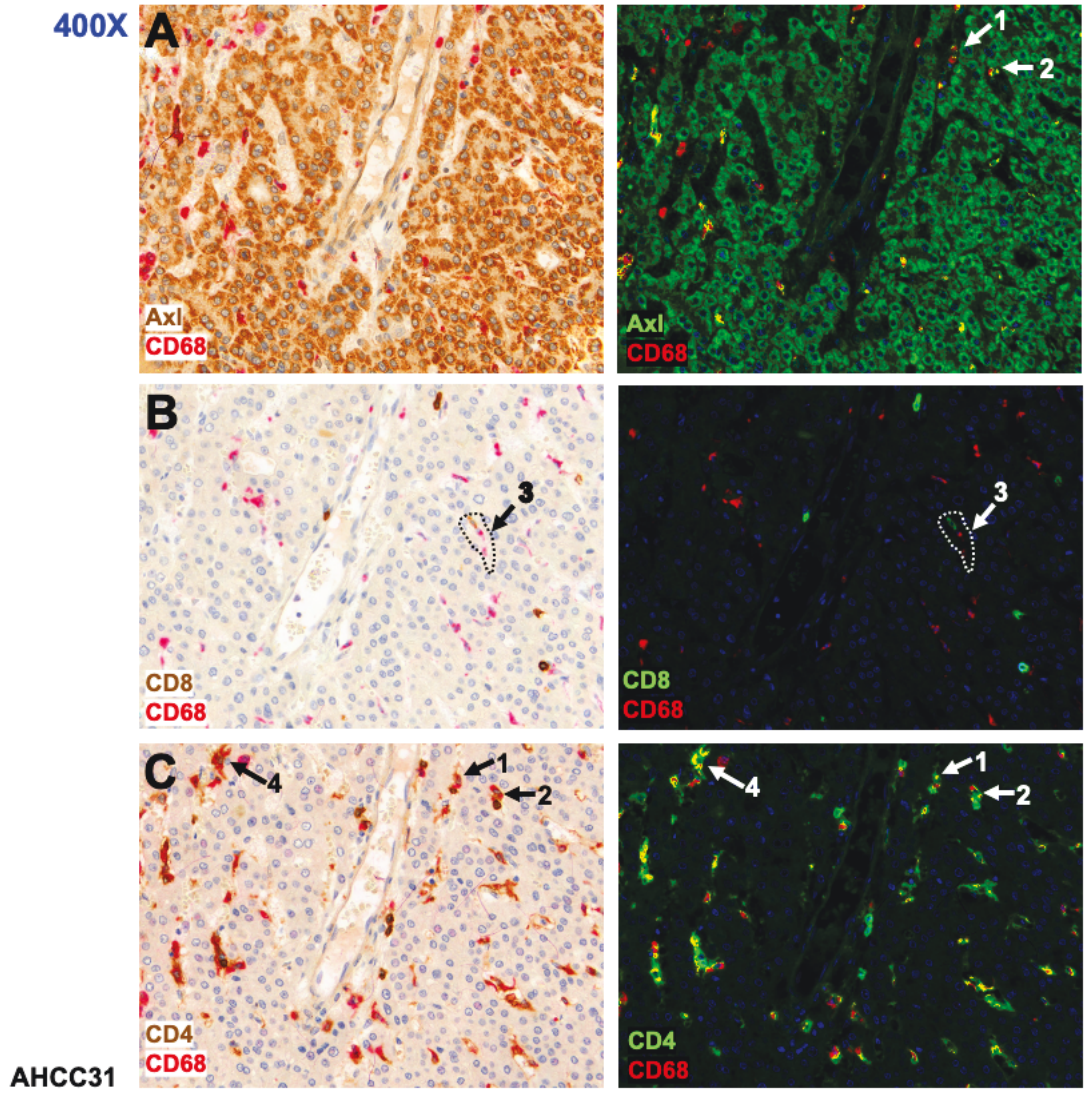

Figure 2.14: Axl+ macrophages can be found in proximity with T lymphocytes in the tumour microenvironment

At high magnification, Axl+CD68+ macrophages can be seen in direct contact with T lymphocytes. Occasional CD8+ T cell contact is seen – arrow 3, panel B. CD4+ T cells (Panel C) are found between macro-trabecular cords of HCC; there is direct cell to cell contact with CD68+ cells (arrows 1 and 2) which appear to be Axl positive (see left image, Panel A). Arrow 4 highlights evidence of CD4+CD68+ cells.

2.4 Discussion

This histological review of the myeloid cell compartment in both liver parenchyma and within the tumour microenvironment confirms the presence of both MerTK and Axl positive myeloid cells in hepatocellular carcinoma. This has not been previously described in the published literature. Enumeration did not demonstrate a significant expansion of TAM-RTK positive macrophages within the tumour environment when compared with the background liver. MerTK+ macrophages were more numerous in tumours, but this was not statistically significant. Conversely, there were significantly less Axl+ macrophages identified in tumours when compared with the surrounding liver.

Direct comparison of treated and untreated tumours did not demonstrate a significant difference in the number of MerTK or Axl positive macrophages seen in viable tumour. Within treated cases there was a modest but statistically significant enrichment of MerTK positive macrophages within lesions when compared with background liver, which has a significant reduction in the number of MerTK positive macrophages when compared with cirrhotic livers without HCC (Figure 2.4D). The reasons for this are not clear and could reflect migration of macrophages to the site of chemoembolization, however background liver in these cases was taken from distant liver or the contralateral lobe at explant, and overall macrophage number was not depleted in these cases.

In practice, patients undergoing locoregional therapy require compensated liver disease; the differences in numbers of MerTK positive macrophages could reflect a degree of decompensation in the control cases, particularly in without HCC who underwent transplantation on account of UKELD score, and not on oncological indications. Increased intrahepatic MerTK positive macrophages have previously been described, both in cirrhosis

and in decompensated liver disease (Bernsmeier *et al.*, 2015) and this finding was replicated in this study when comparing MerTK positive macrophages in cirrhosis with pathological controls.

Simple numerical evaluation of myeloid cells may not reflect of the immune context of a lesion. Myeloid cells are functionally diverse and can have opposing functions in the tumour microenvironment, with established data supporting the presence of tumour associated macrophages with both favourable (Edin *et al.*, 2012) and poor prognosis (Yeung *et al.*, 2015), related to the skewing of the macrophage population towards either a pro-inflammatory, M1-like TAMϕ or towards an alternatively activated, regulatory M2-like TAMϕ, respectively. Recent work has demonstrated that the composition of macrophage populations within lesions in hepatocellular carcinoma can directly predict survival, based on a skew towards a pro-inflammatory, PDL1+ macrophage and away from a suppressive CD169+ phenotype. (C. Wu *et al.*, 2020). Such a model does not rely on expansion of myeloid cell numbers to indicate pathological relevance.

Furthermore, studies have shown that macrophages within specific locations or niches within the TME can be associated with differing clinical outcomes – Dai et al. demonstrated that micro-localisation of macrophages within islets in non-small cell lung cancer was associated with improved survival, whereas macrophages in the stroma were associated with reduced survival (Dai *et al.*, 2010). In this sample of patients both MerTK and Axl positive macrophages were identified in stromal clusters within tumour nests, as well as evenly distributed in well differentiated lesions as 'Kupffer-like' macrophages. It is not known if these have migrated into the TME from the surrounding parenchyma or have differentiated in situ from circulating monocytes. Although classically non-migratory, there is evidence using in-

vivo microscopy demonstrating Kupffer cells' ability to move within hepatic sinusoids (MacPhee, Schmidt and Groom, 1992). Given these shared macrophage niches between MerTK and Axl, further work is needed to prove if these are dual positive macrophages. There is no published work examining the function and phenotype of cells expressing both receptors and this warrants further investigation if such cells are confirmed in a larger cohort of patient samples. In support of this finding, recent work by Pinato et al. has demonstrated peri-tumoural Kupffer cells expressing Gas-6, a central ligand for TAM-RTK signalling (Pinato *et al.*, 2019), raising the possibility of autocrine induction of signalling in these cells.

MerTK positive macrophages were seen other niches within the TME; notably within dense inflammatory infiltrates containing other mononuclear immune cells (Fig 2.1C) and as multinucleate aggregates of macrophages around areas of necrosis and prior embolization. In both cases these macrophages were not positive for Axl. MerTK's role in the periphery of areas of necrosis has been postulated in human atherosclerotic plaques – here, it is postulated that cleavage of surface MerTK from efferocytotic macrophages releases soluble Mer; this can act as a decoy receptor for phosphatidylserine, resulting in ineffective efferocytosis and the promotion of tissue necrosis (B. Cai *et al.*, 2017). It is interesting to note that macrophages seen further into the areas of necrosis appear MerTK negative; this could potentially be because of cleavage of surface MerTK in a similar manner and clearly demonstrates the varied phenotypic and functional array of macrophages even within the same location.

Recent work by Chen et al., 2019 and previously by Kuang et al., 2009 looked at peri-tumoural and stromal monocytes in hepatitis B related HCC. They describe an upregulation of PDL1+HLA-DR+ monocytes with potent capacity to attenuate anti-tumour T-cell responses and an association with reduced survival. This phenotype could be recreated by uptake of

tumour tissue fragments including hyaluronan. Further work is needed to ascertain if the MerTK+ stromal and peri-tumoural macrophages identified in this study, especially those pronounced in the peri-tumoural regions in tumours both with and without locoregional therapy have a similar phenotype, or indeed co-express PD-L1, possibly after uptake of apoptotic and necrotic tumour tissue fragments.

Attempts were made in this study to identify if TAM-RTK dual positive macrophages did co-localise with CD4 and CD8 T cells. Areas of interaction within immune infiltrates were found in which both CD4 and CD8 T cells were found in direct cell contact with macrophages, often in aggregates. These aggregates were demonstrated to be MerTK positive; Axl positivity was more difficult to confirm using this approach on account of high background tumour staining for Axl (Fig 2.12, A – D). Data from murine xenograft models of both solid organ and haematological malignancies has shown that MerTK CD11b+ myeloid cells have the capacity to impair cytotoxic T cell responses through the production of anti-inflammatory, pro-resolution cytokines including IL-10 (Cook *et al.*, 2013). It would be pertinent therefore to ascertain if there is significant regional staining of IL-10 within these intra-tumoural infiltrates in these cases.

There are limitations to this histological case review that must be acknowledged when making conclusions from the findings. The sample size analysed was modest (n=22 cases, n=10 controls), however the data from enumeration of TAM-RTK positive cells demonstrates some consistent findings and patterns in macrophage density as discussed above. In addition, detailed review of the macrophage distribution and phenotype was undertaken with the supervision and expert review of a consultant hepatobiliary histopathologist to assure that

immunohistochemistry had been performed accurately, and that there was concordance in relation to the observations made.

Enumeration of the dual positive cells was undertaken manually, and although technique agreed with expert review, it was exclusively undertaken by the author. Such an approach does leave the analysis open to unintended systematic bias, despite the selection of random high-powered fields for analysis. This could be addressed in future work with independent verification of the enumeration or using automated cell counting software in a larger sample. In addition to this, random sampling could result in misleading results if there are large variations in the density of cells detected between individual high-powered fields. This was evaluated (*data not shown*); the majority of cases showed relatively consistent values between high powered fields. Large multinucleate aggregates in the periphery of necrotic tumour tissue were not included in this enumeration, and high-powered fields were sampled from tumour nests in order to remove this source of variation. Furthermore, counting individual cells in this setting was not feasible. This approach does mean that the results of enumeration are likely to underestimate the density of TAM-RTK macrophages in the TME and, in particular, MerTK.

In this study, a pathological control tumour, such as colorectal metastasis, has not been compared alongside hepatocellular carcinoma. Hepatocellular carcinoma is a malignancy which classically develops upon the background of chronic inflammation and fibrosis; in which there is often only subtle differences histologically between malignant and non-malignant or dysplastic tissue, and in which margins between these compartments are often ill-defined. In light of this, priority was given in this analysis to a comparison of the macrophage phenotype between neighbouring tissue compartments in hepatocellular carcinoma, with a view to gaining an understanding of the contribution of TAM-RTK macrophages to this process. Nevertheless,

it is pertinent and important to understand if TAM-RTK macrophages play a similar role in the TME in other solid tumours; moreover, an understanding of the interaction between those in the liver parenchyma with metastatic tumour tissue would help to qualify our understanding of the contribution from resident and recruited macrophage populations respectively.

Difficulties were encountered with assessing dual positive macrophages in some instances, in particular with relation to Axl. Double positive cells included those with overlap of red and green pseudo-fluorescent signal and those in which both red and green signal were seen within the bounds of a distinct cell, with a nucleus. This approach allowed the analysis to include cells with both cytosolic and cell membrane positivity for both TAM-RTKs. High background tumour tissue expression of Axl did complicate some enumeration, as it could be unclear whether staining was from macrophages or tumour cells. This was also pertinent for sinusoidal, Kupffer like macrophages in close proximity with endothelium. Recent work in HCC has demonstrated endothelial expression of Axl in tumour vessels (Chai *et al.*, 2021) and MerTK has been reported on the glomerular endothelium (Zhen, Finkelman and Shao, 2018). Zagorska et al. have similarly described expression of both TAM-RTK markers on hepatic endothelium in mice, but also note there pronounced expression on Kupffer cells as well (Zagorska, Paqui G. Través, *et al.*, 2020). This could have resulted in false positive identification of dual positive macrophages with cell surface TAM-RTK positivity. To address this, multiplex immunohistochemical staining using a number of markers, including endothelial marker CD31 would be beneficial to help ascertain if Axl and MerTK endothelial cell expression could interfere with interpretation of macrophage TAM-RTK expression.

Despite these considerations, histological evaluation of HCC tissue has confirmed the presence of both MerTK and Axl positive macrophages in the TME. In particular, MerTK positive

macrophages have been identified in dense infiltrates both within tumour nests, in stromal clusters and in the periphery at the boundary with surrounding liver in the case of necrotic embolised disease. TAM-RTK expression has been identified in macrophages with varied morphology, and a differential abundance of MerTK and Axl positive CD68+ cells has been seen when lesions are assessed based on the differentiation status of the tumour. Both MerTK and Axl positive macrophages have been identified near CD4 and CD8 T cells within the TME, raising the possibility of cross-talk between these immune cell populations.

Taken together these data have confirmed aspects of this part of the study's hypothesis. There is a need to gain further phenotypic information about MerTK and Axl positive macrophages in the tumour microenvironment – this is something that is limited using immunohistochemistry (due to the small number of markers that can be stained simultaneously before the signal is affected) and is hampered by the problem of potentially high background signal within non-macrophage cell populations. Enumeration of cells has not identified a clear enrichment by density within the tumour, however not all regions of the TME could be readily assessed by manual cell counting. As a result, there may be an underestimation the abundance of MerTK positive macrophages in particular.

Extraction of the myeloid cell populations from fresh tumour and liver tissue will allow for detailed immunophenotyping and characterisation of these cells, help to clarify the proportion of the myeloid cell populations that express MerTK or Axl and remove the confounding factors of overlapping positive signal from background parenchymal tissue or vasculature. Furthermore, targeted immunohistochemistry with 3 epitopes stained in sequence could be employed to ascertain if dual TAM-RTK macrophages express MAC-387, a marker of

monocyte-derived macrophages that have infiltrated from the circulation as opposed to developing from resident macrophage (and monocyte) populations.

CHAPTER 3

Phenotypic characterisation of MerTK and Axl expressing tissue resident monocytes, macrophages and circulating monocytes

3.1 BACKGROUND AND AIMS

3.1.1 Background

Histological evaluation of macrophage MerTK and Axl expression in a case series of patients with HCC has confirmed their presence within the tumour microenvironment and on intrahepatic macrophages *(Chapter 2)*. Previous published work from within our group has characterised the presence of MerTK on Kupffer cells in human liver (Triantafyllou *et al.*, 2017), and indeed both MerTK and Axl expression has been observed on murine Kupffer cells (Zagórska, Paqui G Través, *et al.*, 2020). However, the observation that both receptors are expressed on human tumour associated macrophages is novel.

Although not numerically enriched within the tumour in the cases analysed in Chapter 2, further information about the immune phenotype of these cells was required to characterise their role within the tumour microenvironment. There is experimental data to suggest the existence of varied functional phenotypes within MerTK+ and Axl+ macrophage populations. MerTK+ macrophages are generally thought to have a pro-resolution phenotype; however, their function can vary dependent on the expression of other markers and the clinical context. Within the liver, low HLA-DR co-expression denotes a MerTK+ macrophage subset with a comparatively reduced phagocytic and efferocytotic capacity. Furthermore, both reduced efferocytosis and pro-inflammatory cytokine production can be demonstrated in the same $MerTK^{+}HLA\text{-}DR^{+}$ macrophages from patients with acute liver failure when compared with healthy controls (Triantafyllou *et al.*, 2018). With respect to Axl, expression can be induced by both classical M1-activation trigger lipo-polysaccharide (LPS) and alternative M2-activation trigger dexamethasone (Zagórska *et al.*, 2014), indicating that Axl may be expressed on macrophages across both pro-inflammatory and immune-regulatory contexts.

Myeloid cell populations within the liver derive clear phenotypic differences based on their ontogeny. Tissue resident and embryonically derived Kupffer cells are the predominant resident myeloid cell in the liver (representing over 80% of macrophages at rest), with the remainder derived from circulating monocytes; so-called 'monocyte-derived macrophages' (MoMFs). The proportion of these increase in response to liver injury or chronic inflammation (Liaskou *et al.*, 2012; Heymann and Tacke, 2016). At rest, Kupffer cells have a low surface expression of HLA-DR, express PD-L1 and produce IL-10, resulting in the induction of a tolerogenic T-lymphocyte responses. MoMFs, by comparison, can have a similar immune-regulatory and restorative phenotype, often after uptake of cellular debris in the context of acute liver inflammation (Dal-Secco *et al.*, 2015), but also have distinctive functions: these include maintained antigen presentation capacity, pronounced CD4+ T lymphocyte activation and pro-inflammatory cytokine production including IL-1β, TNF-α and IL-6 (Liaskou *et al.*, 2012). Recent work has shown that in mouse models of liver injury, Kupffer cells and monocyte-derived macrophages isolated at the same stage of resolution have differing gene expression profiles, highlighting clear persistent differences based on ontogeny (Zigmond *et al.*, 2014).

Taken together, these data confirm that (a) macrophage ontogeny can determine phenotypically distinct populations within the liver and that (b) MerTK positive populations exhibit varied functions depending on their co-expression of other immune phenotypic markers, such as HLA-DR.

The tumour environment provides yet further opportunity for phenotypically distinct MerTK (and Axl) positive macrophage populations. Firstly, ontogeny is different to the liver: macrophages in this compartment are thought to be exclusively derived from the circulation, without a resident population. Secondly, the tumour microenvironment could provide

additional triggers for MerTK and Axl expression, with areas of hypoxia and the presence of apoptotic cells. In the liver, it has been demonstrated that trafficking through hepatic endothelium and uptake of cellular debris drives the development of differentiated, MoMFs (Liaskou *et al.*, 2012) and this up-regulates MerTK expression (Triantafyllou *et al.*, 2018). Areas of inflammation within tumours have the potential to drive Axl versus MerTK expressing macrophage populations.

3.1.2 Hypothesis

It is hypothesised that infiltrating monocytes and myeloid cells recruited into the tumour microenvironment are subject to multiple and varied triggers for both MerTK and Axl expression and that these are more pronounced than in the background liver. Tumour associated myeloid cell populations could therefore have higher MerTK and Axl expression than those from background or control liver tissue, even if not significantly numerically expanded by immunohistochemistry.

It is postulated that co-expression of immunophenotypic markers on both monocytes and macrophages will highlight functional differences between distinct TAM-RTK positive myeloid cell populations in HCC. Differences in phenotype may be determined by both ontogeny and microenvironmental cues. Ascertaining these population specific differences is especially important in the translational context, as a non-targeted approach to receptor blockade, affecting phenotypically divergent cell populations with opposing functions can result in attenuation of therapeutic impact.

3.1.3 Aims

In order to evaluate this hypothesis, the broad aims of this chapter were:

1) to assess co-expression of a range of immunophenotypic markers in MerTK and Axl positive myeloid cells extracted from human tissue
2) to assess co-expression in both monocyte-derived macrophages, the total macrophage population and myeloid derived suppressor cells in tumour, background liver and non-HCC liver
3) to quantify MerTK and Axl surface expression (by MFI or % positivity) between comparable myeloid cell populations across tumour and background liver to assess if there is an expansion of TAM-RTK expressing macrophages in HCC
4) to identify environmental cues for signalling via MerTK and Axl by assessing homogenates of liver and tumour tissue for known ligands of MerTK and Axl signalling.
5) To characterise both the circulating monocyte phenotype and levels of circulating TAM-RTK ligands in HCC, to help establish if there is a circulating TAM-RTK+ monocyte phenotype that has potential to act as a biomarker.

As described previously, cases with prior chemoembolization have a modest enrichment of MerTK+ macrophages when compared with their surrounding liver and often have dense MerTK+ macrophage infiltrates at the tumour boundaries. In light of this, a subsidiary aim of this chapter was:

6) To assess if circulating monocyte phenotype before and up to 6 weeks after chemoembolization reflects this, possibly because of trafficking through embolised tumour and liver tissue.

3.2 METHODS

3.2.1 Patient selection, recruitment and tissue sample collection

Patient selection and recruitment into the study has been described elsewhere (Chapter 7). Samples collected for this part of the study included fresh liver, tumour tissue and peripheral blood samples from patients undergoing liver transplantation or hepatic resection for hepatocellular carcinoma. Blood from patients in the hepatocellular carcinoma clinic at King's College Hospital undergoing locoregional therapy with chemoembolization was also collected prior to treatment and at 2 time points after treatment (24hrs and 6 weeks).

Liver Tissue Collection

Surgical teams were made aware of the patient's consent in advance by email. A member of the study team attended theatre prior to surgery to ensure tissue collection was undertaken in a timely manner and that suitable containers for collection were available. In cases of liver transplantation, transplant co-ordinators were informed in advance of patients' enrolment into the study; when an organ was offered and transplantation due to proceed a member of the study team would be informed in order to attend theatres.

Tissue was collected from theatre immediately after explantation or resection and transferred in sterile conditions (in a collection bag, on ice) to the histopathology laboratory for immediate sectioning and tissue collection. If samples were collected out of hours (after 6pm) without a histopathologist immediately available, collected tissue samples were stored overnight on ice in Roswell Park Memorial Institute (RPMI) 1640 medium supplemented with 1% penicillin-streptomycin and 5% fetal bovine serum in a temperature controlled cold room at 4^{o}C.

Liver tissue was sectioned by a consultant histopathologist as soon as practicable after tissue collection (and, if relevant, storage) and always within 12 hours of surgery. Tissue was sectioned in 5mm intervals and inspected macroscopically. Radiologically known tumours were confirmed and remaining tissue examined for further lesions. In all cases, macroscopically viable tumour tissue was taken for cell extraction, and clear from the margins of the lesion with background liver. Visibly necrotic tissue was not used for extraction. Liver parenchymal tissue was sampled from as far as possible from both the resection margin and from the lesion. In the case of liver explants, this was taken from the contralateral lobe of the liver, if this contained no tumours after sectioning, or from the caudate lobe. For hepatectomy and limited segmentectomy specimens, tissue was taken from an area as distant as possible from any lesions or cauterised liver tissue.

Collected tissue was then weighed. A piece of tissue (liver and tumour) less than 1g was snap frozen and stored immediately at -80^{o}C. The remainder was immediately placed in RPMI 1640 medium (ThermoFisher Scientific, UK) supplemented with 1% penicillin-streptomycin and 5% fetal bovine serum (ThermoFisher Scientific, UK) at 4^{o}C and transferred to the laboratory for tissue homogenisation and cell extraction.

3.2.2 Clinical data acquisition

Supporting clinical data from the cases recruited and analysed were obtained from the electronic medical records at King's College Hospital. Such data included blood results (including alpha-fetoprotein levels), demographic data and information as to the aetiology of underlying liver disease, where appropriate. These data were collected with the patients' consent and stored in a secure password protected database on an approved laptop computer. Official histopathological reports for each case were also stored digitally on this device. In

accordance with requests from the local research ethics committee, backup data was stored on an external hard-drive and kept on hospital premises in a locked cabinet.

3.2.3 Isolation of peripheral blood mononuclear cells and serum from blood samples

Peripheral blood was taken before surgery or after consent was given in the outpatient clinic. A total of 40ml of blood was collected from a peripheral vein in four 9ml lithium heparin tubes, with one SST tube sample collected (4ml). Lithium heparin samples were kept on a roller at room temperature if it was not possible to immediately isolate peripheral blood mononuclear cells. The SST tube was not place on the roller, allowed to coagulate and serum collected by centrifugation of the coagulated sample at 15000 rpm for 10 minutes. Serum samples were aspirated from above the coagulated cells, stored in 100ml aliquots and immediately frozen at -80ºC. If not for immediate centrifuge, SST tubes were kept at 4oC for a maximum of 2 hours before serum collection.

Blood collected in lithium heparin bottles was mixed 1:1 with sterile phosphate buffered saline (PBS, Life Technologies, UK). Diluted blood was layered directly onto 15ml of Ficoll-Paque (GE Healthcare, UK) and spun for 20 minutes at 1200 rpm, with no brake applied to the centrifuge. After centrifugation, the buffy layer was aspirated using a Pasteur pipette and washed with 25ml of PBS at 1200rpm for 10 minutes at room temperature, to remove platelets. After centrifugation, the supernatant was discarded and the pellet re-suspended in 25ml of PBS. Ten microlitres of this was taken and mixed with 10µl of trypan blue and used for counting of cells using a haemocytometer. This re-suspended cell suspension was centrifuged once more for 10 minutes at 1800rpm. After this, the supernatant was once again discarded and the cell pellet ready for analysis. If required, at this point cells were stored by re-suspending in 1ml of CS10 Cryostor cell storing medium (10% DMSO; Stemcell Technologies, UK) and placing in

a graduated cell cooling device (CellCool, Biocision, US) in the freezer at -80°C. Once frozen, if longer periods of storage were required then samples were transferred on dry ice to liquid nitrogen. Graduated cooling and DMSO prevent cell rupture during the freezing process to protect viability on thawing. Cells were stored up to a maximum concentration of 1x 10^7 cells/ml.

3.2.4 Isolation of mononuclear cells from liver and tumour tissue

Tissue was kept on ice and submerged in supplemented media (as above) prior to homogenisation. Tissue was weighed at the time of collection after diagnostic sectioning; up to 150g of liver tissue could be processed using the following protocol at one time. Tissue pieces were cut using a sterile scalpel and forceps into 5mm cubes. Parenchymal tissue was inspected and macroscopically visible vessels and bile ducts were removed prior to subsequent homogenisation. Tissue pieces were rinsed with ice cold phosphate buffered saline (PBS, Life Technologies, UK) until visible blood was no longer visible and then placed into Miltenyi GentleMacs dissociator C-tubes (Miltenyi Biotec, UK), in accordance with the manufacturer's guidance: care was taken not to fill the tubes and supplemented RPMI media (as above) was added. C-tubes were loaded onto the dissociator and tissue was then homogenised on the "mouse_spleen_01_01" setting for 1 minute. Homogenised slurry was poured through a 70 μm steel mesh into 500ml glass beakers. Beakers with 70 μm steel mesh secured with adhesive tape were prepared in advance and autoclaved to maximise sterility. Fully homogenised tissue was rinsed through the mesh using up to 500ml of ice-cold PBS. Solid tissue remaining on the mesh was discarded.

The filtrate was poured into 50ml falcon tubes and spun at 500rpm for 3 minutes at 4°C to separate large debris and sediment. The supernatant was collected in fresh 50ml Falcon tubes

and spun at 2000rpm for 5 minutes at 4°C. Pellets from this centrifugation step were collected, washed in PBS and combined until the total cell pellet from the tissue was resuspended into 40ml of PBS. Each time the cells were washed using ice cold PBS, centrifuging for 5 minutes at 2000rpm. Two separate 50ml falcon tubes with 15ml of Ficoll-Paque (GE Healthcare, UK) were layered with 20ml of the cell suspension for density gradient centrifugation. This was centrifuged in the same manner as above, and the cell monolayer collected and red cell lysis was performed using ACK red cell lysis buffer (Thermofisher Scientific, UK). Thereafter, cells were counted using trypan blue and a haemocytometer, resuspended in 1ml of Cryostor CS10 (Stemcell Technologies, UK), placed on ice for 10 minutes and then placed in a CellCool cell storage container (Biocision, US) for graduated cell freezing and then placed in a freezer at -80°C for cryopreservation. Cells were stored at a range of concentrations from 1 – 10 million cells/ml.

3.2.5 Immunophenotyping of mononuclear cells using multicolour flow cytometry

Frozen cells were thawed in a water bath at 37°C for 1 minute, before washing cells in un-supplemented RPMI 1640 medium and counting the cells using a haemocytometer. Cells were then resuspended in 500µl of phosphate buffered saline (PBS) before incubation with viability dye in the dark, at 4°C for 30 minutes. After washing the cells with 1ml of flow cytometry staining buffer (FACS buffer, eBioscience, UK), the cells were resuspended in 100µl of FACS buffer (at a concentration of no more than 1x 10^7 cells/ml) and a pre-made cocktail of mouse anti-human antibodies labelled with fluorescent markers according to the panel (see Appendix). Samples were incubated at 4°C for 30minutes in the dark, before washing in FACS buffer and acquiring the samples on a BD FACS Fortessa machine. Compensation was undertaken to minimise spectral overlap, using Ultracomp eBead compensation beads (Life Technologies, UK) – one drop of beads was added to 100µl of FACS buffer and 1µl of each antibody used in

the panel was added, using separate tubes for each fluorochrome. These were incubated in the dark for 30mins at 4^{o}C, in the same way as the samples, before washing with 1ml of FACS buffer and resuspending in 100µl of FACS buffer in order to run the samples on the machine prior to running the samples.

Panels were designed with support from BD biosciences to minimise spectral overlap and optimisation was undertaken to determine the optimal volume of antibody to use per test (using both healthy PBMCs and extracted liver mononuclear cells) and calculating staining indices using a range of volumes of added antibody. The Fortessa was optimised before every run using cytometer setup and tracking beads to ensure optimal performance.

The panel designed allowed for gating to identify monocytes according to the DR-exclusion gating strategy (Abeles *et al.*, 2012) and macrophages in a similar fashion to that used by Bernsmeier *et al.,*(Bernsmeier *et al.*, 2018). This panel included CD14 (PE-Cy7, BD Biosciences UK), CD16 (APC-H7, BD Biosciences, UK), HLA-DR (BV510, BD Biosciences, UK), MerTK (APC, R&D Systems, UK) and Axl (AF488, R&D Systems, UK). The viability dye was Alexa-Fluor 700, (BD Biosciences, UK). A lineage marker included CD3, CD15, CD19, CD56 on PerCP Cy 5.5 (all BD Biosciences, UK). Two separate panels with this same common 'backbone' were devised in order to analyse a wide range of markers of co-expression using available channels on Red, Blue and Violet lasers of the BD LSR Fortessa machine (BD Biosciences, UK).

To accurately quantify the proportion of positive cells for each marker, an FMO (fluorescence minus one) was generated for each antibody added to the cocktail, using surplus cells of the same type as those being studied. FMOs were generated for all markers of interest at every run

of samples. Cell samples from tissue were filtered through a 35μm filter when added to polystyrene FACS tubes to help clear any debris and prevent the machine blocking.

3.2.6 Preparation of tissue homogenates

Snap frozen tissue taken at the time of diagnostic sectioning and stored in liquid nitrogen was utilised for generating tissue homogenates. Frozen samples were cut into pieces of weight less than 0.05g (or as close as possible to this), and into cubes of approximately 5mm in width where feasible, using liquid nitrogen chilled scalpels to cut tissue. To minimise contamination, sterile equipment was used and the process undertaken in a sterilised hood within the laboratory. Samples were then weighed.

A sterilised and UV irradiated steel bead and 1.5ml of PBS with Halt Protease Inhibitor Cocktail (Thermofisher Scientific, UK) was added to 2ml eppendorfs; to this, the snap frozen tissue chips were added. Tissue was then homogenised by placing sealed eppendorfs onto TissueLyser II (Qiagen, Manchester, UK) at 30Hz for 2 minutes. Tissue homogenate was centrifuged at 12000rpm for 10 minutes, the supernatant collected and placed into a new Eppendorf before centrifugation once more at 12000rpm for 5 minutes and collection of the supernatant. All steps were undertaken with the tissue and reagents kept on ice between steps to minimise activity of endogenous proteases. Protein in the samples was quantified using the bicinchoninic acid (BCA) assay reagent (Thermofisher Scientific, UK). Briefly, a serial dilution of bovine serum albumin (BSA) in PBS was created and incubated at 37^{o}C for 30 minutes with BCA reagent, generating a colour change which was read using plate reader Fluorostar Optima at 650nm. Using this standard curve, unknown protein concentration values for tissue homogenate samples could be interpolated. Homogenates were spun at 12000rpm for

2 minutes and the supernatant passed through a 35µm filter to remove any debris, before use in assays. Homogenates were stored in liquid nitrogen before use in assays.

3.2.7 Serum and homogenates – enzyme linked immunosorbent assay

ELISA was undertaken according to manufacturers' instructions. The following ELISA kits were used, which were purchased pre-coated: Galectin-3, Gas-6 (both Invitrogen, Thermofisher Scientific, UK) and Pros-1 (ELISAGenie, UK). For homogenates, optimisation was undertaken using two dilutions (1:1 and 1:5) to ensure optimal readings of analyte concentrations. Samples were run in duplicate and the plate read at 450nm on the Multiskan Go plate reader using SkanIt software (Thermo Fisher Scientific, USA). Using the standard dilutions, a sigmoidal log/log 4-PL curve was generated and interpolated using GraphPad Prism v. 8.0 software.

3.2.8 Tissue dissociation, RNA extraction and cDNA synthesis, quantitative PCR

Tissue dissociation

A method outlined by the manufacturer, Qiagen, was followed (RNEasy Mini kit, Qiagen, Germany). Snap frozen tissue was weighed and cut using the method outlined in 3.2.6, with a maximum weight of 0.03g. Tissue pieces were kept on dry ice until the process of tissue homogenisation and RNA extraction could proceed, to minimise endogenous RNAse activity. In summary, tissue was added to a lysis buffer (RLT Buffer) and homogenised using a hand-held pestle and mortar (Cole-Parmer, St Neots, UK) and by passing through a QIAShredder homogeniser column (Qiagen, Germany). The lysate was centrifuged and DNA and RNA precipitated by adding an equal volume of 70% ethanol to the supernatant collected after centrifugation. Precipitate was collected onto RNEasy spin columns and an on-column DNAse digestion was performed by adding pre-formed DNAse and incubating for 15 minutes at room

temperature. After two washing steps using buffer RPE (Qiagen, Germany), the precipitated and purified RNA was collected in RNAse free water and stored at -80ºC until needed for use.

cDNA synthesis

For qPCR (quantitative polymerase chain reaction), cDNA was then generated from the extracted RNA. Briefly, extracted RNA was thawed and kept on ice. PCR tubes were irradiated and the process undertaken in a PCR hood. RNA was added to a mix containing RNAse free water, oligonucleotide primers and deoxynucleoside triphosphate nucleotides (dNTPs). Annealing was allowed by incubating at 65oC for 5minutes before incubation on ice. To this, dithiothreitol (DTT; a reducing agent to help release disulfide bonds on RNA to allow binding of primers), first strand buffer (all Thermofisher Scientific, UK) and an RNAse inhibitor was added before incubating at 37ºC for 2 minutes. Thereafter, reverse transcriptase MMLV was added and thermal cycling undertaken to generate cDNA: 37ºC (15 minutes), 70ºC (15minutes) before cycling down to 4ºC and storage at -20ºC.

Quantitative PCR

Multiplex PCR was performed, using TaqMan primers for genes of interest on fluorophore FAM and housekeeping gene GAPDH on VIC as an internal control. cDNA was added to Taqman 2X mastermix (Thermofisher, UK) which contains DNA polymerase and dNTPs, RNAse and DNAse free water. To this mix, primers for the gene of interest and GAPDH were added and briefly centrifuged. Samples were then processed on a StepOne Plus Real-Time PCR System (Life Technologies, UK) with a preset programme: cDNA was initially denatured at 95ºC for 5 minutes before cycling 40 times between 95ºC for 30 seconds and 60ºC for 1 minute.

3.2.9 Statistical Analysis

Flow cytometry data was analysed using FlowLogic software version 6.0 (Inivai, USA). Given the sample sizes, non-parametric statistical analyses were undertaken to compare groups by surface expression by MFI or %+ve, using Mann-Whitney or Wilcoxon matched pair signed rank test, depending on if an unpaired or paired analysis was required. Kruskal Wallis testing was employed for multiple group comparisons. Similar methods were employed to compare patient demographic and disease parameters between groups, and Chi-squared analysis used to compare categorical data between groups. Non-parametric Spearman correlation analysis was undertaken between recognised disease parameters (such as serum alpha-fetoprotein and MELD score) with markers of interest.

For quantitative PCR, the difference in cycle threshold values between the gene of interest and housekeeping gene GAPDH was measured for each sample (d(CT)). An average d(CT) for non-diseased liver was calculated taken as a baseline. This baseline value was subtracted from d(CT) values for each sample in each tissue group (background liver and tumour) and termed dd(CT). Fold change was calculated using $-\log_2(\text{dd(CT)})$.

3.3 RESULTS

3.3.1 Patient characteristics

The characteristics and clinical parameters of the patients in whom immunophenotyping of extracted mononuclear cells from tissue was analysed by flow cytometry was undertaken is outlined in Table 3.1. There was no statistically significant difference between the control cases and the HCC cases in any of the demographic or clinical parameters measured. It is important to note that both groups contained patients with and without cirrhosis; the ratio of non-cirrhotic cases in each group was not statistically different by Fisher's exact test (p=0.704). There was a higher MELD score in the control population than in the cases with HCC (MELD score 24.5 vs 10, p=0.01). This group contained patients undergoing transplantation for non-HCC related issues, who will have more advanced liver disease. Cases were of a varied aetiology and they were predominantly BCLC stage A, in keeping with the population of patients who are eligible for resection or transplantation. There was no significant difference in the distribution of aetiologies by Chi-squared testing (p=0.063). There was a wide range of tumour sizes; two of the cases were not included in this range as they had multiple lesions.

Variable	Non-HCC Liver n = 12	HCC Liver n = 15	p-value
Age, yrs [range]	57 (43 – 68)	58 (45 – 82)	0.495[c]
Sex [M:F]	7:5	10:5	0.706[a]
Cirrhotic: Non-cirrhotic	7:5	7:8	0.704[a]
Aetiology (if cirrhotic)			
Alcohol	5	2	
NAFLD	1	3	
Viral	0	5	
A1AT	0	1	
PBC	1	0	
Dual aetiology	0	1	
Sporadic	-	3	0.063[b]
BCLC Stage (HCC)			
0	-	1	
A	-	13	
B	-	1	
C	-	0	-
AFP [IU/ml]	-	8.5 (2 – 10618)	-
Tumour Size [mm]	-	47 (15 - 140)	-
Platelet count [x10^9/ml]	130 (61 – 310)	223 (60 – 594)	0.378[c]
Bilirubin (μmol/L)	78 (7 – 326)	16 (4 – 122)	0.341[c]
INR	1.25 (0.91 – 3.11)	1.18 (0.98 – 2.01)	0.642[c]
MELD Score (if cirrhotic)	24.5 (16 – 30)	10 (6 – 21)	**0.01**[c]

Table 3.1: Clinical and physiological characteristics of patients whose liver and tumour tissue were used for extraction of mononuclear cells and to generate tissue homogenates

Abbreviations: HCC = hepatocellular carcinoma, NAFLD = non-alcoholic fatty liver disease, PBC = primary biliary cholangitis, A1AT = alpha-1 antitrypsin deficiency, BCLC = Barcelona Clinic Liver Cancer, AFP = alpha-fetoprotein, IU = international units, MELD = Model for End-Stage Liver Disease, INR = international normalised ratio. Statistical tests used: [a]Fisher's Exact test, [b]Chi-square test, [c]Mann-Whitney U test, [d]Kruskal-Wallis test. Values are written as median with [range].

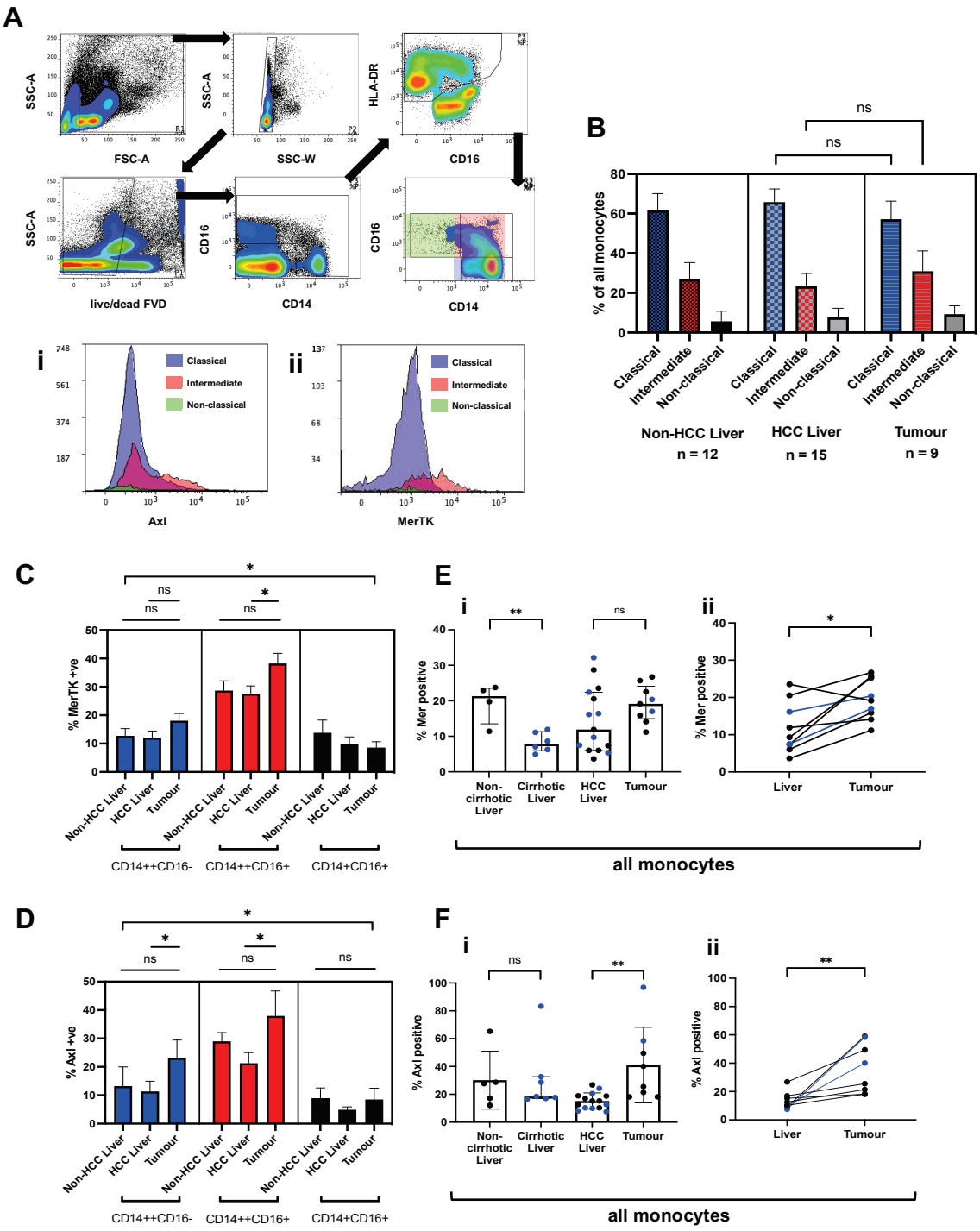

Figure 3.1 Tissue derived monocyte phenotype from patients with HCC reveals an expansion of MerTK and Axl expression on intermediate monocytes and an enrichment in the tumour microenvironment

(A) Schematic of 'HLA-DR exclusion' gating strategy used to identify monocytes; overlays demonstrating the differential surface expression of Axl **(i)** and MerTK **(ii)** in the three sub-populations **(B)** total monocyte subset proportions were similar between groups. **(C)** & **(D)** illustrate surface MerTK and Axl expression, respectively, across the monocyte subsets demonstrating enrichment of expression both in the intermediate subset and in tumour derived intermediate monocytes. Total monocyte MerTK and Axl positivity between the groups is also highlighted in **(E)** and **(F)** respectively; paired analysis of n=8 tumour:liver pairs demonstrated a stronger correlation between tissue and liver TAM-RTK surface expression **(E ii)** and **(F ii)**. In E and F, blue data points represent cirrhotic cases. *Statistical tests – non-parametric analysis was used. For continuous data, group comparisons were made using Mann-Whitney U test (for two groups) or Kruskal Wallis Test when three groups were compared. Paired analysis was by Wilcoxon test; *=p<0.05, **=p<0.01, ns=non-significant.*

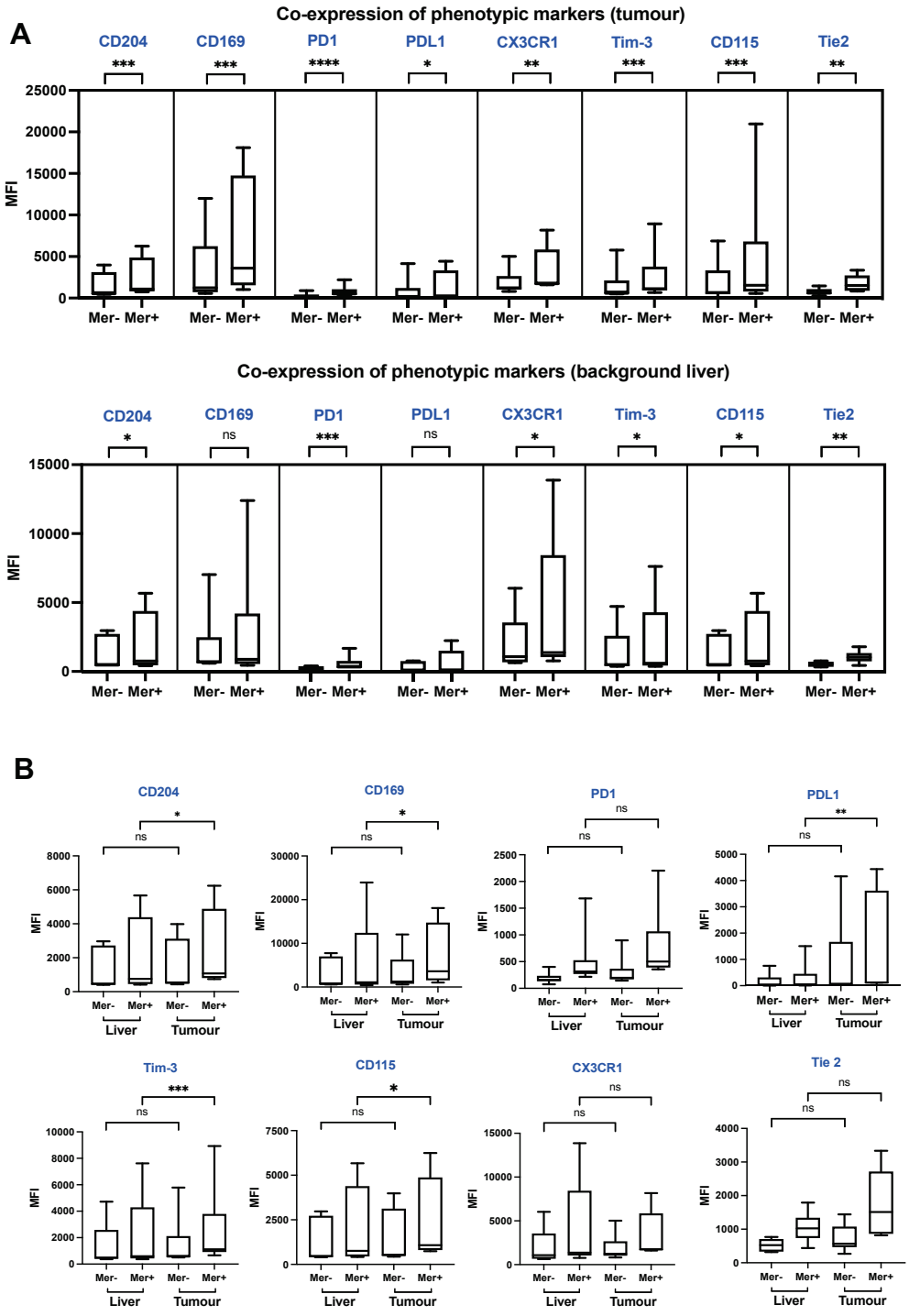

Figure 3.2 Tissue MerTK+ monocyte from patients with HCC co-express higher levels of key tumour associated macrophage markers, some of which are enriched within tumour derived monocytes

(A) MerTK+ tumour and liver derived monocytes were assessed for co-expression of a range of key phenotypic markers **(B)** Surface expression (by MFI) was compared between tumour and liver derived macrophages (MerTK+ve and MerTK-ve) from the same patients. *Statistical tests – non-parametric analysis was used. Box and whisper plots represent median and interquartile ranges respectively. For continuous data, group comparisons were made using Mann-Whitney U test (for two groups). Paired analysis was by Wilcoxon test; *=p<0.05, **=p<0.01, ***=p<0.001, ****=p<0.0001, ns=non-significant. Abbreviations: MFI – median fluorescence intensity; Mer = MerTK. Markers of interest are labelled in blue above each graph.*

3.3.2 TAM receptor tyrosine kinase surface expression is higher on CD14++CD16+ intermediate monocytes

Tissue monocytes and their subsets were identified using the established DR-exclusion gating strategy (Abeles et al, 2012), Fig 3.1A. Fluorescence minus one (FMO) controls were used for all markers to ascertain the gates for positive expression of MerTK and Axl on monocytes and their subsets. Median fluorescence intensity of co-expressed markers on positive and negative populations were compared.

Analysis from 28 patients was undertaken (15 patients with HCC; and 12 control cases). Most monocytes were of the classical subset (CD14++CD16-) across the control cases (63.6%), background liver (66.1%) and tumours (56.4%). Intermediate monocytes comprised 26%, 24.9 and 26.5% of the total in these groups respectively; there was a trend towards an increase in intermediate monocytes in tumour tissue but this was not statistically significant ($p = 0.186$); the proportion of non-classical monocytes in tumour monocytes was also higher (median 10.5% vs 7.3%) but this was not statistically significant ($p = 0.0979$), Fig 3.1 B.

For MerTK, surface expression was highest within the intermediate subset of monocytes (median 29.89% compared with 13.44% on classical monocytes and 9.47% on non-classical monocytes in all samples analysed; $p = 0.0189$ in Kruskal-Wallis test, Fig 3.1 C). For Axl, a similar pattern was noted, with median 23.81% positive in the intermediate subset of monocytes, with 13.05% and 6.8% respectively in the classical and non-classical monocyte subsets (Kruskal Wallis p-value 0.0135 Fig 3.1 D).

Surface Axl positivity on intermediate monocytes was highest in tumour samples (median 37.9%) and was significantly higher than in HCC liver (21.2%, $p=0.0407$). Surface MerTK

positivity was highest on intermediate monocytes from tumour samples (median 39.4%) and was significantly higher than in HCC liver (27.8%, p=0.0350).

3.3.3 Tissue infiltrating monocytes expressing MerTK and Axl are expanded in the tumour environment in HCC

When looking at total monocyte population, the percentage of Axl+ monocytes was significantly higher in tumour derived monocytes when compared with background liver (32.83% vs 15.26% respectively, p = 0.0013, Fig 3.1 C). This pattern was replicated with MerTK+ monocytes, however it did not meet statistical significance – 19.16% of tumour derived monocytes MerTK+ compared with 11.91% in background HCC liver; p=0.1693, Fig 3.1 D. Paired analyses were undertaken of tumour monocytes with background liver from the same case. When analysed in this manner, there was a significant increase in the percentage of monocytes positive for both Axl (32.83% vs 11.48% Axl+; p=0.0078) and MerTK (19.16% vs 9.31% MerTK+; p=0.0195).

3.3.4 MerTK+ and Axl+ monocytes co-express phenotypic markers of a tumour-associated macrophage phenotype

When the whole tumour monocyte population is analysed, both MerTK+ and Axl+ monocytes express higher amounts of all markers assessed (by MFI) when compared with their MerTK- and Axl- counterparts (Fig 3.2A, 3.3A). These include those typically associated with tumour associated macrophages, such as CD204 (MerTK p=0.0128; Axl p=0.0039), CD115 (MerTK p=0.0128; Axl p=0.0038) and CD169 (MerTK p=0.0003, Axl p=0.0026), and with a monocyte derived macrophage phenotype e.g. CX3CR1 (MerTK p=0.0038).

When comparing tumour MerTK+ and Axl+ monocytes with their counterparts from HCC liver, only MerTK has a tumour specific phenotype, with significant but modest increases in

PDL1 (p=0.0312), Tim-3 (p=0.007), CD204 (p=0.0312) and CD169 (p=0.0106). Indeed, in Axl+ tumour monocytes there was a non-significant decrease in all of these markers, by comparison (Fig 3.2 B, 3.3B).

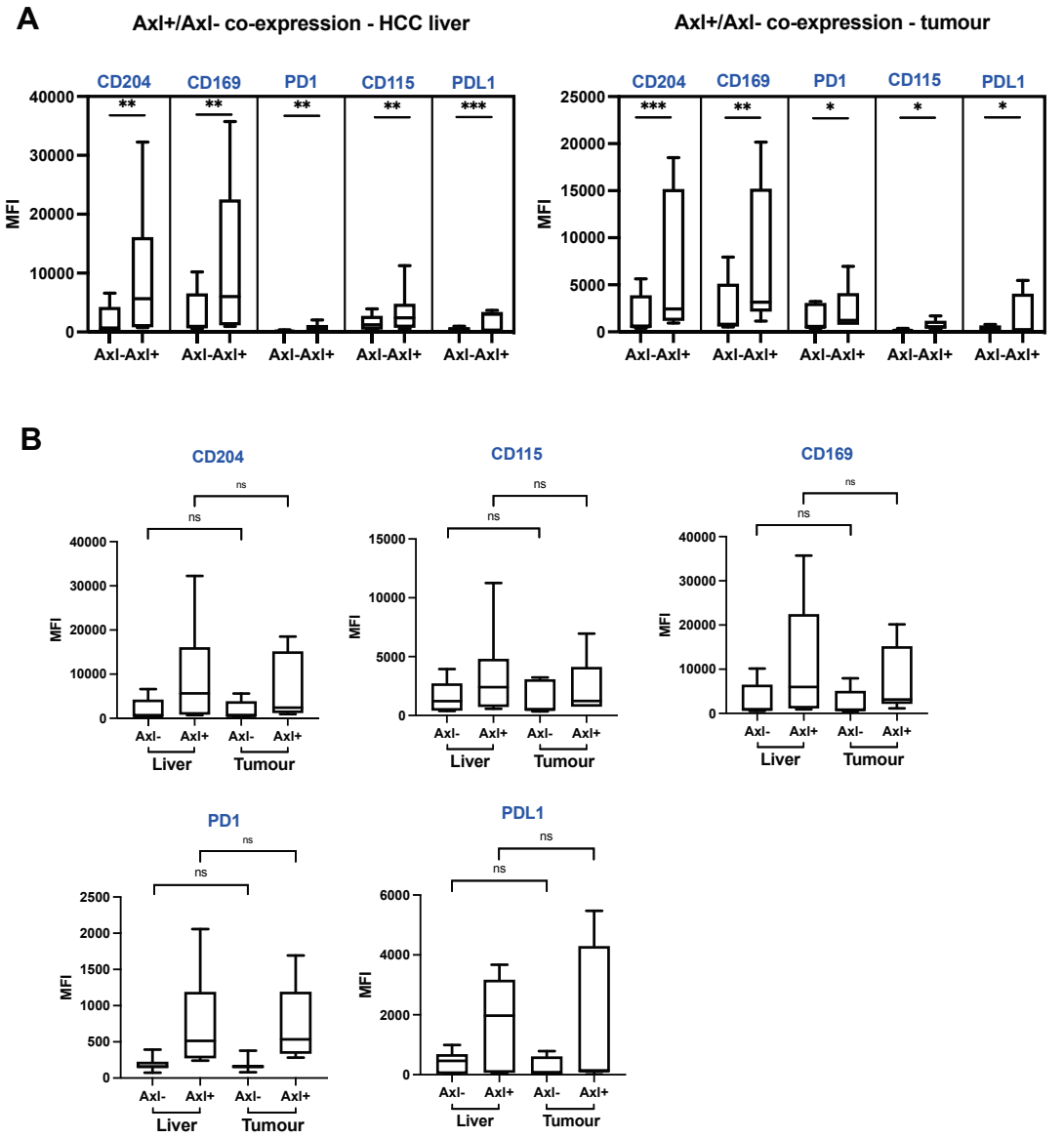

Figure 3.3 Tissue Axl+ monocyte from patients with HCC co-express higher levels of key tumour associated macrophage markers, some of which are enriched within tumour derived monocytes

(A) Tumour and liver derived monocytes were assessed for co-expression of a range of key phenotypic markers, comparing the Axl+ and Axl- monocyte populations **(B)** Expression levels (by MFI) were compared, in Axl+ve macrophages, between tumour and liver derived macrophages from the same patients. *Box and whisper plots represent median and interquartile ranges respectively. Statistical tests – non-parametric analysis was used. For continuous data, group comparisons were made using Mann-Whitney U test. Paired analysis was by Wilcoxon test; *=p<0.05, **=p<0.01, ***=p<0.001, ns=non-significant. Abbreviations: MFI – median fluorescence intensity. Markers of interest are labelled in blue above each graph.*

3.3.5 Macrophages express higher MerTK and Axl than myeloid derived suppressor cells and possess a tumour specific phenotype

Extracted mononuclear cells were stained using a separate panel of markers to identify both tumour and liver resident macrophages. Given the heterogeneity of resident liver macrophage populations, using a broad panel with common macrophage markers allowed for all populations to be captured and analysed: macrophages were defined as CD14+, Lineage (CD3/CD19/CD56/CD15)–, HLA-DR+. A similar strategy was employed by Bernsmeier *et al.* in circulating monocytes in liver disease, with the CD14+, Lineage (CD3/CD19/CD56/CD15)– HLA-DR– population defined as myeloid derived suppressor cells (Bernsmeier *et al.*, 2018). The gating strategy employed is outlined in Fig 3.4A.

The majority of CD14+Lineage– cells were DR+ (Fig 3.4 B) and although raw percentage values were small, there were significantly less CD14+Lineage–DR- cells in the tumour tissue when compared with the background liver (1.34% vs 4.52%, p=0.0154). MerTK and Axl surface expression by MFI in CD14+Lineage-HLA-DR+ cells was significantly higher when compared with CD14+Lineage-DR- cells (MerTK p=0.012; Axl p=0.0001, Fig 3.4 C). This pattern was seen when both background liver (MerTK p=0.0308; Axl p=0.018) and tumour macrophages (MerTK p=0.031; Axl p=0.0139) were compared with the CD14+Lineage-HLA-DR- cells separately (Fig 3.4 D).

CD14+Lineage-HLA-DR+ macrophages from all tissues were assessed for expression of markers reflecting differentiation (CD163 and CD204 reflecting M2, or alternative activation state), function (Tie-2) or a tumour associated phenotype (PD1, PDL1, CD169, CD115 and Tim-3). The results are presented in Figure 3.5. As would be expected, tumour derived CD14+Lineage-DR+ macrophages had an enriched expression of markers associated with

tumour associated macrophages, with significant increase in the proportion of macrophages in the tumour expressing CD163 (56.1% vs 33.9%; p=0.0138), CD204 (65.4% vs 48.1%; p=0.0409), PD1 (13.7% vs 6.9%; p=0.021), PDL1 (23.7% vs 11.2%; p=0.015) and Tim-3 (58.4% vs 43.1%; p=0.0155) when compared with background HCC liver. Tumour derived macrophages did not have a significant increase in all TAMϕ markers, however: CD169 (53.4% vs 41.8%; p=0.217) and CD115 (51.9% vs 40.6%; p=0.202) surface expression was not increased in this sample.

Resident macrophages from cirrhotic livers had increased expression of CD163 (56.1% vs 33.9%; p=0.0138) and Tie-2 (74.2% vs 39.1%; p=0.044) when compared with non-cirrhotic liver.

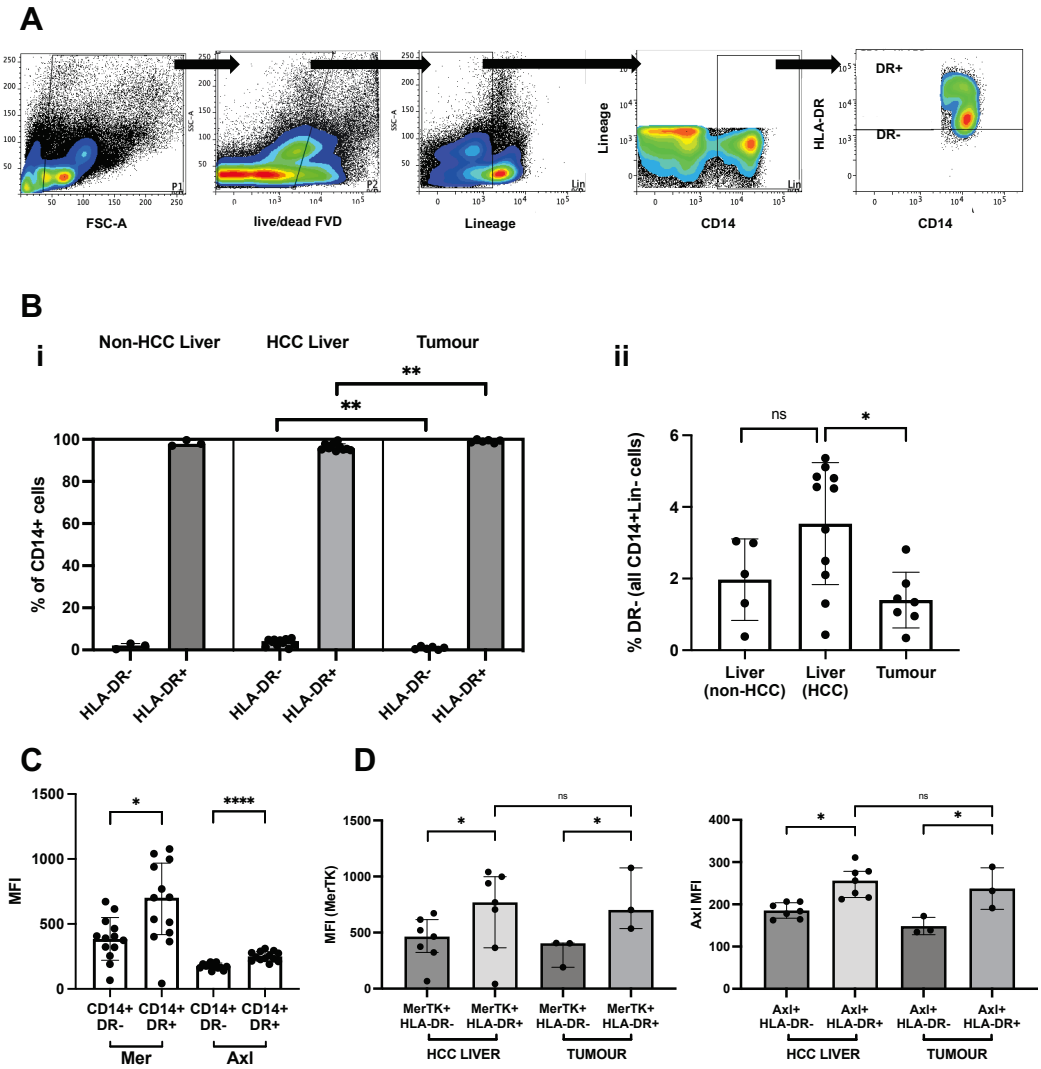

Figure 3.4 Tissue macrophage and myeloid derived suppressor cell (MDSC) phenotyping in HCC:

A small minority are MDSCs and HLA-DR+ macrophages are enriched in the tumour; TAM-RTK expression is higher on macrophages than MDSCs in both compartments. The gating strategy employed to isolate macrophages and MDSCs is demonstrated in **(A);** 12 HCC cases, 7 tumours and 5 non-HCC controls were phenotyped. **(B)** The percentage of CD14+ cells that were macrophages (HLA-DR+) and MDSCs (HLA-DR-) across tissue type and disease state shows that the overwhelming majority are macrophages, but that these are further enriched in the tumour tissue. **(C)** MerTK and Axl surface expression by MFI is higher in the HLA-DR+ macrophage population than the MDSCs across both TAM-RTKs and in both liver and tissue samples. *Statistical tests – non-parametric analysis was used. For continuous data, group comparisons were made using Mann-Whitney U test. Paired analysis was by Wilcoxon test; *=p<0.05, **=p<0.01, ***=p<0.001, ****=p<0.0001, ns=non-significant. Abbreviations: MFI – median fluorescence intensity.*

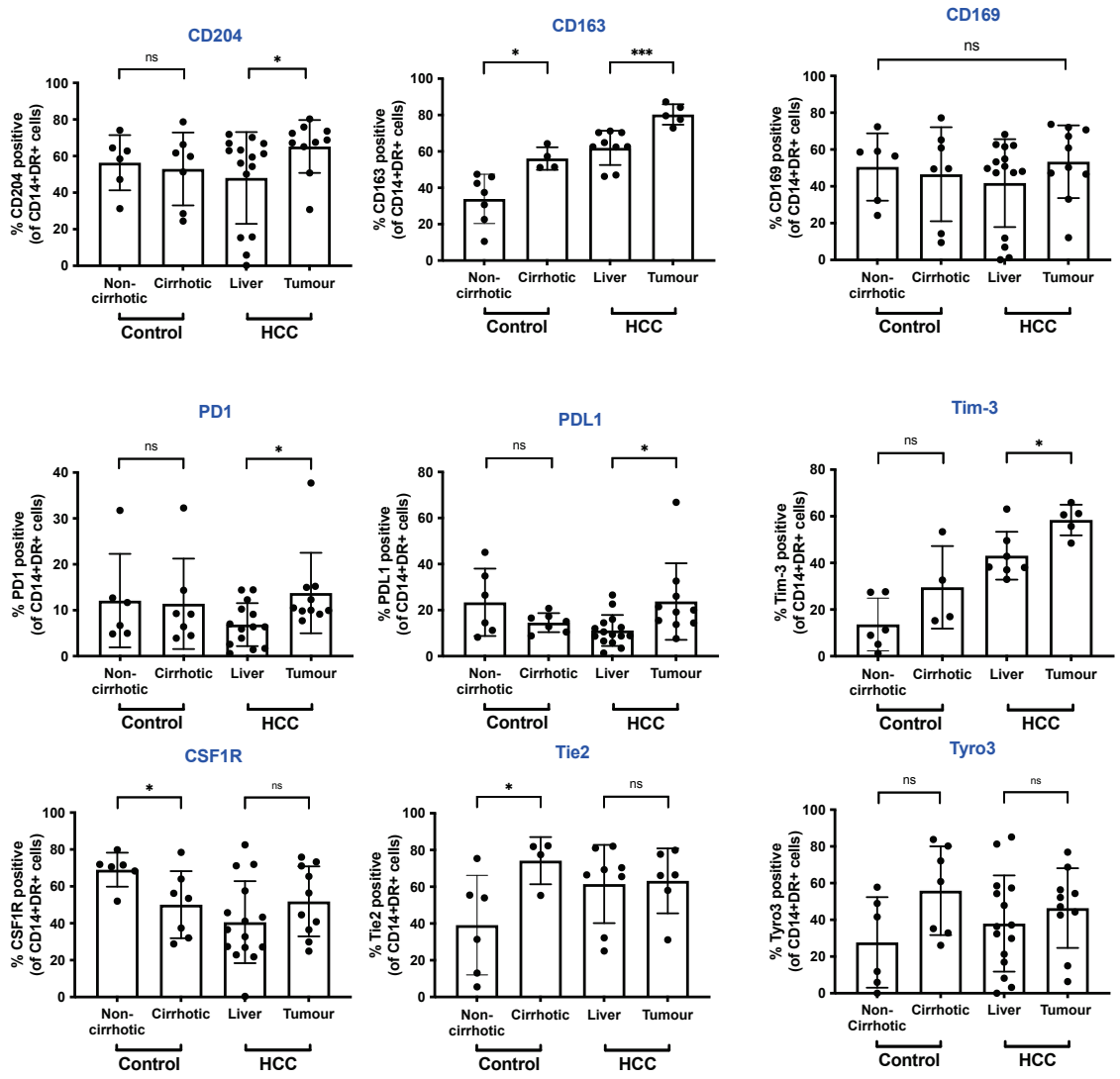

Figure 3.5 Tissue macrophage immune phenotyping in hepatocellular carcinoma

Tumour associated macrophages (isolated using the gating strategy outlined in Figure 3.4) express well-established markers of an M2-like TAMϕ phenotype (CD204 and CD163) and immune checkpoint molecules PD1, PDL1 and Tim-3. *Statistical tests – non-parametric analysis was used. Group comparisons were made using Mann-Whitney U test. *=p<0.05, ***=p<0.001, ns=non-significant. Graphs are labelled with the phenotypic marker of interest in blue. Abbreviations: TAMϕ – tumour associated macrophage*

3.3.6 An *HLA-DRhi* macrophage subset is expanded in hepatocellular tumours

Note was taken of the impression of two sub-populations within CD14+Lin-DR+ macrophages, when gated by HLA-DR surface expression (Fig 3.6 A, final panel on right). A significant increase in the proportion of macrophages with a 'CD14+Lin-DRhi' phenotype was identified in samples derived from tumour when compared with either control or background

liver macrophages (81.8% vs 58.3%; p=0.0007, Fig 3.6B). Furthermore, 'CD14+Lin-DR^{HI}' macrophages express significantly higher surface MerTK and Axl when compared with 'CD14+Lin-DR^{LO}' macrophages in the same tissue (MerTK p<0.0001; Axl p=0.0017). However, when comparing tumour derived DRHi macrophages with DRHi macrophages from background HCC liver, a more complex picture emerged. Tumour resident DRHi macrophages had a trend towards *decreased* MerTK expression (MFI 831 vs 656; p=0.246, Fig 3.6C), as well as a reduction in M2-like markers including Tie-2 (MFI 84.3 vs 78.8; p=0.057), CD163 (MFI 83 vs 75; p=0.133) and PD-1 (MFI 17.2 VS 7.3), Fig 3.6D. Conversely, there was a trend towards an increase in Axl (MFI 309 vs 235; p=0.23) and PD-L1 (MFI 17.2 vs 7.2; p=0.0187) expression when the same two populations were compared.

Taken together, these results may help to explain why despite an enrichment of the CD14+Lineage-DRHi macrophage phenotype in the tumour environment (which has a higher surface expression of MerTK by MFI than both CD14+Lineage-DRlo and CD14+Lineage-DR- cells from the same tissue), overall surface expression of MerTK not significantly elevated in all tumour derived macrophages (Fig 3.4D); however the expression levels are low across all of these markers. Axl surface expression was very variable, and this may explain the lack of a significant elevation in Axl expression in all macrophages despite the findings within sub-populations.

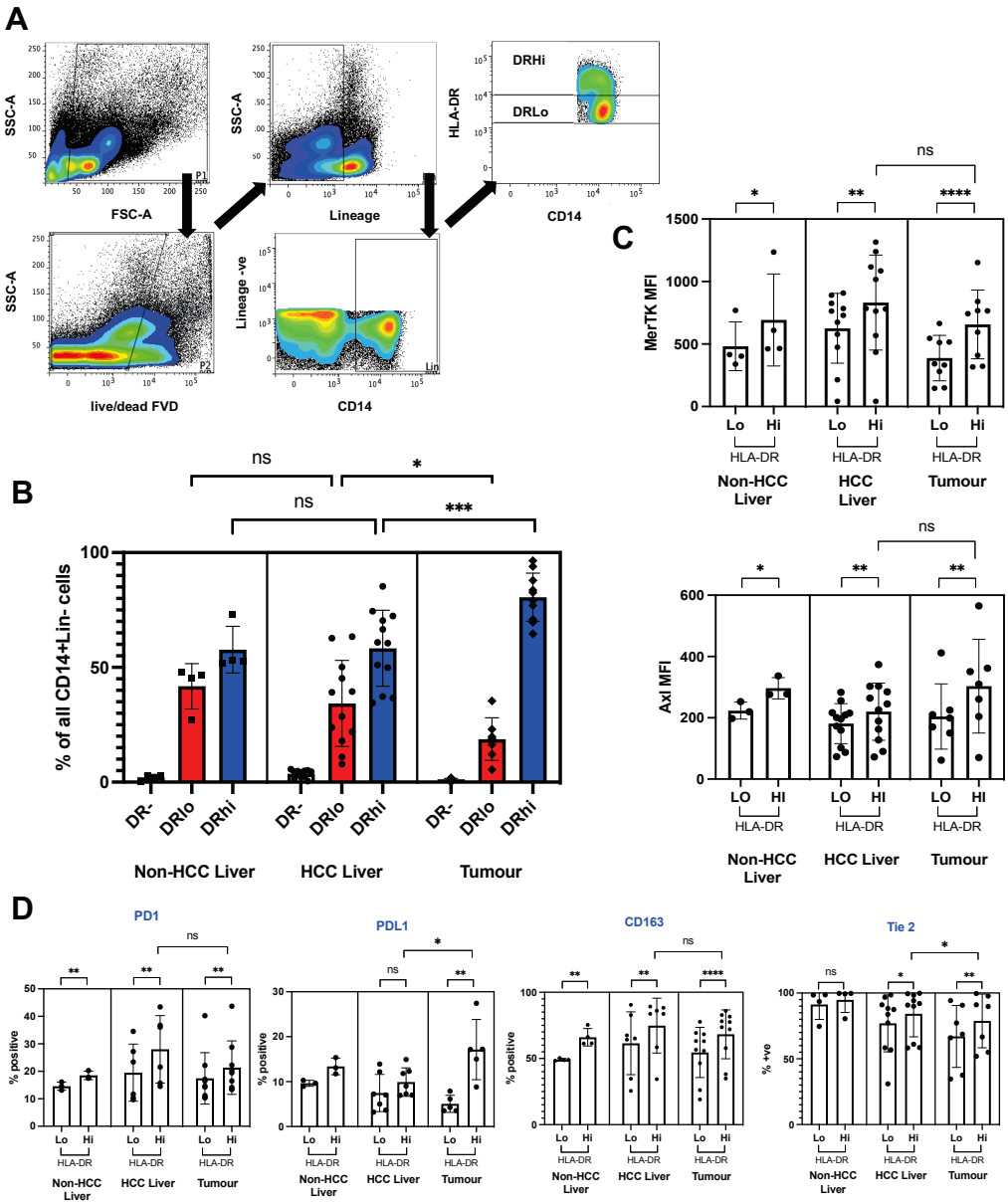

Figure 3.6 An HLA-DR-high expressing subset of macrophages is enriched in the tumour microenvironment in HCC

(A) The gating strategy employed to isolate macrophages and delineate HLA-DR-High and HLA-DR-Low populations is outlined **(B)** HLA-DR expression levels across the three tissue compartments were compared **(C)** MerTK and Axl surface expression by MFI is higher in the HLA-DR-High when compared with HLA-DR-Low populations from the same tissue. **(D)** A similar pattern is seen with other phenotypic markers, with higher surface positivity in HLA-DR-High populations. *Statistical tests – non-parametric analysis was used. For continuous data, group comparisons were made using Mann-Whitney U test. *=p<0.05, **=p<0.01, ***=p<0.001, ****=p<0.0001, ns=non-significant. Abbreviations: MFI – median fluorescence intensity, Lin- = lineage negative.*

3.3.7 Circulating monocyte MerTK and Axl phenotype is not altered in patients with hepatocellular carcinoma

Peripheral blood mononuclear cells were analysed from patients with HCC (n=34) and compared with those with chronic liver disease and cirrhosis, but without HCC (n=11), and with healthy volunteers (n=13). Figure 3.7 summarises the findings, and Table 3.2 outlines the clinical characteristics of the patients recruited. A small minority of cases (n = 2) analysed were patients with HCC without cirrhosis – these non-cirrhotic cases are highlighted as blue points on the graphs, alongside healthy volunteers. Most monocytes are of the classical subset (87.4% in healthy controls); ratios of monocyte subsets were not significantly different between the three groups analysed (p=0.1409, Kruskal-Wallis Test). There was no statistically significant increase in MerTK or Axl positive monocytes in patients with HCC when compared with patients with cirrhosis (MerTK – 14.72% in HCC vs 14.59 in cirrhosis, p=0.6828; Axl – 6.1% in HCC vs 5.7% in cirrhosis, p=0.8917 Fig 3.7 B, C). This persisted when non-cirrhotic HCC cases were excluded from analysis (p= 0.6828, Mann-Whitney test). A stepwise increase in both MerTK and Axl expression across the three groups was noted, and in both instances, this reached significance when comparing monocytes from patients with HCC with healthy volunteers, however the relevance of this is limited given the confounding factor of cirrhosis in the majority of cases.

In keeping with previous published data on analysis of monocyte subsets, MerTK expression was highest on intermediate monocytes (Triantafyllou *et al.*, 2018). MerTK positive intermediate monocytes were not significantly expanded in patients with HCC when compared with those with cirrhosis (57.81% vs 57.12%, p=0.99). Regarding Axl expressing monocytes, in healthy patients Axl expression was highest on non-classical monocytes, but in cirrhosis and HCC intermediate monocytes had the highest surface expression of Axl, and there was a significant increase in Axl+ intermediate monocytes when compared with Axl+ classical

monocytes in HCC (22.34% vs 13.81%, p=0.0291) which was not seen in cirrhotic patients (11.96% vs 4.02%, p=0.222). Circulating monocyte surface expression of both MerTK and Axl did not correlate with serum alpha-fetoprotein (MerTK: r=0.21, p=0.77; Axl r=-0.12, p=0.48) (Fig 3.7 C, D).

3.3.8 Other phenotypic markers are not altered in patients with hepatocellular carcinoma

Other phenotypic markers in circulating monocytes were assessed to ascertain if there was an HCC specific circulating phenotype. A panel of markers related to varied aspects of myeloid function in the hepatic environment were analysed, including homing to liver tissue (CCR2 and CCR5 (Korf *et al.*, 2018)), vascular patrolling and angiogenesis (CX3CR1 and Tie-2) and markers of macrophage differentiation including CD163, CD206, CD301 and CD115. There is evidence that circulating monocytes can traffic through liver parenchyma, acquire markers of macrophage differentiation and reverse migrate back into the circulation in liver disease (Bernsmeier *et al.*, 2015). As such, macrophage differentiation markers may help to evaluate if this is a feature of the behaviour of monocytes in HCC.

Across this panel (see Figure 3.8), there were no significant differences in the markers assessed. However, there was a trend towards an increase in M2-like macrophage marker CD206 (67.2% in HCC vs 52.4% in chronic liver disease, CLD; p=0.1895). CD301 was significantly expanded in cirrhosis and HCC (74.9% in cirrhosis vs 26.1% in non-cirrhotic controls, p=0.0159). CD163, another notable M2-like marker was reduced in both cirrhosis and HCC (5.5% in cirrhosis, 11.4% in healthy controls, p=0.0159)

Variable	Healthy Controls	Cirrhotic Controls	HCC		p-value
			Cirrhotic	Non-cirrhotic	
Number	13	11	34	3	-
Age, yrs [range]	40 [27 – 54]	62 [52 – 73]	69 [33 – 81]	66 [45 – 68]	<0.0001[a]
Sex (M:F)	6:7	8:3	25:9	2:1	0.4495[b]
Aetiology:					
Alcohol	-	7	9	-	
NAFLD	-	2	7	1	
Viral	-	0	10	1	
Autoimmune	-	1	1	-	
Dual aetiology	-	1	3	-	
Other/Sporadic	-	0	4	1	0.1312[b]
AFP (IU/ml)	-	-	9.5 [2 – 32767]	116 [2 – 678]	0.5138[c]
Tumour Size (mm)	-	-	35 [13 – 220]	25.5 [21 – 30]	0.5929[c]
BCLC Stage (HCC)					
0	-	-	4	0	
A	-	-	22	2	
B	-	-	7	0	
C	-	-	1	1	0.128[b]
Platelet count ($x10^9$/ml)	-	164 [60 – 230]	119 [64 – 735]	171 [108 – 184]	0.8683[a] *(0.759[c])*
Bilirubin (µmol/L)	-	15 [8 – 36]	15.5 [3 – 132]	11 [6 – 18]	0.6037[a] *(0.691[c])*
INR	-	1.2 [1.0 – 2.2]	1.15 [0.91 – 2.11]	1.03 [0.93 – 1.08]	0.119[a] *(0.953[c])*
MELD Score (if cirrhotic)	-	10 [6 – 15]	9 [6 – 17]	-	0.792[c]

Table 3.2: Clinical and physiological characteristics of patients whose peripheral blood was utilised to characterise circulating monocyte phenotype
Abbreviations: HCC = hepatocellular carcinoma, NAFLD = non-alcoholic fatty liver disease, AFP = alpha-fetoprotein, IU = international units, MELD = Model for End-Stage Liver Disease, BCLC = Barcelona Clinic Liver Cancer, INR = international normalised ratio. Statistical tests used : [a]Kruskal-Wallis test, [b]Chi-square test, [c]Mann-Whitney U test. Values are written as median with [range]. **These p-values are for Mann-Whitney tests comparing medians between cirrhotic controls and cirrhotic HCC cases i.e.. without adding the non-cirrhotic HCC group into the comparison.*

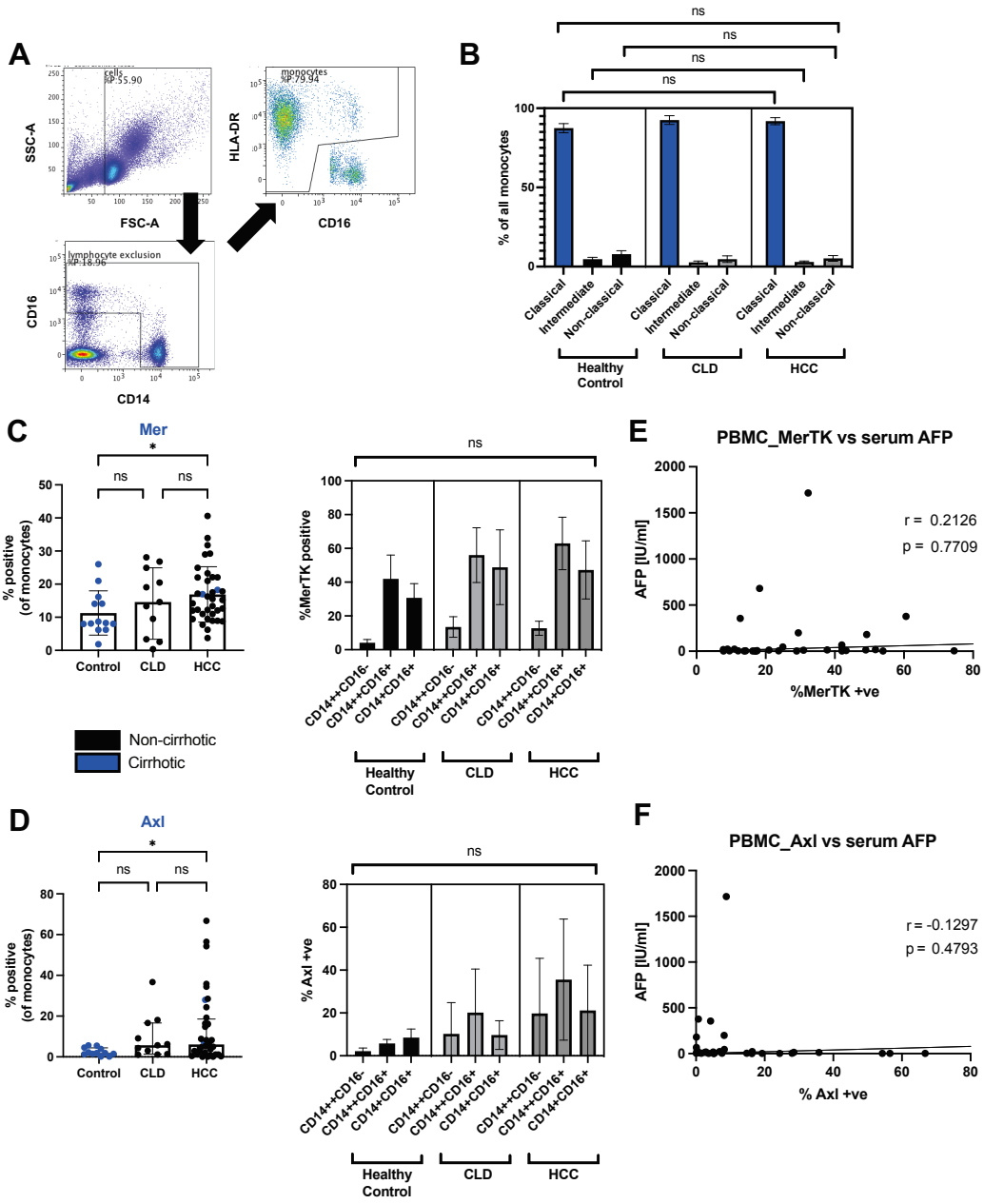

Figure 3.7 Peripheral monocyte MerTK and Axl phenotype in HCC

(A) The gating strategy employed was the same as for the tissue monocytes, and an abbreviated version is presented here **(B)** The majority of monocytes are of the classical subtype and there was no significant difference between the sub-populations across diseased cases and control groups – n=13 non-cirrhotic controls, n=12 people with cirrhosis and n=36 cases with HCC **(C)** MerTK expression was higher on circulating monocytes in patients with HCC, but not when compared with cases with cirrhosis and without HCC. Intermediate monocytes have the highest MerTK expression **(D)** A parallel analysis of Axl on monocytes is presented. In both cases, non-significant correlations between circulating monocyte MerTK or Axl expression and AFP were identified. *Statistical tests – non-parametric analysis was used. For continuous data, group comparisons were made using Mann-Whitney U test. Correlation analysis was performed using Spearman Rank correlation co-efficient in view of sample size. *=p<0.05, ns=non-significant. Abbreviations: AFP – alpha-fetoprotein; CLD – chronic liver disease; FSC – forward scatter; IU – international units; PBMC – peripheral blood mononuclear cells; SSC – side scatter*

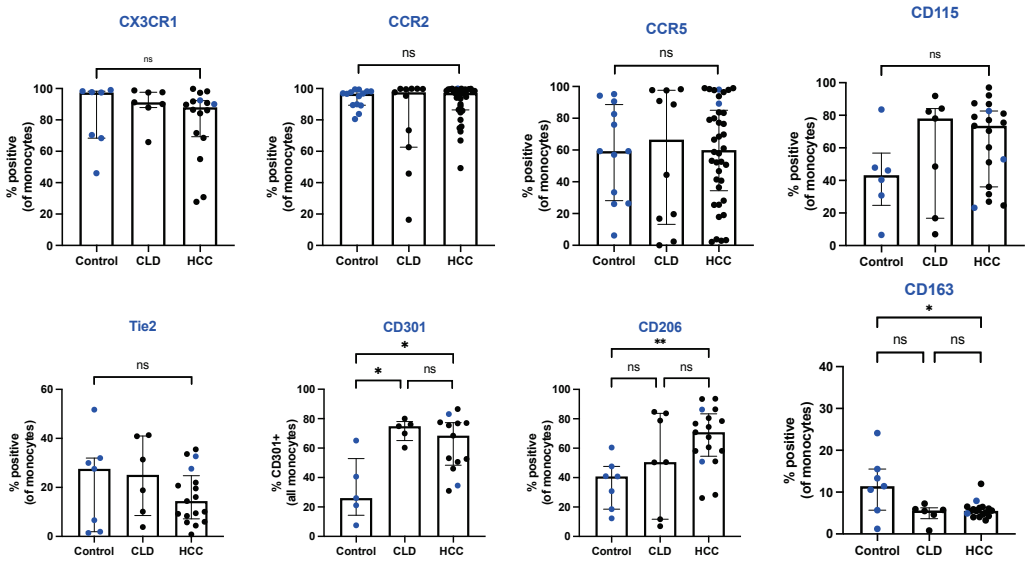

Figure 3.8 Peripheral monocyte MerTK and Axl phenotype in HCC

Circulating monocytes were assessed for expression of a range of phenotypic markers in parallel with MerTK and Axl. *Statistical tests – non-parametric analysis was used. For continuous data, group comparisons were made using Mann-Whitney test or Kruskal Wallis test. *=p<0.05, ns=non-significant. Abbreviations: CLD: chronic liver disease, HCC: hepatocellular carcinoma*

3.3.9 Circulating myeloid derived suppressor cells are expanded in both cirrhosis and in hepatocellular carcinoma and are predominantly MerTK-

Circulating myeloid derived suppressor cells were quantified and characterised (Figure 3.9). MDSCs are often associated with poor prognosis. There was a significant expansion of MDSCs in both cirrhosis and in patients with HCC (20.7% and 24.7% in cirrhosis and HCC respectively, Figure 3.9 B), but there was no significant difference between the two groups. The majority of CD14+Lineage-DR- cells are MerTK negative across all groups (median <1% for both cirrhosis and HCC, Figure 3.9d). There was no significant correlation between MDSC abundance in the circulation and circulating AFP in this small sample.

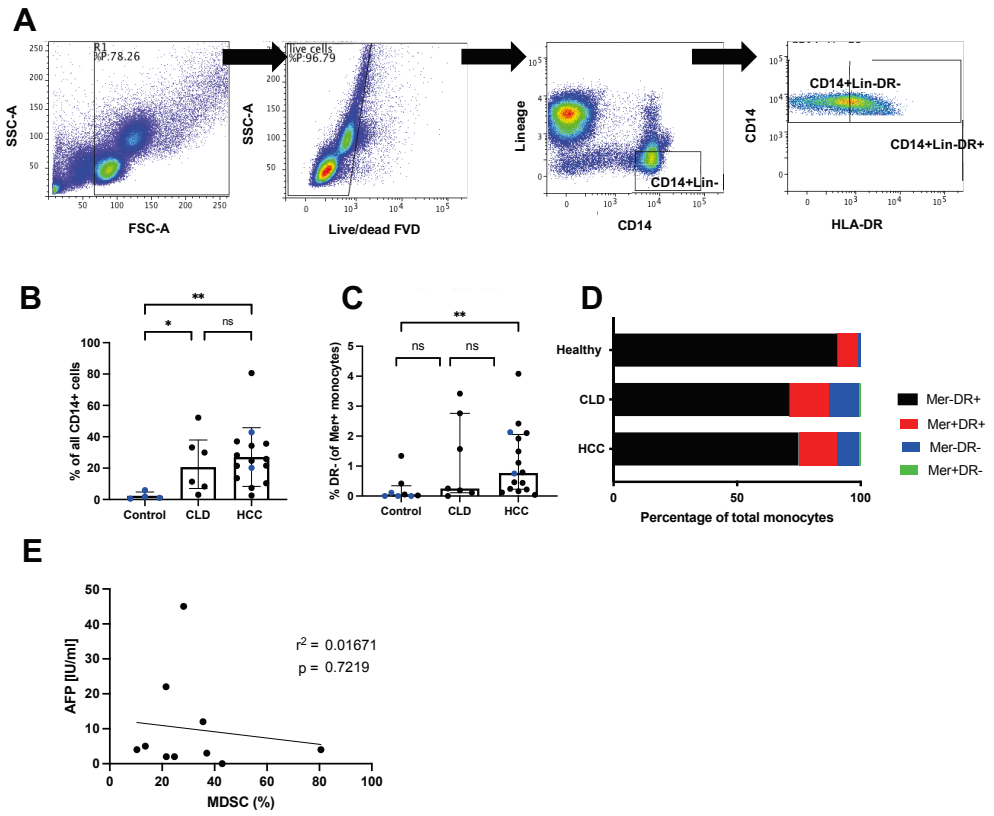

Figure 3.9 The phenotype and abundance of circulating myeloid derived suppressor cells in HCC

(A) A similar gating strategy used for tissue macrophages and myeloid derived suppressor cells was used to quantify and characterise circulating MDSCs in patients with HCC and relevant controls. **(B)** the relative frequencies of MDSCs are presented, with an increase in both chronic liver disease and in patients with HCC. **(C)** There is a small increase in MerTK+ MDSC's in both CLD and HCC, without a significant difference between the two groups. **(D)** The majority of MDSCs are not MerTK positive. **(E)** Serum AFP did not correlate with the abundance of MDSCs in patients with HCC. *Statistical tests – non-parametric analysis was used. For continuous data, group comparisons were made using Mann-Whitney U test or Kruskal Wallis test. *=p<0.05, **=p<0.01, ns=non-significant. Abbreviations: AFP= alpha-fetoprotein, CLD = chronic liver disease, FSC - forward scatter, Lin- = lineage negative, MFI – median fluorescence intensity, SSC – side scatter*

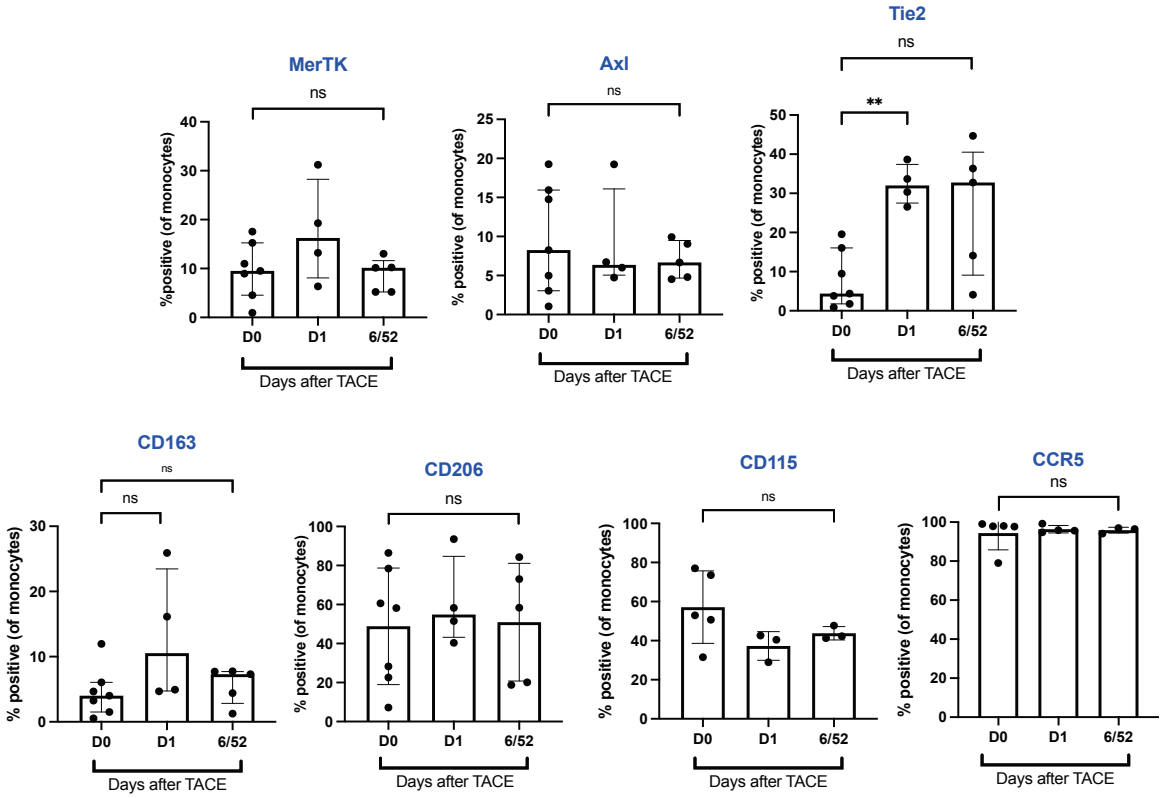

Figure 3.10 Monocyte phenotype after chemoembolization is not significantly or durably altered in patients with HCC

Total monocyte phenotype in patients with HCC undergoing chemoembolisation was characterised. All patients analysed were chemoembolisation naive. Blood was sampled on the day of the procedure (D0), at 24 hours after (D1) and at follow-up 6 weeks later (labelled 6/52). Surface expression of TAM-RTK's and Tie-2 were assessed, as well as markers of tissue homing including CCR5 and macrophage differentiation including CD163, CD206 and CD115 (CSF1R). *Statistical tests – non-parametric analysis was used. For continuous data, group comparisons were made using Mann-Whitney U test or Kruskal Wallis test. *=p<0.05, ns=non-significant. Abbreviations: TACE = transarterial chemoembolisation.*

3.3.9 Tie-2 expression on circulating monocytes is increased after locoregional therapy but TAM receptor tyrosine kinase surface expression is unchanged

Phenotypic analysis of monocytes before and after chemoembolisation did not detect a significant or persistent change in the proportion expressing either MerTK or Axl, or of a range of other markers assessed in this small sample; the phenotype after locoregional therapy is highlighted in Figure 3.10. All cases analysed were in those who were undergoing chemoembolisation for the first time. However, Tie-2 expressing monocytes were elevated at 24hrs after embolization (32% positive on day 1; 4.4% before embolization; p=0.00681). The durability of this phenotypic change was not observed, however, and at 6 weeks there was no

longer a statistically significant elevation in Tie-2 expressing monocytes in patients after therapy, although there was a wide variety in expression at this point.

3.3.9 Tissue concentrations of TAM receptor tyrosine kinase ligands are not significantly elevated in the tumour microenvironment or the circulation

Analysis of tissue homogenates for the presence of ligands for both Axl and MerTK signalling did not show a significant increase in the tumour microenvironment. Figure 3.11 shows the levels of the three key TAM-RTK ligands measured in tumour and liver homogenates from patients with HCC; their clinical details are outlined in Table 3.3. In all three cases, tumour levels of these ligands did not correlate significantly with circulating levels of AFP, but there was a positive correlation between serum AFP and tumour Gas-6. This did not reach statistical significance, however (r^2=0.287, p=0.089). For ligands galectin-3 and protein S, serum and tumour levels did not correlate significantly with each other, either (Figure 3.11 C).

Circulating levels of Galectin-3 and Pros-1 were also measured in a sample of patients and healthy controls. The patient characteristics and clinical parameters of the patients are outlined in Table 3.4; there was no significant difference in any of these parameters between the HCC cases and the pathological control group with cirrhosis and without HCC. Once more, no significant difference was seen between the groups for circulating levels of both Galectin 3 and for Pros-1.

Trial ID	Age (years)	Sex	Aetiology	Tumour Size (mm)	Treated	BCLC Stage	AFP [IU/ml]	Bilirubin (μmol/l)	Platelets (x10^9/ml)	INR	MELD
SHCC23	60	M	Sporadic	180	N	A	30	11	401	1.4	n/a
SHCC26	57	M	Sporadic	240	N	A	32	10	594	1.04	n/a
SHCC47	51	M	ARLD	44	N	A	3	122	86	1.73	21
SHCC53	82	F	Sporadic	57	N	A	78	5	252	1.02	7
SHCC64	45	F	A1AT	100	N	A	442	8	339	1.03	6
SHCC70	79	M	ARLD	23	N	A	2	7	154	1.15	11
SHCC72	57	M	NAFLD	26	Y	A	1	12	107	1.24	9
SHCC77	71	F	ARLD	18	Y	A	3	25	139	1.12	9
SHCC84	81	M	Sporadic	65	N	A	14	29	199	1.17	11
SHCC92	69	M	HFE	40	N	A	2	8	278	1.06	7
SHCC94	59	M	HCV(SVR)	37	N	A	7	9	245	1.02	7
Median (Range) / Ratio	60 (45 – 82)	8:3 (M:F)	-	44 (18 – 240)	2:9 N:Y	-	7 (1 – 442)	10 (5 – 122)	245 (86 – 594)	1.12 (1.02 – 1.73)	9 (6 – 21)

Table 3.3: Clinical parameters and characteristics of cases of HCC in which tissue (tumour and liver) homogenates were extracted

n=12 cases were processed. Median values (range) are highlighted for each parameter; ratios are provided for categorical data. Abbreviations: *HCV (SVR)=hepatitis C virus (sustained virological response), A1AT=alpha-1 antitrypsin deficiency, NAFLD=non-alcoholic fatty liver disease, ARLD= alcohol related liver disease, AFP=alpha-fetoprotein, MELD=Model for End-Stage Liver disease. INR = international normalised ratio, BCLC = Barcelona Clinic Liver Cancer, HFE = hereditary HFE haemochromatosis*

Variable	Healthy Volunteer	Cirrhosis	HCC	p-value
Number	5	11	25	-
Age, yrs [range]	54 (51 – 69)	61 (50 – 72)	65 (45 – 84)	0.229[a]
Sex [M:F]	2:3	9:2	20:5	0.140[b]
Aetiology				
Alcohol	-	10	9	
NAFLD		1	6	
Viral	-	0	2	
A1AT		0	1	
Sporadic	-	0	2	
Dual aetiology	-	0	5	0.086[b]
BCLC Stage (HCC)				
0	-	-	1	
A	-	-	20	
B	-	-	4	
C	-	-	0	-
AFP [IU/ml]	-	-	9 (2 – 33429)	-
Tumour Size [mm]	-	-	39 (17 – 100)	-
Platelet count [x10^9/ml]	-	189 (52 – 301)	154 (42 – 401)	0.886[c]
Bilirubin (μmol/L)	-	18 (8 – 45)	15 (5 – 122)	0.899[c]
INR	-	1.2 (1.0 – 1.9)	1.24 (1.0 – 2.91)	0.832[c]
MELD Score (if cirrhotic)	-	10 (6 – 22)	10 (6 – 22)	0.898[c]

Table 3.4: Clinical and physiological characteristics of cases (and relevant controls) used for ELISA

Abbreviations: HCC = hepatocellular carcinoma, AFP = alpha-fetoprotein, IU = international units, NAFLD = non-alcoholic fatty liver disease, A1AT = alpha-1 antitrypsin deficiency, BCLC = Barcelona Clinic Liver Cancer, INR = international normalised ratio, MELD = Model for End-Stage Liver Disease. Statistical tests used: [a]Kruskal-Wallis test, [b]Chi-square test, [c]Mann-Whitney U test, Values are written as median with [range].

Variable	Non-HCC Liver n = 11	HCC Liver n = 12	p-value
Age, yrs [range]	56 (43 – 68)	57 (50 – 82)	0.457[a]
Sex [M:F]	7:4	9:3	0.667[b]
Cirrhotic: Non-cirrhotic	6:5	6:6	>0.999[b]
Aetiology (if cirrhotic)			
Alcohol	3	4	
NAFLD	1	2	
Viral	0	2	
Sporadic	0	3	
PBC	1	0	
PSC	1	0	
Dual aetiology	0	1	0.288[c]
BCLC Stage (HCC)			
0	-	1	
A	-	11	
B	-	0	
C	-	0	-
AFP [IU/ml]	-	6 (2- 78)	-
Tumour Size [mm]	-	44 (11 – 140)	-
Platelet count [x10^9/ml]	175 (61 – 310)	247 (64 – 594)	0.585[a]
Bilirubin (μmol/L)	43 (7 – 326)	15 (4 – 122)	0.520[a]
INR	1.17 (0.91 – 3.11)	1.165 (1.02 – 1.73)	0.925[a]
MELD Score (if cirrhotic)	10 (6 – 30)	9 (6 – 21)	0.093[a]

Table 3.5: Clinical and physiological characteristics of cases used for qPCR

Abbreviations: HCC = hepatocellular carcinoma, AFP = alpha-fetoprotein, IU = international units, NAFLD = non-alcoholic fatty liver disease, A1AT = alpha-1 antitrypsin deficiency, PBC = primary biliary cholangitis, PSC = primary sclerosing cholangitis, BCLC = Barcelona Clinic Liver Cancer, AFP = alpha-fetoprotein, INR = international normalised ratio, MELD = Model for End-Stage Liver Disease. Statistical tests used: [a]Mann-Whitney U test, [b]Fisher's exact test, [c]Chi-square test. Values are written as median with [range].

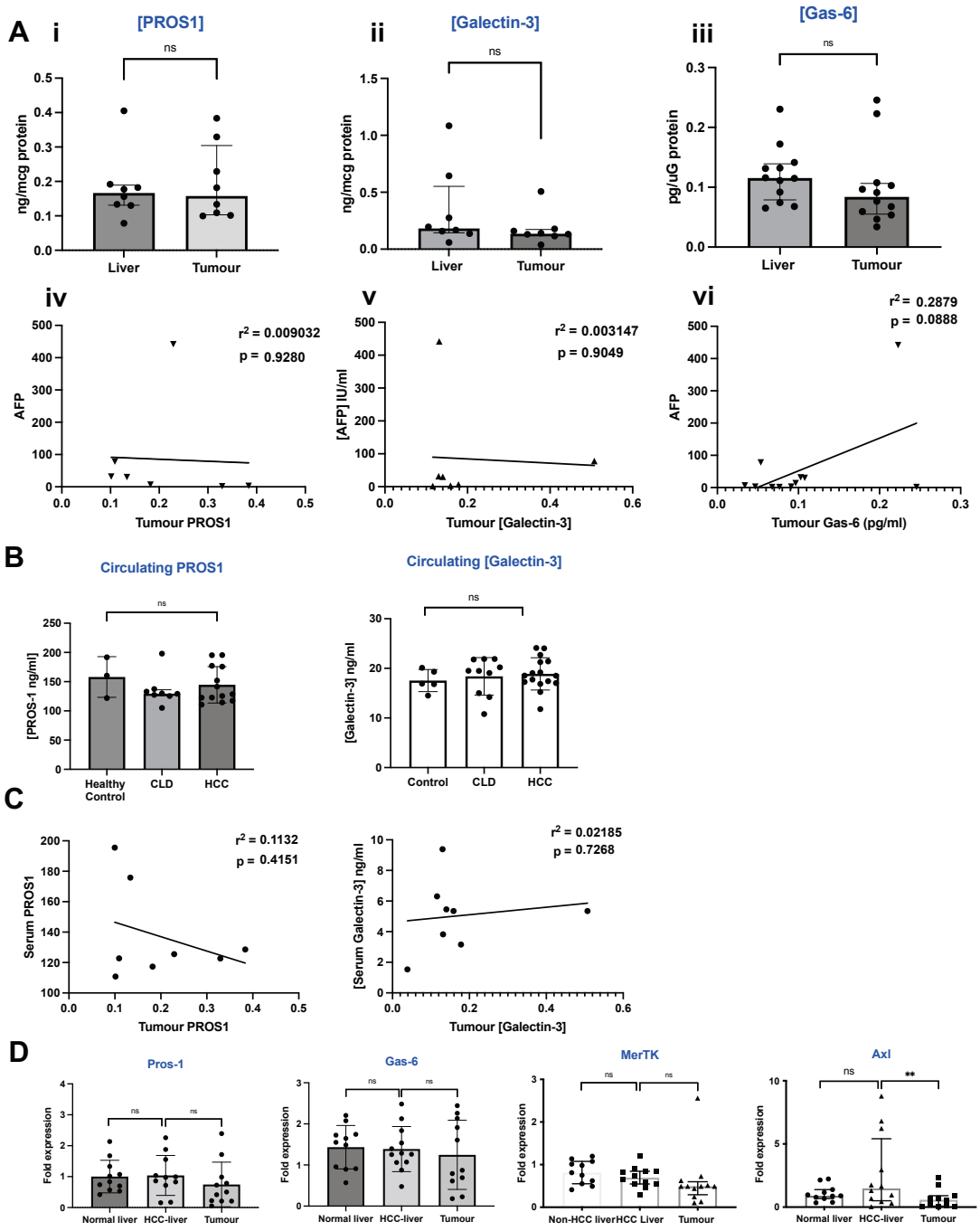

Figure 3.11 Circulating and tissue levels of TAM-RTK ligands, measured by both ELISA and quantitative PCR are not significantly elevated in the tumour microenvironment or in the circulation in patients with HCC

(A) Tumour and paired liver homogenates (n=8) from patients with HCC were analysed for levels of the 3 main TAM-RTK ligands – Protein S (also known as Pros1), Galectin-3 and Gas-6 by ELISA **(i – iii)**. Analyte levels were normalised to tissue protein content. Tissue levels of all analytes were plotted against serum alpha-fetoprotein to assess for correlation with TAM-RTK ligand expression **(iv – vi)**. **(B)** Circulating levels of Pros1 and Galectin-3 were also quantified by ELISA of serum samples: n=5 healthy volunteers, n=12 pathological controls (cirrhosis without any HCC) and n=13 patients with HCC. **(C)** Circulating and intra-tumoural levels of Galectin-3 and Protein S were assessed for correlation between the levels within each compartment **(D)** Tissue expression of MerTK, Axl and both Protein S and Gas-6 (another key TAM-RTK ligand) was quantified by qPCR.

PCR data is presented as fold change in expression compared with the average background expression from control liver samples.
*Statistical tests – non-parametric analysis was used. Group comparisons were made using Mann-Whitney U test (2 datasets) or Kruskal Wallis test (>2 datasets). For paired analysis, Wilcoxon testing was used. Correlation was assessed using the Spearman rank correlation co-efficient. **=p<0.01, ns=non-significant. Abbreviations: AFP= alpha-fetoprotein, PROS1 = protein S.*

3.3.10 Tissue expression of both TAM receptor tyrosine kinase receptors and their key ligands is not enriched within the tumour environment

Tissue expression of both MerTK and Axl was assessed by quantifying extracted RNA from both tumour and liver from cases of n=12 cases of HCC and compared with non-HCC liver controls (n=11). The clinical and demographic characteristics of each group is compared and outlined in Table 3.5. There was no differential expression of either receptor between pathological control tissue or surrounding liver of those with HCC. Pathological control samples included livers from patients with cirrhosis but without HCC (n=6), or those with no parenchymal liver disease who were undergoing resection for either a benign lesion (n=2), for metastatic deposit from colorectal malignancy (n=3). Furthermore, there was a trend towards a reduction in the expression of both TAM-RTKs in the tumour tissue, with a significant reduction in the expression of Axl in the tumour when compared with surrounding liver (p=0.020). Levels of key ligands Pros-1 and Gas-6 were similarly not increased in either HCC background liver or tumour tissue.

These findings were surprising, given the histological evidence of abundant Axl expression on tumour parenchyma seen by immunohistochemistry. RNA extraction and purity was checked using spectrophotometry prior to cDNA synthesis. The reduced RNA in the tumour may be a result of a reduced ability to extract RNA from the tumour tissue after homogenisation, as RNA was not normalised to tissue weight. However, it was cirrhotic liver that was the most challenging to homogenise by mechanical means, not the tumour tissue.

3.4 DISCUSSION

Immunophenotyping of intrahepatic and circulating mononuclear cells isolated from fresh tissue specimens and peripheral blood in human HCC has allowed for further interrogation of both macrophage and monocyte TAM-RTK phenotype in patients with hepatocellular carcinoma. Using established monocyte and macrophage gating strategies, both populations have been evaluated for TAM-RTK expression, co-expression of key immunophenotypic markers, the proportions of key functional subsets and the proportion of myeloid derived suppressor cells.

Tissue monocyte phenotype

The total tumour monocyte population has an expansion of both Axl and MerTK, although the latter only achieves statistical significance upon paired analysis. The majority of intra-hepatic and intra-tumoural monocytes are of the classical subtype, with approximately a quarter being of the intermediate subtype. Although not reaching statistical significance, there was a modest expansion of intermediate monocytes in intra-tumoural monocytes. For both MerTK and Axl, surface expression was highest on intermediate monocytes and significantly higher on intra-tumoural intermediate monocytes when compared with intra-hepatic intermediate monocytes. For Axl, a significant expansion of Axl+ cells was also seen in classical monocytes, resulting in a modest but significant expansion of Axl positive monocytes overall.

Increased TAM-RTK expression on intermediate monocytes has been described previously: work from within our group demonstrated elevated MerTK in this population in both circulating and intrahepatic monocytes (Triantafyllou *et al.*, 2018). The proportion of MerTK+ intermediate monocytes in patients with cirrhosis in that work was around 30%, and is comparable with the data from this study, where approximately 30% of intermediate

monocytes are MerTK positive in both HCC and non-HCC control liver samples. Intermediate monocyte Axl surface expression has not been characterized in the published literature and this study provides some insights into this. Brenig *et al.*, characterised Axl expression on all circulating monocytes in cirrhosis. These cells composed between 10% to 20% of the total monocyte population in compensated cirrhosis (Brenig *et al.*, 2019). This proportion compares favourably with the circulating Axl+ total monocyte percentage seen in this study (median 18.48%). Axl+ monocytes in Brenig *et al.*, have elevated HLA-DR and CD16 co-expression: a similar profile of increased HLA-DR has been described in circulating (Asmussen *et al.*, 2021) and in hepatic intermediate monocytes (Liaskou *et al.*, 2012) and was noted when originally described: Loms Ziegler-Heitbrocken *et al.* reported elevated HLA-DR and CD16+ expression (Loms Ziegler-Heitbrockon *et al.*, 1993). Taken together, these data support our observation that tissue Axl+ monocytes are enriched within intermediate monocytes; consistent with Axl+ monocytes described in Brenig *et al*. The circulating phenotype described in our study differs, however, without an enrichment of intermediate monocytes. The reasons for this are not immediately clear.

Samples were cryopreserved and thawed before batch analysis, which may have impacted upon the proportions of the monocyte subsets characterized in this study, for both PBMCs and for tissue extracted mononuclear cells. Samples collection and cell extraction was undertaken at King's College Hospital; however, flow cytometry was performed at St Mary's Hospital. Specimens were often obtained late in the afternoon after surgery and cell extraction often completed out of hours. As a result, cryopreservation allowed for storage and transport of cell samples before batch staining and analysis. There is data to suggest that freeze-thaw cycles can disproportionately affect intermediate monocytes in peripheral blood monocytes (Rundgren *et al.*, 2018), with the median percentage dropping from 2.4% to undetectable levels after

cryopreservation. This process may have reduced the proportion of intermediate monocytes observed and the total percentage of all monocytes positive for either MerTK or Axl.

Work by Liaskou et al. has shed light on the functional importance of the intermediate monocyte population in liver disease. They demonstrate that this population is recruited from the circulation, differentiates within tissue in response to microenvironmental cues including TGF-β and IL-10, can behave in a plastic fashion with either macrophage or dendritic cell fates and secretes pro-fibrogenic and pro-inflammatory cytokines including TNF-α, IL-6, IL-Iβ, CCL2 and IL-13. These cells have an enhanced capacity to phagocytose and to activate T cells. (Liaskou *et al.*, 2012). In this way, such cells display similar characteristics to M1 differentiated tumour associated macrophages (K. Wu *et al.*, 2020).

It is therefore potentially significant that both MerTK and Axl are most abundantly expressed in this subset of monocytes, and that they are further enriched upon intermediate monocytes from the tumour microenvironment. MerTK and Axl expression on intermediate monocytes could denote a pro-inflammatory, wound healing and resolution phenotype of monocyte in HCC, driven by established triggers for TAM-RTK expression and signalling in the TME. These include issue hypoxia and the presence of apoptotic cells and phosphatidylserine. Hypoxia inducible transcription factors HIF1 and HIF2 directly trigger the transcription of Axl (Rankin *et al.*, 2014).

Other triggers for TAM-RTK signalling and expression include circulating Gas-6 can be overexpressed in solid tumours. Released from endothelial cells after tissue damage (Ekman *et al.*, 2010), it binds to both MerTK and Axl on the myeloid cell surface in the presence of phosphatidylserine and activates signalling (Lemke, 2013). In addition, Galectin-3 has been

found to be upregulated in a number of solid tumours (Newlaczyl and Yu, 2011). However, in this study an elevated level of neither Gas-6 nor Galectin-3 was detected in tumour homogenates when compared with surrounding tissue, when normalized for protein concentration. A similar pattern was also seen when levels of both ligands were normalized by tissue weight. These ligands are therefore not likely to be driving signalling in this context. It has been noted that secretory leucocyte protease inhibitor (SLPI) is another mediator that can promote a MerTK+ phenotype in liver tissue; tumour levels of this mediator would be pertinent to evaluate in further studies.

MerTK+ and Axl+ monocyte co-expression analysis has helped to further elucidate function and relevance in the tumour microenvironment. In keeping with the 'M1- TAMϕ like' phenotypic characteristics of the intermediate monocyte subset described above, tumour resident MerTK+ monocytes have higher surface expression of CD169 (a marker associated with improved outcomes in patients with HCC) when compared with liver monocytes (C. Wu *et al.*, 2020). However, the overall picture is skewed towards a regulatory phenotype: the same MerTK+ population overexpresses several M2- TAMϕ phenotypic markers including CD204, CD115 (also known as CSF1R) and Tim-3. Signalling through CD115 promotes an M2 like phenotype and poor prognosis in HCC (H. Cai *et al.*, 2017). Tim-3 expression has been described on tumour associated macrophages in HCC and is associated with poor survival (Yan *et al.*, 2015). Furthermore, tumour derived MerTK monocytes co-express significantly higher surface PD-L1. PD-L1+ tumour associated macrophages in patients have also been associated with reduced overall survival (W. Zhang *et al.*, 2020).

Axl+ monocytes differ from MerTK, with a reduction in the surface expression in all of these markers, including CD169 when tumour and liver macrophages are compared. None of these

differences met statistical significance, however, and the variability of Axl surface expression seen on all monocytes may be one reason for this finding. Axl+ monocytes are more abundant in the tumour microenvironment (median %+ve 32.83% vs 19.16% for MerTK), however, so their skewing towards a more activated, M1-like phenotype is perhaps more pathologically relevant as a result. Such a reciprocal phenotypic profile may suggest that MerTK+ and Axl+ monocytes may have divergent phenotypes within the tumour microenvironment. Further work is required to determine if this reflects a divergence in function, and the contribution of each to the total myeloid cell milieu.

Co-expression of potentially contradictory phenotypic markers in both MerTK+ and Axl+ tumour derived monocytes could reflect varied phenotypes within different tumour niches and immune contexts. Furthermore, it is now increasingly accepted that a dichotomous 'M1/M2' approach to macrophage phenotype, or even one that places macrophages on a scale between these two distinct cell types, is likely to be inaccurate and misleading, with transcriptomic analyses extending this scale into a network of related subsets (Xue *et al.*, 2014). The finding in this study that M1 and M2 markers can be expressed on the same macrophages has been previously described (Chong *et al.*, 2015). With relation to tumour associated macrophages this dichotomy has been shown to be inaccurate: M2 markers CD163 and CD206 are found on M1 TAMϕs in gastrointestinal tumours, for example (Elliott *et al.*, 2017).

Macrophage Phenotype

Employing a broad gating strategy for macrophages (see paragraph 3.3.5) allowed for the total macrophage population to be assessed, combining sub-populations of differing ontogeny, differentiation and activation state. In doing so, a broad comparison of the tissue compartments

could be undertaken and population wide differences in expression explored. In addition, myeloid derived suppressor cells could be evaluated simultaneously.

In the liver, the majority of macrophages are Kupffer cells, with a minority that derived from circulating monocytes. These are termed monocyte-derived macrophages (MoMFs) and are likely to be derived from intermediate monocytes (Heymann *et al.*, 2015). The contribution of intermediate monocytes to the total tumour myeloid population is not clear, however. As there is no resident population, tumour associated macrophages principally derive from circulating classical monocytes (Olingy *et al.*, 2019) and differentiate in situ. The intermediate monocyte tumour phenotype we describe in this study will most likely have derived from circulating classical monocytes and differentiate in a manner similar to those in the liver (Liaskou *et al.*, 2012); further work is needed to confirm this in a model of hepatocellular carcinoma.

In this study, the overwhelming majority of cells were CD14+Lineage-DR+, with a statistically significant reduction in the percentage of MDSCs in tumour derived macrophages. Comparison of macrophage phenotype between compartments revealed the expansion in the tumour microenvironment of macrophages expressing of 'M2-like' markers including CD204, and CD163 in addition to PD-L1 and Tim-3.

It is important to note that given the small percentage of MDSCs identified using this gating strategy, meaningful flow cytometry analysis using FMOs was difficult to undertake as the event count not high enough to make for reliable evaluation of % positivity. For this reason, total surface expression of MerTK and Axl in MDSCs was measured using mean fluorescence intensity. Finding a reduction in both MerTK expression in myeloid derived suppressor cells is in keeping with previous observations from circulating MDSCs gated in the same manner in

chronic liver disease (Bernsmeier *et al.*, 2018), however this has not been described for Axl before. These data correspond well with the observation that MerTK is a marker of a differentiated M2c macrophage (Zizzo *et al.*, 2012).

Gating on the entire HLA-DR+ population revealed the presence of both 'HLA-DR-high' and 'HLA-DR-low' subsets. Comparative analysis between the two compartments revealed enrichment of HLA-DR-high macrophages within the tumour. These co-express slightly reduced CD163, Tie-2 and PDL1 when compared with the liver derived HLA-DR+ population, although only Tie-2 reached statistical significance. These macrophages could therefore possess an M1, or classically activated tumour associated macrophage (TAMϕ) phenotype. M1 TAMϕs have been described in previous studies and are associated with good prognostic outcomes in patients with solid tumours (Tan et al., Frontiers in Oncology 2020). Given the magnitude of the trends seen, this assumption is not entirely secure and warrants validation in a larger cohort.

The reduced frequency of similar M1-like macrophages in the surrounding liver could reflect the tolerogenic phenotype of Kupffer cells in steady state. Within the liver, variations in HLA-DR expression on macrophages are associated with alterations in function. Kupffer cells express variable levels of MHC Class II antigens, dependent on the environmental context. In steady state, they have a tolerogenic role and induce regulatory CD4+ T cells. However in the setting of liver injury this phenotype alters, with a reduction in surface expression of regulatory phenotypic marker PD-L1, a capacity to induce pro-inflammatory IFN-γ CD4 T cells (Heymann *et al.*, 2015) and higher HLA-DR expression (Triantafyllou *et al.*, 2018).

MerTK and Axl expression is generally higher in these HLA-DR^{HI} subsets, across all groups of macrophages phenotyped. In support of this, gene expression analysis between MerTK- and MerTK+ healthy monocytes by Triantafyllou *et al.* demonstrates significant upregulation of a range of MHC Class II antigens. Furthermore, MerTK+ monocytes in the setting of acute liver injury possess higher HLA-DR than MerTK+ monocytes from healthy patients. This HLA-DR^{hi}, population possessed a reduced expression of M2 phenotypic markers CD163 and CD204 (Triantafyllou *et al.*, 2018) in a similar manner to the trends that we describe in the tumour associated macrophages in this study. Triantafyllou *et al.* define this population as possessing a pro-resolution phenotype, with enhanced efferocytotic and phagocytic capacity.

Tumour derived macrophages exhibited a divergent pattern of surface expression of Axl and MerTK, skewed towards higher Axl+, lower MerTK and an M1- TAMϕ 'like' phenotype. Modulations in MerTK and Axl surface positivity by MFI did not achieve statistical significance, however. It is not clear how MerTK and Axl positive macrophages may functionally differ in the tumour microenvironment, but data from studies in ischaemic reperfusion cardiac injury has shown that Axl+ macrophages can attenuate the pro-resolving functions of MerTK+ macrophages through the release of pro-inflammatory cytokine IL-Iβ (DeBerge *et al.*, 2021). A similar role in the tumour microenvironment may explain the M1-TAMϕ skewing seen in this sample, but further work is needed to test this hypothesis.

Peripheral blood phenotype

Analysis of the peripheral circulation was undertaken to identify a circulating monocyte (PBMC) phenotype in HCC; in particular, one that might echo the intrahepatic monocyte and macrophage TAM-RTK phenotype. PBMCs were noted for the marked reduction in intermediate monocytes, but their frequency in healthy controls is in keeping with comparative

data – classical monocytes typically account for between 85% to 90% of all monocytes and non-classical between 5 to 10% (Wong *et al.*, 2012). In this sample, classical monocytes accounted for 87.4% and non-classical monocytes 7.9%, which is broadly comparable. Patients with chronic liver disease and HCC had a higher proportion of classical monocytes (>90%) and a reduction in both non-classical and intermediate monocytes, which accounted for 2.7% and 2.9% of monocytes in cirrhosis and HCC respectively.

This is a clear difference in the composition of monocytes by their subsets when compared with the intrahepatic populations. Nevertheless, a very slight increase in total MerTK and Axl was seen but it was not statistically significant; this may alter with a larger sample. The percentage of monocytes positive for MerTK and Axl in healthy controls and in compensated cirrhosis was broadly similar to that observed in previous work (Triantafyllou *et al.*, 2018; Brenig *et al.*, 2019). The circulating phenotype is predominantly of the classical monocyte subset and therefore represents the TAM-RTK phenotype before migration into tissue. Previous work has demonstrated elevated serum Gas-6 in HCC (Mukherjee *et al.*, 2016); further work is required to determine if serum levels correlate with % positivity for both MerTK and Axl on circulating monocytes and may represent a circulating driver for the circulating monocyte phenotype.

Circulating myeloid derived suppressor cell phenotype was also characterised and found to be elevated in both cirrhosis and HCC, but not significantly expanded in HCC when compared with patients with cirrhosis. The proportions of CD14+ cells that are classified as MDSCs (20.7% and 24.7% in cirrhosis and HCC respectively) are broadly in keeping with that reported by Bernsmeier *et al.,* (Bernsmeier *et al.*, 2018) in cirrhosis and with Hoechst *et al.,* in HCC (Hoechst *et al.*, 2008). Circulating MDSC percentage correlated negatively with serum AFP

but did not achieve statistical significance. This negative correlation is surprising, as both are known to be risk factor for reduced survival in HCC (Bai *et al.*, 2017; X. Zhang *et al.*, 2019). Further work is needed to ascertain MerTK and Axl expression on these cells, however it would be expected to be similar to those seen in the tissue.

Review of the monocyte phenotype after chemoembolization is limited by the sample size – there were significant practical difficulties in obtaining these samples as most patients recruited had routine follow-up blood tests at a local hospital or with their general practitioner. Nevertheless, in this small group it was notable that Tie-2 expression remained elevated at 6 weeks. Tie-2 expression is highest on the intermediate monocyte subset, and has previously been shown to denote a subset of monocytes that promote re-vascularisation (Patel *et al.*, 2013). Further work on a larger cohort of patients will be required to ascertain if this pro-angiogenic population is recruited to hypoxic areas of embolised tissue after TACE and if circulating Tie-2 expressing monocytes are of prognostic significance; inappropriate angiogenesis in treated tumours could help lesions to re-vascularise and recur.

Limitations have impacted on the interpretation of results and must be acknowledged. Firstly, the gating strategy for macrophages involved a panel that did not include macrophage marker CD11b or dendritic cell CD11c. This has the potential to result in mislabelling of dendritic cells as macrophages. Both markers are expressed both cell types, however (Collin, Mcgovern and Haniffa, 2013) and tumour derived macrophages analysed in this study using this gating strategy expressed elevated differentiated M2 macrophage CD163, suggesting the phenotyping is broadly accurate.

Thereafter, sample size has impacted on the interpretation of results. Significant difficulties were experienced with viable cell yield after cryopreservation of tissue extracted mononuclear cells, resulting in a significant proportion of cases in which thawed cells were not abundant enough to perform phenotypic analysis on either or both phenotyping panels.

These findings from flow cytometry are contradictory when compared with data on the enumeration of TAM-RTK positive cells identified using immunohistochemistry. Whereas a reduction in Axl positive macrophages was seen by this method, cell analysis by flow cytometry has revealed an entirely different result. This may be because manual enumeration of Axl in the tumour environment was complicated by high background signal on hepatocytes and the sinusoidal epithelium, making the identification of discrete Axl+CD68+ cells more challenging and resulting in an underestimation in the tumour microenvironment.

Regarding MerTK, immune phenotyping has confirmed the same modest increase in MerTK expressing monocytes in HCC that was seen with immunohistochemistry, but this was not seen when macrophages were analysed. The reduction in MerTK expression on tumour macrophages was unexpected; perhaps this could reflect a degree of contamination with dendritic cells, which constitutively express higher Axl and less MerTK than macrophages at rest (Zagórska *et al.*, 2014). The trend was subtle, however, and the MerTK MFI of the total macrophage population was not significantly altered between liver and tumour samples (Figure 3.4 D).

Taking the data from phenotyping the tissue myeloid compartment together, combining data from monocytes and macrophages has identified a number of consistent findings. In summary:

1) Tumour monocytes have an increased surface expression of Axl and MerTK than in the surrounding liver compartment. Axl+ monocytes are the more abundant of the two.
2) Axl and MerTK positive tumour monocytes have a divergent expression profile of immunophenotypic markers, with a skewing towards activated, M1-like phenotype.
3) Axl and MerTK expression are highest on the intermediate tissue monocyte population
4) Tumour macrophages may demonstrate a slight reduction in MerTK surface expression and an elevation in Axl expression, but neither reach statistical significance.
5) Tumour macrophages echo monocyte populations with a skewing towards a pro-inflammatory, HLA-DR-high phenotype with a reduction in co-expression of M2 markers including CD163 and Tie-2 in addition to MerTK.

CHAPTER 4

In vitro co-culture and conditioning of monocytes and monocyte- derived macrophages to recapitulate the tissue microenvironment and interrogate myeloid cell function

4.1 BACKGROUND AND AIMS

My data thus far has shown that in HCC, patients have a modest expansion of MerTK and Axl expressing monocytes in the circulation and within the tumour microenvironment. Intrahepatic monocytes have an expansion of intermediate monocyte subset, in keeping with previous published data on infiltrating monocytes in chronic liver disease. Immune phenotyping of extracted mononuclear cells has shown that the proportion of infiltrating monocytes in the tumour that express TAM-RTK was higher than in the surrounding liver, with a higher expression of HLA-DR on MerTK and Axl positive monocytes and macrophages and an enrichment of an HLA-DR high expressing macrophage phenotype in the tumour microenvironment.

These phenotypes may be the result of exposure to microenvironmental cues, most probably within the tissue compartments themselves. Thus far, data in this study has not identified a significant increase in the levels of circulating ligands for MerTK and Axl signalling (including Galectin-3 and Pros-1) or of elevated levels of TAM-RTK ligands within the tumour microenvironment. However, elevated circulating Gas-6 in patients with HCC has been previously described in recent related work to this study (Mukherjee *et al.*, 2016), and there are a range of other known triggers for TAM-RTK expression which have already been discussed: these include products of cholesterol metabolism after ingestion of apoptotic cells for MerTK (A-Gonzalez *et al.*, 2009; Nelson *et al.*, 2013) and areas of relative tissue hypoxia for Axl (Rankin *et al.*, 2014).

In addition to this, detailed review of lesions in Chapter 1 has identified instances of intrahepatic TAM-RTK expressing macrophages co-localising with CD4 and CD8 T cells, both

in tumour nests and in areas with stroma. Cook *et al.* have described how MerTK expression on myeloid cells impairs infiltration of tumours with cytotoxic CD8+ T cells in mouse models of colorectal malignancy: MerTK knockout within leucocytes resulted in increased T cell infiltration and a reduction in tumour growth (Cook *et al.*, 2013). As a result, we sought to investigate the functional impact of MerTK+ myeloid cell interaction with T lymphocytes *in vitro.*

Hypothesis and aims

It was hypothesised that the intra-tumoural monocyte and macrophage phenotype may be driven by microenvironmental mediators within the tumour microenvironment in hepatocellular carcinoma. Using *ex vivo* conditioning and co-culture experiments, this intra-tumoural and intra-hepatic macrophage phenotype could therefore be recapitulated using tissue homogenates from patients with hepatocellular carcinoma. Macrophages conditioned in this way will up-regulate expression of TAM-RTKs in response and share a functional profile in keeping with the tissue resident macrophages *in vivo*. As such, TAM-RTK expressing macrophages would be expected to have a cytokine profile skewed towards an M2-like phenotype, with a reduction in pro-inflammatory cytokine production in response to antigenic stimulation. Moreover, monocytes and macrophages conditioned in this way will exhibit attenuated capacity to elicit effective, pro-inflammatory adaptive immune responses.

In support of this hypothesis, the aims of this chapter were as follows:

1) To generate M0, undifferentiated monocyte-derived macrophages and expose them to tumour and liver homogenates to derive a tissue resident phenotype in response to putative microenvironmental mediators

2) To assess phenotype and function in these conditioned macrophages by quantifying surface expression of MerTK and Axl (as well as by quantitative PCR) and cytokine production in response to LPS stimulation.
3) To condition healthy monocytes with sera from patients with liver disease and HCC before entering these monocytes into an autologous co-culture with CD4 and CD8 T-cells, to assess the effect of increased MerTK and Axl expression on antigen presentation and T cell proliferation.

4.2 METHODS

4.2.1 M0 macrophage conditioning

Monocyte-derived macrophages (MoMFs) were generated from healthy CD14+ monocytes using a protocol adapted from (O'Brien *et al.*, 2014).

4.2.1.1 CD14+ cell isolation by magnetic bead isolation

For this process, the CD14+ monocyte isolation kit (Miltenyi Biotec, UK) was used and manufacturer's instructions followed. All steps were performed on ice to improve yield and purity. Briefly, PBMCs from healthy donors or from patients undergoing venesection for hereditary haemochromatosis but without any evidence of liver disease, were isolated as previously described. The isolated mononuclear cells were re-suspended in MACS (magnetic associated cell sorting) buffer (reconstituted to manufacturer's instructions) and incubated with CD14+ labelled magnetic 'microbeads' for 15 minutes at 4^{o}C. The ratio of beads was scaled up according to the number of PBMCs in the suspension, in accordance with manufacturer's instructions. After incubation and washing in MACS buffer, the cells were applied to a column (LS column) using a pipette, over a 35μm mesh to remove clumps and debris. The column was attached to a MACS separator which helped to activate a magnetic field which would allow for isolation of cells attached to the magnetic beads in the suspension. The column was then washed using MACS buffer and by using a plunger, purified cells were collected. This process was repeated using the effluent (i.e. passed over a second LS Column) to increase CD14+ monocyte yield and purity; cells were then counted using a haemocytometer.

4.2.1.2 Monocyte culture and M0 macrophage differentiation

Isolated CD14+ monocytes were then re-suspended in X-Vivo medium (Lonzo, UK) supplemented with 10% Human AB serum (Sigma-Aldrich, UK), 1% Penicillin-streptomycin (Thermofisher Scientific, UK) and 1% L-glutamine at a concentration of 1million cells/ml and

plated onto 6 well polystyrene tissue culture plates (Corning, UK). 4 million cells were plated per well and then left to adhere to the plate at 37^{o}C in an incubator for an hour. Thereafter, media was aspirated and replaced, this time with X-vivo media supplemented in the same way as before, but with 20ng/ml of M-CSF (macrophage colony stimulating factor, Sigma Aldrich) supplemented. The cells were resuspended in enough media to leave them at a concentration of 1million CD14+ cells/ml and placed in an incubator. On day 4 and day 6 of culture, the cells were inspected and the media changed and replaced with the same, M-CSF supplemented X-vivo media. Non adherent cells were removed at each point. Macrophages were ready for use on Day 7. Media was aspirated using a lifting solution containing PBS, 10mM EDTA and 4mg/ml of lidocaine. This was added and the cells left at room temperature for 20 minutes, before scraping the cells off using a cell scraper. At this point, if required, macrophages were counted using a haemocytometer and phenotyping performed as previously described (Paragraph 3.2.5) using a panel of antibodies to known macrophage markers: CD14 (PE-Cy7, BD Biosciences UK), CD16 (APC-H7, BD Biosciences, UK), HLA-DR (BV510, BD Biosciences, UK), MerTK (APC, R&D Systems, UK) and Axl (AF488, R&D Systems, UK). The viability dye was Alexa-Fluor 700, (BD Biosciences, UK).

4.2.2 Macrophage conditioning and stimulation

Media was aspirated off to dryness and the cells resuspended in X-vivo media supplemented with the following: 10% human AB serum, 1% penicillin-streptomycin, L-glutamine (1%) and 25% tissue homogenate. The final concentration of cells to medium was kept constant (i.e. 1 million cells/ml, based on the original number of cells plated). The production of tissue homogenates is outlined elsewhere (Paragraph 3.2.6). Cells were left to incubate for a further 48hours at 37^{o}C before functional assays, further immunophenotyping by flow cytometry (as described above) or cell lysis and RNA extraction for qPCR.

In those wells in which cytokine responses of cultured macrophages to antigenic stimulus was planned, the media was changed and replaced with unsupplemented RPMI 1640 supplemented with 100ng/ml lipopolysaccharide (InvivoGen, France) and incubated for 6 hours. After 6 hours, the supernatants were collected, centrifuged at 15000rpm for 5 minutes and the supernatants stored in eppendorfs (after filtering through a 35μm mesh) at -80oC.

4.2.3 Cell lysis and RNA extraction

In wells in which cell lysates were required to quantify gene expression, cells were lifted as described above, washed in 3ml of PBS and centrifuged in FACS tubes at 15000rpm for 5 minutes. Cells were re-suspended in 350μl of Qiagen RLT buffer (Qiagen, Germany) supplemented with 1% β-mercaptoethanol and placed in 2.5ml eppendorfs. RNA extraction followed manufacturer's instructions using a RNeasy Mini Kit (Qiagen, Germany). To summarise: once re-suspended in RLT lysis buffer the cells were vortexed for 1 minute to disrupt the cell membranes, and an equal volume of 70% ethanol added to precipitate RNA. This solution was collected on RNEasy spin columns to collect RNA. After washing with RW1 and RPE buffers, the eluted RNA was washed off and collected using RNAse free water. Extracted RNA was then used to generate cDNA and subsequent qPCR as described in Paragraph 3.2.8.

4.2.4 Measurement of cytokines in culture supernatants by MSD

Frozen and stored supernatants collected from macrophages that had been exposed to LPS stimulation (and relevant controls) were thawed and assayed using a custom cytokine array developed by Meso Scale Discovery (MSD, Rockville, US). Samples were diluted 1:1 and added to pre-formed 'U-plex' plates to measure levels of the following cytokines or analytes:

IL-1b, IL-6, IL-8, IL-10, IL-12p70, TNF-a, VEGF and Arginase-1. Plates were read on the Sector Imager 2400 apparatus (Gaithersburg, MD). All experiments were performed according to the manufacturer's instructions.

4.2.5 Monocyte and T-cell autologous co-culture

PBMCs were collected from healthy donors or HFE haemochromatosis patients as described above. During CD14+ monocyte extraction, after passing the PBMC suspension labelled with CD14+ beads over the LS column, the CD14- fraction of cells that flowed through was kept and utilised for isolation of autologous T-cells. First, CD8+ T cells were isolated using a CD8+ positive selection kit (Miltenyi Biotec, UK) and counted. The process was similar to that for CD14+ monocytes, using 20µl of CD8+ beads and 80µl of MACS buffer per 10 million cells. Once collected, the CD8- fraction was utilised: a CD4+ T cell positive selection kit was used – this labelled all other cell types with beads, leaving untouched CD4+ T cells to pass through the column. CD4 and CD8 T cells were counted and cryopreserved using fetal calf serum supplemented with 10% DMSO.

CD14+ monocytes were counted and re-suspended in RPMI 1640 supplemented with 10% fetal calf serum (Sigma- Aldrich, UK), 1% penicillin-streptomycin (Thermofisher Scientific, UK). 500000 cells were plated per well, in a total volume of 400µl of media with the addition of 20% (100µl) of human serum (either healthy controls or from patients with HCC or liver disease). Cells were incubated for 24hrs at 37^{o}C to condition them.

After incubation, adherent cells were retrieved from the bottom of the wells mechanically using a cell scraper or pipette tip, washed in PBS and counted. At this point, phenotyping using the same panel of antibodies listed above was undertaken to characterise TAM-RTK expression

and viability of monocytes. Monocytes ready for addition to co-culture were kept on ice in RPMI 1640 media supplemented with 10% Human AB solution and 1% penicillin-streptomycin ('T cell media'), whilst T cells were prepared.

Frozen CD4 and CD8 T cells were thawed, re-suspended in T cell media at a minimum concentration of 1 million cells/ml and counted. T cells were stained using CFSE to assess proliferation: cells were incubated in a 1μM solution of CFSE dye in the dark for 10 minutes at room temperature. After incubation, CFSE was washed using cold RPMI media and the cells re-suspended in T cell media. CD4 and CD8 T cell suspensions were added to round bottom 96 well plates. To this, monocytes were added in a ratio of 1 monocyte: 4 T cells. Care was taken to re-suspend all populations in media to facilitate this ratio of antigen presenting cell to T lymphocytes, and to ensure that both populations are not at a concentration greater than 1 million cells/ml. A pool of HLA class restricted peptides was added to the monocyte: T cell co-culture. For CD8 T cells, Class I peptides and for CD4 co-cultures, Class II peptides (Cellular Technology Limited, USA). These were added to achieve a concentration of 2μg/ml and are peptides related to common environmentally experienced antigens such as measles or influenza.

Co-cultures were placed in the incubator for 3 days for CD8 T cells and for 6 days for CD4 T cells. This duration was decided based on observations of reduced viability of CD8+ T cells beyond 72 hours in this system. At the end of the co-culture, T cells were collected and assessed for viability and proliferation by flow cytometry (CFSE stain is fluorescent on the same channel as that used for FITC stained samples). Percentage proliferation was calculated from the proportion of daughter cells seen as distinct peaks to the left of the original peak.

4.3 RESULTS

4.3.1 *Ex vivo* conditioning with tumour homogenates stimulates Axl expression in monocyte-derived macrophages; MerTK expression is not significantly altered but may be suppressed

Healthy monocyte-derived macrophages (MoMFs) were conditioned with paired tumour and liver homogenates from n=4 patients with HCC (trial IDs SHCC47, SHCC70, SHCC84, SHCC92 – clinical details and disease characteristics are outlined in Table 3.3). The results are presented in Figure 4.1. MoMF viability was good after culture, with over 90% of cells alive in all groups. MoMFs have high basal surface expression of MerTK, and this is not significantly altered after conditioning with tissue homogenates. At a genetic level, however, MoMFs experience a reduction in expression of MerTK after exposure to tumour homogenate, although this did not reach statistical significance (Fold change from baseline 0.75 vs 1.72 for tumour vs liver homogenate conditioning, p=0.114). The relationship with Axl expression was distinct, however: A significant increase in surface expression of Axl after conditioning with tumour homogenates was seen (median %+ve 6.37% vs 2.6%; p=0.029). This is coupled with an increase at the level of transcription – (fold change 2.11 vs 0.04; p=0.029).

4.3.2 Cytokine production by M0 macrophages in response to stimulation with LPS is skewed towards a M2 phenotype after conditioning with liver and tumour homogenates

Figure 4.1 D presents the results from the MSD cytokine array from supernatants after conditioned macrophages were stimulated with lipopolysaccharide (LPS). One sample had no detectable analytes across all samples and cytokines (SHCC92) and was excluded from the data presented here. Although not meeting statistical significance, most likely on account of the sample size, there is a clear trend towards a reduction in the production of M1 cytokines (IL-1β, TNF-α and IL-6) and an increase in production of VEGF. There was no significant difference in the cytokine production between tumour and liver cases.

Table 4.1: Clinical parameters and characteristics of cases from which serum was used to condition monocytes before co-culture with CD4+ and CD8+ T cells:

Trial ID	Age (years)	Sex	Aetiology	Tumour Size (mm)	Treated	Cirrhosis	BCLC Stage	AFP [IU/ml]	Bilirubin (μmol/l)	Platelets ($x10^9$/ml)	INR	MELD
HV 6	53	F	-	-	-	N	-	-	-	-	-	-
HV 7	54	F	-	-	-	N	-	-	-	-	-	-
CLD 4	65	F	ARLD	-	-	Y	-	-	9	164	1.0	6
CLD 5	48	F	NAFLD	-	-	Y	-	-	46	81	1.5	15
SHCC19	77	M	ARLD	37	Y	Y	B	2	6	269	1.06	7
SHCC47	51	M	ARLD	44	N	Y	A	3	122	86	1.73	21
DC17	45	M	ARLD	-	-	Y	-	-	341	156	2.00	26
DC19	56	F	ARLD	-	-	Y	-	-	177	176	1.50	20

Healthy volunteer serum (HV) and CLD (chronic liver disease) serum were used as control populations and decompensated liver disease patients as a positive control Abbreviations: *ARLD= alcohol related liver disease, NAFLD= non-alcoholic fatty liver disease, AFP=alpha-fetoprotein, MELD=Model for End-Stage Liver disease. INR = international normalised ratio, BCLC = Barcelona Clinic Liver Cancer*

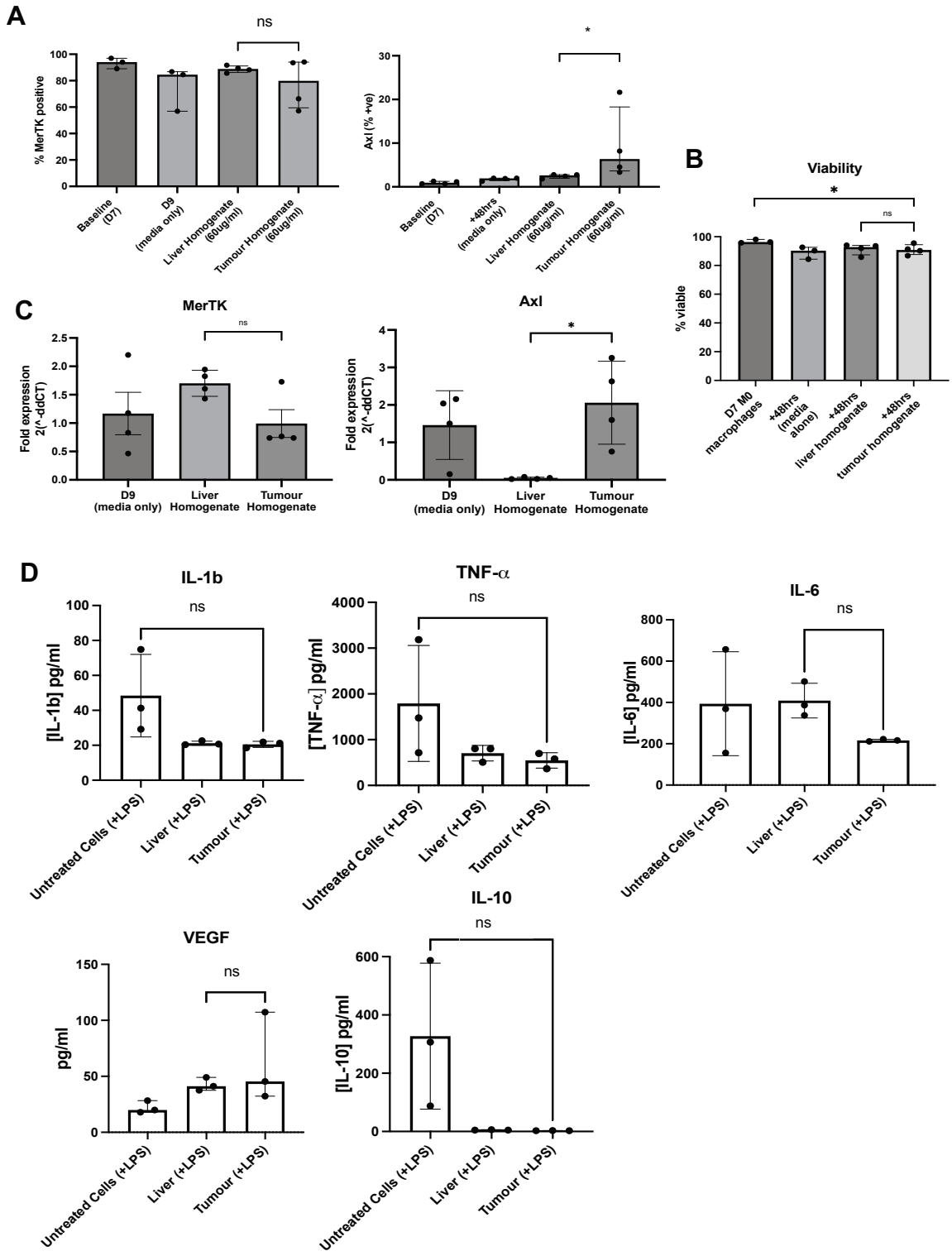

Figure 4.1: Conditioning monocyte-derived macrophages with tissue homogenates up-regulates surface Axl expression and skews cytokine production in response to antigenic stimuli

Monocyte derived M0 macrophages derived from a healthy volunteer were conditioned with paired liver and tumour tissue homogenates from n=4 cases of HCC. Surface expression (A) and qPCR (C) was performed to assess the response in terms of TAM-RTK expression. Cell viability after conditioning was preserved (B). (D) Conditioned macrophages were stimulated with lipopolysaccharide and cytokine production assayed using cytokine array technology (MSD). *Data is presented as median with interquartile ranges. Statistical analysis was non-parametric, using Mann Whitney and Kruskal Wallis testing where appropriate; ns = non-significant; *=p<0.05.*

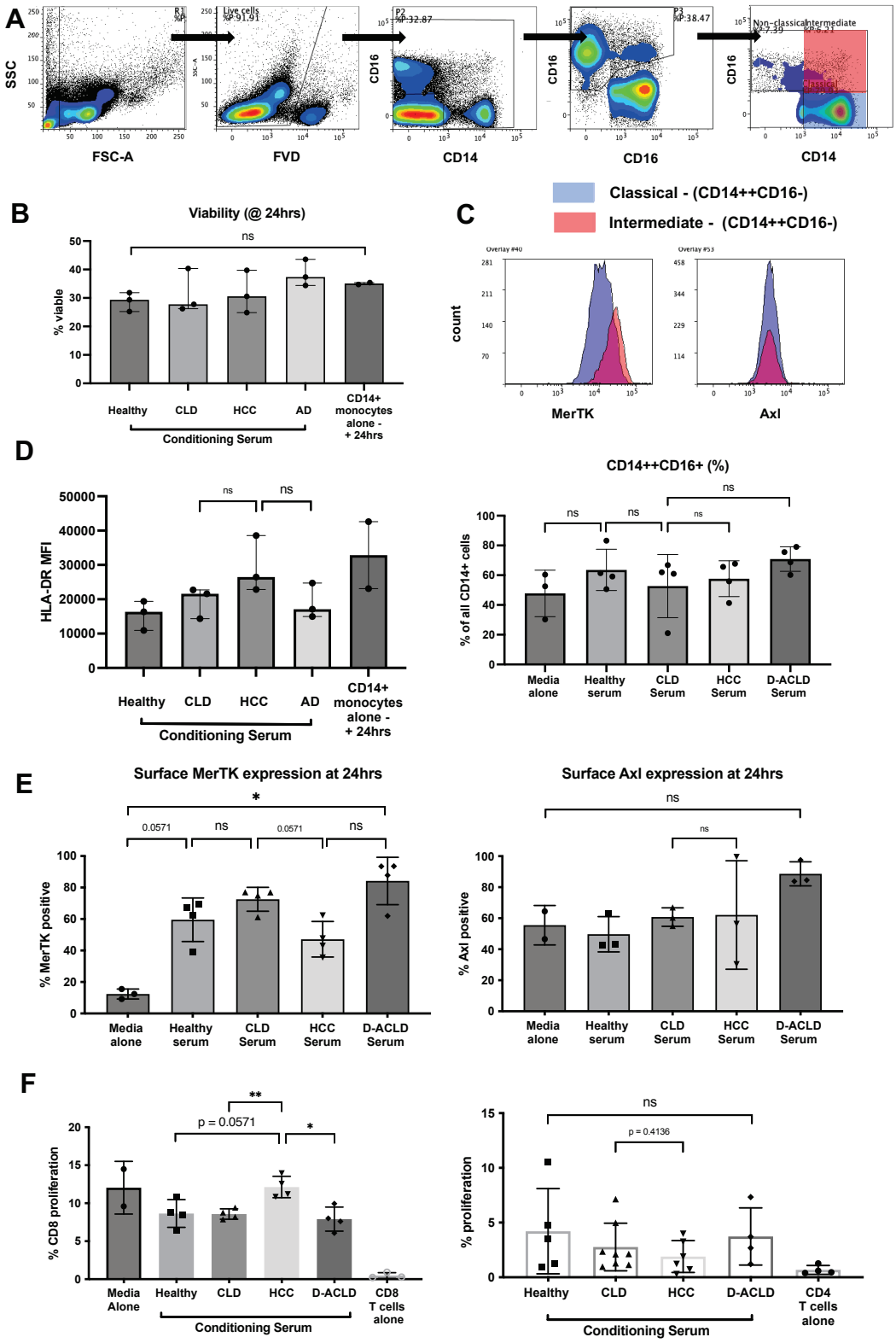

Figure 4.2: Conditioning monocytes with sera from patients with liver disease and HCC recapitulates the tissue monocyte phenotype and impairs antigen presentation and recall responses by autologous cytotoxic T cells

Healthy monocytes were conditioned with sera for 24hrs (n=2 for each group). Data presented here is combined from separate runs using autologous cells from two healthy volunteers. **(A)** conditioned monocytes were phenotyped using the DR exclusion gating strategy **(B)** Viability of monocytes after culture was less than 50%

(C) Intermediate monocytes express higher MerTK expression than classical monocytes **(D)** HLA-DR expression and proportion of intermediate monocytes was measured. **(E)** Surface TAM-RTK expression after conditioning was measured by flow cytometry **(F)** Antigen recall responses of autologous CD8 and CD4 T cells was measured after 6 and 3 days of co-culture with conditioned monocytes respectively. *Data presented here is represented as median with range; statistical analyses are non-parametric (Mann-Whitney or Kruskal Wallis test; *=p<0.05, **=p<0.01).*

4.3.3 Monocytes conditioning with sera from patients with liver disease recapitulates aspects of the tissue resident monocyte phenotype

Healthy monocyte conditioning with sera from patients with liver disease, HCC and healthy controls resulted in a significant alteration in monocyte phenotype. Clinical data for the patients and volunteers whose sera was used is outlined in Table 4.1. Conditioning resulted in an increase in HLA-DR surface expression and in the proportion of monocytes of the intermediate phenotype, although this did not reach statistical significance and was not specific to HCC sera – this is a similar finding to that seen in tissue monocytes phenotyped in Chapter 3. Figure 4.2C shows that MerTK expression, not Axl, is enriched on the intermediate population after serum conditioning. This pattern was seen across all groups and was not specific to HCC serum. MerTK expression was lower in cases with HCC when compared with cirrhotic controls (45.4% vs 75.9% MerTK+; p=0.057). Axl expression was not significantly altered by serum conditioning, except after conditioning with acute decompensated patient serum, although this did not reach clinical significance (Kruskal Wallis p-value=0.306).

4.3.4 Cytotoxic T cell antigen recall responses are attenuated in when co-cultured with monocytes with higher MerTK expression

Autologous co-cultures yielded interesting results when compared with the post-conditioning surface MerTK expression profiles of the monocytes used to generate antigen recall responses (Figure 4.2 F). Data presented is from 2 separate runs using CD14, CD4 and CD8 cells from 2 separate healthy volunteers. Firstly, CD4 T cell co-cultures did not produce significant proliferation responses, and there was no significant difference across the groups. In CD8+ T cells, however, there was a significant reduction in proliferation after conditioning with serum

from patients with cirrhosis and an increase when cultured with HCC serum conditioned monocytes. The reason for this difference was not immediately clear, as both groups utilised cases with cirrhosis. However, it was notable that the reduction in proliferative response was seen with a higher surface MerTK expression. Although not seen in the cases with HCC, these data may demonstrate that higher MerTK expression on monocytes is a marker of an impaired capacity to activate T lymphocytes, which may have clinical relevance in the tumour microenvironment.

4.4 DISCUSSION

Conditioning healthy volunteer monocytes and M0 macrophages using both sera and tissue homogenates from patients with HCC has been demonstrated in these experiments to alter both phenotype and function in both myeloid cell populations. Although limited somewhat by a small sample size, clear trends in MerTK and Axl expression were seen after monocyte derived macrophage (MDM) conditioning with tumour homogenate, with opposing effects. Tumour homogenate conditioning resulted in a trend towards skewing cytokine production away from an M1 phenotype.

It is perhaps not surprising that these homogenates had such an effect – MerTK expression is particularly sensitive to efferocytotic cues, and this highly filtered homogenate could not provide the phosphatidylserine to trigger signalling and MerTK expression. This lack of signalling is evident from the lack of IL-10 production by these macrophages after conditioning with homogenates – IL-10 can promote MerTK expression through a positive feedback loop (Zizzo *et al.*, 2012). The homogenates used were assayed for Gas-6 and Pros-1 (Figure 3.11A) – although both ligands were present in the homogenates, they are not enriched in the tumour when compared with the background liver; therefore, stimulation of Axl expression in this context may not be Gas-6 dependent. Furthermore, Pros-1 is now known not to be a ligand for Axl (Graham *et al.*, 2014a). LPS is a known trigger for Axl expression, as part of a negative feedback loop after activation of interferon signalling (Rothlin *et al.*, 2007); however in this experiment LPS treatment occurred after phenotyping of conditioned macrophages. Further work is required to ascertain which microenvironmental mediator(s) may be driving this Axl+ phenotype in tumour macrophages.

Monocytes demonstrated an increase in a differentiated intermediate monocyte phenotype, with an increase in MerTK surface expression in all groups. This effect has been described in monocytes after cultured on plastic alone (Liaskou *et al.*, 2012); however there was a further increase in MerTK expression with serum from diseased patients. Although the sample size was small, there was a trend towards an HLA-DR high, intermediate monocyte enriched monocyte phenotype after culture with diseased serum, which was most pronounced with acutely decompensated patients' sera and was not specific to tumour serum.

Cytotoxic T cell co-culture experiments in this study suggest that higher MerTK surface expression is associated with attenuated T cell proliferation. This experiment has some limitations in its applicability to the tumour microenvironment, however. Firstly, antigen recall responses are not a key function of T lymphocytes within the tumour microenvironment - any changes in this aspect of T cell function may not be representative of the effect MerTK myeloid cells have on T cells in cancer. In addition, monocytes are not professional antigen presenting cells and so the effects seen may not be relevant to tumour biology. Nevertheless, this data is encouraging and echoes that from Cook *et al.* (mentioned above) demonstrating the regulatory effect of MerTK on CD8 T cell activation. Further intriguing work has shown that this regulatory effect may be reciprocated – activated CD8 T cells can externalise Pros-1 and phosphatidylserine patches on their external surface after activation by antigen presenting cells, thereby engaging with TAM receptors (MerTK and Axl) on their surface and inhibiting further activation (Carrera Silva *et al.*, 2013). This interaction has until now only been described with dendritic cells.

Limitations with these experiments need to be acknowledged. In addition to the small sample size, conclusions from the results of these experiments are limited by the lack of use of an

inhibitory strategy for both MerTK and Axl to dissect the effect of each signalling cascade on the phenotype and function. Repeating these assays after gene silencing of MerTK and Axl separately would allow for more durable assertions to be made. Furthermore, re-designing of the co-culture assays to assay CD8 and CD4 T cell phenotype for markers of exhaustion (e.g. surface expression of PD1 or CTLA-4, for example, or markers of a Treg phenotype such as FoxP3) would be more context specific. Altering the assay to use tumour antigen in place of HLA class I and II restricted peptide would also be more representative of events within the tumour microenvironment. It would be pertinent to repeat the conditioning of monocytes with tissue homogenates. This would allow direct comparison of the effect of tissue derived mediators on M0 monocyte derived macrophage and tissue monocyte phenotype in HCC.

In summary, in addressing the aims of this chapter, the following has been demonstrated *in vitro*:

1) The tissue monocyte phenotype seen in the extracted hepatic and tumour derived monocytes from patients with HCC (as outlined by surface expression of MerTK, Axl and HLA-DR) can be partially recapitulated after conditioning healthy monocytes with sera both from patients with liver disease and those with HCC. This effect is not specific to HCC cases, however, and did not reach statistical significance.
2) In monocyte-derived macrophages, Axl expression (both on the cell surface and at gene expression level) is stimulated by tumour homogenates; MerTK is not similarly affected but is down-regulated. Cytokine production is skewed away from an M1 phenotype after developing this phenotype.
3) Higher MerTK expression on antigen presenting cells can attenuate CD8 T cell activation.

CHAPTER 5

Transcriptomic profiling of tissue macrophages reveals a distinct tumour associated phenotype

5.1 Background and Aims

5.1.1 Background

Characterisation of the MerTK and Axl myeloid cell phenotype in hepatocellular carcinoma has been undertaken topographically using immunohistochemistry and through immunophenotyping of extracted mononuclear cells by flow cytometry. Using conditioning and co-culture experiments *in vitro*, potential drivers for MerTK and Axl expression and evaluation of myeloid cell function have been explored. These methods have identified the MerTK and Axl on intra-tumoural monocytes and macrophages, however the data has yielded some conflicting results regarding the relative frequencies and abundance of MerTK and Axl expression within the tumour microenvironment – namely between immunohistochemistry and flow cytometry.

There are likely a number of causative factors for these conflicting findings. The first is related to the practicalities of cellular extraction - the population of mononuclear cells extracted mechanically from tissue may differ from those enumerated by immunohistochemistry. Not all cells extracted may survive the process of mechanical dissociation, and some may be left adherent to tissue. Macrophages and other resident myeloid cells can congregate around areas of fibrosis, both in the hepatic parenchyma and within tumours. This tissue was very difficult to mechanically dissociate and such cell populations may not have been successfully isolated. Enumeration of double positive cells by immunohistochemistry was challenging in areas with large inflammatory infiltrates: individual cells were difficult to isolate and count (an issue particularly with MerTK), or in areas with high background signal – in the case of Axl. This may have resulted in an underestimation of cells within the tumour microenvironment when counting using this method.

Another factor affecting the data is the difficulty with defining and comparing myeloid cells populations using immunophenotypic markers. Resident and infiltrating hepatic myeloid cell populations share many phenotypic markers, both with each other and with tumour derived myeloid cells, but are known to have distinct genetic signatures (MacParland *et al.*, 2018; Laviron and Boissonnas, 2019). Comparative analyses using monocyte gating and a broader macrophage gating strategy has shown some consistent observations – namely that MerTK and Axl expression is more pronounced on myeloid cells with higher HLA-DR expression, and that HLA-DR is skewed towards a higher expression profile in the tumour microenvironment. However, a lack of reliable distinguishing phenotypic markers for human Kupffer cells has made evaluation of the contribution of this key population (and its tumour associated, 'Kupffer-like' macrophage population, seen histologically in well to moderately differentiated lesions) difficult to determine and quantify. The results of the analysis could have been confounded by the lack of positive gating on CD11b on the macrophage panel.

Finally, surface expression of both MerTK and Axl is not an accurate reflection of MerTK and Axl signalling and activity, as both are regulated by surface cleavage after induction of signalling (Axelrod and Pienta, 2014; Cai *et al.*, 2020). In this way, a significant proportion of TAM-RTK expressing cells with active signalling cannot be identified using flow cytometry of surface markers.

There is a growing body of evidence that tumour derived myeloid cell populations are niche and immune-context specific, with varied responses to antigenic or environmental tissue inflammatory responses (Condeelis and Pollard, 2006; Halaby *et al.*, 2019). Furthermore, they are plastic and can therefore be modulated in response to the presence of cytokines (Sánchez-Martín *et al.*, 2011; Candido *et al.*, 2018) and activation of central signalling pathways such as

PI3 kinase (Li *et al.*, 2020) and ligation of CD40 on the cell surface (Beatty *et al.*, 2011). The expression of particular phenotypic markers may not reflect their function within the tumour environment in different contexts (Yang, McKay, Jeffrey W. Pollard, *et al.*, 2018).

A number of novel methods and technologies have recently been employed in order to interrogate the intratumoural heterogeneity of macrophage populations, including single-cell RNA sequencing (Bao *et al.*, 2021) and mass cytometry (CyTOF) (Halaby *et al.*, 2019). The utility of gaining this degree of resolution in our understanding of macrophage populations is beneficial from a mechanistic perspective and is essential to our understanding of the varied immune landscape within and even between different tumours.

5.1.2 Hypothesis

In view of the need to better understand the MerTK and Axl macrophage phenotype within the tumour and between this microenvironment and the surrounding liver, transcriptomic profiling of both tumour and liver derived myeloid cell populations was undertaken. This would allow for a whole-population analysis to be made at the gene-expression level and, crucially, for comparisons to be made between tissue compartments and disease states. Accepting that there is the possibility for both intra-tumoural and inter-lesional heterogeneity of macrophage phenotype. analysis of identically gated macrophage populations across a sample of cases would allow for any clear phenotypic and functional distinctions to be identified, thereby identifying clear signatures that may direct future avenues of therapeutic intervention.

5.1.3 Aims

The specific aims of this part of the study were as follows:

1) To isolate a purified macrophage population using fluorescence activated cell sorting from both liver and tumour tissue from patients with HCC.
2) To undertake transcriptomic profiling of individual cases using gene expression analysis technology Nanostring.
3) To compare both tumour associated macrophages with the surrounding liver populations for expression of both of MerTK and Axl, and a range of downstream signalling proteins.
4) To undertake a similar comparison between treated and untreated lesions to ascertain the effect of locoregional therapy on MerTK and Axl expression.
5) To explore any tumour or locoregional therapy specific transcriptional signatures that relate to macrophage phenotype and function.
6) To interrogate HCC and liver tissue for evidence of downstream signalling related to MerTK and Axl, extracting protein and performing phosphoproteomic analysis to identify if there is active signalling within these tissue compartments. *(This had originally been planned for extracted macrophage cell lysates in a similar manner to the transcriptomics; however due to a paucity of samples with excess viable cells, snap frozen tissue was analysed instead).*

5.2 Methods

5.2.1 Patient recruitment and sample selection

Patients and samples were recruited and collected in the same manner as for immunophenotyping as in Chapter 3. Tissue sampling and storage has been previously described in Chapter 3. Mononuclear cells were kept cryopreserved in liquid nitrogen in preparation for 'batch processing' shortly before transcriptomic kits were available for sample analysis. Samples were selected initially on the basis of cell yield, initially prioritising cases with ample cells. Cases in which less than 2 million mononuclear cells were stored after extraction were not thawed on this basis.

5.2.2 Fluorescence activated cell sorting

Cryopreserved cell eppendorfs were thawed in a water bath at 37ºC and washed in 5ml of RPMI 1640 media to remove cryopreservation media. Viable cells were then counted using a haemocytometer as previously described and filtered through a 30μm filter to remove debris, before being stained using viability dye FVD AF700 as previously described (Chapter 3), for 20 minutes in the dark at 4ºC. After washing in FACS buffer, cells were resuspended in 50μml of brilliant staining buffer (BD Biosciences, UK) for every 10 million live cells and the full panel of antibodies required were added – for cell numbers over 10 million, the volume of antibody was scaled up as appropriate to maintain the same concentration of antibody. Antibodies added were: CD14 (PE-Cy7), CD1lb (PE), CD3, CD15, CD19, CD56 (all on PerCP Cy5.5), HLA-DR (BV510) – all antibodies were manufactured by BD Biosciences, UK, and the volume per test was the same as that used for phenotyping. FMOs were made at the same time to allow for gating on positive populations. The sorting was undertaken on a FACS Aria III at the Imperial College London St Mary's Campus FACS Sorting Facility, by the facility

manager. Sorted cells were collected into 10% fetal bovine serum and 1% penicillin-streptomycin supplemented media and stored on ice.

5.2.3 Cell lysate preparation and transcriptomics

Isolated cells were immediately lysed by centrifugation at 15000rpm for 5 minutes, aspiration of supernatant and re-suspension in Qiagen RLT buffer (Qiagen, Germany) supplemented with 1% β-mercaptoethanol. 2µl of RLT buffer with 1% β-mercaptoethanol was added for every 20000 cells in each sample, multiplying up the volume added accordingly. A minimum of 2µl was used. After vortexing for 1minute the lysates were immediately stored at -80oC.

5.2.3.1 Gene expression analysis – Transcriptomics

Cell lysates were transferred to University College London Nanostring facility on dry ice. Lysates were thawed and incubated overnight with reporter and capture probes for 16hrs on a thermal cycler, before being immobilised on cartridges using the nCounter Prep Station (Nanostring Technologies, Seattle, US). The Myeloid codeset panel was used, and Nanostring nCounter® XT GX Human Immunology V2 assay set up. The codeset panel contains 742 genes of interest, including MerTK, Axl, Tyro3 and downstream signalling proteins from TAM-RTK signalling cascades in immune regulation.

To summarise the Nanostring technology, native RNA extracted from the samples is allowed to bind to capture and reporter probes; there are pairs of capture and reporter probes for each of the 742 genes in the panel and these are allowed to bind overnight. The RNA-probe complexes are then immobilised on a solid cartridge and the reporter probe signal (which is emitted fluorescence) is read directly by the nCounter Sprint Profiler machine. Light signal for

each probe is unique and signal intensity can be quantified to measure abundance of each RNA fragment. Copy count data was retrieved and analysis undertaken using nSolver version 4.0 software initially for quality control; further analysis of copy count data was analysed with statistical assistance using the RStudio platform environment (R Foundation for Statistical Computing, Vienna, Austria). Further detail on statistical analysis is provided below.

5.2.4 Tissue homogenisation, peptide and phosphopeptide extraction

Snap frozen tissue was homogenised for protein extraction as described in *Chapter 3.* These homogenates were subject to the same protein quantification by BCA assay and homogenates used for quantification of proteins of interest by ELISA.

Frozen tissue fragments were pulverised using a tissue pulveriser and the fragments immediately added to a 1ml of a mix of both Halt Protease inhibitor and Halt Phosphatase Inhibitor (both at 1% concentration and diluted in M-PER Mammalian Extraction Buffer, all manufactured by Thermofisher Scientific). This was incubated at 4^{o}C for 15minutes before centrifugation at 15000rpm for 10 minutes and the supernatant transferred to a new vial, and protein quantification undertaken using the Bradford Assay. Lysates were transferred to Barts Centre (Cancer Research UK) Queen Mary University London, for mass spectrometry under the direction and supervision of Dr David Britton and Professor Pedro Cutillas. Briefly, samples were enriched for phosphopeptides using a method summarised in Montoya *et al.,* (Montoya *et al.*, 2011) and peptides and phosphopeptides analysed by liquid chromatography/mass spectrometry (LC-MS/MS) using a LTQ-Orbitrap mass spectrometer; peptide quantification and normalisation was undertaken using a method summarised in Casado *et al.,* (Casado *et al.*, 2013).

5.2.5 Immunohistochemistry

Double epitope enzymatic immunohistochemistry was undertaken using the same protocol outlined in **2.2.3**. Rabbit anti-human C1Q antibody (Agilent, US) was used at a 1:100 dilution in combination with CD68 at the same dilution used in previous double epitope stains.

5.2.6 ELISA (Enzyme Linked Immunosorbent Assay)

Samples (serum, tissue homogenates) were thawed, centrifuged and added according to the manufacturer's instructions (Invitrogen, Thermofisher Scientific, UK). For the C1q ELISA, serum was added at a 1:1000 dilution, and cell culture supernatants in a 1:1 dilution. Homogenates were added at a 1:5 dilution. Samples were run and analysed as described previously in **3.2.7**; a 5-parameter curve fit was used to interpolate values and the dilution factor used to calculate the true values before presenting raw values.

5.2.7 *In vitro* M0 macrophage differentiation and conditioning

This was undertaken as previously described in paragraph 4.2.1 to 4.2.3, including stimulation with lipopolysaccharide, cell surface staining by flow cytometry, RNA extraction and collection of cell supernatants. Cells were stained with the same panel of antibodies but also with rabbit anti-human C1q-FITC (abcam, Cambridge, UK).

5.2.8 Intra-cellular staining by flow cytometry

Conditioned macrophages were concurrently analysed using flow cytometry using standard protocols for surface expression and for intra-cytoplasmic expression of C1q. Briefly, cells were lifted and stained in the same manner as previously described (Paragraph 4.2.1). Once washed, 100µl of intracellular fixation buffer (BD Biosciences, UK) was added to each polystyrene tube and the cell pellet vortexed at the bench. After incubation for 20 minutes at

room temperature, and away from direct light the cells are washed in 2ml of Permeabilization buffer as well before centrifuging at 500g for 5 minutes. Thereafter, intracellular staining with C1q-FITC antibody (rabbit anti-human; abcam, Cambridge, UK) was undertaken before washing and re-suspending in FACS buffer and acquiring on the BD LSR Fortessa (BD Biosciences, UK).

5.2.9 Statistical analysis

As previously, statistical analysis for comparison of groups was non-parametric, using Mann-Whitney, Wilcoxon matched pairs signed rank, and Kruskal Wallis testing where appropriate. Categorical data was analysed for significant differences using Chi-squared analysis.

5.2.9.1 Transcriptomics – Nanostring

Samples were analysed in batches and normalisation undertaken manually using the Nanostring nSolver guidelines and using R studio statistical platform. Assistance in bioinformatics was provided by Dr Laura Martinez-Gili, Department of Surgery and Cancer, Imperial College London, who helped to design code to generate correlation matrices and heatmap clustering analyses.

Copy count data was visually inspected initially. Normalisation of data for each sample was undertaken in a two-step process. Firstly, positive control normalisation was performed using the 6 positive controls added each 'lane' – a lane contains the RNA from one sample. Briefly, the geometric mean of the 6 positive controls were calculated for each 'lane' and divided by the arithmetic mean of the geometric means across all samples run on each batch, generating a positive control scaling factor. If the scaling factor was >3 or <0.3, the sample was discarded at this stage. Otherwise, the raw copy count was multiplied by this normalisation factor.

RNA content normalisation was then performed using housekeeping genes – 40 of these were run simultaneously in each lane. Those housekeeping genes with a copy count below that of the highest of the negative controls were excluded from analysis. Housekeeping gene counts across all samples were inspected for variability between them by Spearman rank correlation. A co-efficient matrix and heatmap was generated. Those that varied significantly from other housekeeping genes were removed. Utilising this set of remaining housekeeping genes, a content normalisation factor was calculated for each lane. This was generated in the same manner as the positive control scaling factor (i.e. geometric mean of each lane's housekeeping gene copy counts/ arithmetic mean of all geometric means). Copy count data was then multiplied by this lane specific content normalisation factor, as long as this was less than 10.

After normalisation, samples were subjected to principal component analysis (PCA) and outliers removed. The remaining samples were taken forward for analysis. Comparison of the mean copy count for each gene between groups was performed using a paired Students T-test; p-values were corrected for multiple testing using the Benjamini-Hochberg correction method and false discovery rate (FDR) thresholds at 5% and 10% set. Fold-change and FDR values were $\log_2$ transformed for each gene and plotted as Volcano plots.

Heatmaps were generated focusing on the significantly up or down-regulated genes (at the 5% FDR level) using Z-scores. Significantly upregulated genes were then entered into online Gene Ontology resource and Panther Reactome analysis undertaken to generate pathway analysis (Ashburner *et al.*, 2000; Mi *et al.*, 2019). Significantly enriched processes and pathways are identified and visualised.

5.2.9.2 Proteomics and phosophoproteomics

Results from LC/MS were matched to peptides and phospho-peptides using Mascot searches on the SwissProt/Uniprot online database: online software Mascot identifies peptide sequences from mass spectrometry data and matches them to known peptides on the UniProt online database. Peptides were then mapped to Gene Ontology IDs using online database DAVID (Huang, Sherman and Lempicki, 2008), as described in Casado *et al.,* (Casado *et al.*, 2013), generating a list of peptides and phosphorylated peptides found in tissue samples that map to specific gene ontologies. From this entire dataset, Gene ontology IDs which were related to immunological processes and function were isolated by searching through the dataset using immunological terms and a unique list of peptides and phosphopeptides generated with direct relation to immunological processes and cell populations.

Thereafter, normalised data on the peptide abundance between tumour and liver was compared using a paired Student's T-test, and fold changes calculated between mean peptide abundance values. Benjamini-Hochberg correction for multiple comparisons was undertaken, false discovery rates calculated and rates of 10% and 25% taken as significant. Volcano plots of $\log_2$(Fold change) against log2(FDR) were plotted and significantly upregulated peptides and phosphorylated peptides were analysed using the Gene Ontology resource as above (Ashburner *et al.*, 2000; Mi *et al.*, 2019).

5.3 RESULTS

5.3.1 Patient characteristics – transcriptomics

Samples from sixteen patients with sufficient cells after mechanical dissociation and cell extraction were collected for gene expression analysis. Table 5.1 outlines the clinical details and characteristics of the cases in this series. After removal of outliers and samples which failed quality control, either because of a content normalisation factor outside of the acceptable range (and therefore indicating inadequate RNA quantity) or because the sample was an outlier on principal component analysis, 9 pairs remained which could be analysed. Table 5.2 outlines details of cell yield from each case, if it was excluded from analysis and if so, on what basis. Of the nine cases taken forward, 3 had undergone prior chemoembolization: 2 of which were cases of tumour 'down-staging' before transplantation, the third case receiving chemoembolisation before hepatic resection. Treated and untreated groups are outlined and compared in Table 5.3. There are no significant differences between the groups, although the sample sizes for comparison are small, making statistical comparisons less reliable. One of the tumour samples (SHCC76, an untreated case) was excluded from the paired analysis because the liver sample from the same case was an outlier on principal component analysis; however it was used in the secondary analysis comparing macrophages from treated and untreated tumours (Figure 5.5).

5.3.2 Cell sorting and yield

Cells were sorted according to the gating strategy outlined in Figure 5.1. To summarise, live single cells were isolated using a viability dye. A lineage gate used to label (and therefore exclude) T cells (CD3), B cells (CD19), NK Cells (CD56) and neutrophils (CD15) by gating on the lineage negative population. Thereafter, CD14+CD11b+ positive cells were positively selected and collected. HLA-DR+ and HLA-DR- cells were sorted, counted and collected in

RPMI. The yield of HLA-DR- cells was low, and the majority were less than 3000 cells. On this basis, they were not taken forward for analysis as this was likely to yield insufficient RNA for effective analysis.

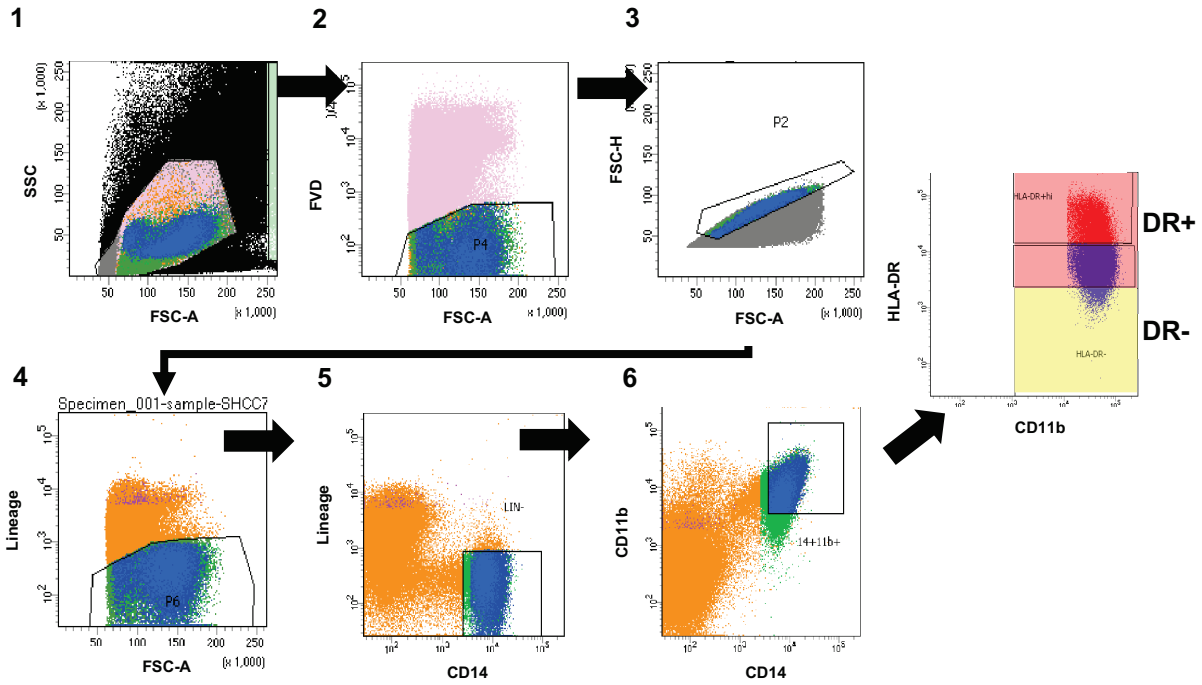

Figure 5.1: Fluorescence activated cell sorting (FACS) gating strategy for macrophages Mononuclear cells were stained using a panel of fluorescent antibodies (details in paragraph 5.2.2). Gating sequence is in numerical order: mononuclear cells were selected from the total cell population (1), before gating on live cells (2), excluding doublets (3) and excluding cells that stain positive for any of the lineage markers (4). CD14+CD11b+ cells were then positively selected (5 & 6). HLA-DR+ cells are macrophages; HLA-DR- cells are myeloid derived suppressor cells.

Trial ID	Age (years)	Sex	Aetiology	Tumour Size (mm)	Treated	AFP [IU/ml]	Bilirubin (μmol/l)	Platelets ($x10^9$/ml)	INR	MELD
SHCC19	77	M	ARLD	37	Y	2	6	269	1.06	7
SHCC23	60	M	Sporadic	180	N	30	11	401	1.4	10
SHCC36	58	F	ARLD	14	N	143	12	182	1.14	7
SHCC47	51	M	ARLD	44	N	3	122	86	1.73	21
SHCC51	57	M	NAFLD/ALD	25	Y	3	14	136	1.3	9
SHCC53	82	F	Sporadic	57	N	78	5	252	1.02	7
SHCC60	70	M	ARLD	27	N	76	14	90	1.45	11
SHCC64	45	F	A1AT	100	N	442	8	339	1.03	6
SHCC70	79	M	ARLD	23	N	2	7	154	1.15	11
SHCC72	57	M	NAFLD	26	Y	1	12	107	1.24	9
SHCC76	81	F	ARLD	28	N	7	20	136	1.25	10
SHCC77	71	F	ARLD	18	Y	3	25	139	1.12	9
SHCC84	81	M	Sporadic	65	N	14	29	199	1.17	11
SHCC85	79	M	NAFLD	25	N	95	9	268	1.18	8
SHCC89	55	M	HCV(SVR)	17	N	3	8	184	1.2	9
SHCC94	59	M	HCV(SVR)	37	N	7	9	245	1.02	7
Median (Range) / Ratio	65 (45 – 82)	11: 5 (M:F)	-	27.5 (14–180)	4:12 (Y:N)	7 (2 – 442)	11.5 (5 -122)	183 (86- 401)	1.17 (1.02 – 1.73)	9 (6 – 21)

Table 5.1: Clinical parameters and demographics of cases in which macrophage transcriptomics was attempted

Macrophages from n=16 cases were sorted for transcriptomics using FACS; RNA was extracted from cell lysates and Nanostring gene expression analysis undertaken. 742 genes were analysed; comparative expression between tumour and surrounding liver macrophages was undertaken. All patients were BCLC stage A meeting either Milan Criteria for transplantation or fit for resection according to Barcelona staging, with only one case (SHCC47) having decompensated disease. Median values and (range) are highlighted for each parameter; ratios are provided for categorical data. Abbreviations: *NAFLD=non-alcoholic fatty liver disease, ARLD= alcohol related liver disease, HCV (SVR)=hepatitis C virus (sustained virological response), A1AT=alpha-1 antitrypsin deficiency, AFP=alpha-fetoprotein, INR= international normalised ratio, MELD=Model for End-Stage Liver disease, FACS = fluorescence activated cell sorting*

Trial ID	Treated	Tumour Cell Yield (DR+)	Liver Cell Yield (DR+)	Pair used in analysis? (Y/N)	If No: reason for exclusion
SHCC19	Y	7016	8871	Y	-
SHCC23	N	24760	96065	Y	-
SHCC36	N	2584	56121	Y	-
SHCC47	N	30707	163722	Y	-
SHCC51	Y	7686	52888	Y	-
SHCC53	N	39266	139955	Y	-
SHCC60	N	2933	2575	N	Content normalization factor (tumour macrophages)
SHCC64	N	25013	40272	Y	-
SHCC70	N	10695	72389	Y	-
SHCC72	Y	3376	40272	N	Content normalization factor (tumour macrophages)
SHCC76	N	34150	3835	N	PCA outlier (liver macrophages)*
SHCC77	Y	3155	15595	Y	-
SHCC84	N	16782	131347	N	PCA outlier (tumour macrophages)
SHCC85	N	5372	12461	N	Content normalization factor (tumour macrophages)
SHCC89	N	5335	31034	N	Content normalization factor (tumour macrophages)
SHCC94	N	16600	8098	N	Content normalization factor (liver & tumour macrophages)
Treated Y:N	4:12 (Y:N)	-	-	-	-

Table 5.2: Yield of macrophages from cell sorting of extracted mononuclear cells from cases of HCC and their surrounding liver

Sixteen cases were sorted using the gating strategy outlines in Figure 5.1. CD14+CD11b+HLA-DR+ macrophage yield was measured after each cell sort. Despite some cases with less than 5000 cells, cell lysates from all 16 cases were analysed using nCounter Nanostring technology. Cases that were subsequently excluded are noted on the right of the table; the reason for this is provided alongside. **NB: SHCC76 tumour HLA-DR+ cells were used when comparing treated and untreated tumours (Figure 5.5).*

	Treated (n=3)	Untreated (n=6)	p-value
Age	71 (57 – 77)	59 (45– 82)	0.908
Sex (M:F)	2:1	3:3	0.999
Aetiology			
- ARLD	2	3	
- NAFLD	1	1	
- Other	0	2	0.509*
Bilirubin (mmol/L)	14 (6 – 25)	9.5 (5 – 122)	0.748
Platelets ($x10^9$/ml)	139 (136 – 269)	217 (86 – 401)	0.752
AFP (IU/ml)	3 (2-3)	54 (2 – 442)	0.064
MELD score	9 (7 – 9)	8.5 (6 – 21)	0.556
Lesion size (mm)	25 (18 – 37)	50.5 (14 – 180)	0.433

Table 5.3: Clinical characteristics of the two sub-groups analysed by transcriptomics

Tumour macrophages from cases with (n=3) and without (n=6) prior chemoembolization were compared using Nanostring transcriptomics technology. The clinical and demographic characteristics of the groups are compared and are broadly similar (Statistical analyses: Mann-Whitney test for numerical data; Fisher's exact test for categorical data and *Chi squared testing). *Abbreviations: ALD = alcohol related liver disease; NAFLD = non-alcoholic fatty liver disease; AFP = alpha-fetoprotein; MELD = model for end-stage liver disease. Data are presented as median with (range).*

5.3.3 Tumour associated macrophages possess hallmarks of reduced activity of MerTK and Axl signalling

Figure 5.2 outlines a volcano plot demonstrating a distinct tumour specific phenotype for macrophages isolated from patients with HCC, with a clear separation of genetic expression between both populations. When tumour and liver macrophages were compared, 100 genes of the 742 were significantly different after Benjamini-Hochberg correction with a false discover rate (FDR) of 5%; with the FDR set at 10%, this rose to 199. Cluster heatmap analysis was performed (Figure 5.3A), outlining a clear tumour related gene signature. The majority of statistically significant genes were downregulated in the tumour associated macrophages. The observation that there is an overall downregulation in gene expression in the tumour derived population is a similar finding to the expression profile by qPCR from tumour tissue seen in Chapter 3 (see paragraph 3.3.10).

Table 5.4 below highlights a selection of key genes of interest relating to TAM-RTK signalling in macrophages. Firstly, CD68 expression was high and similar in each population, indicating that a highly pure macrophage population had been isolated. For both MerTK and Axl, there was an increase in fold change expression in the tumour derived population, but this did not meet statistical significance, with non-significant p-values ($p=0.29$ for Axl, $p=0.18$ for MerTK). TAM-RTK expression is therefore not significantly upregulated in the tumour microenvironment in HCC, based on this sample of cases.

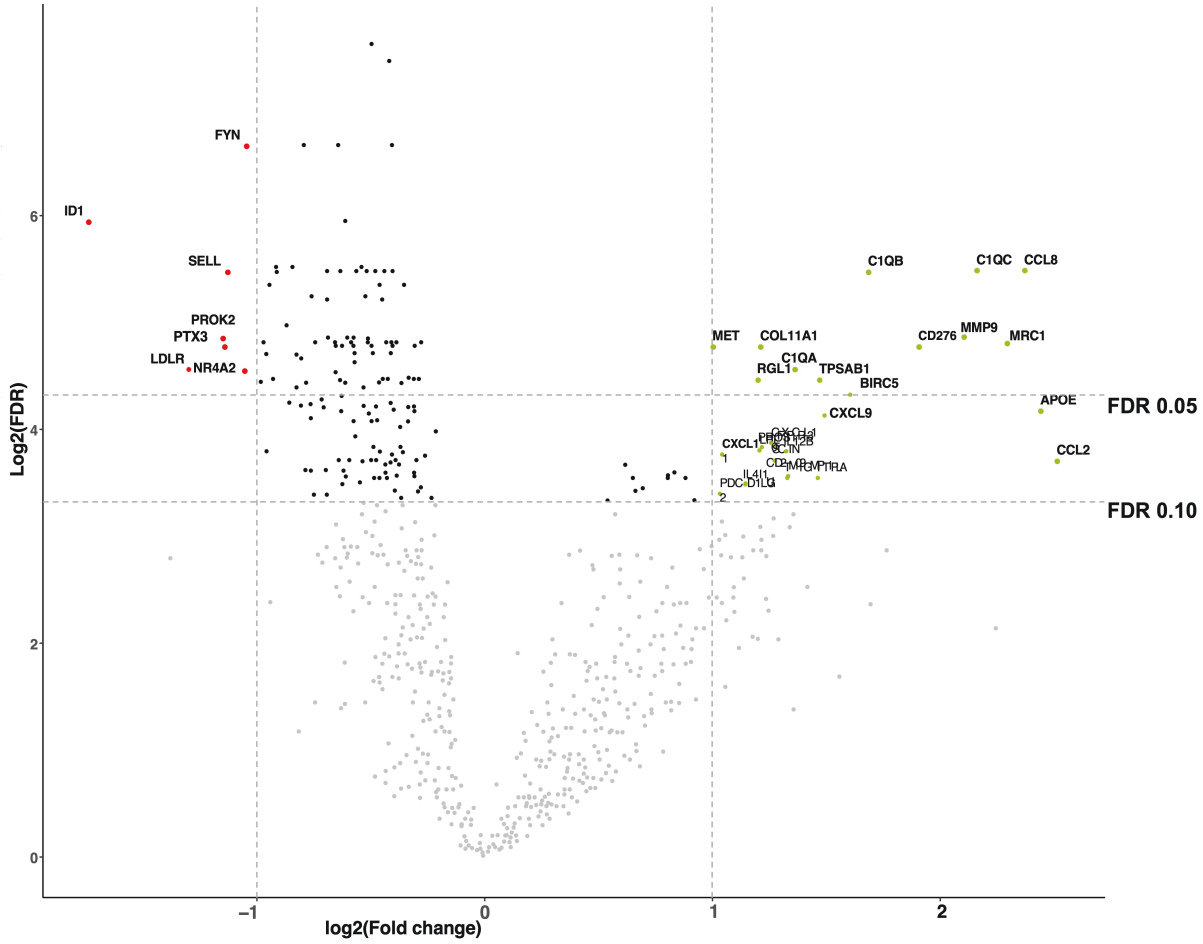

Figure 5.2: Transcriptomic profiling of macrophages from patients with HCC outlines a clear tumour associated macrophage phenotype

Nanostring analysis of n=9 sample pairs extracted from patients with HCC was performed; tumour associated macrophages were compared directly with liver macrophages from the same patients. Volcano plot of log2(fold change) against $\log_2$(FDR) after paired T-test analysis; horizontal dashed lines indicate FDR of 0.10 and 0.05. Vertical dashed lines demarcate a fold change between tumour and liver of at least 2. Red genes to the left are significantly downregulated in tumour associated macrophages; green genes to the right are upregulated. Abbreviations: *FDR – false discovery rate*

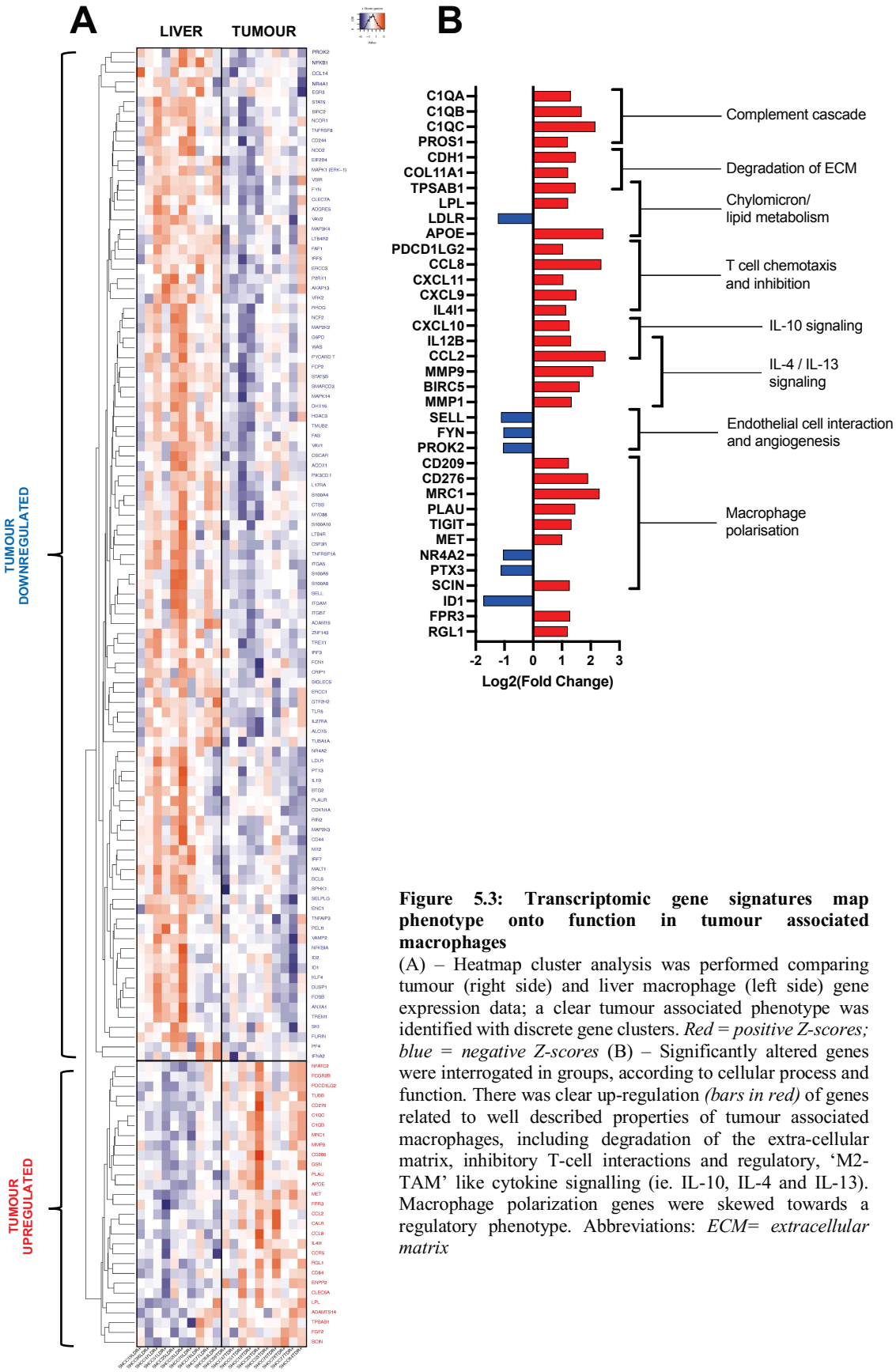

Figure 5.3: Transcriptomic gene signatures map phenotype onto function in tumour associated macrophages

(A) – Heatmap cluster analysis was performed comparing tumour (right side) and liver macrophage (left side) gene expression data; a clear tumour associated phenotype was identified with discrete gene clusters. *Red = positive Z-scores; blue = negative Z-scores* (B) – Significantly altered genes were interrogated in groups, according to cellular process and function. There was clear up-regulation *(bars in red)* of genes related to well described properties of tumour associated macrophages, including degradation of the extra-cellular matrix, inhibitory T-cell interactions and regulatory, 'M2-TAM' like cytokine signalling (ie. IL-10, IL-4 and IL-13). Macrophage polarization genes were skewed towards a regulatory phenotype. Abbreviations: *ECM= extracellular matrix*

Gene	**Liver** (normalised, log2-transformed)	**Tumour** (normalised, log2-transformed)	**p-value**	**Benjamini Hochberg p-value**
AXL	5.797871337	6.346844662	0.29263158	0.44596829
MERTK	8.764676788	9.05776657	0.18647948	0.32903268
TYRO3	3.453539727	3.173484138	0.42316576	0.58029986
ERK-1	9.608972433	9.202379493	**5.58E-05**	**0.009933**
PIK3CD	9.381693326	8.746839145	**0.00060401**	**0.02248537**
PIK3CG	8.882938448	8.482883484	0.0683079	0.18385244
AKT-1	8.468921756	8.192695553	**0.036747481**	**0.128395131**
SOCS1	6.967789062	7.011870433	0.90204585	0.94864159
SOCS3	10.44391961	9.94455917	**0.01467427**	**0.07657926**
STAT1	10.70625593	10.80729821	0.662962457	0.769579226
STAT3	9.053239752	8.837907565	0.29060933	0.44471981
STAT6	10.38063847	9.813878836	**0.00073402**	**0.02248537**
NFKB1	7.17932564	6.76724058	**0.00720639**	**0.05350737**
NFKBIA	13.0641274	12.2978371	**0.00721069**	**0.05350737**
TGFB1	10.0416538	9.70505581	**0.00474595**	**0.04486051**
IL12B	1.00230469	2.31163061	**0.01299951**	**0.07268742**
IFNAR1	8.984943193	8.775691131	0.12248731	0.25728817
IFNAR2	9.588254411	9.280118796	**0.018483**	**0.08496824**
IL10	6.275867429	6.248609973	0.92404429	0.95505574
HLA-DRA	13.73397125	13.99186642	0.16083561	0.3016453
HLA-DRB3	12.76720534	12.97392884	0.24080243	0.3917974
PROS1	4.389588193	5.589682475	**0.01212291**	**0.07077641**
CCR2	9.349860419	9.032591003	0.30277782	0.45704484
CD68	10.99316572	10.9144305	0.66842106	0.77365353

Table 5.4 Log transformed mean copy count data for genes related to MerTK and Axl signalling after comparative transcriptomic analysis of tumour and liver macrophages in HCC

Gene expression data for key genes related to TAM-RTK signalling and macrophage phenotype are outlined above, comparing paired tumour and liver samples. Individual p-values are provided from a paired Student's T-test of $\log_2$ transformed (mean copy count) comparing tumour and liver. Benjamini-Hochberg p=values are provided to give a false discovery rate; those that are less than 0.10 are highlighted in bold.

Downstream transcription factors and signalling molecules of TAM-RTK signalling reveal a clearer picture. A range of key downstream targets are significantly downregulated, perhaps indicating a reduction in signalling through MerTK and Axl. These include ERK-1, PI3-kinase and AKT. Furthermore, SOCS3 (but not SOCS1) and TGF- β is downregulated; these are further downstream of both MerTK and Axl signalling cascades. IL-12β is more highly expressed in the tumour environment (p=0.01, 0.07 after BH correction) – this M1 polarising

cytokine is inhibited by MerTK signalling. The observation that IL-10 is not significantly different between the compartments is equally significant. This cytokine forms part of a positive feedback loop for MerTK expression and would be expected to be elevated in cell populations with active MerTK signalling (Graham *et al.*, 2014a).

There are other indicators of a more nuanced picture, however. Expression of MerTK ligand Pros-1 is significantly elevated in tumour associated macrophages (p=0.01; 0.07 after BH correction). Ubil *et al.* describe how Pros-1 derived from tumour cells prevents M1 cytokine release in macrophages; an effect mediated via MerTK signalling (Ubil *et al.*, 2018). From our data, Pros-1 production has not resulted in a significant upregulation of MerTK expression, however. Pros-1 mediated activation of MerTK signalling in macrophages results in the production of IL-10 (Maimon *et al.*, 2021), which has not been observed either. Therefore, the significance of this observation with respect to activation of MerTK signalling is not immediately apparent.

NFκβ is significantly downregulated in the tumour (p=0.007, 0.05 after BH correction). Signalling through this central transcription factor is negatively regulated by MerTK (Camenisch *et al.*, 1999), but it can be activated by Axl in cancer cell lines (Paccez *et al.*, 2015). NFκβ is a critical central transcription factor with an established role in classical activation of macrophages, generating an M1 phenotype. Active NFκβ signalling in macrophages can help to limit tumour progression in mouse models of ovarian cancer (Hoover *et al.*, 2020). Downregulation at a population level, therefore, would suggest a skewing of tumour associated macrophages in this dataset towards an M2-like, immune regulatory phenotype.

NFκβ has a wide array of potential ligands and regulatory mechanisms (Dorrington and Fraser, 2019), making it difficult to attribute differential NFκβ expression to MerTK or Axl mediated signalling alone. In support of the complexity of NFκβ expression and signalling, expression of a key inhibitory protein, IκBα (gene NKFBIA; p=0.007, 0.05 after BH correction) is also downregulated. IκBα can help regulate oscillations in transcription of NFκβ in response to activating upstream signals. In doing so, this affects the temporal dynamics of NFκβ mediated transcription and can result in epigenetic changes that modulate the inflammatory response to environmental triggers (Cheng *et al.*, 2021). The significance of loss of this role in the tumour microenvironment has not been investigated.

Attenuation of pro-inflammatory cytokine induced signalling can be mediated by MerTK and Axl binding to subunits of the IFN receptor (Rothlin *et al.*, 2007). In this analysis there was a non-significant reduction in expression of subunit IFNAR1 (p=0.12, 0.26 after Benjamini-Hochberg (BH) correction) and, notably, a significant reduction in subunit IFNAR 2 (p=0.01, 0.08 after BH correction). IFNAR2 has been described to be upregulated in Axl+ dendritic cells in which there is active Axl signalling. This may suggest that active Axl signalling is not evident in these macrophages; however, it is important to note that this signalling pathway mediated through IFNAR subunits has not been described in macrophages, but in dendritic cells only.

HLA-DR expression was examined between the compartments, in view of the consistent finding of enriched, 'HLA-DR^{HI}' populations in the tumour by flow cytometry. On this analysis, there was no significant difference between the two tissue compartments but overall expression is very high between both populations (p=0.16 and 0.24 respectively for HLA-DRA and HLA-DRB3; 0.30 and 0.39 after BH correction). These data would suggest that the

enrichment in surface HLA-DR expression in the tumour microenvironment identified by flow cytometry is not reflected in a differential expression of HLA-DR at the level of transcription.

Given that HLA-DR is consistently co-expressed at higher levels on MerTK+ and Axl+ macrophages, this finding provides further evidence that tumour associated macrophages do not up-regulate expression of MerTK and Axl when compared with hepatic counterparts. As a marker of differentiation in monocytes and macrophages, high HLA-DR expression in both populations confirms that cells sorted and compared in this analysis were well differentiated, echoing the predominantly 'HLA-DR^{HI}' phenotype seen at flow cytometry. A significant down-regulation of ID1, a gene found overexpressed in less differentiated myeloid derived suppressor cells, provides further phenotypic confirmation of this (Figure 5.3 B) (Melief *et al.*, 2020).

5.3.4 Tumour associated macrophages have a distinct phenotype outlined by gene expression analysis

Figure 5.2C and 5.3A highlight the existence of a specific gene expression signature in tumour associated macrophages in HCC. Table 5.4 outlines some key genes related to TAMϕ function, and their expression in both liver and tissue macrophages. Figure 5.3 B also highlights key genes identified at least 2-fold difference (up or down) from liver macrophages, arranging them by cellular function and process.

Firstly, a significant upregulation of CD276 in the tumour derived population is notable. CD276 is a monocyte derived macrophage marker; therefore, this underlines that the predominant ontogeny of tumour associated macrophages in HCC is from circulating

monocytes, and that (as expected) the liver has a higher population of resident macrophages, i.e. Kupffer cells.

Gene	Liver (normalised, log2-transformed)	Tumour (normalised, log2-transformed)	p-value	Benjamini Hochberg p-value
C1QB	7.856628511	9.539171808	**0.00058728**	**0.02248537**
C1QC	7.152574423	9.310957998	**0.00046113**	**0.02248537**
C1QA	7.354231432	8.655949065	**0.0043437**	**0.042579**
TREM1	10.2620231	9.317400361	**0.00092783**	**0.02455664**
S100A8	13.67969289	12.70952182	**0.00221825**	**0.03565704**
S100A9	15.03359746	14.07496361	**0.00354376**	**0.0382237**
STAB1	7.948344379	8.487919691	**0.02491455**	**0.09940778**
LPL	3.920182289	5.126552523	**0.012411903**	**0.07193468**
LDLR	6.790238227	5.565101427	**0.004026594**	**0.039963943**
APOE	5.299543795	7.738079464	**0.008216873**	**0.055289806**
CD274	3.513980215	4.570884365	0.03399812	0.12439865
TREM2	5.098224665	6.863290432	0.04198	0.13742671
IDO1	5.387036182	6.34909004	0.05370256	0.15505395
IDO2	1.592352736	2.223201802	0.25581991	0.40543116
ARG1	1.833455514	3.250580478	0.06317328	0.17416523
ARG2	3.636323118	3.642896837	0.98824944	0.99451211
CD163	9.00998918	9.555481031	0.16693165	0.3068142
VEGFA	9.170238034	9.17098891	0.99858295	0.99982262
VEGFC	1.021185241	1.484995558	0.49105006	0.64130032
CD47	9.793779498	9.646289123	0.17453688	0.31495974
MARCO	4.762723818	5.42106942	0.22286738	0.37206044
CD14	11.62322277	11.36923231	0.38824589	0.54587422
CD16	11.06166968	11.34635934	0.31689542	0.47385116
CSF1R	7.258720277	7.400153913	0.36781057	0.52715089
CX3CR1	8.505120375	8.746267931	0.39960028	0.55761445

Table 5.5: Log transformed mean copy count data for genes related to tumour-associated macrophage function after comparative transcriptomic analysis

Gene expression data for key genes related to TAM-RTK signalling and macrophage phenotype are outlined above, comparing paired tumour and liver samples. Individual p-values are provided from a paired Student's T-test of $\log_2$ transformed (mean copy count) comparing tumour and liver. Benjamini-Hochberg p=values are provided to give a false discovery rate; those that are less than 0.10 are highlighted in bold.

Other typical characteristics of tumour associated macrophage are apparent. An increase in expression of both IDO1 and ARG1 was demonstrated, although both did not reach statistical significance. These genes have both been described as key features of the altered metabolic signature in tumour associated macrophages (Schupp *et al.*, 2017). There was a reduction in

M1 polarising gene TREM1 (BH p-value=0.0245) (Yang *et al.*, 2019) with an increase in TREM2 expression on tumour associated macrophages (p=0.04, albeit non-significant after BH correction, p=0.1374). TREM-2 expression is associated with wound healing in liver injury (Coelho *et al.*, 2021) and increased expression is associated with poor responses to immunotherapy (Molgora *et al.*, 2020). In addition, 'M2-like' cytokine production through genes including IL4IL and IL-12B and TIGIT are increased. TIGIT is an immune checkpoint that has been demonstrated to skew macrophages towards a regulatory phenotype (Noguchi *et al.*, 2019). Tumour associated macrophages in this study overexpress PLAU – a gene that has been demonstrated to induce a pro-fibrotic, M2 phenotype (Meznarich *et al.*, 2013). Taken together with reduced NFκβ transcription and a significant increase in the expression of CD206/MRC1, the profile of gene expression in these tumour associated macrophages is in keeping with a phenotype that is permissive of tumour progression and skewed away from classical activation and production of pro-inflammatory cytokines.

There is significant upregulation of genes related to other well described attributes of tumour associated macrophages. This includes genes related to degradation of the extracellular matrix such as matrix metalloproteases MMP9 and MMP1, chemokines involved in T-cell chemotaxis - CXCL9 and CXCL11 (de Masson *et al.*, 2022) and inhibition of T cell activation such as PDL2 (Latchman *et al.*, 2001). There was a reduction in genes related to endothelial cell interaction and angiogenesis, however: a key tumour promoting function of tumour associated macrophages, the tumour derived population saw reduced expression of L-selectin (SELL) and transcription factor FYN, which is downstream of vascular endothelial growth factor (VEGF) (Werdich and Penn, 2005). PROK2 has been similarly described to be pivotal in promoting angiogenesis in cancer cell lines (Kurebayashi *et al.*, 2015) and has reduced expression in the tumour environment. This pattern of PROK2 expression has been previously

described in HCC (Monnier *et al.*, 2008), with PROK2 being expressed more highly on Kupffer cells.

5.3.5 Gene ontology enrichment analysis highlights key functional characteristics of tumour associated macrophages in HCC

5.3.5.1 Ontology results

Interrogation of significantly upregulated genes has helped to identify a tumour associated macrophage phenotype. Pathway enrichment analysis using the Gene Ontology database has further helped to elucidate a hierarchy of enriched functions within this population in HCC. Table 5.6 and Figure 5.4 illustrate the pathways and aspects of function identified. When taken together with the volcano plot of differential gene expression (Figure 5.2), four key features were identified: chylomicron remodelling and altered lipid metabolism, breakdown of the extracellular matrix and matrix metalloprotease activation, cytokine signalling mediated through IL-10, IL-13 and IL-4, and activation and regulation of the complement cascade.

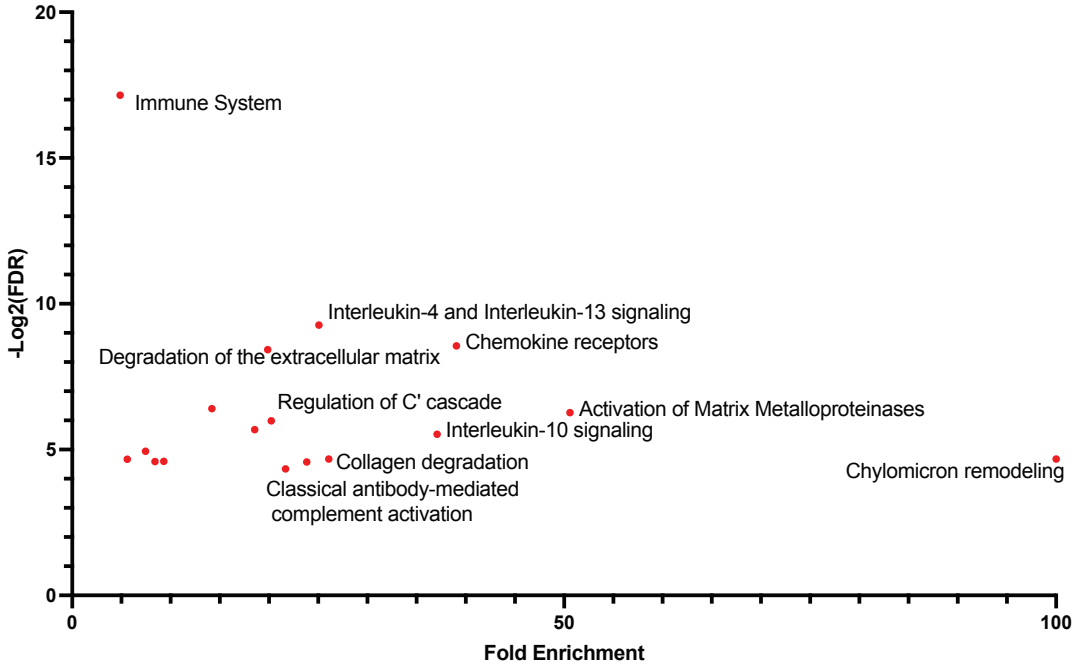

Figure 5.4: Gene ontology analysis of upregulated genes by pathway and function analysis
This graphical representation of the data in Table 5.5 helps to visualise the degree of enrichment of specific cellular processes and functions within TAM from patients with HCC, based on transcriptomic analysis. *Abbreviations: FDR – false discovery rate.*

Reactome Pathway with hierarchy	Fold enrichment	p-value	-Log2(FDR)
Chylomicron remodelling	**100**	2.04E-04	4.67300254
Activation of Matrix Metalloproteinases	**50.59**	3.64E-05	6.26534457
↳ Degradation of the extracellular matrix	**19.87**	5.83E-06	8.42476513
Chemokine receptors bind chemokines	**39.05**	4.25E-06	8.55979192
↳ Peptide ligand-binding receptors	**14.2**	2.83E-05	6.40506933
↳ Class A/1 (Rhodopsin-like receptors)	**8.41**	3.16E-04	4.59074485
Interleukin-10 signalling	**37.1**	8.69E-05	5.52616115
↳ Signalling by Interleukins	**7.45**	1.43E-04	4.94341647
↳ Cytokine Signalling in Immune system	**5.59**	2.21E-04	4.66932688
Collagen degradation	**26.08**	2.35E-04	4.67668758
Interleukin-4 and Interleukin-13 signalling	**25.07**	1.95E-06	9.26979047
Classical antibody-mediated complement activation	**23.85**	3.03E-04	4.57346686
↳ Creation of C4 and C2 activators	**21.68**	3.97E-04	4.33642766
↳ Complement cascade	**18.55**	7.05E-05	5.68038207
Regulation of Complement cascade	**20.23**	5.08E-05	5.98393163
G alpha (i) signalling events	**8.83**	2.53E-04	4.66566056

Table 5.6: Gene ontology analysis of upregulated genes defines an hierarchy of enrichment and outlines key functional characteristics of tumour associated macrophages in HCC

Up-regulated genes were entered into online database, Panther, for gene ontology enrichment analysis by Reactome pathway. Enrichment scores for key cellular processes are generated by mapping the number of genes within a particular pathway (or pathways) that are found enriched within a sample.

5.3.5.2 Lipid Metabolism, the extracellular matrix and cancer cell migration

Genes related to lipid metabolism are strongly differentially expressed in tumour macrophages in this sample, with elevated LPL (lipoprotein lipase) and APOE (apolipoprotein E) and reduced expression of the LDL receptor, LDLR (Table 5.5). Recent work has identified lipid metabolism as a metabolic switch in tumour associated macrophages that promotes pro-inflammatory cytokine production and may be beneficial for tumour clearance (Rabold *et al.*, 2020). There is also growing evidence that altered lipid metabolism in tumour associated macrophages is directly linked to cancer cell motility and migration. Zheng *et al.* describe higher ApoE expression on M2-skewed tumour associated macrophages in gastric cancer.

Furthermore, exosomes expressing ApoE released from these macrophages can then activate PI3K/Akt signalling in tumour cells, resulting in increased tumour cell migration (Zheng *et al.*, 2018). A further recent study demonstrated a similar mechanism in prostate cancer. Tumour cell released IL-1β can stimulate LDL uptake from the tumour microenvironment by scavenger receptor MARCO (a well-recognised tumour associated macrophage marker). The resultant lipid loaded TAMϕs release CCL6, which promotes tumour cell migration and motility (Masetti *et al.*, 2021).

It is not clear if any such process is underway in HCC, and MARCO expression was not significantly elevated in this sample. However, it is notable that these two functions were enriched on pathway analysis together; matrix metalloproteases MMP1 and MMP9 are also elevated in tumour macrophages in this study (BH p-values 0.08 and 0.03 respectively): these are directly involved in breakdown of the extracellular matrix to promote tumour migration and metastasis. This mechanistic link poses questions specific to HCC – lipid accumulation in tumour phagocytes (particularly in steatohepatitic lesions or in those related to NAFLD cirrhosis) may play a mechanistic role in tumour biology.

5.3.5.3 Complement cascade component C1Q expression in tumour associated macrophages

There was a notable clustering of up-regulated genes from the complement cascade – all 3 sub-component chains of the C1Q complex: C1QA, C1QB and C1QC (BH p-values= 0.0224, 0.0224 and 0.0426 respectively, see Table 5.5). Other components of the complement cascade were not significantly elevated, including C3, C4A and C5. Notably, PTX3 is significantly downregulated within the macrophage population (p=0.002, 0.03 after BH correction). Pentraxin 3 is a well-established ligand of C1q and plays a role both in regulating activation of

the classical pathway of complement activation in the circulation via Factor H, as well as promoting C1q mediated efferocytosis and cytotoxicity by binding to apoptotic cells and pathogens (Bottazzi *et al.*, 2010). Recent work has characterised a parallel role for PTX3 within the tumour microenvironment. By helping to prevent overactivation of complement via Factor H it prevents C5a mediated chemotaxis of monocytes to the tumour via CCL2. CCL2 promotes M2 macrophage polarisation, resulting in the accumulation of tumorigenic TAMϕs within the lesion (Bonavita *et al.*, 2015). Notably, in our analysis there is a significant upregulation of CCL2, perhaps suggesting that a lack of PTX3 is having this very effect.

There are other mechanisms by which C1q can play a deleterious role within the tumour microenvironment. In a mouse model of melanoma, C1q deficient mice have a much slower progression of disease and increased survival (Bulla *et al.*, 2016) and C1QA, B, C expression are associated with poor prognosis in breast cancer (Winslow *et al.*, 2015). Tumour derived C1r, C1s, C3, C4 interacts with macrophage derived C1q, resulting the activation of the complement cascade, opsonisation and recruitment of an inflammatory infiltrate into the tumour microenvironment (Roumenina *et al.*, 2019). C1q is a well-known opsonin for apoptotic cells (Ogden *et al.*, 2001). Downstream of C1q binding, macrophages are skewed towards a regulatory phenotype (Benoit *et al.*, 2012) have enhanced efferocytotic activity and increased survival (Pulanco *et al.*, 2017).

In this way, C1q functions in a manner similar to MerTK. Crucially, C1q mediated efferocytosis in macrophages has been demonstrated to act via MerTK dependent mechanism in murine macrophages (Galvan *et al.*, 2014). It is therefore possible that the M2 skewed phenotype seen in tumour associated macrophages in this sample is a result of direct action of autocrine C1q, produced after efferocytosis. Indeed, APOE is another gene known to be up-

regulated after efferocytosis and is expressed at a significantly higher level in the tumour derived population, as described above. This would be consistent, therefore, with a post-efferocytosis macrophage phenotype. Although a significant increase in MerTK expression has not been observed in this analysis, expression is higher in the tumour population and the proportion of MerTK that is phosphorylated (and therefore active in signalling) is not known.

5.3.6 Prior treatment with locoregional therapy alters the transcriptomic profile of macrophages, but MerTK and Axl are unchanged

In order to explore the effect of chemoembolisation on macrophage phenotype in HCC, tumour associated macrophages (TAMϕs) from cases with embolization prior to surgery were compared with those from patients in whom no embolization had been given. In addition to exploring the effect of tissue necrosis and hypoxia on TAM-RTK expression, a further aim of this sub-analysis was to ascertain if the dense infiltrates of MerTK+ macrophages seen at immunohistochemistry around areas of necrosis could be further characterise at a transcriptional level. As described above, Table 5.3 outlines the patient characteristics and clinical parameters of each group.

Figure 5.5 summarises this analysis and although there is a clear separation of gene expression, only 6 genes were significantly differentially expressed between the groups at a false discovery rate (FDR) of 0.10, with 9 genes when the FDR was increased to 0.20. Table 5.7 lists the genes with FDR <0.20. One gene was significantly up-regulated in cases with prior chemoembolisation – CCL22 (p=0.0001; 0.03 after BH correction). All other significant genes were downregulated after treatment, including Tyro-3 (p=0.0001; 0.04 after BH correction). Within this group, reduction in AIF1 expression is notable – expression is associated with M2 tumour associated macrophages in HCC and with disease progression (H. Cai *et al.*, 2017). In

addition, reduction in histone de-acetylase 3 (HDAC3) may be of clinical relevance – HDAC inhibitors have been shown to improve tumour responses to checkpoint inhibitor therapy by skewing macrophage phenotype towards anti-tumour immunity and inhibiting the recruitment of MDSCs (Li *et al.*, 2021). Both examples suggest an alteration in the skewing of macrophage phenotype towards anti-tumour immunity. Increased CCL22 expression after therapy, however, is less encouraging: CCL22 can promote chemotaxis of regulatory T cells and macrophage released CCL22 has been demonstrated to contribute to sorafenib resistance in HCC (Wiedemann *et al.*, 2019; Gao *et al.*, 2020).

Gene expression of MerTK and Axl was not significantly different between the groups; whereas before both receptors were up-regulated in the tumour environment, in this case, MerTK expression is lower in treated cases (albeit without statistical significance).

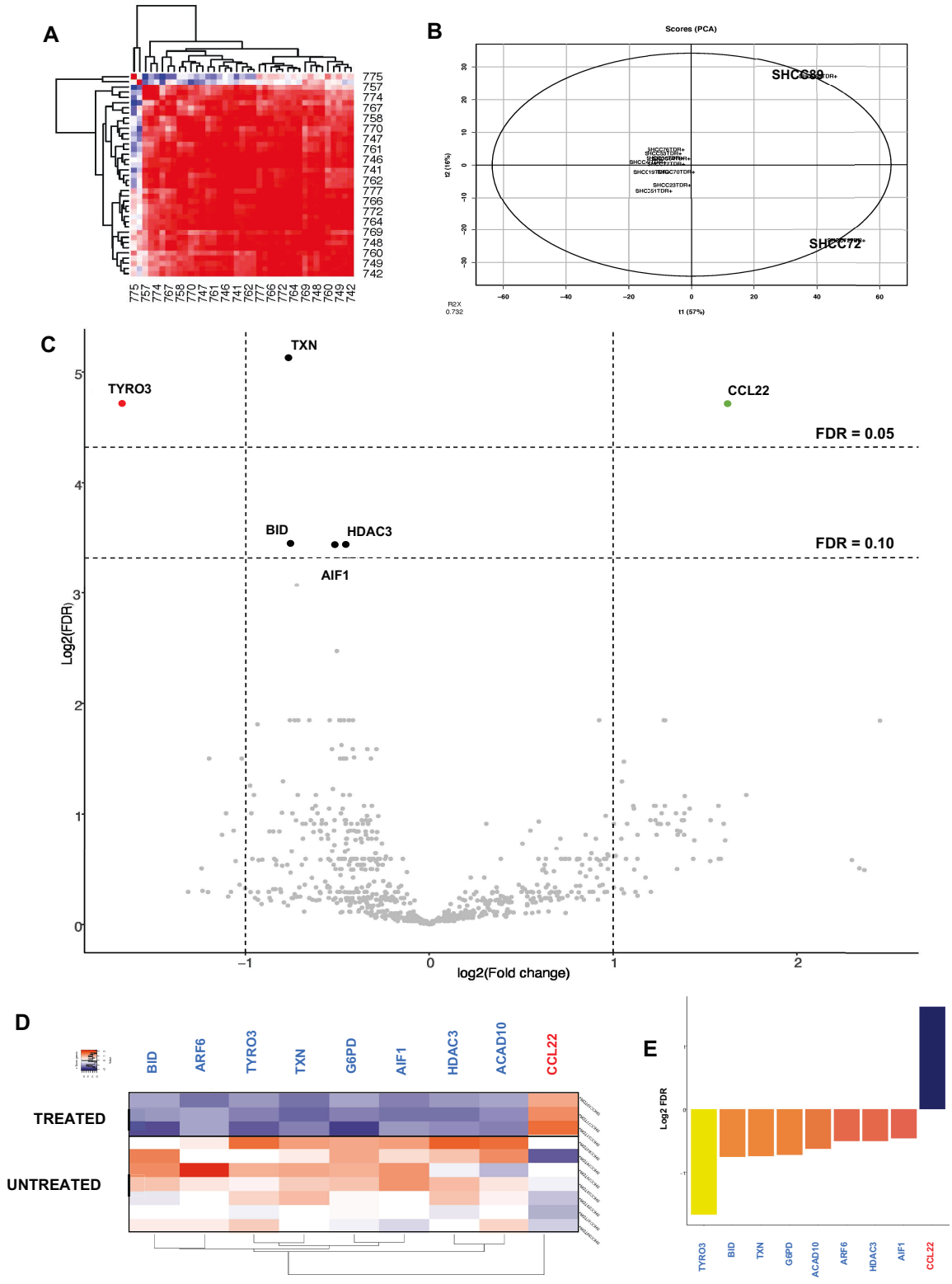

Figure 5.5: Macrophages isolated from treated HCC lesions display a distinct gene expression pattern when compared with tumour associated macrophages from untreated tumours

(A) Correlation of housekeeping genes was analysed *(as in paired analysis with liver macrophages, Figure 5.2);* three housekeeping genes were removed. (B) Principal component analysis was then used to remove outliers from the analysis, as before, resulting in removal of SHCC72 and SHCC89. (C) Volcano plot of log_2(fold change) between treated (n=3) and untreated (n=7) cases against log_2(FDR). (D) Heatmap and (E) bar chart of genes with a significant log2(fold change), at a false discovery rate of 0.20

Gene	Untreated HCC (**mean,** normalised, log2-transformed)	Treated HCC (**mean** normalised, log2-transformed)	p-value	BH p-value
TXN	9.139765162	8.396788664	3.59E-05	**0.028506759**
CCL22	2.196797103	3.819498491	0.00014433	**0.038199387**
TYRO3	3.0334467	1.364057745	0.000130796	**0.038199387**
AIF1	11.19784996	10.73609267	0.00048691	**0.092152286**
BID	9.180174653	8.424611688	0.000696365	**0.092152286**
HDAC3	7.373920089	6.868026899	0.000695705	**0.092152286**
ACAD10	6.045268525	5.417637026	0.001197752	**0.118876882**
G6PD	7.665749648	6.942697556	0.001056851	**0.118876882**
ARF6	9.549837582	9.04375809	0.002043319	**0.180266131**
MERTK	8.50045379	8.07090503	0.38286813	0.81980676
AXL	5.58885985	6.20512777	0.24197197	0.71422209

Table 5.7: Log transformed mean copy count data of relevant genes after comparative transcriptomic analysis between treated and untreated cases of HCC
Gene expression data from tumour associated macrophages comparing cases with prior chemoembolisation (n=3) and those without any form of locoregional therapy before surgery (n=6). Individual p-values are provided from a paired Student's T-test of $\log_2$ transformed (mean copy count) comparing the groups. Benjamini-Hochberg p=values are provided to give a false discovery rate; those that are less than 0.20 are highlighted in bold.

5.3.7 Proteomic analysis of tumour and liver tissue from patients with HCC

Both proteomic and phosphoproteomic analysis of tissue from eight patients with HCC was undertaken to identify if there is enrichment of both peptides and phosphopeptides related to downstream signalling from MerTK and Axl in HCC. This analysis had originally been planned to be undertaken on extracted mononuclear cells. However sufficient cells were not available after completing recruitment of patients into the study, based upon the requirements of cells for effective analysis (over 10 million per sample) and the percentage of mononuclear cells that express MerTK or Axl (between 20 – 50%, based on flow cytometry).

In lieu of this, tissue was used in its place. The immune component of the signal from the tissue was isolated using targeted search terms and comparative analysis is presented for proteomics in Figure 5.6 and Figure 5.7 for phosphoproteomics. The clinical characteristics of the cases

used for this paired analysis are outlined in Table 5.8**.** The majority were cirrhotic (n=6; 2 cases were sporadic HCC without chronic liver disease).

5.3.7.1 Proteomic analysis

A total of 6273 peptides were isolated and identified by liquid chromatography-mass spectrometry (LC-MS). Of these, 326 peptides were compared between tumour and liver after those related to immunity and immune cell function were extracted from the data. Firstly, Axl was not detected by proteomics in either tumour or liver tissue. The reason for this is not clear, as the protein extraction was successful and satisfactory yields were reported by the team at Queen Mary University London who conducted the mass spectrometry. MerTK peptide was elevated in tumour tissue, but this did not meet statistical significance (fold change 1.47; p=0.106; 0.351 after Benjamini-Hochberg correction). Transcription factors downstream of MerTK AKT and STAT3 were elevated as well but did not meet statistical significance (AKT: fold change 2.51; p=0.207; BH p-value 0.468, STAT3: fold change 1.17, p-value 0.367, after BH correction 0.622).

The volcano plot highlights a few key peptides that are differentially expressed. n=32 genes had an FDR less than 0.25, which was the level set for statistical significance given the small sample size. Significant up-regulation of LCP1 (Uniprot name PLSL) in the tumour indicates both that extraction of the immune signal was effective (LCP1 codes for lymphocyte cytosolic protein) and suggests that there is an enrichment of an inflammatory infiltrate in the tumours in this sample of cases. Amongst other significant proteins was a significant down-regulation of complement cascade proteins C4a and C4b in tumour tissue (fold change 0.21, p=0.0003, 0.027 after BH correction). In addition to this, pathway enrichment analysis of the statistically significant proteins has highlighted activation of C3 and C5 as significantly enriched in the

tumour tissue. This seemingly contradictory finding may reflect that formation of the C3 convertase results from the breakdown of C4 into fragments. In light of prior data from transcriptomics regarding an upregulation of C1q expression in tumour macrophages, this data may suggest that there are intralesional accumulation of downstream complement cascade proteins. Further work is needed to characterise this further.

Pathway analysis and peptide abundance suggests that lipid metabolism is altered in the tumour microenvironment, with activation of clearance pathways for chylomicrons and LDL, and enrichment of apolipoprotein B in the tumour tissue. This echoes enrichment of APOE seen in the transcriptomic analysis of macrophages and adds further evidence for the importance of lipid metabolism in the immune context of the tumour microenvironment.

5.3.7.2 Phosphoproteomic analysis

A total of 13472 phosphorylated peptides were isolated by LC-MS, and after immune signal extraction, 1740 remained. No phosphorylated MerTK or Axl was identified in the phosphoproteomic datasets. Both were searched for from the entire dataset, before isolating out immune function related phosphopeptides. Only 6 phosphopeptides were statistically significant and pathway analysis revealed enrichment of expected immune related signalling pathways. This included the ErbB pathway, which activates AKT and MAPK. These are downstream of MerTK and Axl. There was a downregulation of phosphorylated peptide BAD; this protein usually promotes cell death and apoptosis, so a reduction in the amount of phosphorylated BAD may suggest that there is less apoptotic signalling in the tumour, which would be expected in this context.

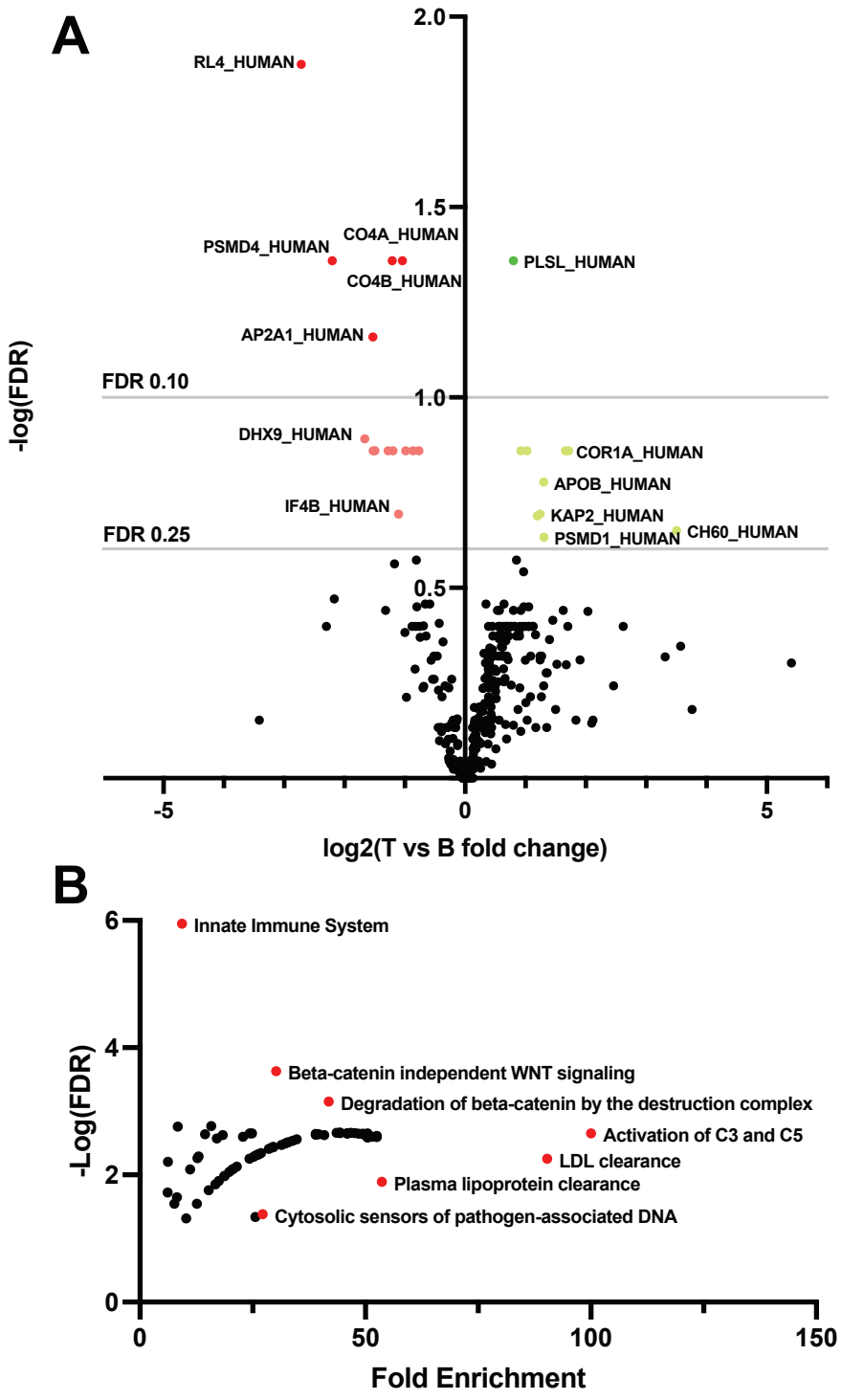

Figure 5.6: Comparative proteomic analysis of paired tumour and liver tissue from patients with HCC
(A) n=8 patients' tissue was homogenised and analysed by liquid chromatography mass spectrophotometry (LC/MS). Peptides were quantified and for this analysis, those related to immune function were extracted from the data and compared. The volcano plot outlines peptides significantly upregulated (to the right, in green) in the tumour tissue; those in red are less abundant in the tumour. Proteins are labelled using their UniProt database entry name. Paired student's t-test of log2 transformed values of peptide quantity is plotted against –log transformed (FDR). **(B)** Pathway analysis using gene ontology enrichment analysis by Reactome pathway – fold enrichment is plotted against $-\log_{10}$(FDR) – all those highlighted in red are statistically significant, with $p<0.05$)
Abbreviations: FDR – false discovery rate

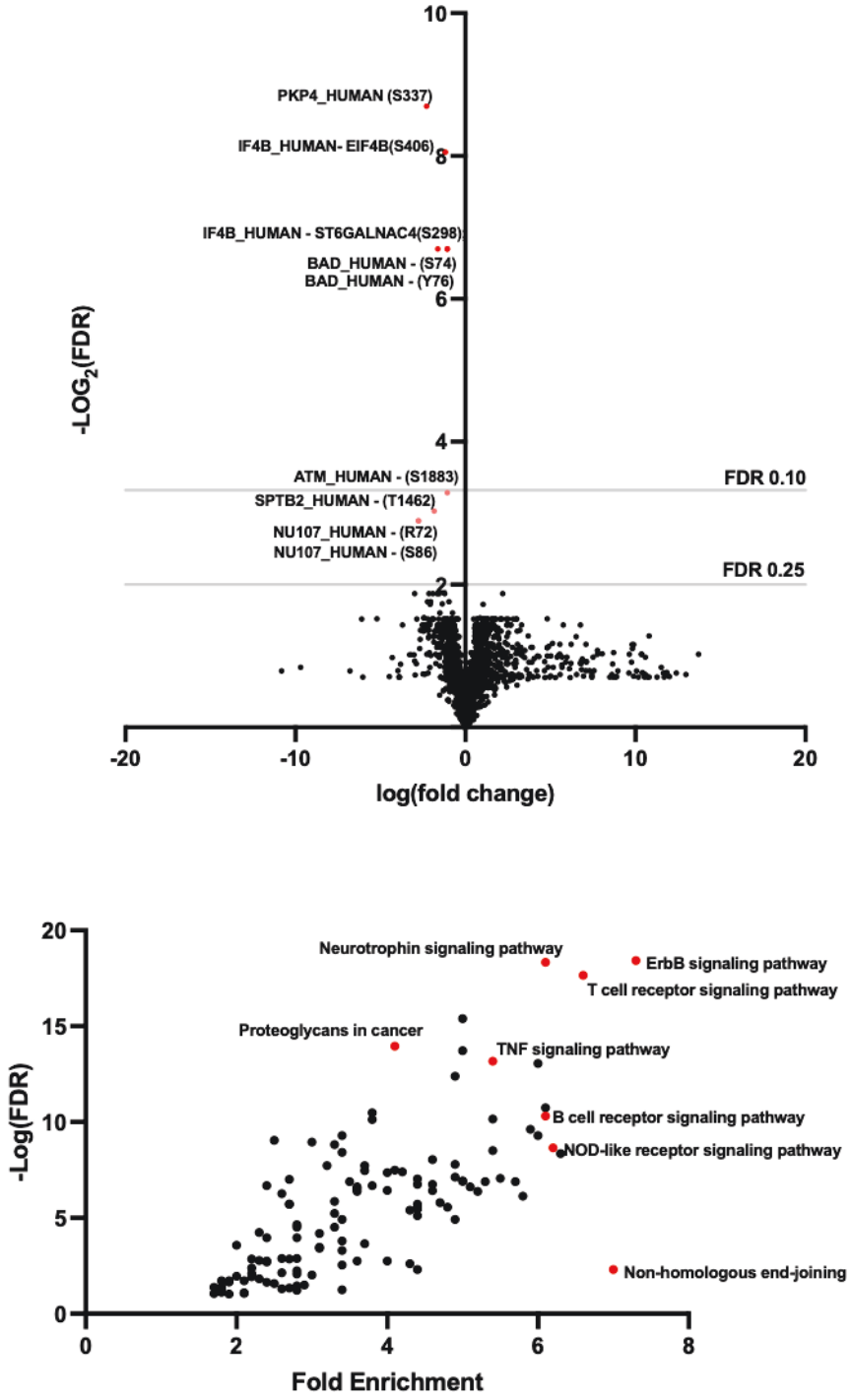

Figure 5.7: Comparative phosphoproteomic analysis of paired tumour and liver tissue from patients with HCC

n=8 patients' tissue analysed by liquid chromatography mass spectrophotometry (LC/MS). Phosphopeptides related to immune function were extracted from the data and compared between liver and paired tumour tissue. The volcano plot (top) outlines differential phosphopeptide abundance after Benjamini Hochberg correction. Those in red are less abundant in the tumour. Phosphorylation site is in brackets after each phosphopeptide. Phosphorylated proteins are labelled using their UniProt database entry name; the phosphorylation site is in brackets. Paired student's t-test of log2 transformed values for phosphopeptide quantity was performed to generate p=values. Pathway analysis using gene ontology enrichment analysis by Reactome pathway (bottom): fold enrichment is plotted against $-\log_{10}$(FDR). All those highlighted in red are statistically significant; $p<0.05$. *Abbreviations: FDR – false discovery rate*

Trial ID	Age (years)	Sex	Aetiology	Tumour Size (mm)	Treated	AFP [IU/ml]	Bilirubin (μmol/l)	Platelets (x10^9/ml)	INR	MELD
AHCC31	52	M	ALD	Multifocal	Y	28	27	64	1.15	9
SHCC01	65	M	A1AT	10	N	38	7	186	1.06	6
SHCC02	54	M	NAFLD	55	N	3	18	243	1.11	8
SHCC14	60	M	ALD	34	Y	2	54	83	1.54	6
SHCC21	55	M	HCV (SVR)	30	N	31	4	171	1.05	7
SHCC23	60	M	Sporadic	180	N	30	11	401	1.4	n/a
SHCC26	57	M	Sporadic	240	N	32	10	594	1.04	n/a
SHCC27	67	M	ALD	18	N	5	13	306	1.49	11
Median (Range) / Ratio	58.5 (52 – 67)	-	-	34 (10 – 240)	6:2	29 (2 – 32)	12 (4 - 54)	214 (64 – 594)	1.13 (1.04 - 1.54)	7.5 (6 – 11)

Table 5.8: Clinical parameters and characteristics of cases of HCC in which proteomics and phosphoproteomics analysis was undertaken

n=8 cases were analysed, with tissue taken from tumour and from surrounding or background liver. Median values (range) are highlighted for each parameter; ratios are provided for categorical data. Abbreviations: *HCV (SVR)=hepatitis C virus (sustained virological response), A1AT=alpha-1 antitrypsin deficiency, NAFLD=non-alcoholic fatty liver disease, ARLD= alcohol related liver disease, AFP=alpha-fetoprotein, MELD=Model for End-Stage Liver disease. INR = international normalised ratio*

5.3.8 C1q expressing macrophages are seen in the tumour microenvironment but circulating and tissue levels of C1q are not elevated in HCC

In light of data suggesting a role for the complement cascade (and more specifically C1q) in the tumour microenvironment in HCC, characterisation of C1q expression in the tumour by immunohistochemistry was performed. As for MerTK and Axl, double epitope enzymatic immunohistochemistry for C1q+CD68+ macrophages was undertaken. Representative images from 2 cases are shown in Figure 5.8. True colour images demonstrate the presence of mild background staining for C1q on hepatocytes, and areas with clusters of dual C1q+CD68+ cells which are more apparent at higher magnification. These are evident in both the tumour nests and in the periphery. Arrow 2 highlights the presence of C1q+CD38- cells with clear Kupffer-like morphology in the tumour periphery. These are like Mer+CD68- cells seen in this earlier double stain, outlined in Figure 2.4. It is possible that these cells express low levels of CD68, given their morphology which is typical for Kupffer cells. Staining with M2 macrophage marker CD163 may help to clarify their phenotype further.

Circulating levels of C1q was measured in sera of patients with HCC and relevant controls groups. Their clinical characteristics and parameters are compared in Table 3.4. Tissue levels of C1q were also assayed and clinical parameters for the cases from which the homogenates were obtained are outlined in Table 3.3 (CHECK). Circulating levels of C1q were not significantly elevated in patients with HCC when compared with patients with cirrhosis (5.36ng/ml (HCC) vs 5.91ng/ml (CLD); p= 0.239, Figure 5.9A). When the 25 cases of HCC were divided by prior history of chemoembolisation or by AFP secretion, no significant differences were seen (p=0.82 for chemoembolised vs untreated; p=0.69 for AFP secretor vs non-AFP secretor; Figure 5.9 B). Serum C1Q did not correlate significantly with serum AFP (Spearman correlation coefficient r= -0.005773; p=0.9748). Tissue levels of C1Q in tissue

homogenates were measured (Figure 5.9D) – C1q was normalised to the protein content in the homogenate (ng/mcg protein) and to the weight of the tissue (ng/g tissue). By each means of normalisation, there was a reduction in serum C1q in the tumour environment when compared with liver tissue (0.003143ng/mcg vs 0.000608 ng/mcg protein; p=0.0269, Wilcoxon test). Finally, there was no significant correlation between serum and tumour C1q concentrations (Spearman correlation r = -0.223; p=0.5517).

5.3.9 *In vitro* conditioning of monocyte-derived macrophages with tissue homogenates promotes C1Q surface expression and C1q+ macrophages possess a MerTK^{hi}/HLA-DR^{hi} phenotype

In vitro conditioning experiments were undertaken, in parallel those performed to assess macrophage MerTK and Axl phenotype after tissue homogenate conditioning. The tissue homogenates used were from the same patients. Conditioning resulted in an increase in surface expression of C1q (Figure 5.10 A), which was statistically significant across the disease and control groups (Kruskal-Wallis p-value= 0.0011) but there was no significant difference between the surface expression when conditioned with tumour vs liver homogenates (32.4% vs 27.1%). Considering the possibility of surface staining being the result of adherence of soluble C1q from the homogenates onto the cell surface, cells were permeabilised and total cell staining performed, i.e. including cytosolic staining (Figure 5.10 B). The intracellular component of total cell staining after permeabilisation and was calculated by performing surface staining without permeabilisation in parallel and subtracting this value from total cell staining value. There were no significant differences between the group but perhaps a trend towards a reduction in intracellular C1q in tumour conditioned macrophages. The results seen here are echoed after assessing C1q expression by quantitative PCR, with a trend towards less C1q expression after tumour homogenate conditioning (Figure 5.10 C).

Immune phenotyping of the C1q positive cells did demonstrate a familiar, HLA-DR^{hi} phenotype with higher MerTK expression on C1q+ macrophages. This co-expression of C1q and MerTK has been previously described - C1q promotes efferocytosis through induction of expression of MerTK (Galvan *et al.*, 2014); it is possible that a similar mechanism is active in this setting; however further work is needed to confirm this.

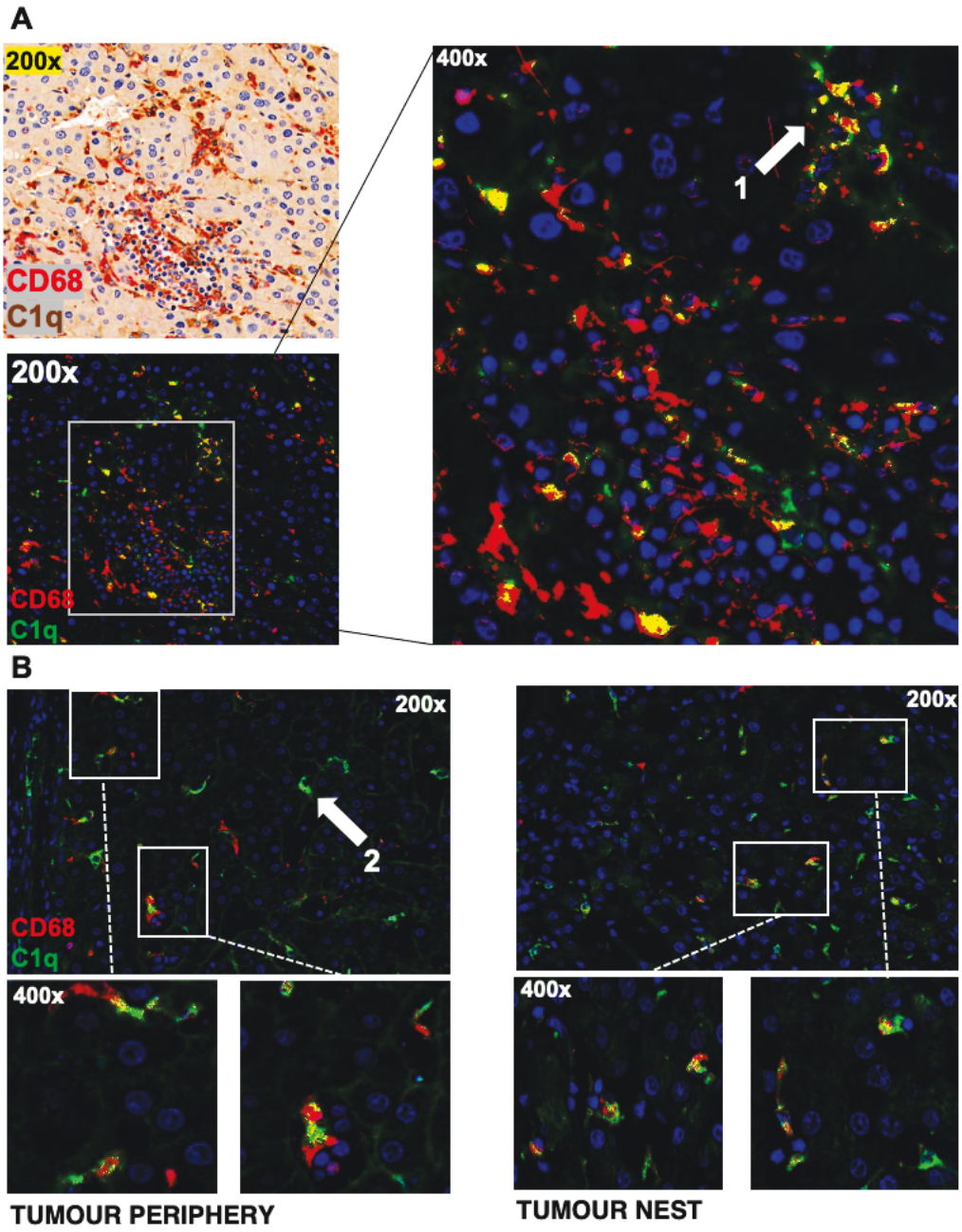

Figure 5.8: C1q expressing macrophages are evident in the tumour microenvironment in HCC

Double epitope enzymatic immunohistochemistry was performed on formalin fixed, paraffin embedded sections from lesions. CD68, a macrophage marker, was stained using permanent red and appears red on the true colour **(A)** and pseudo-immunofluorescent images. C1Q was stained using DAB, a brown stain in true colour, is labelled fluorescent green on pseudo-immunofluorescence. Areas of overlapping signal appear yellow; images taken at low (200X) and high magnification (400x) **(A)** true colour and pseudo-immunofluorescent images from within a tumour lesion demonstrate clusters of C1Q positive macrophages between cords of hepatocellular tissue (Arrow 1). **(B)** Further examples of C1q+CD68+ macrophages in the tumour microenvironment, in different locations. Arrow 2 demarcates a number of C1Q+CD68- cells with Kupffer-like morphology.

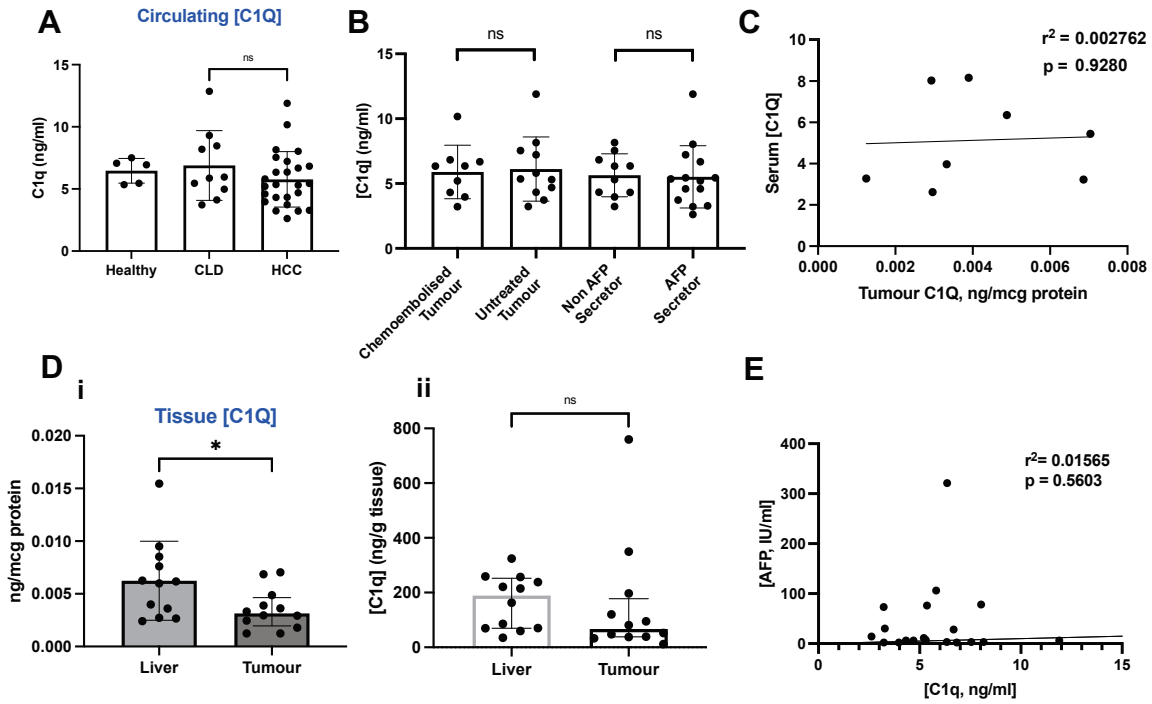

Figure 5.9: C1q levels are not elevated in the circulation or within the tumour microenvironment in HCC

(A) Circulating [C1q] was measured from sera of patients with HCC (n=25) and with pathological (n=10) and healthy controls (n=5) **(B)** Cases were grouped and compared according to prior chemoembolization status, or by AFP secretion and **(C)** Circulating C1Q and serum AFP were directly compared to assess for correlation **(D)** Tissue homogenate C1Q levels were measured in tumour and surrounding liver in n=12 cases; **(I)** – normalised to protein by weight; **(ii)** – normalised to tissue weight. **(E)** circulating and intratumoural [C1Q] levels were assessed for correlation. Data expressed as median with interquartile ranges. Mann-Whitney tests for unpaired and Wilcoxon tests used for paired analyses respectively; Spearman Correlation co-efficients calculated and presented. *=p <0.05.

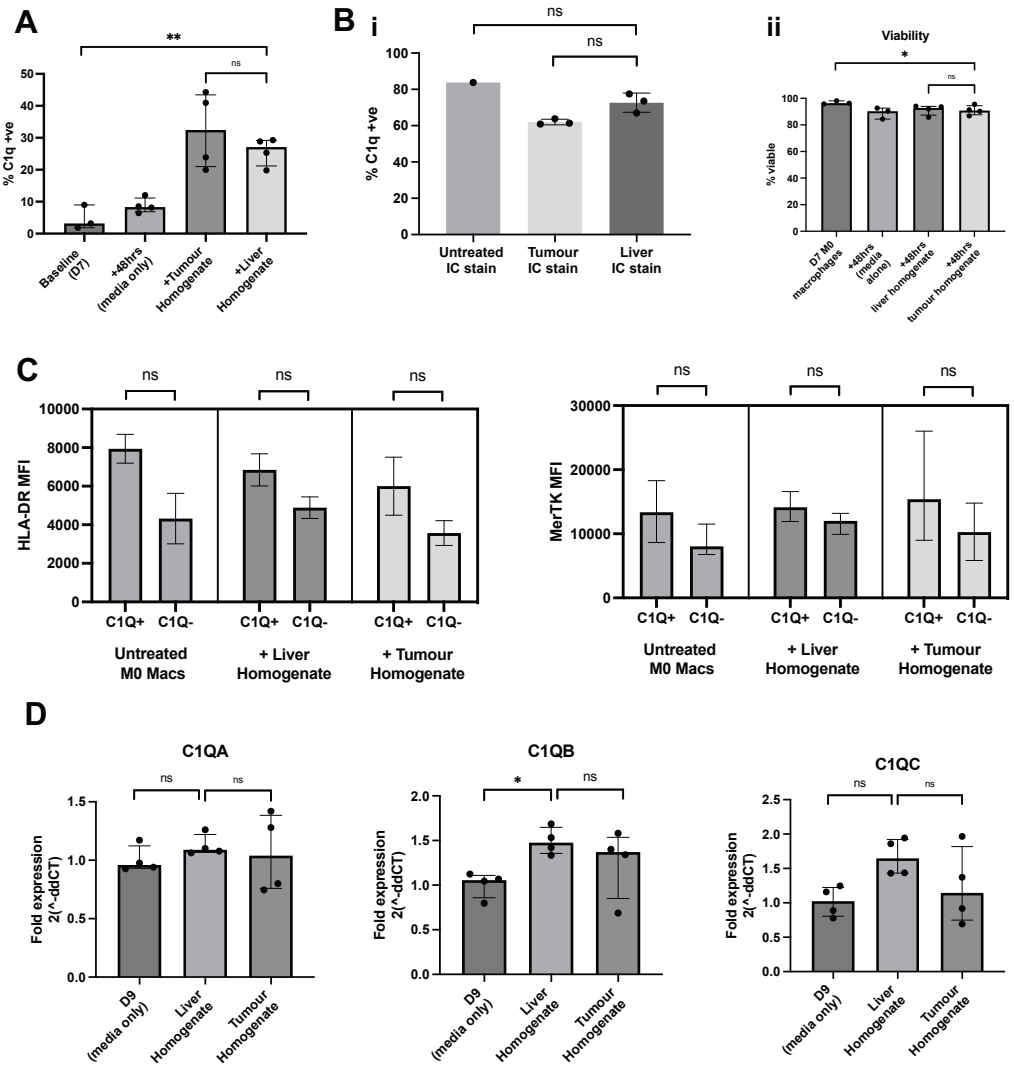

Figure 5.10: In vitro conditioning of M0 macrophages with tissue homogenate upregulates C1q expression

(A) Surface C1q expression was measured by flow cytometry after 48hrs incubation of monocyte derived M0 macrophages with media supplemented with 25% tumour and liver homogenates**. (B)** Combined surface and intracellular staining was performed compared with surface only staining to assess total cellular C1q expression in each conditioning state; viability was measured in all conditions using fixable viability dye when staining lifted cells from individual wells **(C)** C1q+ macrophages after conditioning were assessed for co-expression of HLA-DR and MerTK **(D)** Quantitative PCR using RNA extracted from conditioned macrophages was performed after 48hrs. Data expressed as median with interquartile ranges. Mann-Whitney tests were used for unpaired and Wilcoxon tests used for paired analyses respectively. *=p <0.05.

5.4 DISCUSSION

The primary aim of this chapter was to clearly define the phenotype of tumour associated macrophages in HCC, and to ascertain if MerTK and Axl expression was significantly increased within this population. This was particularly pertinent to the aims of the study in view of some of the conflicting results in terms of MerTK and Axl phenotype when comparing myeloid cells extracted from the tumour environment were phenotyped and gated using a macrophage or monocyte gating strategies. In defining and characterising a clear macrophage population and performing transcriptomic analysis, this analysis has helped to clarify and confirm the tumour associated macrophage phenotype in HCC. Using pathway analysis and by interrogating groups of up-regulated genes, this analysis has further helped to characterise tumour associated macrophage function.

Gene expression analysis has been able to definitively ascertain if there is differential expression of MerTK and Axl between these compartments. Although there was an increase in both MerTK and Axl expression within tumour associated macrophages, this did not reach statistical significance and there was a clear transcriptional profile towards a reduction in downstream signalling from both members of the TAM-RTK family. After the limitations of immunohistochemistry and some conflicting results from immunophenotyping using macrophage and monocyte gating strategies, the characterisation of macrophage phenotype in relation to TAM-RTK expression has been determined definitively. In addition, proteomic analysis of tumour and liver tissue did not provide evidence of enriched MerTK or Axl within the tumour microenvironment. Phosphoproteomics did not identify phosphorylated MerTK, Axl or any of their well-established canonical downstream signalling targets.

The tumour associated population possessed a transcriptional profile in keeping with key aspects of tumour associated macrophage function; thereby validating the findings. This profile included activation of matrix metalloproteases, a skewing towards an M2-like cytokine profile (IL-12 and IL-4/IL-13 signalling) and increased expression of markers of an M2 phenotype including CD206, CD209 and PLAU (with reduction of M1 marker TREM1). CCL8 was markedly upregulated in the tumour population and has been noted to have pro-tumoural effects in HCC – a recent study demonstrated the capacity of CCL8 to induce epithelial to mesenchymal transition in cancer cell lines, which is pivotal to metastasis. Expression of CCL8 was promoted by tissue hypoxia and also results in an increased recruitment of monocytes into the tumour which can differentiate into TAMϕs (Cassetta *et al.*, 2019; Graham and Pollard, 2022).

Gene ontology and pathway enrichment analysis helped to further define key aspects of function associated with the tumour derived population, highlighting the importance of lipid metabolism, chylomicron remodelling and regulation and activation of the complement cascade. These aspects of function are potentially linked – uptake of breakdown products of cell apoptosis and necrosis (two abundant processes within the liver) includes cholesterol metabolites and phosphatidylserine. This process can be initiated by C1q, resulting in lipid laden post-efferocytotic macrophages which can promote tumour progression through the production of chemokines including CCL6 and CCL8 to promote tumour progression and metastasis.

In keeping with a ‘post-phagocytic’ model of tumour associated macrophage function was the notable increase in expression of Stabilin-1 in this population. Also known as CLEVER-1, it is well described as a scavenger receptor, with ligands including oxidised-LDL and

extracellular matrix proteins (Li *et al.*, 2011; Workman and Sage, 2011). In homeostasis it plays a key role in clearance of cellular debris after localised tissue damage, including after inflammatory insults and demarcates an M2 macrophage phenotype (Patten and Shetty, 2019), with Stabilin-1 knockout macrophages producing increased amounts of pro-fibrotic mediators such as CCL3 (Rantakari *et al.*, 2016). Stabilin-1 is well described on tumour associated macrophages in a range of human cancers (Werno *et al.*, 2010; David *et al.*, 2012; Riabov *et al.*, 2016). It is possible that both Stabilin-1 and C1q act in a co-operative manner to promote clearance of intra-tumoural cellular breakdown products and in doing so engender a pro-resolution, wound healing M2- TAMϕ phenotype in HCC.

It is pertinent to note that these interconnected processes closely relate to a key aspect of MerTK (and Axl) function – namely efferocytosis. Moreover, (Galvan *et al.*, 2014) have demonstrated that MerTK can act downstream of C1q in macrophages. Further work is required to determine how these pathways interact and if they co-operate in the tumour environment in HCC, despite a lack of a significant upregulation of the TAM-RTKs in this sample. Through *in vitro* assays it has been demonstrated here that C1q expression can be promoted on the surface of macrophages after conditioning with tissue homogenates and that high C1Q expression is associated with higher MerTK expression. However, C1q expression at a genetic level was not triggered: further experiments should be conducted using apoptotic and necrotic cellular debris to ascertain if it is these key breakdown products that generate this phenotype *in vivo.*

Comparison of the treated and untreated tumours has shown that there is an encouraging switch in phenotype with a reduction in AIF1 and HDAC3, which would skew the phenotype towards

an activated M1 like phenotype. In helping to skew TAMϕ phenotype away from a tumour-promoting phenotype, this may be one aspect by which chemoembolisation is effective.

Limitations of these analyses need to be acknowledged. Firstly, it is worthy to note that there was difficulty in obtaining sufficient cell numbers from the stored mononuclear cell extracts, and a significant number of cases were excluded from this analysis on account of poor cell yield. Considering this poor yield, it was not feasible to sort cells according to both MerTK and Axl positivity, or by HLA-DR status on account of a concern that there may not be sufficient cells within each group to yield meaningful amounts of RNA. As a result it was not possible to undertake these analyses; however we note that similar MerTK restricted analyses have been performed in other disease contexts (Triantafyllou *et al.*, 2018).

As well as cell yield affecting the ability to compare specific macrophage sub-populations, it was also not feasible to conduct phosphoproteomic analysis by LC/MS on these cells. The resultant phosphoproteomic and proteomic analyses on snap frozen tissue, therefore, have limited scope in addressing the specific question related to our hypothesis – namely in demonstrating if there is active downstream signalling from MerTK and Axl. Furthermore, a bioinformatic method of extracting the 'immune signal' from the total phosphoproteomic dataset was vulnerable to introducing bias and limited the applicability of results from this form of analysis. Further work on this dataset, with an unbiased approach, is required.

Another limitation to this analysis was the necessity to cryopreserve the macrophages and monocytes extracted before analysis. This has the potential to have resulted in loss of myeloid cell populations that are more vulnerable to cryopreservation and thawing. The technical logistics of obtaining liver cells and being able to immediately sort and lyse them for analysis

was not available in conducting this study and would be required in order to ensure purity of the results if this study were to be expanded and performed in a wider cohort of patients.

An increasing array of novel techniques for in-depth phenotypic analysis are now available; of these, single cell RNA sequencing is perhaps the best known. Other techniques, such as CyTOF can also provide a detailed profile of subgroups and individual cells within a tissue or lesion (Williams, Yeh and Soloff, 2016). Recent work with single cell sequencing has provided insight into the landscape of T lymphocytes in hepatocellular carcinoma (Zheng *et al.*, 2017; Ho *et al.*, 2021). To date, no such analysis has been performed for myeloid cells. These two single-cell RNA sequencing studies demonstrate that there is clear heterogeneity within the tumour microenvironment, with variations in the frequency and phenotype of different immune cell populations within a tumour. In addition, there is evidence here of variability between individual lesions, and of variations within immune cell populations themselves.

Transcriptomics performed using Nanostring (or similar methods of gene expression array) have some limitations when compared with these technologies. By pooling all macrophage lysates from one lesion together into one sample for analysis, the composition and contribution of individual sub-populations and intra-tumoural niches (for example, those seen in stromal clusters as opposed to those with a more differentiated, Kupffer life appearance such as those demonstrated at histological review in Chapter 2) is lost. Furthermore, with a limited array of genes analysed (the Nanostring Myeloid Codeset is pre-determined), it is an inherently biased approach to genetic expression analysis.

The effects of this 'pooling' of cells can be seen in the data when comparing transcriptomic data with results from characterising the macrophage and monocyte population by flow

cytometry. Whereas in the latter it was possible to identify a clear expansion of an HLA-DR^{HI} phenotype within the tumour, with an enrichment of this sub-population in the tumour extracted myeloid populations, this observation was lost in analysing the entire macrophage population as a whole and was evident in the data – we saw high levels of HLA-DR expression in both compartments, but there was no significant difference between the groups. Furthermore, when assessing the cytokine profile of the entire macrophage population by transcriptomic analysis, there was evidence of skewing towards an M2-like phenotype by transcriptomics.

Whilst this is in keeping with established paradigms on the deleterious effects of this population in the tumour microenvironment, this does not reflect some of the co-expression data that has been generated by flow cytometry. In these data, Axl+ monocytes were found to be more abundant than Mer+ monocytes (by frequency), and although not statistically significant in this sample, there was a trend towards the Axl+ monocyte population displaying a reduction in classical, M2 like tumour associated macrophage markers such as CD204, CD115 and PDL1; this diverged from the MerTK+ population which had higher expression of these same markers. If this effect is to be believed then it could be expected that there would be an M1-like skewing in the macrophage population. Indeed, this is what we see on review of the macrophage phenotype by flow cytometry, with the HLA-DR^{HI} phenotype in the tumour enriched and expressing lower CD163.

It is suggested that these conflicts and inconsistencies within – and between – the gene expression and flow cytometry data may be the result of a few other key factors. These include acknowledging that surface expression using flow cytometry is an inaccurate measure of gene expression, given that we know MerTK and Axl can be cleaved from the cell surface and act as a decoy receptor for their own ligands to regulate their own signalling (Graham *et al.*, 2014a;

Akalu, Rothlin and Ghosh, 2017). It is also now widely accepted that the strict M1/M2 paradigms of cytokine expression, which are based on functional readouts of macrophages *in vitro* do not reflect phenotype or function *in vivo.*

One method that is hoped can help to resolve some of these inconsistencies is the use of spatial transcriptomic profiling. This technology combines single cell sequencing and unbiased gene expression analysis at a cellular level with histological and topographical data from tissue sections (Achim, Vergara and Pettit, 2018). Such technologies offer the potential to gain an understanding of the range of intra-tumoural niches of macrophages and crucially, how they interact with their surrounding cell populations. If applied in the context of this study, it would help to characterise the phenotype of macrophage populations that were not amenable to analysis after mechanical cell extraction – this includes those macrophages in areas of tissue that were difficult to dissociate, such as areas of necrotic tumour and the interface between the liver parenchyma in cases where the tumour had developed a fibrous capsule.

Despite these limitations with aspects of transcriptomics in comparison with newer spatial and single cell technologies, there is a clear merit in being able to avoid the complexities of niche resident populations with varied function to gain a more clinically relevant 'headline' view of the most important driving phenotype within a lesion. In doing this, this study has highlighted exciting data on a pro-efferocytotic, C1q expressing macrophage phenotype within the tumour microenvironment, with classical, M2-like tumour associated macrophage phenotypic characteristics. Encouragingly, whilst not statistically enriched for MerTK and Axl, these macrophages share clear phenotypic features of TAM-RTK expressing macrophages. Crucially, C1q expressing macrophages rely on MerTK signalling in order to conduct efferocytosis (Zizzo *et al.*, 2012). The mechanisms by which C1q and MerTK interact is not

clear, and in this study, a lack of significant MerTK stimulation in the tumour associated macrophages might suggest another means by which C1q acts in this environment.

Important further work is required to understand what is driving the production of C1q in the tumour microenvironment by these macrophages – classically this is thought to be in relation to antigenic stimuli (Hoekzema *et al.*, 1989; Faust and Loos, 2002), but what the trigger is in the tumour has not yet been characterised. A recent study has identified C1q production in response to chronic inflammation within the hepatic parenchyma, with tumorigenic effects. C1q activated the β-catenin pathway in hepatic progenitor cells, resulting in proliferation but without differentiation and an expansion of undifferentiated progenitor cells. Inhibition of C1q blocked activation of the β-catenin pathway within HCC tumours (Ho *et al.*, 2020). It is possible that in this study we have identified the same C1q producing population of macrophages, which would suggest an inflammatory niche within the tumour environment is driving it.

Further work on this question will include determining which inflammatory contexts within the tumour microenvironment drive C1q expression; something that could be answered with spatial transcriptomics. In addition, immunohistochemistry of a wider cohort of HCC patients should be undertaken, staining not only for C1q but for other components of the complement cascade, given the results of other studies highlighting the classical cascade as promoting tumour progression (Roumenina *et al.*, 2019).

In summary, in this chapter we have made the following observations:

1) Tumour associated macrophages do have an increased expression of both MerTK and Axl, but this did not reach statistical significance.
2) Downstream signalling targets of TAM-RTK activation were not stimulated or up-regulated in tumour associated macrophages.
3) Proteomic and phosphoproteomic analysis of tumour tissue did not reveal evidence of phosphorylated Axl or MerTK, but the ErbB pathway, which includes downstream transcription factor Akt, was enriched in the tumour.
4) The tumour associated macrophage population is characterised by a gene expression profile of genes promoting efferocytosis, with upregulation of C1q and Stabilin-1 and an M2-skewed cytokine and functional profile.
5) Conditioning of M0 macrophages with filtered tumour and liver homogenates does not stimulate C1Q expression at a genetic level but does increase surface expression; C1q+ macrophages exhibit higher MerTK surface expression.

6. CONCLUDING REMARKS

The aims of this thesis were to characterise the MerTK and Axl expressing myeloid cell compartment in HCC. Given the clear therapeutic potential in expanding our range of immunotherapeutic options, seeking to ascertain if this immune regulatory family of tyrosine kinase inhibitors is a potential target is pertinent for a few key reasons. Firstly, it plays a key role in regulating the immune response and has effects upon a range of immune cell populations. Secondly, it has a role in promoting tumour progression through a number of means, including the fact that Axl is overexpressed in HCC and cabozantinib, a second line therapy for HCC, has direct inhibitory actions upon Axl. Thirdly, it has established pathogenic roles in chronic liver disease. Through a combination of detailed immunohistochemical analysis and review, immune phenotyping of extracted mononuclear cells and transcriptomic analysis of the tumour associated macrophage compartment, the following has been observed.

Synthesis of results:

Immunohistochemistry has identified that there are both MerTK and Axl expressing macrophages in the tumour microenvironment, and that they have differing distributions and frequencies: Axl appears to be less abundant in the TME but seen reliably in the liver; MerTK is seen in both compartments but there is a subset of cases in which dense MerTK positive infiltrates can be seen – both at the sites of prior chemoembolisation and in stromal clusters. There were limitations to this analysis but it has been possible to survey and characterise TAM-RTK expression across a range of tumour types and niches.

Immunophenotyping was performed and confirmed the presence of both TAM-RTKs on both intratumoural monocytes (which are most likely monocyte-derived macrophages), with enrichment of both molecules on the surface in the tumour microenvironment. There were

divergent co-expression profiles but this signal was muted and the sample size was small. However, this divergent profile of function between MerTK and Axl has been described previously (Zagórska, Paqui G. Través, *et al.*, 2020). The macrophage phenotyping was perhaps limited in its scope, yielding some conflicting results but clearly highlighting the presence of an HLA-DR^{HI} phenotype in the tumour microenvironment. Taken together with previous published work from our group demonstrating that an HLA-DR^{HI} phenotype is associated with potent phagocytic and efferocytic capabilities (in MerTK+ HLA-DR^{HI} monocytes in liver failure (Triantafyllou *et al.*, 2018)) this data may point towards a population of macrophages that are enhanced in their ability to phagocytose. This profile also is in keeping with recent transcriptomic studies reporting higher expression of HLA-DR in TAMϕs (Aizarani *et al.*, 2019).

This assertion is further backed up by the enrichment of a key efferocytotic marker in C1q, as identified by transcriptomics. This signal, in conjunction with aspects of lipid metabolism and activation of matrix metalloproteases points to a mechanism that has been recently outlined in prostate cancer (Masetti *et al.*, 2021) whereby the process of becoming laden with lipid results in an alteration in cytokine production that can further promote tumour progression and metastasis. This will need further investigation in HCC. Furthermore, we have noted some encouraging M1 like phenotypic signs in HCCs that have undergone treatment (reduction in AIF1 expression) – this is key to our understanding of mechanism of the benefit offered by this therapy, and crucially points to another role for immunotherapy – in order to promote and sustain responses, using macrophage-based immunotherapy may improve outcomes from chemoembolisation.

Limitations have been acknowledged – one aspect that has the potential to limit the applicability of the findings is that the tumours phenotyped in this study are not reflective of those in need of new systemic therapies at present (i.e. those with advanced disease) – current practice does not routinely require biopsy of patients with advanced disease before therapy but a number of trials are now ongoing and this is changing. This will be crucial and it would be important to repeat some of this phenotypic characterisation using macrophages from biopsy specimens of patients with intermediate or advanced disease.

In vitro analyses were limited in their scope and would benefit from further repeats, and with adaptations to reflect the tumour in the co-cultures, but it was encouraging to see that Axl expression could be induced by culturing with homogenates – there is evidence that the experiment works but will need further adaptations and trials with a range of other micro-environmental cues (such as hypoxia, or high lactate) to simulate the TME more accurately.

Another key limitation was cell yield and its effect on the ability to perform more direct comparative transcriptomic analyses – in particular, MerTK+ vs MerTK-, Axl+ vs Axl- and HLA-DR^{HI} vs the HLA-DR^{LO} population in tumour macrophages. Further work with more samples would be required for this and if a better yield was possible, this would allow for a more meaningful immune cell phosphoproteomic profiling to be performed. In this study, immune cells extraction was not optimised for transcriptomics, for example by using collagenases and RNAses within the buffers used to incubate and digest the tissue. This was intentional, as both surface MerTK and Axl are cleaved by collagenases and this would have impaired cell surface phenotyping by flow cytometry. Further attempts at cell extraction using these reagents may help to improve cellular yield and the quality of transcriptomic data obtained.

With the advent of spatial transcriptomics and neighbourhood analysis, these technologies could be employed – particularly in tumours with dense MerTK positive infiltrates – to gain further understanding at a topographic level of the varied phenotypes of macrophages. In addition, an unbiased RNA-sequencing based approach for tumour derived macrophage populations would potentially add to the growing field of understanding of macrophage function in HCC – the defined array of genes offered by Nanostring analysis limits the interpretability of these findings in the wider context of the complex heterogeneity of myeloid cell populations in the TME.

In addition to these practical limitations and difficulties experienced during the course of this work, there is merit in considering a different approach to gaining understanding of efferocytotic function and TAM-RTK signalling in hepatocellular carcinoma. In a human study, this is best assessed by assaying expression of MerTK, Axl and other key proteins in the efferocytotic pathways at a genomic and proteomic level using an unbiased approach (such as RNA sequencing and proteomics on a purified immune cell population), before embarking on further experiments to interrogate the function of these signalling pathways using knockout models in cell lines or murine models of hepatocellular carcinoma – from the findings in this thesis it is clear that TAM-RTK expressing myeloid cells are present in the TME; their pathophysiological role at present, however, remains uncharacterised and given that both MerTK and Axl were not identified in the phosphoproteomic analyses, they may not be significant in the wider context of tumour biology in HCC. Analysis of the existing unbiased, full phosphoproteomic dataset will be of further benefit in understanding the key signalling cascades of interest within the tumour microenvironment and may help to identify new therapeutic targets in HCC.

7. RECRUITMENT

Patients were recruited into the study using ethics that were approved at the local ethics committee. The approval code was 15/LO/0363.

Inclusion criteria included all adults, with capacity. Exclusion criteria were those with active Hepatitis B or C infection, or currently on any immunotherapy. Patients were recruited from the transplant wait-list, surgical clinic or local HCC-MDT, and from the HCC clinic at Kings College hospital.

The following flow chart outlines the recruitment over the period January 2017 – September 2019:

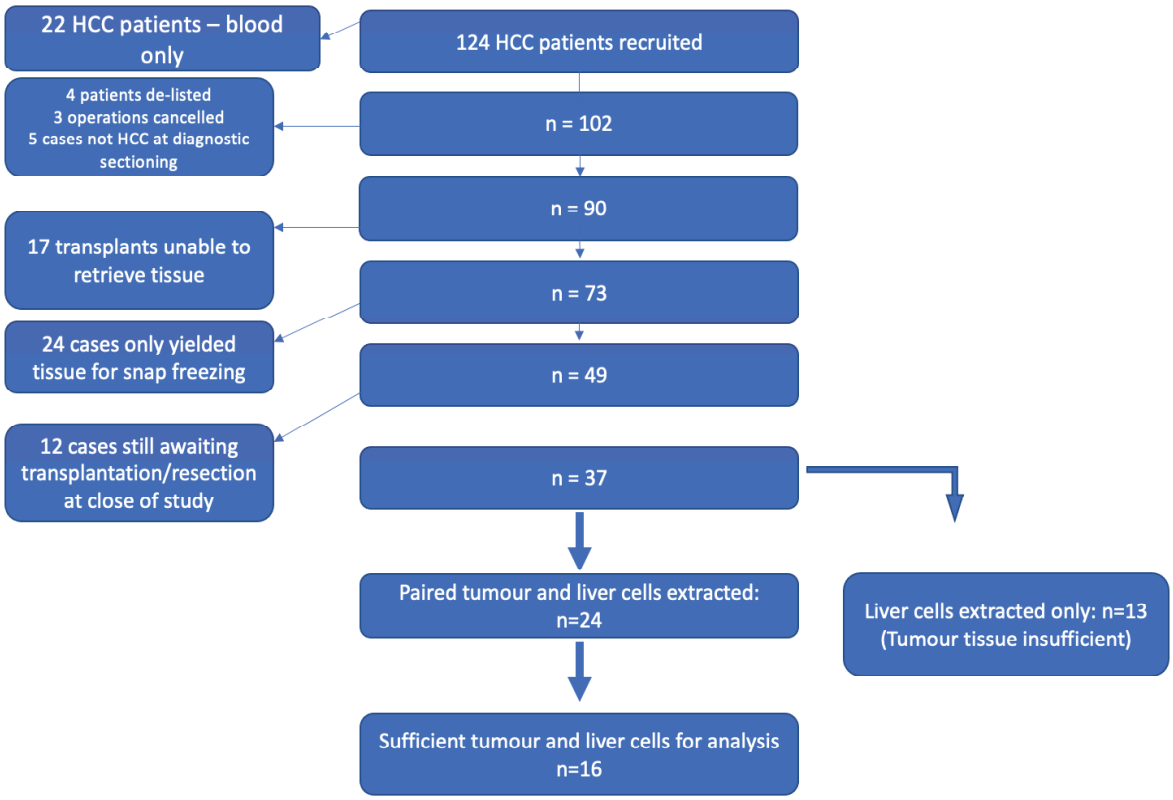

8. REFERENCES

A-Gonzalez, N. *et al.* (2009) 'Apoptotic cells promote their own clearance and immune tolerance through activation of the nuclear receptor LXR.', *Immunity*, 31(2), pp. 245–258. doi: 10.1016/j.immuni.2009.06.018.

Abeles, R. D. *et al.* (2012) 'CD14, CD16 and HLA-DR reliably identifies human monocytes and their subsets in the context of pathologically reduced HLA-DR expression by CD14hi/CD16neg monocytes: Expansion of CD14hi/CD16pos and contraction of CD14lo/CD16pos monocytes in acute liver failure', *Cytometry Part A*, 81 A(10), pp. 823–834. doi: 10.1002/cyto.a.22104.

Achim, K., Vergara, H. M. and Pettit, J.-B. (2018) 'Spatial Transcriptomics: Constructing a Single-Cell Resolution Transcriptome-Wide Expression Atlas.', *Methods in molecular biology (Clifton, N.J.)*. United States, 1649, pp. 111–125. doi: 10.1007/978-1-4939-7213-5_7.

Aggarwal, B. B., Vijayalekshmi, R. V and Sung, B. (2009) 'Targeting inflammatory pathways for prevention and therapy of cancer: short-term friend, long-term foe.', *Clinical cancer research : an official journal of the American Association for Cancer Research*. United States, 15(2), pp. 425–430. doi: 10.1158/1078-0432.CCR-08-0149.

Aizarani, N. *et al.* (2019) 'A human liver cell atlas reveals heterogeneity and epithelial progenitors', *Nature*, 572(7768), pp. 199–204. doi: 10.1038/s41586-019-1373-2.

Akalu, Y. T., Rothlin, C. V. and Ghosh, S. (2017) 'TAM receptor tyrosine kinases as emerging targets of innate immune checkpoint blockade for cancer therapy', *Immunological Reviews*, 276(1), pp. 165–177. doi: 10.1111/imr.12522.

Ali, M. Y. *et al.* (2005) 'Activation of dendritic cells by local ablation of hepatocellular carcinoma', *Journal of Hepatology*, 43(5), pp. 817–822. doi: 10.1016/j.jhep.2005.04.016.

Ashburner, M. *et al.* (2000) 'Gene Ontology: tool for the unification of biology', *Nature Genetics 2000 25:1*. Nature Publishing Group, 25(1), pp. 25–29. doi: 10.1038/75556.

Asmussen, A. *et al.* (2021) 'Monocyte subset distribution and surface expression of HLA-DR

and CD14 in patients after cardiopulmonary resuscitation', *Scientific Reports 2021 11:1*. Nature Publishing Group, 11(1), pp. 1–12. doi: 10.1038/s41598-021-91948-z.

Axelrod, H. and Pienta, K. J. (2014) 'Axl as a mediator of cellular growth and survival', *Oncotarget*. Oncotarget, 5(19), pp. 8818–8852. doi: 10.18632/ONCOTARGET.2422.

Bai, D. S. *et al.* (2017) 'The prognostic correlation of AFP level at diagnosis with pathological grade, progression, and survival of patients with hepatocellular carcinoma', *Scientific Reports*. Nature Publishing Group, 7(1). doi: 10.1038/S41598-017-12834-1.

Bao, X. *et al.* (2021) 'Integrated analysis of single-cell RNA-seq and bulk RNA-seq unravels tumour heterogeneity plus M2-like tumour-associated macrophage infiltration and aggressiveness in TNBC', *Cancer immunology, immunotherapy : CII*. Cancer Immunol Immunother, 70(1), pp. 189–202. doi: 10.1007/S00262-020-02669-7.

Bárcena, C. *et al.* (2015) 'Gas6/Axl pathway is activated in chronic liver disease and its targeting reduces fibrosis via hepatic stellate cell inactivation.', *Journal of hepatology*, 63(3), pp. 670–678. doi: 10.1016/j.jhep.2015.04.013.

Beatty, G. L. *et al.* (2011) 'CD40 agonists alter tumor stroma and show efficacy against pancreatic carcinoma in mice and humans', *Science (New York, N.Y.)*. Science, 331(6024), pp. 1612–1616. doi: 10.1126/SCIENCE.1198443.

Benoit, M. E. *et al.* (2012) 'Complement Protein C1q Directs Macrophage Polarization and Limits Inflammasome Activity during the Uptake of Apoptotic Cells', *The Journal of Immunology*, 188(11), pp. 5682 LP – 5693. doi: 10.4049/jimmunol.1103760.

Bernsmeier, C *et al.* (2018) 'CD14 + CD15 − HLA-DR − myeloid-derived suppressor cells impair antimicrobial responses in patients with acute-on-chronic liver failure', *Gut*, 67, pp. 1155–1167. doi: 10.1136/gutjnl-2017-314184.

Bernsmeier, C. *et al.* (2015) 'Patients with acute-on-chronic liver failure have increased numbers of regulatory immune cells expressing the receptor tyrosine kinase MERTK', *Gastroenterology*. W.B. Saunders, 148(3), pp. 603-615.e14. doi:

10.1053/J.GASTRO.2014.11.045.

Bilzer, M., Roggel, F. and Gerbes, A. L. (2006) 'Role of Kupffer cells in host defense and liver disease.', *Liver international : official journal of the International Association for the Study of the Liver*. United States, 26(10), pp. 1175–1186. doi: 10.1111/j.1478-3231.2006.01342.x.

Bonavita, E. *et al.* (2015) 'PTX3 Is an Extrinsic Oncosuppressor Regulating Complement-Dependent Inflammation in Cancer', *Cell*. Elsevier, 160(4), pp. 700–714. doi: 10.1016/j.cell.2015.01.004.

Bottazzi, B. *et al.* (2010) 'An Integrated View of Humoral Innate Immunity: Pentraxins as a Paradigm', *http://dx.doi.org/10.1146/annurev-immunol-030409-101305*. Annual Reviews , 28, pp. 157–183. doi: 10.1146/ANNUREV-IMMUNOL-030409-101305.

Brar, G. *et al.* (2020) 'Hepatocellular Carcinoma Survival by Etiology: A SEER-Medicare Database Analysis', *Hepatology Communications*. John Wiley & Sons, Ltd, 4(10), pp. 1541–1551. doi: https://doi.org/10.1002/hep4.1564.

Brenig, R. *et al.* (2019) 'Expression of AXL receptor tyrosine kinase relates to monocyte dysfunction and severity of cirrhosis'. doi: 10.26508/lsa.201900465.

Bulla, R. *et al.* (2016) 'C1q acts in the tumour microenvironment as a cancer-promoting factor independently of complement activation.', *Nature communications*, 7, p. 10346. doi: 10.1038/ncomms10346.

Buonaguro, L. *et al.* (2019) 'Immunotherapy in hepatocellular carcinoma', *Annals of Hepatology*. Elsevier Espana S.L., 18(2), pp. 291–297. doi: 10.1016/J.AOHEP.2019.04.003.

Cai, B. *et al.* (2017) 'MerTK receptor cleavage promotes plaque necrosis and defective resolution in atherosclerosis', *The Journal of clinical investigation*. J Clin Invest, 127(2), pp. 564–568. doi: 10.1172/JCI90520.

Cai, B. *et al.* (2020) 'Macrophage MerTK Promotes Liver Fibrosis in Nonalcoholic Steatohepatitis', *Cell Metabolism*. Elsevier Inc., 31(2), pp. 406-421.e7. doi:

10.1016/j.cmet.2019.11.013.

Cai, H. *et al.* (2017) 'Colony-stimulating factor-1-induced AIF1 expression in tumor-associated macrophages enhances the progression of hepatocellular carcinoma', *OncoImmunology*. Taylor & Francis, 6(9), p. e1333213. doi: 10.1080/2162402X.2017.1333213.

Camenisch, T. D. *et al.* (1999) 'A novel receptor tyrosine kinase, Mer, inhibits TNF-alpha production and lipopolysaccharide-induced endotoxic shock', *Journal of Immunology*, 162(6), pp. 3498–3503. Available at: http://www.jimmunol.org/content/162/6/3498.full.pdf.

Cancer Research UK (2019) *Liver cancer mortality statistics | Cancer Research UK*. Available at: http://www.cancerresearchuk.org/health-professional/cancer-statistics/statistics-by-cancer-type/liver-cancer/mortality#ref-2 (Accessed: 25 July 2022).

Candido, J. B. *et al.* (2018) 'CSF1R + Macrophages Sustain Pancreatic Tumor Growth through T Cell Suppression and Maintenance of Key Gene Programs that Define the Squamous Subtype', *Cell reports*. Cell Rep, 23(5), pp. 1448–1460. doi: 10.1016/J.CELREP.2018.03.131.

Carrera Silva, E. A. *et al.* (2013) 'T cell-derived protein S engages TAM receptor signaling in dendritic cells to control the magnitude of the immune response.', *Immunity*, 39(1), pp. 160–170. doi: 10.1016/j.immuni.2013.06.010.

Casado, P. *et al.* (2013) 'Kinase-substrate enrichment analysis provides insights into the heterogeneity of signaling pathway activation in leukemia cells', *Science Signaling*. American Association for the Advancement of Science, 6(268). doi: 10.1126/SCISIGNAL.2003573/SUPPL_FILE/DATASET3.XLS.

Cassetta, L. *et al.* (2019) 'Human tumor-associated macrophage and monocyte transcriptional landscapes reveal cancer-specific reprogramming, biomarkers, and therapeutic targets', *Cancer cell*. Elsevier, 35(4), pp. 588–602.

Chai, Z. T. *et al.* (2021) 'AXL Overexpression in Tumor-Derived Endothelial Cells Promotes Vessel Metastasis in Patients With Hepatocellular Carcinoma', *Frontiers in Oncology*. Frontiers Media S.A., 11, p. 1801. doi: 10.3389/FONC.2021.650963/BIBTEX.

Cheng, Q. J. *et al.* (2021) 'NF-κB dynamics determine the stimulus specificity of epigenomic reprogramming in macrophages.', *Science (New York, N.Y.)*, 372(6548), pp. 1349–1353. doi: 10.1126/science.abc0269.

Chong, B. F. *et al.* (2015) 'A subset of CD163+ macrophages displays mixed polarizations in discoid lupus skin', *Arthritis research & therapy*. Arthritis Res Ther, 17(1). doi: 10.1186/S13075-015-0839-3.

Coelho, I. *et al.* (2021) 'Trem-2 Promotes Emergence of Restorative Macrophages and Endothelial Cells During Recovery From Hepatic Tissue Damage', *Frontiers in immunology*. Front Immunol, 11. doi: 10.3389/FIMMU.2020.616044.

Collin, M., Mcgovern, N. and Haniffa, M. (2013) 'Human dendritic cell subsets', *Immunology*. Wiley-Blackwell, 140(1), p. 22. doi: 10.1111/IMM.12117.

Collman, R. *et al.* (1990) 'Macrophage-tropic strains of human immunodeficiency virus type 1 utilize the CD4 receptor', *Journal of virology*. J Virol, 64(9), pp. 4468–4476. doi: 10.1128/JVI.64.9.4468-4476.1990.

Condeelis, J. and Pollard, J. W. (2006) 'Macrophages: Obligate Partners for Tumor Cell Migration, Invasion, and Metastasis', *Cell*. Elsevier, 124(2), pp. 263–266. doi: 10.1016/J.CELL.2006.01.007.

Cook, R. S. *et al.* (2013) 'MerTK inhibition in tumor leukocytes decreases tumor growth and metastasis', *Journal of Clinical Investigation*, 123(8), pp. 3231–3242. doi: 10.1172/JCI67655.

Crispe, I. N. *et al.* (2006) 'Cellular and molecular mechanisms of liver tolerance', *Immunological Reviews*. Blackwell Publishing Ltd, 213(1), pp. 101–118. doi: 10.1111/j.1600-065X.2006.00435.x.

Dai, F. *et al.* (2010) 'The number and microlocalization of tumor-associated immune cells are

associated with patient's survival time in non-small cell lung cancer', *BMC cancer*. BMC Cancer, 10. doi: 10.1186/1471-2407-10-220.

Dal-Secco, D. *et al.* (2015) 'A dynamic spectrum of monocytes arising from the in situ reprogramming of CCR2+ monocytes at a site of sterile injury', *The Journal of Experimental Medicine*. The Rockefeller University Press, 212(4), p. 447. doi: 10.1084/JEM.20141539.

David, C. *et al.* (2012) 'Stabilin-1 expression in tumor associated macrophages.', *Brain research*, 1481, pp. 71–78. doi: 10.1016/j.brainres.2012.08.048.

DeBerge, M. *et al.* (2021) 'Macrophage AXL receptor tyrosine kinase inflames the heart after reperfused myocardial infarction', *The Journal of clinical investigation*. J Clin Invest, 131(6). doi: 10.1172/JCI139576.

Delgado Martínez, C., Gómez-Rubio, M. and Gómez-Domínguez, C. (2021) 'Is hepatitis C direct-acting antiviral therapy a risk factor for the development and recurrence of hepatocellular carcinoma? Narrative literature review and clinical practice recommendations.', *Annals of hepatology*. Mexico, 21, p. 100225. doi: 10.1016/j.aohep.2020.05.007.

Dighe, A. S. *et al.* (1994) 'Enhanced in vivo growth and resistance to rejection of tumor cells expressing dominant negative IFN gamma receptors.', *Immunity*. United States, 1(6), pp. 447–456. doi: 10.1016/1074-7613(94)90087-6.

Dorrington, M. G. and Fraser, I. D. C. (2019) 'NF-κB signaling in macrophages: Dynamics, crosstalk, and signal integration', *Frontiers in Immunology*. Frontiers Media S.A., 10(APR), p. 705. doi: 10.3389/FIMMU.2019.00705/BIBTEX.

Dunn, G. P. *et al.* (2002) 'Cancer immunoediting: From immunosurveillance to tumor escape', *Nature Immunology*, 3(11), pp. 991–998. doi: 10.1038/ni1102-991.

Edin, S. *et al.* (2012) 'The Distribution of Macrophages with a M1 or M2 Phenotype in Relation to Prognosis and the Molecular Characteristics of Colorectal Cancer', *PLOS ONE*. Public

Library of Science, 7(10), p. e47045. doi: 10.1371/JOURNAL.PONE.0047045.

Ekman, C. *et al.* (2010) 'Plasma concentrations of Gas6 (growth arrest specific protein 6) and its soluble tyrosine kinase receptor sAxl in sepsis and systemic inflammatory response syndromes', *Critical care (London, England)*. Crit Care, 14(4). doi: 10.1186/CC9233.

Elliott, L. A. *et al.* (2017) 'Human tumor-infiltrating myeloid cells: Phenotypic and functional diversity', *Frontiers in Immunology*. Frontiers Research Foundation, 8(FEB), p. 86. doi: 10.3389/FIMMU.2017.00086/BIBTEX.

European Association for the Study of the Liver (2018) 'EASL Clinical Practice Guidelines: Management of hepatocellular carcinoma.', *Journal of hepatology*. Netherlands, 69(1), pp. 182–236. doi: 10.1016/j.jhep.2018.03.019.

Fattovich, G. *et al.* (2004) 'Hepatocellular carcinoma in cirrhosis: incidence and risk factors.', *Gastroenterology*. United States, 127(5 Suppl 1), pp. S35-50. doi: 10.1053/j.gastro.2004.09.014.

Faust, D. and Loos, M. (2002) 'In vitro Modulation of C1q mRNA Expression and Secretion by Interleukin-1, Interleukin-6, and Interferon-g in Resident and Stimulated Murine Peritoneal Macrophages', *Immunobiology*. Elsevier, 206(4), pp. 368–376.

Finn, R. S. *et al.* (2020) 'Atezolizumab plus Bevacizumab in Unresectable Hepatocellular Carcinoma', *New England Journal of Medicine*. Massachusetts Medical Society, 382(20), pp. 1894–1905. doi: 10.1056/NEJMoa1915745.

Gaipl, U. S. *et al.* (2006) 'Clearance of apoptotic cells in human SLE.', *Current directions in autoimmunity*. Switzerland, 9, pp. 173–187. doi: 10.1159/000090781.

Galvan, M. D. *et al.* (2014) 'Complement protein C1q and adiponectin stimulate Mer tyrosine kinase-dependent engulfment of apoptotic cells through a shared pathway.', *Journal of innate immunity*, 6(6), pp. 780–792. doi: 10.1159/000363295.

Gao, Y. *et al.* (2020) 'CCL22 signaling contributes to sorafenib resistance in hepatitis B virus-associated hepatocellular carcinoma', *Pharmacological Research*, 157, p. 104800. doi:

https://doi.org/10.1016/j.phrs.2020.104800.

GBD 2019 Diseases and Injuries Collaborators (2020) ‘Global burden of 369 diseases and injuries in 204 countries and territories, 1990-2019: a systematic analysis for the Global Burden of Disease Study 2019.’, *Lancet (London, England)*, 396(10258), pp. 1204–1222. doi: 10.1016/S0140-6736(20)30925-9.

Graham, D. K. *et al.* (2014a) ‘The TAM family: Phosphatidylserine-sensing receptor tyrosine kinases gone awry in cancer’, *Nature Reviews Cancer*, 14(12), pp. 769–785. doi: 10.1038/nrc3847.

Graham, N. and Pollard, J. W. (2022) ‘An acid trip activates protumoral macrophages to promote hepatocellular carcinoma malignancy’, *The Journal of Clinical Investigation*. The American Society for Clinical Investigation, 132(7). doi: 10.1172/JCI158562.

Greten, T. F., Wang, X. W. and Korangy, F. (2015) ‘Current concepts of immune based treatments for patients with HCC: From basic science to novel treatment approaches’, *Gut*, 64(5), pp. 842–848. doi: 10.1136/gutjnl-2014-307990.

Grivennikov, S. I., Greten, F. R. and Karin, M. (2010) ‘Immunity, Inflammation, and Cancer’, *Cell*. Elsevier Inc., 140(6), pp. 883–899. doi: 10.1016/j.cell.2010.01.025.

Guidotti, L. G. *et al.* (2015) ‘Immunosurveillance of the liver by intravascular effector CD8(+) T cells.’, *Cell*. United States, 161(3), pp. 486–500. doi: 10.1016/j.cell.2015.03.005.

Guilliams, M. *et al.* (2022) ‘Spatial proteogenomics reveals distinct and evolutionarily conserved hepatic macrophage niches.’, *Cell*. United States, 185(2), pp. 379-396.e38. doi: 10.1016/j.cell.2021.12.018.

Hadden, J. W. (2003) ‘Immunodeficiency and cancer: prospects for correction.’, *International immunopharmacology*. Netherlands, 3(8), pp. 1061–1071. doi: 10.1016/S1567-5769(03)00060-2.

Halaby, M. J. *et al.* (2019) ‘GCN2 drives macrophage and MDSC function and

immunosuppression in the tumor microenvironment', *Science immunology*. Sci Immunol, 4(42). doi: 10.1126/SCIIMMUNOL.AAX8189.

Heymann, F. *et al.* (2015) 'Liver Inflammation Abrogates Immunological Tolerance Induced by Kupffer Cells'. doi: 10.1002/hep.27793/suppinfo.

Heymann, F. and Tacke, F. (2016) 'Immunology in the liver — from homeostasis to disease', *Nature Reviews Gastroenterology &Amp; Hepatology*. Nature Publishing Group, a division of Macmillan Publishers Limited. All Rights Reserved., 13, p. 88. Available at: http://dx.doi.org/10.1038/nrgastro.2015.200.

Higashi, T., Friedman, S. L. and Hoshida, Y. (2017) 'Hepatic stellate cells as key target in liver fibrosis.', *Advanced drug delivery reviews*, 121, pp. 27–42. doi: 10.1016/j.addr.2017.05.007.

Ho, D. W.-H. *et al.* (2021) 'Single-cell RNA sequencing shows the immunosuppressive landscape and tumor heterogeneity of HBV-associated hepatocellular carcinoma.', *Nature communications*, 12(1), p. 3684. doi: 10.1038/s41467-021-24010-1.

Ho, T.-C. *et al.* (2020) 'Complement C1q mediates the expansion of periportal hepatic progenitor cells in senescence-associated inflammatory liver', *Proceedings of the National Academy of Sciences*. Proceedings of the National Academy of Sciences, 117(12), pp. 6717–6725. doi: 10.1073/pnas.1918028117.

Hoechst, B. *et al.* (2008) 'A New Population of Myeloid-Derived Suppressor Cells in Hepatocellular Carcinoma Patients Induces CD4+CD25+Foxp3+ T Cells', *Gastroenterology*, 135(1), pp. 234–243. doi: 10.1053/j.gastro.2008.03.020.

Hoekzema, R. *et al.* (1989) 'Biosynthesis of normal and low-molecular-mass complement component C1q by cultured human monocytes and macrophages', *Biochemical Journal*. Portland Press Ltd., 257(2), pp. 477–486.

Hoover, A. A. *et al.* (2020) 'Increased canonical NF-kappaB signaling specifically in macrophages is sufficient to limit tumor progression in syngeneic murine models of

ovarian cancer', *BMC Cancer*, 20(1), p. 970. doi: 10.1186/s12885-020-07450-8.

Huang, D. W., Sherman, B. T. and Lempicki, R. A. (2008) 'Systematic and integrative analysis of large gene lists using DAVID bioinformatics resources', *Nature Protocols 2009 4:1*. Nature Publishing Group, 4(1), pp. 44–57. doi: 10.1038/nprot.2008.211.

Jenne, C. N. and Kubes, P. (2013) 'Immune surveillance by the liver.', *Nature immunology*. United States, 14(10), pp. 996–1006. doi: 10.1038/ni.2691.

K., A.-A. G. *et al.* (2022) 'Tremelimumab plus Durvalumab in Unresectable Hepatocellular Carcinoma', *NEJM Evidence*. Massachusetts Medical Society, 1(8), p. EVIDoa2100070. doi: 10.1056/EVIDoa2100070.

Kanwal, F. and Singal, A. G. (2019) 'Surveillance for Hepatocellular Carcinoma: Current Best Practice and Future Direction.', *Gastroenterology*, 157(1), pp. 54–64. doi: 10.1053/j.gastro.2019.02.049.

Karlsen, T. H. *et al.* (2022) 'The EASL–Lancet Liver Commission: protecting the next generation of Europeans against liver disease complications and premature mortality', *The Lancet*. Elsevier B.V., 399(10319), pp. 61–116. doi: 10.1016/S0140-6736(21)01701-3/ATTACHMENT/82513520-DAB3-430E-A196-83F57E6FC6C3/MMC1.PDF.

Kew, M. C. (2003) 'Synergistic interaction between aflatoxin B1 and hepatitis B virus in hepatocarcinogenesis.', *Liver international : official journal of the International Association for the Study of the Liver*. United States, 23(6), pp. 405–409. doi: 10.1111/j.1478-3231.2003.00869.x.

Korf, H. *et al.* (2018) 'The Role of Monocytes and Macrophages in Acute and Acute-on-Chronic Liver Failure', *Frontiers in Immunology | www.frontiersin.org*, 9, p. 2948. doi: 10.3389/fimmu.2018.02948.

Kudo, M. *et al.* (2018) 'Lenvatinib versus sorafenib in first-line treatment of patients with unresectable hepatocellular carcinoma: a randomised phase 3 non-inferiority trial', *The Lancet*. Elsevier, 391(10126), pp. 1163–1173. doi: 10.1016/S0140-6736(18)30207-1.

Kurebayashi, H. *et al.* (2015) 'Prokineticin 2 (PROK2) is an important factor for angiogenesis in colorectal cancer', *Oncotarget*. Oncotarget, 6(28), pp. 26242–26251. doi: 10.18632/ONCOTARGET.4385.

Latchman, Y. *et al.* (2001) *PD-L2 is a second ligand for PD-1 and inhibits T cell activation*. Available at: http://immunol.nature.com.

Laviron, M. and Boissonnas, A. (2019) 'Ontogeny of Tumor-Associated Macrophages', *Frontiers in immunology*. Front Immunol, 10, p. 1799. doi: 10.3389/FIMMU.2019.01799.

Lee, Y.-J. *et al.* (2012) 'Preventing cleavage of Mer promotes efferocytosis and suppresses acute lung injury in bleomycin treated mice.', *Toxicology and applied pharmacology*. United States, 263(1), pp. 61–72. doi: 10.1016/j.taap.2012.05.024.

Lemke, G. (2013) 'Biology of the TAM receptors.', *Cold Spring Harbor perspectives in biology*, 5(11). doi: 10.1101/cshperspect.a009076.

Lemke, G. and Rothlin, C. V (2008) 'Immunobiology of the TAM receptors.', *Nature reviews. Immunology*, 8(5), pp. 327–336. doi: 10.1038/nri2303.

Lencioni, R. *et al.* (2016) 'Sorafenib or placebo plus TACE with doxorubicin-eluting beads for intermediate stage HCC: The SPACE trial.', *Journal of hepatology*. Netherlands, 64(5), pp. 1090–1098. doi: 10.1016/j.jhep.2016.01.012.

Li, Man *et al.* (2020) 'Remodeling tumor immune microenvironment via targeted blockade of PI3K-γ and CSF-1/CSF-1R pathways in tumor associated macrophages for pancreatic cancer therapy', *Journal of controlled release : official journal of the Controlled Release Society*. J Control Release, 321, pp. 23–35. doi: 10.1016/J.JCONREL.2020.02.011.

Li, R. *et al.* (2011) 'Role of liver sinusoidal endothelial cells and stabilins in elimination of oxidized low-density lipoproteins.', *American journal of physiology. Gastrointestinal and liver physiology*, 300(1), pp. G71-81. doi: 10.1152/ajpgi.00215.2010.

Li, X. *et al.* (2021) 'HDAC inhibition potentiates anti-tumor activity of macrophages and

enhances anti-PD-L1-mediated tumor suppression', *Oncogene*, 40(10), pp. 1836–1850. doi: 10.1038/s41388-020-01636-x.

Liaskou, E. *et al.* (2012) 'Monocyte Subsets in Human Liver Disease Show Distinct Phenotypic and Functional Characteristics'. doi: 10.1002/hep.26016.

Linger, R. M. A. *et al.* (2008) 'TAM receptor tyrosine kinases: biologic functions, signaling, and potential therapeutic targeting in human cancer.', *Advances in cancer research*, 100, pp. 35–83. doi: 10.1016/S0065-230X(08)00002-X.

Liu, P., Chen, L. and Zhang, H. (2018) 'Natural Killer Cells in Liver Disease and Hepatocellular Carcinoma and the NK Cell-Based Immunotherapy.', *Journal of immunology research*, 2018, p. 1206737. doi: 10.1155/2018/1206737.

Liu, Y. *et al.* (2022) 'Single-Cell Transcriptomic Analysis Reveals Macrophage-Tumor Crosstalk in Hepatocellular Carcinoma.', *Frontiers in immunology*. Switzerland, 13, p. 955390. doi: 10.3389/fimmu.2022.955390.

Liu, Y *et al.* (2023) 'Identification of a tumour immune barrier in the HCC microenvironment that determines the efficacy of immunotherapy.', *Journal of hepatology*. Netherlands, 78(4), pp. 770–782. doi: 10.1016/j.jhep.2023.01.011.

Liu, Z. *et al.* (2019) 'The trends in incidence of primary liver cancer caused by specific etiologies: Results from the Global Burden of Disease Study 2016 and implications for liver cancer prevention', *Journal of Hepatology*, 70(4), pp. 674–683. doi: https://doi.org/10.1016/j.jhep.2018.12.001.

Llacuna, L. *et al.* (2010) 'Growth arrest-specific protein 6 is hepatoprotective against murine ischemia/reperfusion injury.', *Hepatology (Baltimore, Md.)*, 52(4), pp. 1371–1379. doi: 10.1002/hep.23833.

Llovet, J. M. *et al.* (1999) 'Natural history of untreated nonsurgical hepatocellular carcinoma: rationale for the design and evaluation of therapeutic trials.', *Hepatology (Baltimore, Md.)*. United States, 29(1), pp. 62–67. doi: 10.1002/hep.510290145.

Llovet, J. M. (2005) ‘Updated treatment approach to hepatocellular carcinoma’, *Journal of Gastroenterology*, 40(3), pp. 225–235. doi: 10.1007/s00535-005-1566-3.

Llovet, J. M. *et al.* (2008) ‘Sorafenib in Advanced Hepatocellular Carcinoma’, *New England Journal of Medicine*, 359(4), pp. 378–390. doi: 10.1056/NEJMoa0708857.

Llovet, J. M. *et al.* (2016) ‘Hepatocellular carcinoma’, *Nature Reviews Disease Primers*, 2(1), p. 16018. doi: 10.1038/nrdp.2016.18.

Llovet, J. M. *et al.* (2021) ‘Hepatocellular carcinoma’, *Nature Reviews Disease Primers*, 7(1), p. 6. doi: 10.1038/s41572-020-00240-3.

Llovet, J. M. and Bruix, J. (2003) ‘Systematic review of randomized trials for unresectable hepatocellular carcinoma: Chemoembolization improves survival.’, *Hepatology (Baltimore, Md.)*. United States, 37(2), pp. 429–442. doi: 10.1053/jhep.2003.50047.

Llovet, J. M., Fuster, J. and Bruix, J. (2004) ‘The Barcelona approach: Diagnosis, staging, and treatment of hepatocellular carcinoma’, *Liver Transplantation*, 10(S2), pp. S115–S120. doi: 10.1002/lt.20034.

Loms Ziegler-Heitbrockon, H. W. *et al.* (1993) *Monocyte subsets 2053 The novel subset of CDl4+/CDl6+ blood monocytes exhibits features of tissue macrophages**, *Eur. J. Immunol*.

Lu, Q. and Lemke, G. (2001) ‘Homeostatic regulation of the immune system by receptor tyrosine kinases of the Tyro 3 family.’, *Science (New York, N.Y.)*. United States, 293(5528), pp. 306–311. doi: 10.1126/science.1061663.

MacParland, S. A. *et al.* (2018) ‘Single cell RNA sequencing of human liver reveals distinct intrahepatic macrophage populations’, *Nature Communications*, 9(1), pp. 1–21. doi: 10.1038/s41467-018-06318-7.

MacPhee, P. J., Schmidt, E. E. and Groom, A. C. (1992) ‘Evidence for Kupffer cell migration

along liver sinusoids, from high- resolution in vivo microscopy', *American Journal of Physiology - Gastrointestinal and Liver Physiology*, 263(1 26-1). doi: 10.1152/AJPGI.1992.263.1.G17.

Maimon, A. *et al.* (2021) 'Myeloid cell-derived PROS1 inhibits tumor metastasis by regulating inflammatory and immune responses via IL-10.', *The Journal of clinical investigation*, 131(10). doi: 10.1172/JCI126089.

Masetti, M. *et al.* (2021) 'Lipid-loaded tumor-associated macrophages sustain tumor growth and invasiveness in prostate cancer', *Journal of Experimental Medicine*, 219(2), p. e20210564. doi: 10.1084/jem.20210564.

de Masson, A. *et al.* (2022) 'Macrophage-derived CXCL9 and CXCL11, T-cell skin homing, and disease control in mogamulizumab-treated CTCL patients', *Blood*. American Society of Hematology, 139(12), pp. 1820–1832. doi: 10.1182/BLOOD.2021013341.

Melief, J. *et al.* (2020) 'High expression of ID1 in monocytes is strongly associated with phenotypic and functional MDSC markers in advanced melanoma', *Cancer Immunology, Immunotherapy*. Springer, 69(4), p. 513. doi: 10.1007/S00262-019-02476-9.

Meznarich, J. *et al.* (2013) 'Urokinase Plasminogen Activator Induces Pro-Fibrotic/M2 Phenotype in Murine Cardiac Macrophages', *PLOS ONE*. Public Library of Science, 8(3), p. e57837. doi: 10.1371/JOURNAL.PONE.0057837.

Mi, H. *et al.* (2019) 'PANTHER version 14: more genomes, a new PANTHER GO-slim and improvements in enrichment analysis tools', *Nucleic acids research*. Nucleic Acids Res, 47(D1), pp. D419–D426. doi: 10.1093/NAR/GKY1038.

Mittal, S. *et al.* (2016) 'Hepatocellular Carcinoma in the Absence of Cirrhosis in United States Veterans is Associated With Nonalcoholic Fatty Liver Disease.', *Clinical gastroenterology and hepatology : the official clinical practice journal of the American Gastroenterological Association*, 14(1), pp. 124–31.e1. doi: 10.1016/j.cgh.2015.07.019.

Molgora, M. *et al.* (2020) 'TREM2 Modulation Remodels the Tumor Myeloid Landscape,

Enhancing Anti-PD-1 Immunotherapy', *Cell*. NIH Public Access, 182(4), p. 886. doi: 10.1016/J.CELL.2020.07.013.

Monnier, J. *et al.* (2008) 'Prokineticin 2/Bv8 is expressed in Kupffer cells in liver and is down regulated in human hepatocellular carcinoma.', *World journal of gastroenterology*, 14(8), pp. 1182–1191. doi: 10.3748/wjg.14.1182.

Montoya, A. *et al.* (2011) 'Characterization of a TiO2 enrichment method for label-free quantitative phosphoproteomics', *Methods (San Diego, Calif.)*. Elsevier, 54(4), p. 370. doi: 10.1016/J.YMETH.2011.02.004.

Mukherjee, S. K. *et al.* (2016) 'MER Tyrosine Kinase Positive Tumour Associated Macrophages Are a Novel Therapeutic Target in Hepatocellular Carcinoma', *Journal of Hepatology*. Elsevier, 64(2), pp. S574–S575. doi: 10.1016/S0168-8278(16)01046-1.

Nakanishi, M. *et al.* (2008) 'Abscopal effect on hepatocellular carcinoma.', *The American journal of gastroenterology*. United States, pp. 1320–1321. doi: 10.1111/j.1572-0241.2007.01782_13.x.

Nault, J. C. *et al.* (2013) 'High frequency of telomerase reverse-transcriptase promoter somatic mutations in hepatocellular carcinoma and preneoplastic lesions', *Nature communications*. Nature Publishing Group, 4(1), pp. 1–7.

Nelson, E. R. *et al.* (2013) '27-Hydroxycholesterol links hypercholesterolemia and breast cancer pathophysiology.', *Science (New York, N.Y.)*, 342(6162), pp. 1094–1098. doi: 10.1126/science.1241908.

Newlaczyl, A. U. and Yu, L. G. (2011) 'Galectin-3--a jack-of-all-trades in cancer', *Cancer letters*. Cancer Lett, 313(2), pp. 123–128. doi: 10.1016/J.CANLET.2011.09.003.

Noguchi, Y. *et al.* (2019) 'Human TIGIT on porcine aortic endothelial cells suppresses xenogeneic macrophage-mediated cytotoxicity', *Immunobiology*. Immunobiology, 224(5), pp. 605–613. doi: 10.1016/J.IMBIO.2019.07.008.

O'Brien, A. J. *et al.* (2014) 'Immunosuppression in acutely decompensated cirrhosis is mediated by prostaglandin E2.', *Nature medicine*, 20(5), pp. 518–523. doi: 10.1038/nm.3516.

Ogden, C. A. *et al.* (2001) 'C1q and mannose binding lectin engagement of cell surface calreticulin and CD91 initiates macropinocytosis and uptake of apoptotic cells', *The Journal of experimental medicine*. The Rockefeller University Press, 194(6), pp. 781–796.

Olingy Huy Q Dinh Catherine C Hedrick, C. E. and Catherine Hedrick, C. C. (no date) 'Monocyte heterogeneity and functions in cancer'. doi: 10.1002/JLB.4RI0818-311R.

Paccez, J. D. *et al.* (2015) 'Inactivation of GSK3β and activation of NF-κB pathway via Axl represents an important mediator of tumorigenesis in esophageal squamous cell carcinoma', 26. doi: 10.1091/mbc.E14-04-0868.

Paolino, M. *et al.* (2014) 'The E3 ligase Cbl-b and TAM receptors regulate cancer metastasis via natural killer cells', *Nature*, 507(7493), pp. 508–512. doi: 10.1038/nature12998.

Pascut, D., Pratama, M. Y. and Tiribelli, C. (2020) 'HCC occurrence after DAA treatments: molecular tools to assess the post-treatment risk and surveillance', *Hepatic Oncology*. Future Medicine, 7(2), p. HEP21. doi: 10.2217/hep-2020-0010.

Patel, A. S. *et al.* (2013) 'TIE2-expressing monocytes/macrophages regulate revascularization of the ischemic limb', *EMBO Molecular Medicine*. John Wiley & Sons, Ltd, 5(6), pp. 858–869. doi: 10.1002/EMMM.201302752.

Patten, D. A. and Shetty, S. (2019) 'The Role of Stabilin-1 in Lymphocyte Trafficking and Macrophage Scavenging in the Liver Microenvironment', *Biomolecules* . doi: 10.3390/biom9070283.

Petrillo, M. *et al.* (2015) 'Polarisation of tumor-associated macrophages toward M2 phenotype correlates with poor response to chemoradiation and reduced survival in patients with locally advanced cervical cancer', *PLoS One*. Public Library of Science San Francisco, CA USA, 10(9), p. e0136654.

Pinato, D. J. *et al.* (no date) 'Integrated analysis of multiple receptor tyrosine kinases identifies Axl as a therapeutic target and mediator of resistance to sorafenib in hepatocellular carcinoma'. doi: 10.1038/s41416-018-0373-6.

Pulanco, M. C. *et al.* (2017) 'Complement Protein C1q Enhances Macrophage Foam Cell Survival and Efferocytosis', *The Journal of Immunology*. American Association of Immunologists, 198(1), pp. 472–480. doi: 10.4049/JIMMUNOL.1601445.

Qi, N. *et al.* (2013) 'Development of a Spontaneous Liver Disease Resembling Autoimmune Hepatitis in Mice Lacking Tyro3, Axl and Mer Receptor Tyrosine Kinases', *PLoS ONE*, 8(6), pp. 1–11. doi: 10.1371/journal.pone.0066604.

Rabold, K. *et al.* (2020) 'Enhanced lipid biosynthesis in human tumor-induced macrophages contributes to their protumoral characteristics', *J Immunother Cancer*, 8, p. 638. doi: 10.1136/jitc-2020-000638.

Rahib, L. *et al.* (2014) 'Projecting cancer incidence and deaths to 2030: the unexpected burden of thyroid, liver, and pancreas cancers in the United States.', *Cancer research*. United States, 74(11), pp. 2913–2921. doi: 10.1158/0008-5472.CAN-14-0155.

Rahman, Z. S. M. *et al.* (2010) 'Impaired apoptotic cell clearance in the germinal center by Mer-deficient tingible body macrophages leads to enhanced antibody-forming cell and germinal center responses.', *Journal of immunology (Baltimore, Md. : 1950)*, 185(10), pp. 5859–5868. doi: 10.4049/jimmunol.1001187.

Ramachandran, P. *et al.* (2019) 'Resolving the fibrotic niche of human liver cirrhosis at single-cell level.', *Nature*. England, 575(7783), pp. 512–518. doi: 10.1038/s41586-019-1631-3.

Rankin, E. B. *et al.* (2014) 'Direct regulation of GAS6/AXL signaling by HIF promotes renal metastasis through SRC and MET', *Proceedings of the National Academy of Sciences*, 111(37), pp. 13373–13378. doi: 10.1073/pnas.1404848111.

Rantakari, P. *et al.* (2016) 'Stabilin-1 expression defines a subset of macrophages that mediate

tissue homeostasis and prevent fibrosis in chronic liver injury', *Proceedings of the National Academy of Sciences*. Proceedings of the National Academy of Sciences, 113(33), pp. 9298–9303. doi: 10.1073/pnas.1604780113.

Reig, M. *et al.* (2016) 'Unexpected high rate of early tumor recurrence in patients with HCV-related HCC undergoing interferon-free therapy', *Journal of hepatology*. Elsevier, 65(4), pp. 719–726.

Reig, M. *et al.* (2022) 'BCLC strategy for prognosis prediction and treatment recommendation: The 2022 update.', *Journal of hepatology*, 76(3), pp. 681–693. doi: 10.1016/j.jhep.2021.11.018.

Riabov, V. *et al.* (2016) 'Stabilin-1 is expressed in human breast cancer and supports tumor growth in mammary adenocarcinoma mouse model', *Oncotarget*. Impact Journals, LLC, 7(21), p. 31097.

Roayaie, S. *et al.* (2013) 'Resection of hepatocellular cancer ≤2 cm: results from two Western centers.', *Hepatology (Baltimore, Md.)*, 57(4), pp. 1426–1435. doi: 10.1002/hep.25832.

Rothlin, C. V. *et al.* (2007) 'TAM Receptors Are Pleiotropic Inhibitors of the Innate Immune Response', *Cell*, 131(6), pp. 1124–1136. doi: 10.1016/j.cell.2007.10.034.

Roumenina, L. T. *et al.* (2019) 'Tumor cells hijack macrophage-produced complement C1q to promote tumor growth', *Cancer Immunology Research*, 7(7), pp. 1091–1105. doi: 10.1158/2326-6066.CIR-18-0891.

Rundgren, I. M. *et al.* (2018) 'Standardization of sampling and sample preparation for analysis of human monocyte subsets in peripheral blood', *Journal of Immunological Methods*. Elsevier B.V., 461, pp. 53–62. doi: 10.1016/J.JIM.2018.06.003.

Saito, T. *et al.* (2014) 'Spontaneous regression of a large hepatocellular carcinoma with multiple lung metastases.', *Gut and liver*, 8(5), pp. 569–574. doi: 10.5009/gnl13358.

Sana, G. *et al.* (2014) 'Adult Human Hepatocytes Promote CD4+ T-Cell Hyporesponsiveness

Via Interleukin-10-Producing Allogeneic Dendritic Cells', *Cell Transplantation*. SAGE Publications Inc, 23(9), pp. 1127–1142. doi: 10.3727/096368913X666421.

Sánchez-Martín, L. *et al.* (2011) 'The chemokine CXCL12 regulates monocyte-macrophage differentiation and RUNX3 expression', *Blood*. Blood, 117(1), pp. 88–97. doi: 10.1182/BLOOD-2009-12-258186.

Schneider, C. A., Rasband, W. S. and Eliceiri, K. W. (2012) *NIH Image to ImageJ: 25 years of image analysis*, *Nature Methods*. doi: 10.1038/nmeth.2089.

Schupp, J. *et al.* (2017) 'Targeting myeloid cells in the tumor sustaining microenvironment', *Cellular Immunology*. Academic Press. doi: 10.1016/J.CELLIMM.2017.10.013.

Seitz, H. M. *et al.* (2007) 'Macrophages and dendritic cells use different Axl/Mertk/Tyro3 receptors in clearance of apoptotic cells.', *Journal of immunology (Baltimore, Md. : 1950)*. United States, 178(9), pp. 5635–5642. doi: 10.4049/jimmunol.178.9.5635.

Shankaran, V. *et al.* (2001) 'IFNγ and lymphocytes prevent primary tumour development and shape tumour immunogenicity', *Nature*. Macmillian Magazines Ltd., 410, p. 1107. Available at: http://dx.doi.org/10.1038/35074122.

Tabrizian, P. *et al.* (2022) 'Ten-Year Outcomes of Liver Transplant and Downstaging for Hepatocellular Carcinoma', *JAMA surgery*. JAMA Surg. doi: 10.1001/JAMASURG.2022.2800.

Tacke, F. (2017) 'Targeting hepatic macrophages to treat liver diseases', *Journal of Hepatology*. European Association for the Study of the Liver, 66(6), pp. 1300–1312. doi: 10.1016/j.jhep.2017.02.026.

Tan, M. L. *et al.* (2020) 'Evaluating the Polarization of Tumor-Associated Macrophages Into M1 and M2 Phenotypes in Human Cancer Tissue: Technicalities and Challenges in Routine Clinical Practice'. doi: 10.3389/fonc.2019.01512.

Triantafyllou, E. *et al.* (2017) 'MerTK expressing hepatic macrophages promote the resolution

of inflammation in acute liver failure', *Gut*, p. gutjnl-2016-313615. doi: 10.1136/gutjnl-2016-313615.

Triantafyllou, E. *et al.* (2018) 'MerTK expressing hepatic macrophages promote the resolution of inflammation in acute liver failure', *Gut*, 67(2), pp. 333 LP – 347. Available at: http://gut.bmj.com/content/67/2/333.abstract.

Trinchet, J.-C. *et al.* (2015) 'Complications and competing risks of death in compensated viral cirrhosis (ANRS CO12 CirVir prospective cohort).', *Hepatology (Baltimore, Md.)*. United States, 62(3), pp. 737–750. doi: 10.1002/hep.27743.

Tu, S. *et al.* (2008) 'Overexpression of interleukin-1beta induces gastric inflammation and cancer and mobilizes myeloid-derived suppressor cells in mice.', *Cancer cell*, 14(5), pp. 408–419. doi: 10.1016/j.ccr.2008.10.011.

Ubil, E. *et al.* (2018) 'Tumor-secreted Pros1 inhibits macrophage M1 polarization to reduce antitumor immune response', *Journal of Clinical Investigation*, 128(6), pp. 2356–2369. doi: 10.1172/JCI97354.

Ugel, S. *et al.* (2015) 'Tumor-induced myeloid deviation: When myeloid-derived suppressor cells meet tumor-Associated macrophages', *Journal of Clinical Investigation*, 125(9), pp. 3365–3376. doi: 10.1172/JCI80006.

Vogel, A. *et al.* (2018) 'Hepatocellular carcinoma: ESMO Clinical Practice Guidelines for diagnosis, treatment and follow-up†', *Annals of Oncology*. Elsevier, 29, pp. iv238–iv255. doi: 10.1093/annonc/mdy308.

Wang, X. *et al.* (2018) 'Age-related changes in expression and signaling of TAM receptor inflammatory regulators in monocytes', *Oncotarget; Vol 9, No 11*. Available at: https://www.oncotarget.com/article/23851/text/.

Werdich, X. Q. and Penn, J. S. (no date) 'Src, Fyn and Yes play differential roles in VEGF-mediated endothelial cell events'. doi: 10.1007/s10456-005-9021-x.

Werno, C. *et al.* (2010) 'Knockout of HIF-1α in tumor-associated macrophages enhances M2 polarization and attenuates their pro-angiogenic responses', *Carcinogenesis*, 31(10), pp. 1863–1872. doi: 10.1093/carcin/bgq088.

Wiedemann, G. M. *et al.* (2019) 'Peritumoural CCL1 and CCL22 expressing cells in hepatocellular carcinomas shape the tumour immune infiltrate.', *Pathology*. England, 51(6), pp. 586–592. doi: 10.1016/j.pathol.2019.06.001.

Williams, C. B., Yeh, E. S. and Soloff, A. C. (2016) 'Tumor-associated macrophages: unwitting accomplices in breast cancer malignancy.', *NPJ breast cancer*, 2, pp. 15025-. doi: 10.1038/npjbcancer.2015.25.

Williams, R. *et al.* (2014) 'Addressing liver disease in the UK: A blueprint for attaining excellence in health care and reducing premature mortality from lifestyle issues of excess consumption of alcohol, obesity, and viral hepatitis', *The Lancet*, 384(9958), pp. 1953–1997. doi: 10.1016/S0140-6736(14)61838-9.

Winslow, S. *et al.* (2015) 'Prognostic stromal gene signatures in breast cancer.', *Breast cancer research : BCR*, 17(1), p. 23. doi: 10.1186/s13058-015-0530-2.

Wong, K. L. *et al.* (2012) 'The three human monocyte subsets: Implications for health and disease', *Immunologic Research*, 53(1–3), pp. 41–57. doi: 10.1007/s12026-012-8297-3.

Workman, G. and Sage, E. H. (2011) 'Identification of a sequence in the matricellular protein SPARC that interacts with the scavenger receptor stabilin-1.', *Journal of cellular biochemistry*. United States, 112(4), pp. 1003–1008. doi: 10.1002/jcb.23015.

Wu, C. *et al.* (2020) 'Myeloid signature reveals immune contexture and predicts the prognosis of hepatocellular carcinoma', *The Journal of Clinical Investigation*. American Society for Clinical Investigation, 130(9), pp. 4679–4693. doi: 10.1172/JCI135048.

Wu, K. *et al.* (2020) 'Redefining Tumor-Associated Macrophage Subpopulations and Functions in the Tumor Microenvironment', *Frontiers in immunology*. NLM (Medline), 11, p. 1731. doi: 10.3389/FIMMU.2020.01731/BIBTEX.

Xu, M. *et al.* (2015) 'Intratumoral delivery of IL-21 overcomes anti-Her2/Neu resistance through shifting tumor-associated macrophages from M2 to M1 phenotype', *The Journal of Immunology*. Am Assoc Immnol, 194(10), pp. 4997–5006.

Xue, J. *et al.* (2014) 'Transcriptome-Based Network Analysis Reveals a Spectrum Model of Human Macrophage Activation', *Immunity*. Cell Press, 40(2), pp. 274–288. doi: 10.1016/J.IMMUNI.2014.01.006.

Yan, W. *et al.* (2015) 'Tim-3 fosters HCC development by enhancing TGF-β-mediated alternative activation of macrophages', *Gut*. BMJ Publishing Group, 64(10), pp. 1593–1604. doi: 10.1136/GUTJNL-2014-307671.

Yang, F. C. *et al.* (2019) 'TREM-1-dependent M1 macrophage polarization restores intestinal epithelium damaged by DSS-induced colitis by activating IL-22-producing innate lymphoid cells', *Journal of Biomedical Science*. BioMed Central, 26(1). doi: 10.1186/S12929-019-0539-4.

Yang, M., McKay, D., Pollard, Jeffrey W, *et al.* (2018) 'Diverse Functions of Macrophages in Different Tumor Microenvironments', *Cancer Research*, 78(19), pp. 5492 LP – 5503. doi: 10.1158/0008-5472.CAN-18-1367.

Yang, M., McKay, D., Pollard, Jeffrey W., *et al.* (2018) 'Diverse Functions of Macrophages in Different Tumor Microenvironments', *Cancer research*. Cancer Res, 78(19), pp. 5492–5503. doi: 10.1158/0008-5472.CAN-18-1367.

Yeung, O. W. H. *et al.* (2015) 'Alternatively activated (M2) macrophages promote tumour growth and invasiveness in hepatocellular carcinoma', *Journal of Hepatology*. European Association for the Study of the Liver, 62(3), pp. 607–616. doi: 10.1016/j.jhep.2014.10.029.

Zagórska, A. *et al.* (2014) 'Diversification of TAM receptor tyrosine kinase function', *nature immunology*, 15. doi: 10.1038/ni.2986.

Zagórska, A., Través, Paqui G, *et al.* (2020) 'Differential regulation of hepatic physiology and injury by the TAM receptors Axl and Mer'. doi: 10.26508/lsa.202000694.

Zagórska, A., Través, Paqui G., *et al.* (2020) 'Differential TAM receptor regulation of hepatic physiology and injury', *bioRxiv*, 3(8), p. 2020.03.13.990143.

Zhang, Q. *et al.* (2019) 'Landscape and Dynamics of Single Immune Cells in Hepatocellular Carcinoma', *Cell*. Elsevier Inc., 179(4), pp. 829-845.e20. doi: 10.1016/j.cell.2019.10.003.

Zhang, T. *et al.* (2020) 'Neoadjuvant therapy and immunotherapy strategies for hepatocellular carcinoma.', *American journal of cancer research*, 10(6), pp. 1658–1667.

Zhang, W. *et al.* (2020) 'IL-6 promotes PD-L1 expression in monocytes and macrophages by decreasing protein tyrosine phosphatase receptor type O expression in human hepatocellular carcinoma', *Journal for ImmunoTherapy of Cancer*, 8, p. 285. doi: 10.1136/jitc-2019-000285.

Zhang, X. *et al.* (2019) 'The prognostic value of myeloid derived suppressor cell level in hepatocellular carcinoma: A systematic review and meta-analysis'. doi: 10.1371/journal.pone.0225327.

Zhang, Y. *et al.* (2013) 'Breakdown of immune homeostasis in the testis of mice lacking Tyro3, Axl and Mer receptor tyrosine kinases.', *Immunology and cell biology*. England, 91(6), pp. 416–426. doi: 10.1038/icb.2013.22.

Zhang, Y. and Wang, X. (2020) 'Targeting the Wnt/β-catenin signaling pathway in cancer', *Journal of Hematology & Oncology*, 13(1), p. 165. doi: 10.1186/s13045-020-00990-3.

Zhen, A. *et al.* (2014) 'CD4 Ligation on Human Blood Monocytes Triggers Macrophage Differentiation and Enhances HIV Infection', *Journal of Virology*. American Society for Microbiology, 88(17), pp. 9934–9946. doi: 10.1128/JVI.00616-14.

Zhen, Y., Finkelman, F. D. and Shao, W. H. (2018) 'Mechanism of Mer receptor tyrosine kinase inhibition of glomerular endothelial cell inflammation', *Journal of leukocyte biology*. J Leukoc Biol, 103(4), pp. 709–717. doi: 10.1002/JLB.3A0917-368R.

Zheng, C. *et al.* (2017) 'Landscape of Infiltrating T Cells in Liver Cancer Revealed by Single-Cell Sequencing', *Cell*. Elsevier, 169(7), pp. 1342-1356.e16. doi: 10.1016/j.cell.2017.05.035.

Zheng, P. *et al.* (2018) 'Tumor-associated macrophages-derived exosomes promote the migration of gastric cancer cells by transfer of functional Apolipoprotein E', *Cell Death & Disease*, 9(4), p. 434. doi: 10.1038/s41419-018-0465-5.

Zhou, Y. *et al.* (2020) 'Blockade of the Phagocytic Receptor MerTK on Tumor-Associated Macrophages Enhances P2X7R-Dependent STING Activation by Tumor-Derived cGAMP.', *Immunity*. United States, 52(2), pp. 357-373.e9. doi: 10.1016/j.immuni.2020.01.014.

Zigmond, E. *et al.* (2014) 'Infiltrating Monocyte-Derived Macrophages and Resident Kupffer Cells Display Different Ontogeny and Functions in Acute Liver Injury', *The Journal of Immunology*, 193(1), pp. 344–353. doi: 10.4049/jimmunol.1400574.

Zizzo, G. *et al.* (2012) 'Efficient Clearance of Early Apoptotic Cells by Human Macrophages Requires M2c Polarization and MerTK Induction', *The Journal of Immunology*. American Association of Immunologists, 189(7), pp. 3508–3520. doi: 10.4049/JIMMUNOL.1200662.

Zucman-Rossi, J. *et al.* (2015) 'Genetic Landscape and Biomarkers of Hepatocellular Carcinoma', *Gastroenterology*. Elsevier, 149(5), pp. 1226–1239. doi: 10.1053/j.gastro.2015.05.061.

9. APPENDIX

Antibody	Fluorochrome	Species	Manufacturer	Volume
Common Markers to both tubes				
CD14	PE- Cy7	Mouse	BD Biosciences	1.5ul
CD16	APC-H7	Mouse	BD Biosciences	1.5ul
HLA-DR	Brilliant Violet 510	Mouse	BD Biosciences	2.5ul
MerTK	APC	Mouse	R & D	2.5ul
Fixable Viability Dye	AF700	Mouse	BD Biosciences	-
Lineage (CD3/CD56/CD19/CD15)	PerCP Cy 5.5	Mouse	BD Biosciences	2.5ul each
Tube 1				
PD-L1	Brilliant Violet 421	Mouse	BD Biosciences	5ul
CD169	Brilliant Violet 650	Mouse	BD Biosciences	5ul
CD204	Brilliant Violet 605	Mouse	BD Biosciences	3ul
PD1	Brilliant Violet 711	Mouse	BD Biosciences	5ul
Tyro 3	PE	Mouse	R & D	3ul
Axl	AF488	Mouse	R & D	3ul
CSF1R	Brilliant Violet 786	Mouse	BD Biosciences	5ul
Tube 2				
Tim-4	Brilliant Violet 421	Mouse	BD Biosciences	5ul
Tim-3	Brilliant Violet 650	Mouse	BD Biosciences	5ul
CX3CR1	Brilliant Violet 605	Mouse	BD Biosciences	5ul
CD163	Brilliant Violet 711	Mouse	BD Biosciences	5ul
Tie2	PE	Mouse	BD Biosciences	5ul
CD172a	AF488	Mouse	BD Biosciences	5ul
CD64	Brilliant Violet 786	Mouse	BD Biosciences	5ul